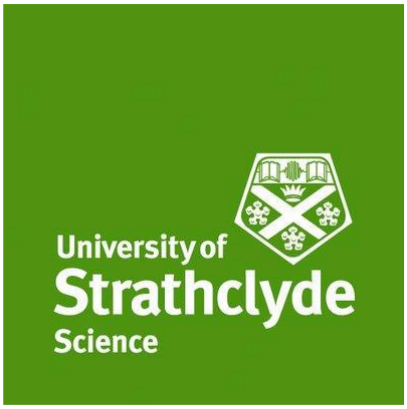

The rational structure-based design of a nanoparticle system presenting a chimeric MenB antigen

Rob Cunliffe

A thesis presented for the degree of
Doctor of Philosophy
from the Institute of Pharmacy and Pharmaceutical Sciences
at the University of Strathclyde

December 2019

Declaration of Authenticity

'This thesis is the result of the author's original research. It has been composed by the author and has not been previously submitted for examination which has led to the award of a degree.' 'The copyright of this thesis belongs to the author under the terms of the United Kingdom Copyright Acts as qualified by University of Strathclyde Regulation 3.50. Due acknowledgement must always be made of the use of any material contained in, or derived from, this thesis.'

Signed: Rob Cunliffe
Date: 16/12/2019

Acknowledgments

The research projected was funded by the European Commission Project Leveraging Pharmaceutical Sciences and Structural Biology Training to Develop 21st Century Vaccines (H2020-MSCA-ITN-2015 grant agreement 675370). Rob Cunliffe is a PhD candidate at the University of Strathclyde (Glasgow, UK) and participated in the project at GSK (Siena, Italy). This project was co-sponsored between the University of Strathclyde and GSK.

Abstract

Bacterial infection by the gram-negative diplococcus *Neisseria meningitidis* serogroup B (MenB) is a leading cause of meningitis and septicaemia. Vaccines rank amongst the most important public health interventions for combatting these diseases. As vaccine development orientates towards more minimalist subunit antigen-based vaccines, new adjuvant systems are increasingly needed to boost immunogenicity. The application of nanoparticles in vaccine formulations has the potential to drive the development of next generation adjuvant systems that improve antigen presentation and overall vaccine immunogenicity. In addition, advances in structural and computational biology have enabled a new era of vaccine design and discovery, Structural Vaccinology, which seeks the rational structure-based design of improved vaccine antigens measured in terms of epitope presentation, stability and ease of production. In this project, a structural vaccinology approach is adopted toward the rational design of a self-assembling ferritin nanoparticle system displaying a chimeric protein antigen to stimulate broad and efficacious immunogenicity against MenB. This chimeric antigen, incorporating epitopes from the NadA3 and PorA MenB antigens seeks to confer broader MenB strain coverage, while its incorporation into a self-assembling ferritin-based nanoparticle system sees the chimeric NadA3-PorA presented in a multicopy format on the ferritin surface, enhancing the immunogenicity. The first part of the thesis describes the *in silico* design of a feasible protein nanoparticle system using X-ray crystallography data. This NadA3-PorA-Ferritin was then expressed and purified, before its epitope presentation was characterised by a range of structural and biochemical approaches, including cryo-electron microscopy (cryo-EM). The immunogenicity of the NadA3-PorA-Ferritin was assessed *in vivo*, revealing that recombinant nanoparticle presentation of the NadA3-PorA enhanced the humoral responses raised against the subunit antigen. Different adjuvant systems to deliver the NadA3-PorA-Ferritin were also examined, demonstrating that an in-house, cationic liposome formulation produced by benchtop microfluidics generated a similar level of immunogenicity as a commercially available MF59-based emulsion adjuvant. Further serological assays were performed to gauge the bactericidal titre resulting from immunisation with the nanoparticle. The work within this project exemplifies a structural vaccinology approach towards the design of a chimeric protein antigen-presenting self-assembling nanoparticle system that is able to confer broad and efficacious protection against MenB.

Keywords: Structural Vaccinology, Nanoparticle vaccine, self-assembling, rational design

List of Posters and Oral Presentations

Cunliffe R, Chatzikleanthous D, Anderluzzi G, Lou Ramirez G, Perrie Y, Ferlenghi I (2017). Developing manufacturing processes for cationic lipid adjuvants: the effect of lipid concentration on liposome size and charge. UK and Ireland Controlled Release Society Symposium, University of Strathclyde, Glasgow, UK. 30-31st May 2017 (poster)

Cunliffe R, Veggi D, Giusti F, Scarselli M, Ferlenghi I (2017). Structure-based antigen modification for improved efficacy of vaccines: nanoparticles as vehicles of heterologous epitopes. Cryo-EM symposium: Introducing the new Cryo-Electron Microscopy Facility for Structural Biology. ESRF, Grenoble, France. 6-7th July 2017 (poster)

Cunliffe R, Veggi D, Giusti F, Scarselli M, Ferlenghi I (2017). Structure-based antigen modification for improved efficacy of vaccines: Nanoparticles as vehicles of heterologous epitopes GSK Vaccines PhD Research Day, Siena, Italy 2017 (poster)

Cunliffe R., Perrie Y. (2018) Process development for the microfluidic-based formulation and purification of cationic liposomes. Academy of Pharmaceutical Sciences at the International Pharmaceutical Federation, Glasgow, UK. Accepted on 08.08.2018 (poster)

Cunliffe R., Perrie Y. (2018) Investigating cationic liposome production by a microfluidic process. SIPBS PhD Research Day, Glasgow, UK. Accepted on 09.11.2018 (poster)

Cunliffe R., Fantoni A., Veggi D., Scarselli M., Ferlenghi I., Perrie Y (2018). Structure-based antigen modification for improved efficacy of vaccines: Nanoparticles as vehicles of heterologous epitopes. GSK Vaccines PhD Research Day, Siena, Italy. Accepted on 30.11.2018 (poster)

Cunliffe R, Perrie Y, Ferlenghi I (2019) Structural vaccinology: The rational design of a ferritin nanoparticle presenting a chimeric antigen Bioinspired Nanomaterials, Glasgow, UK. March 2019 (Oral presentation)

Cunliffe R, Perrie Y, Ferlenghi I (2019) Next-generation vaccines: Self-assembling ferritin nanoparticles presenting chimeric antigens UK and Ireland Controlled Release Society Symposium, Liverpool, UK. June 2019 (poster)

Cunliffe R, Perrie Y, Ferlenghi I (2019) improving vaccine efficacy: The rational structure-based design of a nanoparticle system displaying a chimeric antigen. Controlled Release Society Annual Meeting & Exposition, Valencia, Spain, 2019 (Oral presentation)

Cunliffe R, Perrie Y, Ferlenghi I (2019) Enhancing vaccine potency: self-assembling ferritin nanoparticles as antigen delivery systems. British Society for Nanomedicine, Glasgow, 2019 (Oral presentation)

Cunliffe R, Perrie Y, Ferlenghi I (2019) Enhancing the immunogenicity of a chimeric subunit antigen through surface presentation on a self-assembling protein nanoparticle. APS PharmSci, London, 2019 (poster)

Cunliffe R, Perrie Y, Ferlenghi I (2019) The rational structure-based design of a nanoparticle system presenting a chimeric MenB antigen. PHA-ST-TRAIN-VAC Symposium, Strathclyde, 2019 (Oral presentation)

Cunliffe R, Perrie Y, Ferlenghi I (2019) The rational structure-based design of a nanoparticle system presenting a chimeric MenB antigen. GSK Vaccines PhD Research Day, Siena, Italy (Oral presentation)

Contents

List of tables

Table of figures

Abbreviations

APC	Antigen presenting cell
BCR	B-cell receptor
BSA	Bovine serum albumin
CAF	Cationic adjuvant formulation
ConA	Concanavalin A
CPU	Colony forming units
Cryo-EM	Cryo electron microscopy
DC	Dendritic cell
DDA	Dimethyldioctadecylammonium
DED	Direct electron-detector
DilC	1,1′-Dioctadecyl-3,3,3′,3′-tetramethylindocarbocyanine perchlorate
DLS	Dynamic light scattering
DMG-PEG2000	1,2-dimyristoyl-rac-glycero-3-methoxy-PEG2000
DOTAP	1,2-dioleoyl-3-trimethylammonium-propane
DSPC	1,2-distearoyl-sn-glycero-3-phosphocholine
ELISA	Enzyme-Linked Immunosorbent Assay
FACS	Fluorescence-activated cell sorting
FcR	Fc receptor
fHbp	Factor H binding protein
FRR	Flow rate ratio
GC	Germinal centre
GO	Graphene oxide
HA	Hemagglutinin

HDX-MS	Hydrogen-Deuterium Exchange Mass Spectrometry
HPV	Human papillomavirus
Hsp90	Heat shock protein 90
IEDB	Immune Epitope DataBase
IFNγ	Interferon gamma
IL	Interleukin
IPTG	Isopropyl β-D-thiogalactoside
IMD	Invasive meningococcal disease
IVIS	In Vivo Imaging System
LOD	Limit of detection
LOQ	Limit of quantification
mAb	Monoclonal antibody
MenB	*N. meningitidis* serogroup B
MHC	Membrane-histocompatibility complex
mPES	Modified polyethersulfone
MPL	Monophosphoryl lipid A
NadA3	Neisserial adhesin A variant 3
NHBA	Neisseria heparin-binding antigen
NIR	Near-infrared
NMR	Nuclear Magnetic Resonance
OMV	Outer membrane vesicle
OVA	Ovalbumin
PAMP	Pathogen-associated molecular pattern
PDI	Polydispersity index
PEG	Polyethylene glycol

PLGA	Poly(lactide-co-glycolide)
PorA	Porin A
PROFILER	Phage-based Representation Of Immuno-Ligand Epitope Repertoire
PRR	Pathogen Recognition Receptor
RELION	REgularized LIkelihood OptimizatioN
RI	Refractive index
RSV	Respiratory Syncytial Virus
SBA	Serum Bactericidal Assay
SD	Standard deviation
SDS-PAGE	Sodium dodecyl sulfate polyacrylamide gel electrophoresis
SEC	Size exclusion chromatography
SPR	Surface Plasmon Resonance
TAA	Trimeric autotransporter adhesin
TDB	α,α′-trehalose 6,6′-dibehenate
TEM	Transmission Electron Microscopy
TFF	Tangential Flow Filtration
T_{FH}	T follicular helper cells
TFR	Total flow rate
Th	T helper cell
TLR	Toll-like receptor
TNF-α	Tumor necrosis factor alpha
Treg	Regulatory T-cell
VLP	Virus-like-particle
VR1	variable region 1
VR2	variable region 2

1. Chapter 1

General introduction

1.1 Developing vaccines for *Neisseria meningitidis*

1.1.1 The case for a vaccine against *Neisseria meningitidis*

Bacterial infection by the gram-negative diplococcus *Neisseria meningitidis* is a leading cause of meningitis and septicaemia (Stephens et al., 2007). A bacterium that colonises only humans, it is estimated that about 8 – 25 % of people at any one time are carriers of *N. meningitidis* in their nasopharynx (Stephens, 1999). Transmission from person to person occurs largely through respiratory droplets, leading to the establishment of a carrier state which can endure for days to months.

Both meningitis and septicaemia are manifestations of invasive meningococcal disease (IMD), which occurs when the bacteria break through the protective lining of the nose and throat, entering the bloodstream before successfully evading the innate immune system and multiplying, leading to septicaemia (Rosenstein et al., 2001). In some of these cases, the bacteria cross the blood-brain barrier which results in meningitis. Individuals who contract IMD and survive are often left with permanent disabilities including brain damage, hearing loss and sequelae arising from limb amputation.

Though only a small fraction of people who are exposed to meningococcal bacteria fall ill with the development of IMD, it is however infants and adolescents who are among those highest at risk of developing meningococcal disease. IMD results from the complex interplay of a number of factors, including the virulence of the *N. meningitidis* strain, favourable environmental and host conditions for exposure, colonization, invasion and survival (Rouphael and Stephens, 2012).

Common to all gram-negative bacteria, the cell envelope of *Neisseria meningitidis* is composed of an outer membrane, a peptidoglycan layer and a cytoplasmic inner membrane. Its outer membrane consists of lipooligosaccharides, phospholipids and porin proteins, which enable hydrophilic nutrients to diffuse into the bacterium (Rouphael and Stephens, 2012). Furthermore, invasive disease-causing *N. meningitidis* strains tend to always be encapsulated in a polysaccharide capsule, which aids bacterial survival in the blood by conferring resistance to complement-mediated killing and by inhibiting phagocytosis (Uria et al., 2008). Figure 1-1 shows a schematic diagram of a meningococcal surface with key features labelled.

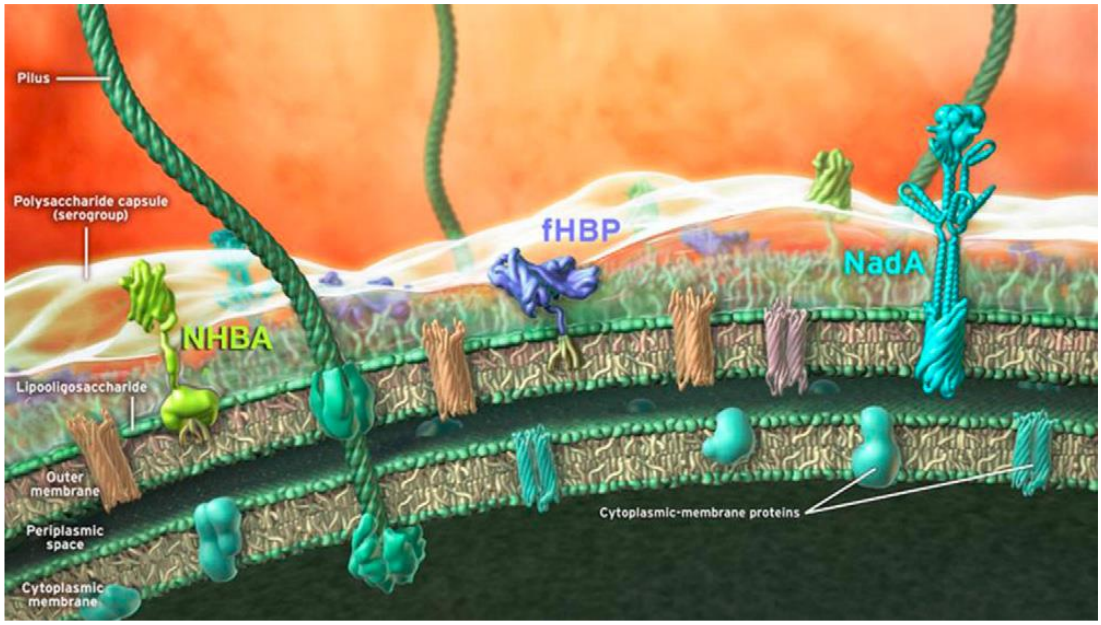

Figure 1-1 Schematic diagram of the *N. meningitidis* bacterial surface. In addition to labelled cellular components, highlighted are three significant proteins NHBA, fHBP, NadA, which are three surface-exposed protein antigens that comprise Bexsero[1], a multivalent vaccine against *N. meningitidis* serogroup B. Image taken from (Serruto et al., 2012).

Virulence of the bacterium is influenced by a range of factors, one of these being the expressed capsule polysaccharide (Stephens, 2009). *N. meningitidis* can be divided into 12 serogroups which are defined by both the immunogenicity and structure of their capsular polysaccharides, with serogroups A, B, C, W, X and Y the cause of almost IMD cases (Stephens et al., 2007).

1.1.2 The challenging path towards a vaccine for *N. meningitidis* serogroup B

Vaccines against *N. meningitidis* developed in the past targeted the capsular polysaccharide (Snape and Pollard, 2005); however, the path towards developing a polysaccharide or glycoconjugate vaccine against *N. meningitidis* belonging to serogroup B (MenB) proved to be particularly difficult. With MenB being a leading cause of IMD in both developed and developing countries, the goal remained to develop a multivalent vaccine to confer broad strain coverage against MenB. A vaccine conferring broad protection is important in not only preventing for the selection of escape variants but also for the fact that changes in serogroup circulation are unpredictable and can occur very quickly (Khatami and Pollard, 2010).

[1] Bexsero is a trademark owned by or licensed to the GSK group of companies.

Vaccine design was hampered by the fact that the polysaccharide capsule of serogroup B contains a derivative of a sialic acid homopolymer that is identical in structure to the human fetal neural cell adhesion molecule of the central nervous system (Hobb et al., 2010). This example of molecular mimicry induces low immunogenicity against serogroup B (Zimmer and Stephens, 2006). Therefore, alternate approaches investigated protein antigens as potential vaccine components. However, high intra-serogroup antigenic diversity such as that displayed by the immunodominant porin protein Porin A (PorA) created further barriers towards the development of a universal vaccine against MenB (Feavers and Pizza, 2009).

In response to epidemic situations, vaccines composed of outer membrane vesicles (OMVs) containing the immunodominant PorA as the major vaccine antigen were developed in a strain specific fashion against MenB clonal strains (Holst et al., 2009). Though enacted with some degree of success, such approaches stimulated a poor immune response in very young children and conferred a short duration of protection (Yogev and Tan, 2011). In addition, due to their strain-specific nature, these approaches did not constitute a vaccination strategy with universal coverage against MenB. For example, given the high antigenic variability of PorA, it was estimated that as many as twenty different PorA variants would be required to cover over 80% of invasive strains in the United States (Tondella et al., 2000).

1.1.3 Arriving at a MenB vaccine by reverse vaccinology

Reverse vaccinology developed in the late 1990s takes advantage of high-throughput DNA sequencing to survey the entire sequenced bacterial genome in a computer-based prediction method for the identification of potential immune-stimulating antigens (Rappuoli, 2000). This is contrary to the labour and time intensive 'classical vaccinology' approach to vaccine development, in which potential antigens are isolated individually from *in vitro* culture and identified using biochemical, immunochemical and microbiological methods.

Bexsero is the first of its kind multicomponent vaccine formulation against MenB, composed of surface-exposed meningococcal proteins originally identified by the reverse vaccinology approach (Serruto et al., 2012). Early in the development of Bexsero, reverse vaccinology was applied to mine the genome of MC58, a virulent strain of MenB (Kelly and Rappuoli, 2005). Surface-exposed proteins of MenB were identified, expressed, purified and their cellular locations determined by techniques including Enzyme-Linked Immunosorbent Assay (ELISA) and fluorescence-activated cell sorting (FACS). The Serum Bactericidal Assay (SBA), which measures

complement-mediated killing via antibody, was used to select for antigens able to elicit bactericidal antibodies and led to the identification of three proteins that went on to form the basis of the Bexsero vaccine. The final vaccine formulation consists of these three surface-exposed meningococcal proteins; Factor H binding protein (fHbp), Neisseria adhesin A (NadA) and Neisseria heparin-binding antigen (NHBA), in addition to outer membrane vesicles expressing PorA (serosubtype 1.4 from the New Zealand strain of MenB) (Serruto et al., 2012).

1.2 Next-generation subunit vaccines

1.2.1 Enhancing the immunogenicity of subunit antigen formulations

Vaccines rank amongst the most important public health interventions for combatting disease and increasing quality of life. Current vaccines that are licensed for use can be divided into three categories: live-attenuated, chemically inactivated ('killed') and subunit vaccines.

The immunising agents in attenuated vaccines are pathogens that have been modified such that they have a greatly diminished pathogenic capability but are still replication-competent. It has been generally observed that live-attenuated vaccines provide a long-term sterilising immunity whereas inactivated ('killed') pathogen vaccines induce more transient responses with a periodic requirement for boosting (Amanna et al., 2007). This can partially be attributed to the fact that live-attenuated vaccines retain pathogen-associated molecular patterns (PAMPs), which are evolutionary conserved pathogen structures recognized by the innate immune system (Maisonneuve et al., 2014; Mogensen, 2009). The innate immune can recognise these PAMPs through germ line-encoded innate microbial sensors known as Pathogen Recognition Receptors (PRRs), of which toll-like receptors (TLRs) are an example. Though attenuated vaccines have the capability to provide lifelong immunity by inducing strong humoral and cell mediated protection, they are disadvantaged in that they carry a risk of reversion to pathogenic state and are unsuitable for use in immunocompromised individuals (Noad and Roy, 2003).

Over the past few decades, vaccinology has been moving away from attenuated and inactivated vaccines and towards the rational design of subunit vaccines whose immunogenicity is focused on specific antigenic epitopes (Rappuoli et al., 2011). Though these subunit formulations have better safety profiles, the lack of microbial PAMPs renders them inherently less immunogenic and so immunostimulatory agents (adjuvants) are often needed (Moyle and Toth, 2013).

A range of adjuvants are licensed for use in vaccine formulations today, including alum (aluminium salts) which was first approved in the United States in the 1920s (Kool et al., 2012). For a long time, this was the only licensed adjuvant in the United States until the licensing of GSK's ASO4 (containing aluminium hydroxide and monophosphoryl lipid A – a TLR agonist) in 2009 (Mbow et al., 2010). Other adjuvants have been licensed for use in Europe including Novartis's MF59 (an oil-in-water emulsion consisting of squalene, Tween 80 and Span 85), GSK's ASO3 (an oil-in-water emulsion containing squalene, Tween 90 and α-Tocopherol) as well as liposome-based formulations (including GSK's AS01 adjuvant) (Mbow et al., 2010; O'Hagan and De Gregorio, 2009).

1.2.2 Nanovaccinology for the improved subunit vaccine formulations

While research is ongoing to establish new adjuvant formulations, subunit vaccine immunogenicity can also be improved through the optimization of nanoparticle-based antigen delivery systems. Nanotechnology is one field that has the potential to address the need for improved subunit antigen delivery systems. The application of therapeutic nanoparticles has undergone rapid maturation over the past two decades, yet nanoparticles in the form of liposomes have had pharmaceutical applications since at least the 1960s (Torchilin, 2005) and today a wide-range of liposome-based formulations exist on the market, including one for morphine and liposome formulations incorporating the chemotherapeutic drug doxorubicin (Bulbake et al., 2017; Burgess et al., 2010)

The application of nanotechnology in the field of vaccinology has undergone a similarly rapid increase in recent development, leading to what has been dubbed the birth of 'Nanovaccinology' (Mamo and Poland, 2012). A range of nanoparticle delivery systems are being deployed in vaccine formulations for their potential as antigen presenting systems to enhance antigen processing and as immunostimulant adjuvants to modulate the immune response. Examples of these nanoparticle platforms acting as adjuvants for the next-generation of subunit vaccines include virus-like-particles, liposomes, emulsions, and self-assembling peptides amongst others.

1.2.3 Virus-like-particles

Virus-like-particles (VLPs) are among the nanoparticle platforms that best exemplify the premise of presenting both antigen and adjuvant together in a manner that mimics the pathogen-immune cell interaction. VLPs are a class of nanoparticles formed by the self-assembly of viral capsid proteins, but they differ however to viral particles in

that they lack the viral genomic material and therefore are not susceptible to reversion (Noad and Roy, 2003).

VLPs are effective antigen presentation systems that harness the evolved viral structure which itself is optimised for interaction with host immune system and they have even been shown to induce potent immune responses in the absence of adjuvant (Zhang et al., 2000). Research by Bachmann et al demonstrated that B cells recognize through their B-cell receptors (BCRs) ordered and highly repetitive displays of antigens spaced at an optimal distance 50 – 100 Å, leading to the activation of the B cells and scaffolding of other components of the innate humoral immune system in a distinctive manner (Bachmann et al., 1993). Such ordered epitope spacing is rare among vertebrate self-antigens; therefore it can be considered as a type of PAMP that B cells have evolved to detect via engagement of the BCRs on their surfaces.

VLP-based nanoparticle vaccine formulations were first introduced as a vaccine against the Hepatitis B virus (McAleer et al., 1984; Valenzuela et al., 1982) in 1986 and since then a VLP-based vaccine against the human papillomavirus (HPV) (Bryan, 2007; Schiller and Lowy, 2012) has also been approved. Though VLPs that have been commercialised to date are based on self-assembly of target protein capsid proteins, VLPs can also act as heterologous delivery systems in which a target antigen from a virus unrelated to that of capsid is presented onto the surface of a VLP. An example of this approach being GSK's malaria vaccine, Mosquirix (RTS,S) in which the malaria antigen is delivered by a hepatitis B VLP (Cohen et al., 2010).

1.2.4 Liposomes

Liposomes are spherical self-assembled vesicles composed of a lipid bilayer enclosing an internal aqueous cavity. Figure 1-2 gives an overview of the structural features of liposomal vesicles.

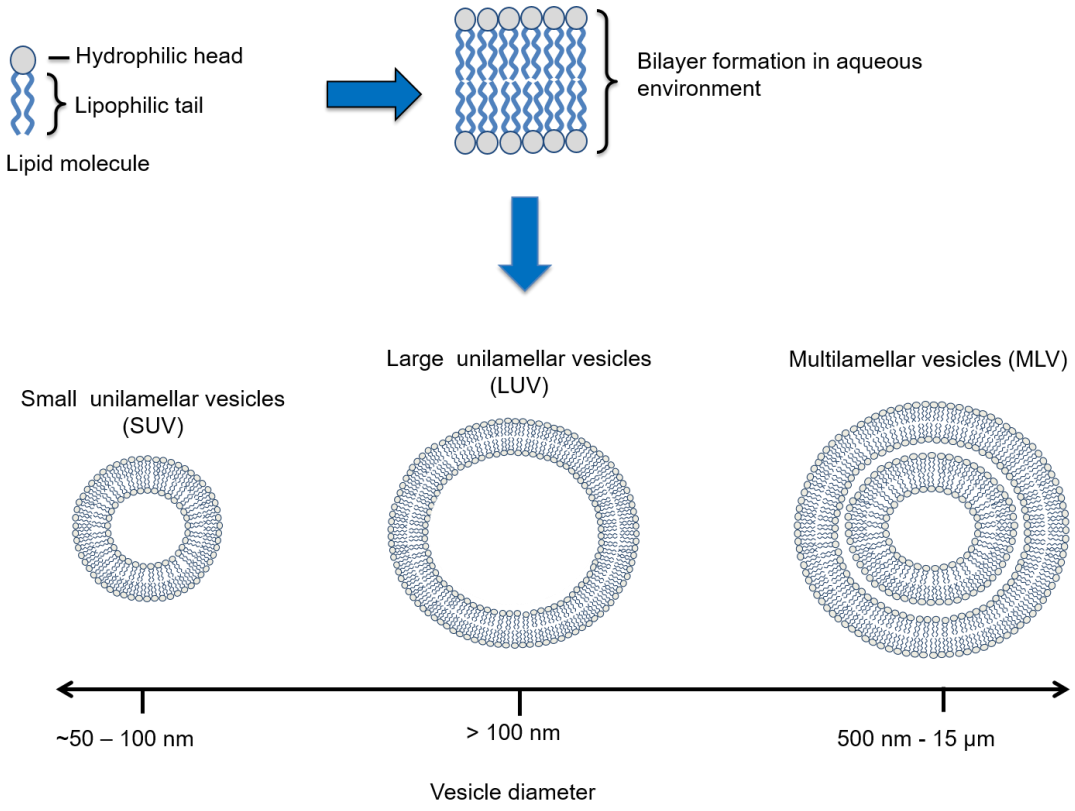

Figure 1-2 A schematic overview of liposomal vesicle structures. Liposomes can be divided into two main types – unilamellar or multilamellar – depending on the number of lipid bilayers that compose them. The larger aqueous core of unilamellar liposomes makes them suitable for the encapsulation of hydrophilic drugs, whereas multilamellar liposomes are ideal for encapsulating hydrophobic drugs (Marasini et al., 2017).

Liposomes are exploited in a variety of nanomedicine formulations. In particular, they have a number of attributes that favours their deployment in vaccine formulations as adjuvants and vehicles for antigen delivery. As well as their biocompatibility and low toxicity, they can provide a long-term controlled release of subunit antigens, protecting them from both physical and chemical degradation. Indeed, liposomes are highly versatile adjuvants whose effects can be tailored by several means, such as the choice of lipids and formulation methods, the way in which antigens are associated (e.g. surface-association or encapsulation) and addition of immunostimulators (Tandrup Schmidt et al., 2016). Moreover, through liposomal delivery, subunit antigens are thereby converted to a more particulate nature which better promotes their uptake by antigen-presenting cells (APCs) (Marasini et al., 2017)

Liposomal-adjuvanted vaccine formulations on the market include GSK's AS01-adjuvanted herpes zoster virus vaccine (Del Giudice et al., 2018) , as well as two available vaccines based on virosome formulations; the vaccines Infexal (against

influenza) and Epaxal (against hepatitis A) (Gluck et al., 2004). Virosomes are virus protein-incorporated lipid vesicles that promote both cell fusion and delivery of viral antigens (Almeida et al., 1975).

The delivery of vaccine antigens using cationic liposome formulations has been shown to be particularly effective, with uptake of positively-charged liposomes by APCs observed to be much higher than when compared to neutral or anionic liposome formulations, which is due to favourable interactions with anionic cell membranes (Foged et al., 2004; Nakanishi et al., 1997). Studies also suggest that the cationic charge is important in being able to retain the liposome formulation at the site of injection, which leads to prolonged antigen presentation to, and subsequent immunostimulation of, APCs (Henriksen-Lacey et al., 2010b; Henriksen-Lacey et al., 2011a).

One hurdle facing the translation of liposome adjuvants from bench to market is their cost-effective production (Perrie et al., 2016). One potential solution to this problem is the production of liposomes by microfluidic processes (Whitesides, 2006), with research demonstrating the applicability of microfluidics as a high-throughput technique for reproducible and controlled liposome production (Joshi et al., 2016; Kastner et al., 2015; Perrie et al., 2016).

1.3 Rationally-designed self-assembling protein nanoparticle systems

In addition to VLPs, there are also many other naturally occurring self-assembling nanoparticle systems that are capable of functioning as high density and structurally ordered antigenic arrays in vaccine formulations. A scenario has been proposed in which a presented high density and structurally ordered antigenic array results in multiple simultaneous binding events to BCRs (López-Sagaseta et al., 2016). This higher avidity binding favours the generation of potent, long-lived protection in germinal centres over the weaker avidity binding shown by monovalent soluble subunit antigens.

Figure 1-3 summarises this proposed mechanism.

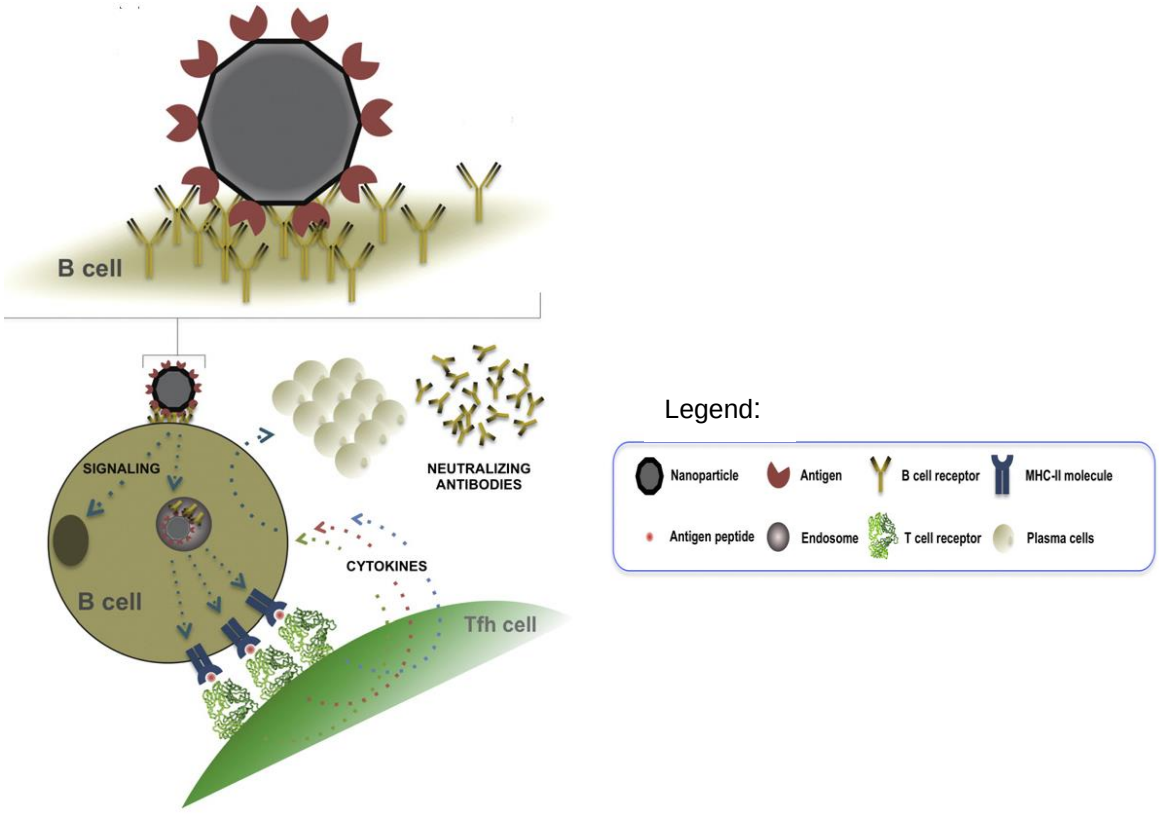

Figure 1-3 The generation of potent, long-lived immune protection in germinal centres by self-assembling nanoparticle antigenic arrays. The multivalent nanoparticle results in higher avidity binding to the BCRs, translating as tighter and prolonged bindings. There is an increase in BCR clustering for multiple and simultaneous engagement with the antigenic epitopes, which effectively traps the nanoparticle and establishes a durable and strong recognition resulting in B-cell intracellular signalling, internalization and processing of the antigen for presentation on MHC molecules to the T follicular helper cells (T_{FH}) found within the germinal centres. This new recognition interaction sees the T_{FH} secrete regulatory cytokines and leads to the differentiation of B cells into plasma cells that secrete antigen-specific antibodies. Diagram adapted from (López-Sagaseta et al., 2016).

Ferritin is a large, almost ubiquitously found protein with a mass of around 450 kDa (Truffi et al., 2016) which serves as an intracellular store of iron, with each molecule of ferritin able to store up to 4500 iron atoms (Arosio et al., 2009). High-resolution structures of ferritin from the bacteria *Helicobacter pylori* revealed that it self-assembles into stable octahedral nanoparticles of around 12 nm in diameter composed of 24 identical monomer subunits, each of which are comprised of a four-alpha-helix bundle structure (Cho et al., 2009). In animals, both light and heavy ferritin monomers instead self-assemble into 24-meric nanoparticles of solely one type or as a mixture of different heavy-light ratios (Granier et al., 2003; Lawson et al., 1991). In

terms of physiological location, ferritin is found in both extracellular and intracellular compartments including the cytosol, nucleus and mitochondria (López-Sagaseta et al., 2016).

The ferritin nanoparticle has been extensively studied and has found use in a number of *in vivo* applications including as a biodiagnostic marker (Geninatti Crich et al., 2006) and as a novel delivery and imaging platform in cancer treatment (Fan et al., 2012). Several studies have used self-assembling proteins, such as ferritin, as multivalent antigen displays in vaccine formulations (Han et al., 2014; Jardine et al., 2013; Kanekiyo et al., 2015; Malmqvist, 1993). Using recombinant DNA technology, genes encoding self-assembling polypeptides such as the ferritin monomer, can be encoded for in sequence with a desired immunogenic epitope and the chimeric nanoparticle is then expressed in a chosen expression system. In addition to their immunogenic ability towards high-quality antibody responses, these self-assembling protein antigens acting as vaccine delivery platforms have the benefits of high purity, safety and tolerability (López-Sagaseta et al., 2016).

Kanekiyo et al. rationally designed a genetic construct which encoded for the influenza hemagglutinin (HA) connected by a short amino acid linker to a *Helicobacter pylori* non-haem ferritin monomer (Kanekiyo et al., 2013), a ferritin that was found to diverge highly at sequence level to its mammalian counterpart. The HA monomer was linked via a short amino acid linker to an N-terminal aspartate residue of the ferritin monomer, as linkage at this position was rationalized to enable HA monomers to trimerize successfully on self-assembly of the ferritin nanoparticle. These chimeric ferritin-HA monomers were proven to successfully self-assemble into nanoparticle presenting eight correctly trimerized HA trimers on the nanoparticle surface in a symmetrically ordered manner. Figure 1-4 shows the overall structure of the HA-ferritin nanoparticle as well as geometrical considerations for the design of the system.

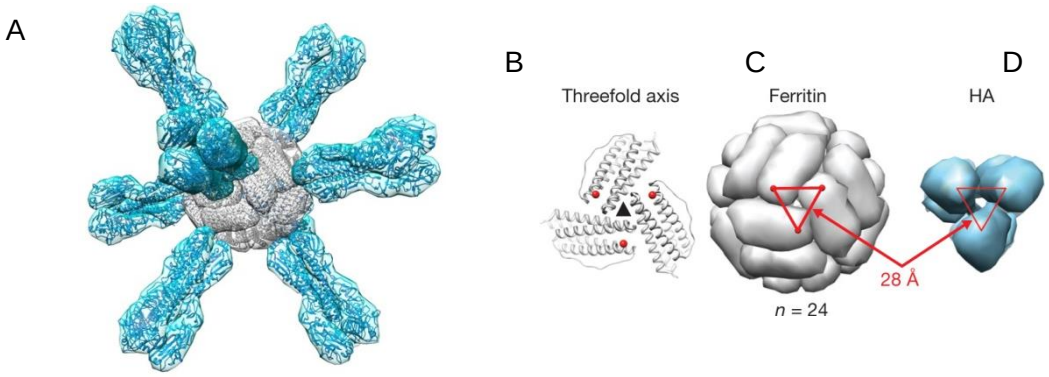

Figure 1-4 Overall structure and deign considerations of the HA-Ferritin nanoparticle A) The overall architecture of the chimeric HA-Ferritin nanoparticle with 8 spikes of the trimeric HA (in blue) presented on the *H. pylori* ferritin (grey) surface B) On the ferritin surface, a potential site for linkage of heterologous epitope is a threefold axis formed by three ferritin monomers. An N-terminal solvent exposed aspartate on each monomer is represented by a red sphere. C) A triangle connecting those three N-terminal aspartates at the threefold axis on the ferritin and D) a triangle connecting the central axis of each HA monomer in the trimer. Both these triangles show comparable side lengths of 28 Å. This geometric overlap enables successful trimerization of the HA on self-assembly of HA-Ferritin monomers into the 24-mer HA-ferritin nanoparticle. Images adapted from Kanekiyo et al., 2013 (Kanekiyo et al., 2013).

In a significant finding *in vivo*, the HA-presenting nanoparticle was able to elicit a broader and more potent immune response in mice compared to a current trivalent inactivated influenza vaccine. In addition, pre-existing anti-*H. pylori* ferritin immunity was not found to interfere with subsequent immunization using the chimeric HA-ferritin nanoparticles, with no reduction in the HA-specific antibody response seen. Furthermore, no evidence was found for the abrogation of immune tolerance and induction of autoimmunity when mice were immunized with the *H. pylori* ferritin-HA chimera.

Another study deployed a similar approach in which a truncated form of the gp350 antigen from the Epstein-Barr virus was presented in a structurally optimised orientation on the surface of either ferritin or encapsulin (Kanekiyo et al., 2015). Encapsulin is another example of a self-assembling polypeptide and forms an icosahedron made of 60 identical subunits (Sutter et al., 2008). The truncated gp350 when presented on either the ferritin or the encapsulin nanoparticles was able to elicit neutralizing antibody titres far exceeding those obtained with the soluble antigen gp350 antigen alone. As improvements in immunogenicity were only seen when the truncated gp350 was presented on the nanoparticles, it was suggested that the nanoparticle presentation conformationally stabilized the truncated antigen.

As both the ferritin and encapsulin nanoparticles were 20 – 50 nm in diameter, it was also suggested that both were likely to be trafficked in a similar manner through the lymph nodes for uptake by dendritic cells (DCs), B cells and macrophages (Irvine et al., 2013; Kanekiyo et al., 2015). In accounting for differences in immunogenicity between the two nanoparticle systems, one of the proposed reasons was that the antigen spacing (at the optimal 50 - 100 Å) on the ferritin allowed for more efficient cross linking of BCRs and therefore stimulated B-cell activation more effectively (Bachmann and Zinkernagel, 1997; Kanekiyo et al., 2015). More recently, another group also utilized the ferritin nanoparticle display system to present native-like HIV-1 envelope glycoprotein timers and reported that the chimeric ferritin nanoparticles were significantly more immunogenic than the soluble trimers when used to immunize mice and rabbits (Sliepen et al., 2015).

1.3.1 Immunological considerations of nanoparticle vaccine formulations

To generate a successful immune response against the subunit antigen, nanoparticle vaccine formulations need to interact with a range of immune cells including innate immune cells, APCs and adaptive immune effector and memory cells (Rosenthal et al., 2014). Size, charge and shape of nanoparticles are all factors that impact antigen uptake by professional APCs such as DCs and macrophages. Both these cell types specialise in the uptake and processing of antigen, therefore active research is focused on understanding the relationship between these cells and efficacious nanoparticle formulations.

Activation and maturation of DCs stimulated by antigen require not only antigen presentation but also the presence of co-stimulatory molecules which are bound by the DCs using PRRs such as TLRs (Banchereau and Steinman, 1998). Nanoparticle adjuvants, such as cationic liposomes, hold promise in their ability to efficiently target APCs, and stimulate antigen uptake while delivering co-stimulatory signals for the generation of potent immune responses (Guy, 2007). Figure 1-5 gives an overview of the interactions taking place.

Nanoparticle vaccines can be modified to include co-stimulatory molecules (PAMPs) to mimic stimulatory signals present on pathogens, thus improving the quality of the innate immune response and the subsequent adaptive response. An example of a TLR agonist used in vaccine formulations is Lipid A, an endotoxic component of Gram-negative bacteria, that has been incorporated into liposomes where it functions as a strong adjuvant and TLR-4 agonist (Steers et al., 2009). The detoxified version

of lipid A, Monophosphoryl lipid A (MPL), is also able to similarly drive PRR signalling and immune cell activation yet it lacks the associated toxicity (Elamanchili et al., 2007). MPL has been included in GSK's adjuvant AS04 (present in GSK's Cervarix vaccine against HPV (Bryan, 2007)) as well as AS01 (also GSK) which is a liposome-based formulation (Garcon and Van Mechelen, 2011).

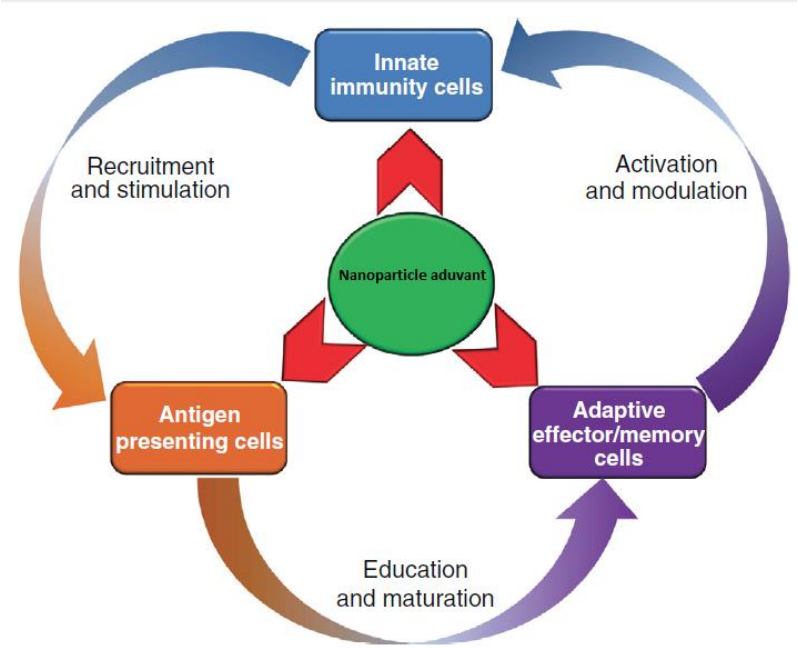

Figure 1-5 Schematic showing the various immune cells that nanoparticle adjuvants need to interact with in order to generate a successful immune response. Nanoparticle vaccine formulations can potentially act as both antigen delivery vehicles and immunostimulators to cells of the immune system including those of innate immunity, antigen presenting cells and adaptive cells. Innate immune cells, such as granulocytes, are activated at the site of vaccine administration to recruit APCs, such as dendritic cells due to the co-stimulatory signals present in the nanoparticle adjuvant. DCs can then migrate to secondary lymphoid tissue such as the lymph nodes, where they can become stimulated directly by nanoparticle adjuvants that have passively drained or been targeted to lymphoid tissue. In the lymphoid tissue, naıve adaptive cells such as T-cells, are selected for either by activated APCs presenting the antigen or direct antigen delivery by the nanoparticle adjuvant. The result is a variety of immune effector subtypes are activated that active immunity via cytokine secretion, antibody production, and cytotoxic delivery, in addition to the memory cells that mediate immunological memory. Adapted from Rosenthal et al, 2014 (Rosenthal et al., 2014).

It has been observed that nanoparticles with a comparable size to pathogens are generally more efficiently recognized and taken up by APCs; distinct APC populations may be targeted by varying nanoparticle size, with larger particles (0.5–5 um) preferentially taken up by peripheral DCs and macrophages at the injection site

whereas smaller particles (20 – 200 nm) are able to exploit circulatory access to the lymphatic system and target DCs residing in the lymph nodes (Manolova et al., 2008; Reddy et al., 2007). In addition to these observations, the mechanism of uptake has also been seen to vary according to nanoparticle size, with smaller particles taken by up primarily by receptor-mediated endocytosis and larger particles taken up by phagocytosis or macropinocytosis (Badiee et al., 2013). The correlation between nanoparticle size and the immune response generated is not quite so straightforward however, and within the literature there is currently no definition of an optimal size range for nanoparticle adjuvants (Oyewumi et al., 2010).

1.3.2 Structural Vaccinology, an emerging era of vaccine design

Advances in structural and computational techniques have increased our capacity to determine antigen structures and form the basis of a new era of vaccine development and discovery dubbed 'structural vaccinology'. The central premise of structural vaccinology is the rational structure-based design of improved vaccine antigens measured in terms of epitope presentation, stability and ease of production. The aforementioned design of self-assembling protein nanoparticles that display heterologous antigens are powerful examples of a rational structure-based approach to vaccine design.

One group deployed a structural vaccinology approach towards the design of a chimeric antigen to combat the antigenic variability of the MenB antigen fHbp and confer broad vaccine coverage (Scarselli et al., 2011). The MenB antigen fHbp (one of the constituent antigens of the Bexsero vaccine) displays high antigenic variability with hundreds of fHbp peptide sequences having been identified across MenB strains (Masignani et al., 2003). These variants are classified into three variant groups that do not display cross-protective immunity against each other. With as little as 65% sequence identity existing between the three variant groups, antigenic variability is a key barrier to overcome to confer breadth of protection.

Prior structural determination by NMR (Nuclear Magnetic Resonance) and X-ray crystallography of the fHbp variant 1.1 formed the blueprint for a fHbp scaffold onto which to graft epitopes from variants 2 and 3, whose size and location were determined by computational analyses and epitope mapping experiments. Over 50 such recombinant fHbp antigens were produced in this way. Bactericidal assays using sera from mice immunized with these recombinant antigens identified an antigen that was broadly cross protective against multiple strains of MenB. Figure 1-6 shows the final chimeric antigen obtained in this way.

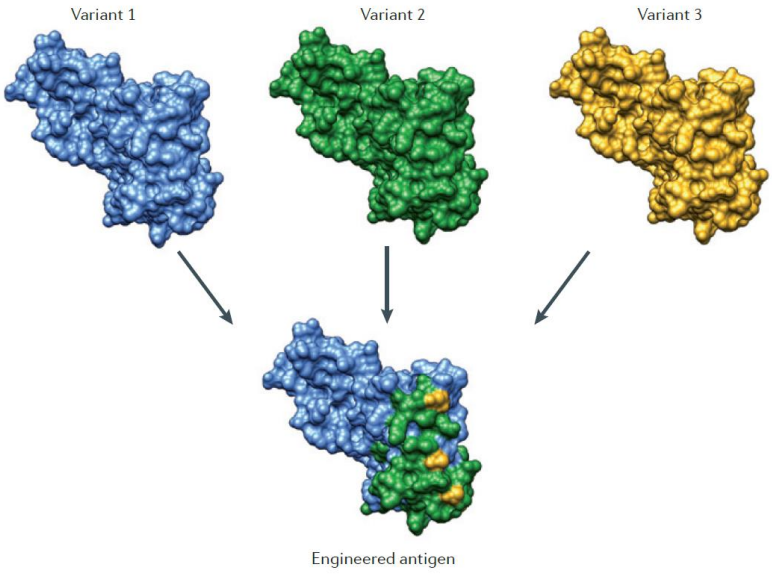

Figure 1-6 The rational structure-based design cross-protective fHbp antigen. Amino acids from the surface of variants 2 and 3 were grafted into the variant 1 structure which resulted in a chimeric antigen able to elicit immunity against all three fHbp variants. Diagram taken from (Dormitzer et al., 2012).

1.3.3 Structure-guided design of a nanoparticle presenting a chimeric MenB antigen

In this project, a structural vaccinology approach has been applied towards the rational design of a ferritin nanoparticle acting as a multivalent antigen presenting system for a chimeric protein antigen against MenB. As described previously, presentation of subunit antigens on ferritin can improve both their immunogenicity and stability. A structure-based approach guides the design of the chimeric protein MenB antigen such that it is comprised of optimally presented immunogenic epitopes derived from two MenB antigens, therefore conferring breadth of protection against MenB and simplifying the final vaccine formulation. This is also one of the first demonstrations of a self-assembling protein nanoparticle displaying a bacterial antigen rather than a viral antigen.

Epitopes from two well-characterized MenB antigens were selected to form the chimeric protein antigen. The first of these antigens was the homotrimeric autotransporter adhesin protein Neisserial adhesin A variant 3 (NadA3), which functioned as a scaffold for insertion of epitopes from the second antigen. The second antigen to contribute epitopes was the porin protein PorA.

1.3.4 NadA3 as a scaffold for the design of a chimeric MenB antigen

NadA is an outer membrane protein which belongs to the trimeric autotransporter adhesin (TAA) family, which are proteins that are known to interact with extracellular matrix proteins and play a role in invasion of target cells (Lyskowski et al., 2011). The general structure of TAAs is a conserved C-terminal integral membrane β-barrel that anchors the protein to the outer membrane connected by a coiled-coil stalk to an N-terminal domain that mediates cell adhesion.

The gene encoding NadA is present in around 50% of pathogenic MenB strains and it is found to mostly associate with three out of four of the hypervirulent MenB strains (Comanducci et al., 2004). NadA has been categorised into two main groups based on sequence homogeneity; group 1 containing the three most common variants, all of which are immunologically cross-reactive and group 2 (Comanducci et al., 2004). Group 1 contains the variant 3 (NadA3) which is present in the Bexsero vaccine as soluble recombinant NadA3 (Serruto et al., 2012).

In vitro studies in which NadA3 was expressed on the surface of *E. coli* cells showed NadA3 to play a role in promotion of adhesion and invasion of Chang epithelial cells (a human conjunctiva cell line widely used in meningococcal pathogenesis studies) (Capecchi et al., 2005). This epithelial adhesive and invasive capacity of NadA3 was initially mapped to the N-terminal globular 'head' region (Capecchi et al., 2005), before then also expanding to neighbouring dimeric coiled-coil structures in receptor interactions (Tavano et al., 2011). Evidence of NadA binding to β1 integrin and triggering an internalization signal have been reported (Nagele et al., 2011) and more recently interactions with the molecular chaperone heat shock protein 90 (Hsp90) have also been characterised, in which bacterial adhesion and invasion mediated by NadA was found to be inversely correlated to the expression of Hsp 90 by Chang epithelial cells (Montanari et al., 2012).

In addition, the presence of NadA-specific receptors on myeloid cells has been investigated in several studies, suggesting that NadA likely exerts an immune-modulatory action on those cells (Franzoso et al., 2008; Mazzon et al., 2007; Tavano et al., 2009). NadA is able to induce high titres of bactericidal antibodies (Bowe et al., 2004) and serum secretions containing antibodies against NadA were identified in convalescent children following a period of IMD, which suggests it is both expressed and immunogenic during IMD (Litt et al., 2004).

To evaluate Bexsero vaccine strain coverage, the Meningococcal Antigen Typing System (MATS) assay was developed as a useful predictor of whether a strain of

MenB would be killed by bacterial antibodies elicited by the Bexsero vaccine (Donnelly et al., 2010). However, when this assay is performed, the estimated coverage from the NadA3 antigen (in relation to the other present vaccine antigens) appears to be very low (Fagnocchi et al., 2013). Under the *in vitro* growth conditions used in the MATS assay, the transcriptional regulator NadR (the major mediator of phase-variable expression of NadA in MenB), maximally represses NadA expression (Fagnocchi et al., 2013; Metruccio et al., 2009). The possibility therefore that the contribution to vaccine coverage by NadA is underestimated due to the *in vitro* conditions used in MATS assay calculation was investigated. Interestingly, human saliva was reported to induce NadA expression to a level comparable to that as achieved by a known alleviator of NadR mediated repression, therefore suggesting that signals present in the oropharyngeal niche of meningococcal colonization are capable of inducing expression of NadA (Fagnocchi et al., 2013; Fagnocchi et al., 2012). Considering this observation, the study concluded that NadA expression levels *in vivo* and during infection are highly immunogenic and that all strains with NadA present may be susceptible to bacterial antibodies elicited by the Bexsero vaccine.

In 2014, an X-ray crystallographic structure of an ectodomain fragment of the variant 5 of NadA (NadA5) as well as a transmission electron microscopy (TEM) analysis of NadA3 was presented (Malito et al., 2014). While both these variants are found to share 46% to 50% sequence identity, they are not immunologically cross-reactive. (Bambini et al., 2014). The crystal structure of the NadA5 homotrimer (Figure 1-7) revealed an almost exclusively coiled-coil architecture, with an N-terminal head domain 40 Å in diameter in which each monomer adopts a novel wing-like fold.

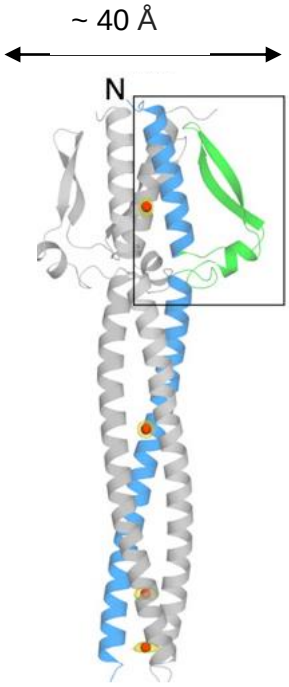

Figure 1-7 Crystal structure of a truncated version of the trimeric NadA variant 5 (NadA5) obtained at 2 Å resolution. The stalk of one monomer is highlighted in blue and the wing-like protrusion for the same monomer is in green. 'N' at the top of the head region is for the N-terminus. Adapted from (Malito et al., 2014).

Epitope mapping experiments for NadA3 in the form of peptide scanning and Hydrogen-Deuterium Exchange Mass Spectrometry (HDX-MS) could map a protective conformational epitope that has contributions from residues deriving from the solvent exposed wing-like protrusions as well from the coiled-coil within the N-terminal head domain. In accounting for the lack of immune-cross reactivity between the two groups of NadA variants, differences in stalk lengths and shifted heptad periodicity in the coiled-coil, as well as areas of low to moderate sequence variability in parts of N-terminal head were suggested as reasons for differences in antibody binding.

Other studies using a phage display-based strategy, PROFILER (Phage-based Representation of Immuno-Ligand Epitope Repertoire), showed that immunization with Bexsero induces antibodies directed predominantly against the N-terminal head region (Domina et al., 2014). A later study using the same technology also identified an antibody which recognizes a conformational epitope in the C-terminal portion of the stalk (Cariccio et al., 2016).

Though initially NadA3 proved to be recalcitrant to crystallization, due mainly to its predicted highly extended and flexible structure, a crystal structure for a less flexible

N-terminal fragment was finally solved (Figure 1-8) (Liguori et al., 2018). In the same paper DSC and SEC-MALLS analyses first defined an N-terminal NadA3 fragment comprising residues 24–170, deemed as NadA3 (24-170), as the minimum region able to exhibit stable trimerization and was taken through for crystallisation trials. The solved structure revealed a continuous 160 Å-long coiled-coil stalk that extended from the head down through to the C-terminus. Though the 3D structures of the NadA5 and NadA3 N-terminal head regions were found to be similar, the structure of the coiled-coil stalk however revealed larger differences, namely in the discovery of two unexpected, highly unusual 11-residue (undecad) coiled-coil repeats, deviating from the canonical 7-residue heptad repeat pattern. In a heptad repeat, the seven residues are accommodated in two helical turns with respect to the coiled-coil axis whereas three helical turns are needed to in the case of the undecad repeat (Parry and Squire, 2017). Though the authors cite that the overall structural roles of these undercards in coiled-coil proteins are poorly understood, it is likely that disruptions of these contributed towards the poor stability of the shorter NadA3 constructs that were recalcitrant to crystallisation.

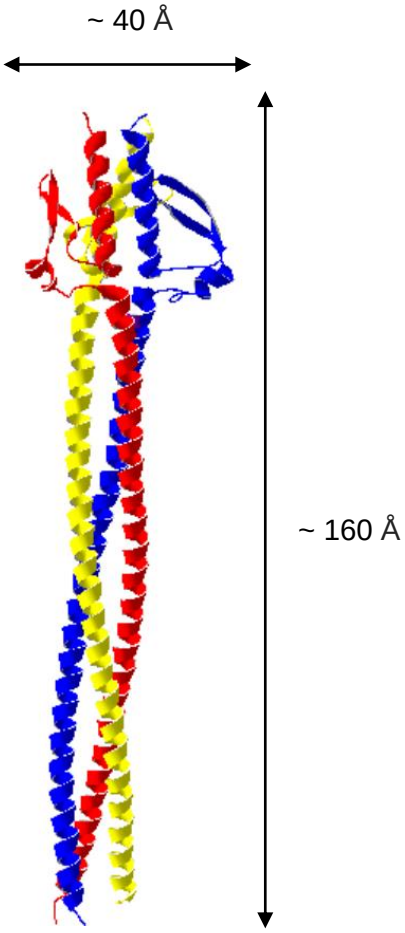

Figure 1-8 Model of the crystal structure of the trimeric NadA3 (24-170) created from PDB ID 6EUN ((Berman et al., 2000; Liguori et al., 2018)) using SwissPdb Viewer (Guex and Peitsch, 1997). Each of the three monomers comprising the trimer are color coded individually.

Another study characterised anti-NadA3 human monoclonal antibodies raised by immunisation with Bexsero and found that only those targeting the N-terminal head domain are capable of inhibiting binding to Chang epithelial cells, thus confirming location of the cell binding domain while also demonstrating these antibodies can also prevent initial bacterial colonization as well as promote killing of meningococcal strains (Giuliani et al., 2018). These structural elucidation and epitope mapping experiments of the NadA3 antigen allowed for an improved understanding of its immunogenicity and opened up the possibility of structure-guided approach towards the design of the chimeric NadA3-PorA antigen.

1.3.5 Identification of a PorA epitope for insertion into NadA3

The second selected antigen from which epitopes will be derived from is the porin protein PorA, which is one of the major immunogenic proteins expressed in the outer membrane of MenB. PorA is cation selective, enabling hydrophilic nutrients to diffuse

into the bacterium (Tommassen et al., 1990) and displays phase-variable expression (random on/off switching) which plays a role in facilitating escape from bactericidal antibodies (Tauseef et al., 2013; van der Ende et al., 1995). Most *N. meningitidis* strains are found to express PorA, though occasionally there are reports of IMD-causing strains lacking PorA (van der Ende et al., 2003). Other roles for PorA include binding to the C4B-binding protein (the major inhibitor of the classical complement pathway) with strains expressing PorA found to be more resistant to serum bactericidal assay killing as a result (Jarva et al., 2005).

PorA itself is trimeric, each of the monomers having a mass of 35 kDa with high β-pleated sheet content, conferring a predicted β-pleated-barrel structural motif with 8 extra membranous loops (Derrick et al., 1999). As mentioned previously, the high intra-serogroup antigenic diversity displayed by PorA was one barrier to a universal vaccine design. Extra membranous loops I and IV, known as variable regions 1 (VR1) and 2 (VR2) respectively, display high nucleotide sequence diversity and so are used for strain typing (Russell et al., 2004). Crucially with regards to vaccine design, VR2 is highly immunogenic, eliciting bactericidal antibodies in humans (Findlow et al., 2005).

Based on this, a PorA VR2 epitope was selected for the chimeric NadA3-PorA antigen generation. The chosen PorA VR2 serosubtype, VR2 14, was amongst the most represented in a subset of MenB strains that were SBA negative in the presence of sera from adolescents vaccinated with Bexsero. Figure 1-9 shows the VR2 serosubtype distribution among SBA negative MenB strains.

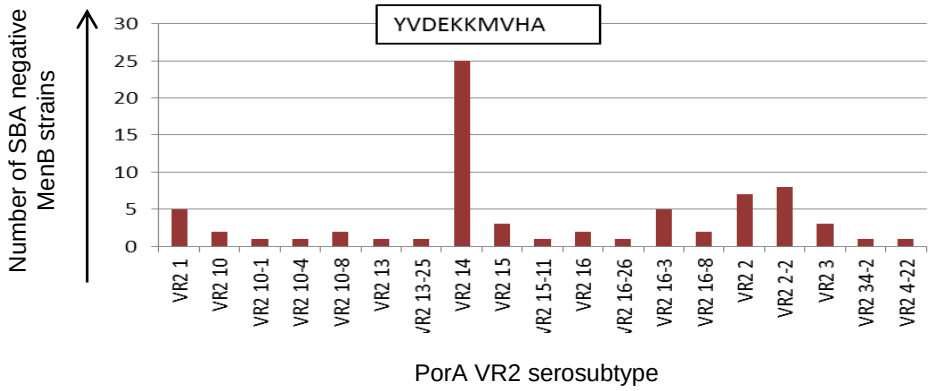

Figure 1-9 The distribution of PorA VR2 serosubtypes from MenB strains that were SBA negative in presence of sera from Bexsero vaccinated adolescents. Along the x-axis are the PorA VR2 serosubtypes. The number of SBA negative strains in which a particular serosubtype is present is displayed on the y-axis. VR2 14 was amongst the most represented serosubtypes in this panel of SBA negative MenB strains. The corresponding amino acid sequence for VR2 14 is shown boxed above the chart.

PorA is an integral membrane protein that is present in OMVs that are included in the Bexsero vaccine. However, the manufacture of these OMVs is complex and subject to regulatory issues (Ulmer et al., 2006). The potential therefore to generate a potent immune response against immunodominant epitopes from an integral membrane protein such as PorA by integrating such epitopes into a soluble protein antigen scaffold i.e. NadA3, would greatly simplify the vaccine formulation. The conformation of the VR2 epitope appears to be a particularly important consideration when attempting to optimally present this epitope; one study in which a PorA VR2 epitope was fixed into its cyclised conformation, mimicking its biological β-turn structure, by conjugating it to a carrier protein was found to induce high bactericidal titres in the SBA (Oomen et al., 2005). Conversely, the linear peptide epitope was not able to elicit bactericidal titres.

1.3.6 Design of the NadA3-PorA-Ferritin nanoparticle

In designing a chimeric antigen, it was envisioned that the known crystal structure of the NadA3 (24-170) domain could be used as a scaffold for the insertion of the PorA VR2 epitope. Using Swiss PDB protein modelling software (Guex and Peitsch, 1997), a stable trimer was modelled in which 32 residues from the NadA3 N-terminal protruding wing motif were removed and the 10 residue-long PorA VR2 14 epitope was inserted into the NadA3 structure, as described in Figure 1-10.

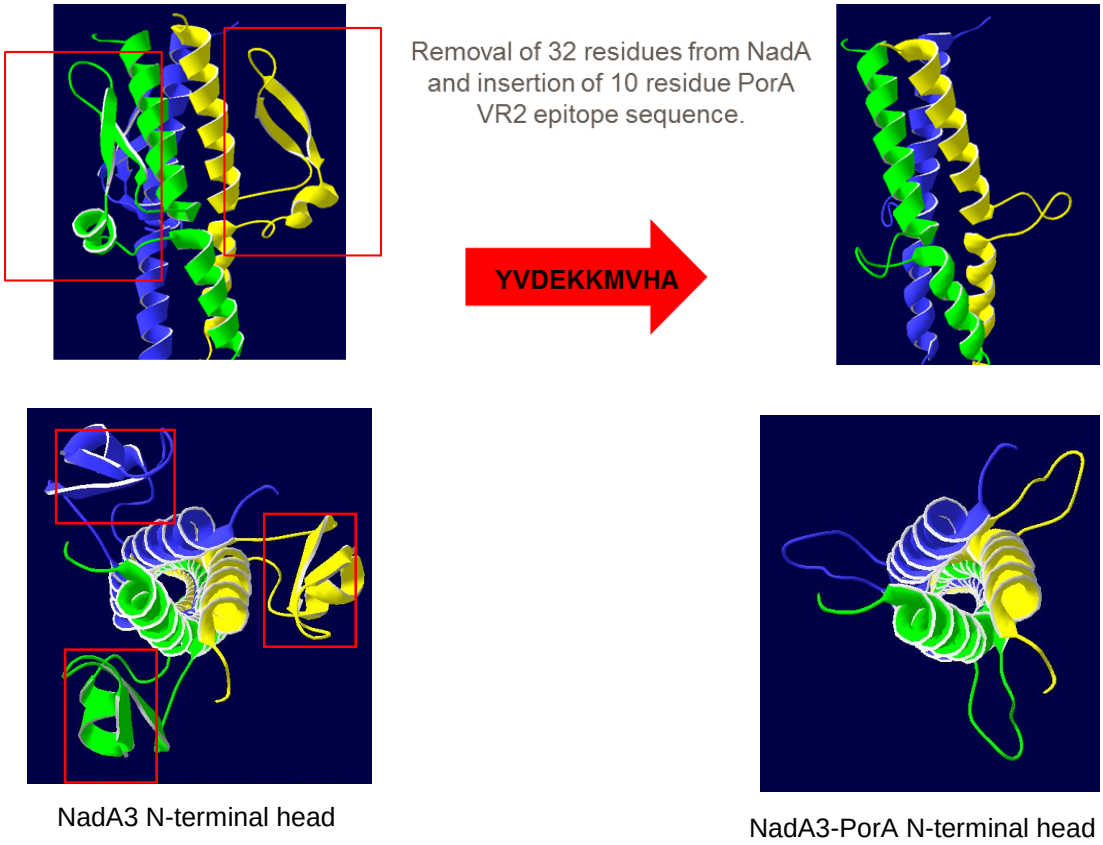

Figure 1-10 Design of the NadA3-PorA chimeric antigen using the NadA3 (24-170) crystal structure as a scaffold. Images on the left show the N-terminal head region looking from the side (upper image) and looking down from the N-terminus (lower image). Images on the right show the corresponding NadA3-PorA chimeric antigen structure following removal of 32 residues from each monomer (boxed in red) and insertion of the 10 residue PorA VR2 14 epitope (shown by the red arrow).

With the structure of the trimeric NadA3-PorA modelled, a DNA sequence was designed that encodes for the NadA3-PorA in sequence with the ferritin. This DNA sequence encodes for a monomer NadA3-PorA linked to the ferritin by a short, flexible glycine and serine rich peptide linker of 4 amino acids. The length of linker sequence was rationally designed such that on self-assembly of the ferritin nanoparticle there would be correct trimerisation of the NadA3-PorA domains. Past work already performed in our lab using a wild type NadA3-Ferritin construct harbouring this linker was shown to enable correct trimerization of the NadA3 on self-assembly of the nanoparticle when expressed in *E. coli*. The NadA-PorA-Ferritin monomer amino acid sequence is detailed in Figure 1-11.

On expression in *E. coli*, 24 of these monomers self-assemble into a ferritin nanoparticle with eight spikes of the NadA-PorA symmetrically displayed on its surface as shown in Figure 1-12.

NadA3(24-170) - Ferritin:

MGSSHHHHHHENLYFQGATNDDDVKKAATVAIAAAYNNGQEINGFKAGETIYDIDEDGTITKKD
ATAADVEADDFKGLGLKKVVTNLTKTVNENKQNVDAKVKAAESEIEKLTTKLADTDAALADTDA
ALDATTNALNKLGENITTFAEETKTNIVKIDEKLEA**SGGS**DIIKLLNEQVNKEMNSSNLYMSMS
SWCYTHSLDGAGLFLFDHAAEEYEHAKKLIVFLNENNVPVQLTSISAPEHKFEGLTQIFQKAYE
HEQHISESINNIVDHAIKSKDHATFNFLQWYVAEQHEEEVLFKDILDKIELIGNENHGLYLADQ
YVKGIAKSRKS

NadA3(24-170) PorA Ferritin:

MGSSHHHHHHENLYFQGATNDDDVKKAATVAIAAAYNNGQEING**YVDEKKMVHA**GLGLKKVVTN
LTKTVNENKQNVDAKVKAAESEIEKLTTKLADTDAALADTDAALDATTNALNKLGENITTFAEE
TKTNIVKIDEKLEA**SGGS**DIIKLLNEQVNKEMNSSNLYMSMSSWCYTHSLDGAGLFLFDHAAEE
YEHAKKLIVFLNENNVPVQLTSISAPEHKFEGLTQIFQKAYEHEQHISESINNIVDHAIKSKDH
ATFNFLQWYVAEQHEEEVLFKDILDKIELIGNENHGLYLADQYVKGIAKSRKS

Figure 1-11 Amino acid sequences of NadA3 (24-170)–Ferritin and NadA3 (24-170) -PorA-Ferritin. Residues from NadA3 are in purple, those underlined in purple represent residues to be removed for PorA insertion. Ferritin residues are green, the PorA VR2 14 epitope residues are **red** and the four amino acid linker is orange. For purification purposes, a 6XHis tag is required (along with its accompanying restriction sequences) and is shown in light blue.

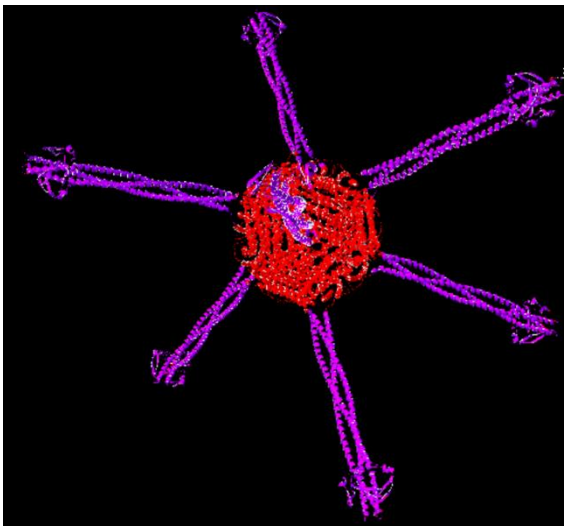

Figure 1-12 The NadA3 (24-170)-PorA-Ferritin nanoparticle modelled using SwissPdb Viewer (Guex and Peitsch, 1997). The ferritin at the centre is shown in red and the NadA3-PorA trimers on the surface are in purple.

During the initial cloning work, two different NadA3-PorA-Ferritin constructs were cloned and transformed into *E. coli*; one using the aforementioned NadA3 (24-170) and another using a longer length NadA3 with the entirety of the stalk (residues 24 – 342). However, attention was focused on the shorter length construct as the shorter stalk was envisioned to create less flexibility problems.

From this point on, any references to the NadA3-PorA-Ferritin nanoparticle refer to the construct with the NadA3 (24-170) as a scaffold unless explicitly stated.

1.4 Structural analysis of vaccine antigens by electron microscopy

Following expression and purification of the NadA3-PorA-Ferritin recombinant nanoparticle, epitope presentation will then be investigated using a variety of biochemical and structural techniques prior to initiating an *in vivo* study. The use of transmission electron microscopy will be able to provide information on the assembly of the nanoparticle, how epitopes are presented and potentially an atomic-level resolution understanding of the NadA3-PorA-Ferritin nanoparticle.

1.4.1 Negative stain Transmission Electron Microscopy

Transmission Electron Microscopy (TEM) continues to be an important technique for studying the structure of biological molecules. In TEM, electrons are transmitted through a sample such that they are absorbed and scattered, before being focused onto an electron detector (Egerton et al., 2004). This adsorption and scattering produces contrast, which is recorded in the resulting TEM image, known as a micrograph. These micrographs depict 2D projections of the sample in which each point represents the sum of the electron density of the 3D object perpendicular to that point on the plane (Belnap, 2015). The wavelength of the electron beam is 100,000 fold shorter than that of visible light, which allows TEM to study biological molecules with atomic-level resolution (Winey et al., 2014).

TEM of biological samples may pose some problems, such as susceptibility to radiation damage induced by the electron beam which breaks chemical bonds and creates free radicals, causing further secondary damage. The column of the microscope though which the electron beam is transmitted is held under a vacuum, which prevents the beam from undergoing coherence degradation due to interactions with gas molecules. Furthermore, dehydration within the vacuum of the microscope requires that samples are also solid and the sample must be suitably thin to avoid image degradation arising from multiple electron elastic and inelastic collisions (Ohi et al., 2004). The inherently poor electron scattering capacity of atoms found within biological material can be overcome by embedding the sample in a layer of dried heavy metal solution, a technique known as negative stain TEM. The improved scattering offered by these heavy metal atoms enables the generation of a functional

electron miscopy image, due primarily to the differential scattering between the surrounding heavy metal layer and the biological sample.

A variety of heavy metal stains are available, with uranyl or tungstate based stains being particularly common. Conventional negative staining sees the biological material absorbed to a glow-discharged (a process which renders the grid hydrophilic) carbon-coated copper or nickel grid followed by application of staining solution before being left to air-dry. Though addition of stain does protect against sample dehydration, embedded particles can undergo various degrees of flattening deformation and the stain application may not be heterogeneous (see Figure 1-13).

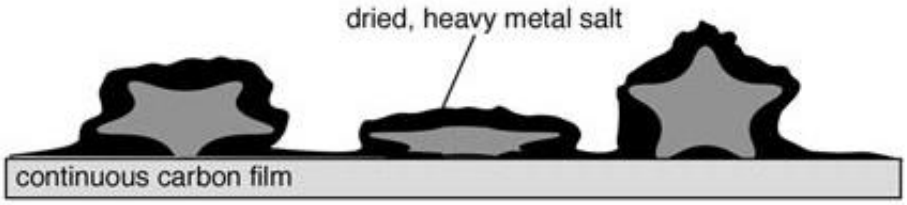

Figure 1-13 Schematic diagram showing macromolecules adsorbed onto the carbon substrate and embedded in the negative stain. The staining does not penetrate the samples, essentially forming a cast instead of the specimen surface at the expense of internal structure information. Artefacts such as sample flattening can also be introduced as depicted in the figure. Image adapted from (Belnap, 2015).

The electron micrographs obtained tend to have a high signal-to-noise ratio and the images obtained are only 2D projections of the desired molecule. To overcome these issues, computational averaging techniques and single-particle analysis are deployed, in which different views of freestanding particles are picked, classified into homologous groups and then combined to yield a 3D reconstruction of the molecule of interest.

A limitation of this technique is that only surface features and internal cavities penetrated by the stain can be depicted, with only partial internal structure revealed. In addition, heavy metal microsalt formation on drying sets a limit of resolution to about 20 Å (Ohi et al., 2004). Another problem is adsorption of the sample to the support in a limited number of preferred orientations, which can lead to loss of information.

1.4.2 Atomic-level resolution by Cryo-EM

Though negative stain TEM is quick and relatively easy to perform, it is however limited by the achievable resolution and lack of internal structural information. Such problems were circumvented by the advent of cryo-EM which preserves the native environment while also reducing the effects of radiation-induced damage in a stain-free approach.

Cryo-EM has been in development as a technique since the 1970s, however recent advances in electron detectors, image processing and software algorithms have seen great strides made in the field of single particle cryo-EM towards reaching atomic-level resolution protein structures (Thompson et al., 2016).

During cryo-EM sample preparation, the sample is vitrified at an extremely rapid rate of freezing of 10^6 °C/s by plunging the sample into a cryogen such as liquid ethane surrounded by liquid nitrogen (Dubochet et al., 1988). This fixes the water in a non-crystalline solid state, known as amorphous or vitreous ice. The sample is then imaged while maintaining liquid nitrogen temperatures, a temperature which has been shown to reduce radiation-induced damage by six-fold compared to ambient temperatures (Dubochet et al., 1988). What this therefore means is that higher electron doses can be used to obtain a higher signal-to-noise ratio while sustaining a lower amount of radiation damage.

Of the hardware advances that contributed to the cryo-EM advances in the past decade, the improvement in electron detectors is one of high importance. Direct electron-detectors (DEDs) cameras represent a significant technological leap from charge-coupled device cameras and film. A key development hurdle overcome was a way to minimize the radiation damage to the DED's silicon chip; this resulted in an increase in the practical chip lifespans measured by numbers of exposures (Nogales, 2016). The use of these DEDs results in images that have high contrast and fast read-outs, with the later feature allowing for a 'movie-mode' that effectively compensates for beam-induced motion of the sample grid (Campbell et al., 2012). High-quality data collection is now a more efficient process and high-resolution structural determination from smaller data sets is now possible. In addition, smaller proteins than ever before also stand a better chance of having their structures solved at atomic-level resolutions (Bai et al., 2013).

Alongside this requirement for fewer particles to build a high-resolution image, improvements in data processing have also played an important role in shortening the structure elucidation process. During the single particle reconstruction process,

thousands of particles must be extracted, classified into their relative 2D orientations and combined to generate the desired 3D structure. Software packages such as RELION (for REgularized LIkelihood OptimizatioN) have been enormously successful in enabling the classification of particle projections into structurally homogenous datasets (Scheres, 2012). These software advances allow for improved classification of heterogeneous samples, allowing for identification of various conformational states (Fernandez et al., 2013).

The advances made in recent years have enabled cryo-EM to become a practical alternative to X-ray crystallography. This is especially exciting with regards to systems that have proven resistant to structural determination by X-ray crystallography; integral membrane proteins, biological polymers such as microtubules and also large molecular assemblies which are only able to be produced and reconstituted in small quantities (He et al., 2013). Future technical advancements in the field will continue with improved electron detectors, reproducible cryo-EM sample preparation methods, phase-plate technology and software that can handle continuous forms of structural variation (Nogales, 2016).

1.5 Aim and objectives

Modern vaccinology faces the challenge of developing improved subunit antigen vaccines that demonstrate enhanced immunogenicity, broad protective immunity and ease of formulation. The aim of this project was to employ a rational structure-based design approach toward the design of a chimeric antigen presented on the surface of a self-assembling protein nanoparticle. The hypothesis is that the chimeric antigen incorporating epitopes from heterologous antigens confers broader strain coverage and the presentation of this subunit antigen in a multivalent fashion on the surface of ferritin can enhance the immune response directed against the subunit antigen.

The objectives of this thesis were:

1. The cloning into a suitable vector from which to express the NadA3-PorA-Ferritin in *E. coli* and its subsequent purification. The acquisition of further control protein antigens in a similar manner to enable comprehensive characterisation of the nanoparticle system.

2. Investigation of the NadA3-PorA-Ferritin epitope presentation through a variety of structural, biochemical and immune-based techniques including, but not limited to; cryo-EM, SPR, and SBA.

3. *In vivo* experiments to assess the efficacy of the NadA3-PorA-Ferritin as a vaccine system. An investigation of the central hypothesis that presentation of the chimeric antigen on ferritin results in enhanced immunogenicity compared to administration of the chimeric subunit antigen alone, and that the chimeric antigen confers broad strain coverage against MenB.
4. The microfluidic production of a cationic liposome adjuvant formulation for the delivery of the NadA3-PorA-Ferritin nanoparticle and an *in vivo* assessment of its immunogenicity.

2. Chapter 2

Purification and epitope characterisation of a rationally-designed nanoparticle antigen

2.1 Introduction

Modern vaccinology faces the challenge of developing improved subunit antigen vaccines that demonstrate improved immunogenicity, broad protective immunity and ease of formulation. In this project, a nanoparticle-based structural vaccinology approach has been investigated toward the development of an improved vaccine antigen against MenB.

In the introduction chapter, the applicability of self-assembling protein nanoparticle systems as subunit antigen presenting systems in vaccine formulations was discussed. Previous studies (Kanekiyo et al., 2015; Sliepen et al., 2015) have made use of ferritin as a scaffold for the display of heterologous vaccine antigens. One such study was that of Kenekiyo et al (Kanekiyo et al., 2013), who engineered a system in which a ferritin nanoparticle was used as a scaffold for the surface-display of multiple copies of the trimeric influenza HA antigen. Display of the subunit antigen HA in this multi-copy format could induce a more potent immune response compared to administration of the subunit antigen alone.

In this study, an approach that combines elements of structural vaccinology and nanovaccinology has been used towards the design of a ferritin nanoparticle that displays a chimeric protein antigen comprising immunogenic epitopes from two MenB antigens. The chimeric antigen incorporates epitopes from two MenB surface exposed antigens found in the Bexsero vaccine against MenB; these antigenic proteins are the NadA3 protein and the Porin protein PorA (Serruto et al., 2012).

The chimeric NadA3-PorA antigen was designed by an *in silico* design process, in which the PorA VR2 14 loop epitope was inserted into the NadA3 (24-170) homotrimer crystal structure. Flexible amino acid linkers linking the NadA3-PorA chimeric antigen to trimeric interfaces on the ferritin surface were then designed to enable correct trimerisation of the chimeric antigen on self-assembly of the nanoparticle. This *in silico* modelling work yielded the starting material for this study, the amino acid sequence of the NadA3-PorA-Ferritin monomer.

This chapter begins with the cloning work to obtain the DNA construct that will encode for the NadA3-PorA-Ferritin monomer. The monomer is then expressed in *E. coli*, where it combines with 23 other NadA3-PorA-Ferritin monomers to assemble into the NadA3-PorA-Ferritin nanoparticle, which then must be purified. Once the purified nanoparticle is obtained, a variety of structural analyses and antibody-based assays are undertaken to examine the epitope presentation on the nanoparticle.

2.1.1. Aim and objectives

The main aim of the work presented in this chapter was validation of the structural vaccinology approach toward antigen design, showing that high resolution structural data can be harnessed to design an improved vaccine antigen that can be stably expressed and that optimally presents immunogenic epitopes.

To achieve this, the objectives were:

1. The cloning, expression and purification of the NadA3-PorA-Ferritin system.
2. The structural characterisation of NadA3-PorA-Ferritin by electron microscopy, in accordance with the structural vaccinology premise that seeks high resolution structural data to guide the rational design of improved vaccine antigens.
3. Further characterisation of epitope presentation on the NadA3-PorA-Ferritin using biochemical-based techniques.

2.2 Materials and methods

2.2.1 Materials

Reagents	Supplier
10X CutSmart buffer	New England Biolabs, Ipswich, MA
10X NEB buffer 3.1	New England Biolabs, Ipswich, MA
Agarose	Sigma, Dorset, UK, Dorset, UK
Amicon Centrifugal Filter Unit	Merckmillipore, Darmstadt, Germany
Ampicilin	In-house GSK, Siena, IT
Ampicilin-Agar plate	In-house GSK, Siena, IT
Anti -Mouse IgG Antibody solution	Sigma, Dorset, UK
Pierce BCA Protein Assay Kit	ThermoFisher, Waltham, MA
BgII restriction enzyme	New England Biolabs, Ipswich, MA
Bio-rad Protein Assay Dye	Bio-rad, Watford, UK
BL21(DE3) competent cells	New England Biolabs, Ipswich, MA
B-PER reagent	ThermoFisher, Waltham, MA
CelLytic express	Sigma, Dorset, UK
CM-5 sensor chip and mouse Antibody Capture Kit	GE Healthcare, Chicago, US
Complete EDTA-free DNase	Sigma, Dorset, UK
Copper/Nickel 300-square mesh grid of carbon/formvar	Agar Scientific, Essex, UK
DNA Primers	Sigma, Dorset, UK
DPN1 restriction enzyme	New England Biolabs, Ipswich, MA
DNase	Sigma, Dorset, UK
DPN1 restriction enzyme	New England Biolabs, Ipswich, MA
FastRuler high range DNA ladder	ThermoFisher, Waltham, MA
FastRuler middle range DNA ladder	ThermoFisher, Waltham, MA
Gel loading buffer	In-house GSK, Siena, IT
GeneRuler 1 Kb DNA ladder	ThermoFisher, Waltham, MA

Glycerol	Sigma, Dorset, UK
GoTaq Green Master Mix	ThermoFisher, Waltham, MA
HBS-P+ buffer	GE Healthcare, Chicago, US
His GraviTrap column	GE Healthcare, Chicago, US
HiTrap Talcon Crude 5 mL	GE Healthcare, Chicago, US
HK100 competent cells	Sigma, Dorset, UK
HTMC	In-house GSK, Siena, IT
Imidazole	Sigma, Dorset, UK
IPTG (isopropyl β-D-thiogalactoside)	In-house GSK, Siena, IT
KAPA mix	Sigma, Dorset, UK
LBPTK media	In-house GSK, Siena, IT
Mach1 competent cells	Sigma, Dorset, UK
MES running buffer	ThermoFisher, Waltham, MA
Millex 0.22 µM filter	Sigma, Dorset, UK
MilliQ Water	In-house GSK, Siena, IT
Nickel carbon/formvar grids	Agar Scientific, Essex, UK
Novex Sharp standard Marker	Sigma, Dorset, UK
NuPAGE LDS Sample buffer 4x	ThermoFisher, Waltham, MA
NuPAGE sample reducing agent 10x	ThermoFisher, Waltham, MA
NuPAGE Novex Bis-Tris 4-12 % gels	ThermoFisher, Waltham, MA
Omega E.Z N.A. HP Plasmid DNA mini kit II	Omega Bio-tek, Norcross, GA
Omega E.Z N.A. Plasmid DNA Midi kit	Omega Bio-tek, Norcross, GA
PBS	In-house GSK, Siena, IT
PBS-BSA (1%)	In-house GSK, Siena, IT
pET-TEV-NadAv3 24-170-4aa linker-Ferritin 5-167	In-house GSK, Siena, IT
pET-TEV-NadAv3 24-342-6aa linker-Ferritin 5-167	In-house GSK, Siena, IT
Quantifoil R1.2/1.3 grids	Electron Microscopy Sciences
SeeBlue Plus2 marker	Sigma, Dorset, UK
Sensor chip NTA	GE Healthcare, Chicago, US
SimplyBlue SafeStain	ThermoFisher, Waltham, MA
SOC media	In-house GSK, Siena, IT
Sodium chloride	Sigma, Dorset, UK
Sodium phosphate	Sigma, Dorset, UK

SuperSignal West Pico PLUS Chemiluminescent Substrate	ThermoFisher, Waltham, MA
SYBR SAFE	ThermoFisher, Waltham, MA
TCA	Sigma, Dorset, UK
Ultracel 100 kDa ultrafiltration disc	Sigma, Dorset, UK
Uranyl acetate	In-house GSK, Siena, IT
Uranyless stain	Electron Microscopy Sciences
Whatman filter Paper No.1	Sigma, Dorset, UK

2.2.2 Cloning to obtain a NadA3-PorA-Ferritin expression plasmid vector

Plasmid DNA minipreps (from in-house banked cells) were performed to obtain DNA templates encoding NadA3(24-170)-Ferritin (with a 6XHis tag at the N- terminus) in a pET-15b expression vector. Primers were designed to enable insertion of the PorA VR2 loop sequence into these DNA templates using the polymerase incomplete primer extension (PIPE) cloning method (Klock and Lesley, 2009). PCR reaction conditions (including primer annealing temperatures and starting template DNA concentration) were screened to enable selection for optimum conditions. The successful PCR reactions were digested using DPN1 (Neb) to remove methylated template DNA, leaving just PCR product. DNA sequences were then transformed into competent HK100 and MACH1 *E. coli*. Colony PCR screening was then performed using screening primers to identify colonies that had been successfully transformed with the NadA3-PorA-Ferritin plasmid DNA. Plasmid DNA was then extracted and was transformed into *E. coli* BL21 (DE3) cells suitable for protein expression. Plasmid DNA was extracted by midi prep (Omega E.Z N.A. Plasmid DNA Midi kit) from the BL21 cells and then sequenced by Sanger sequencing to confirm presence of the pET-15b expression plasmid encoding the NadA3-PorA-Ferritin.

2.2.3 Overexpression and purification of NadA3-PorA-Ferritin

E. coli BL21 (DE3) cells transformed with the NadA3-PorA-Ferritin pET-15b expression plasmid were grown at 20°C for 18 hours in HTMC media (prepared in-house). Protein overexpression was induced by the addition of IPTG (isopropyl β-D-thiogalactoside) to a final concentration of 1 mM and cells were left to express overnight at 20°C. Cells were then harvested by centrifugation at 6400 x g for 20 minutes at 4°C, and were then resuspended in 300 mM sodium chloride, 50 mM sodium phosphate, pH 7.5 and lysed by sonication (Qsonica Q700) with 5 cycles of 30 seconds of sonication (40% amplitude) interspersed with 1 minute on ice. Cell

lysates were clarified by centrifugation at 36,200 g for 45 minutes, and the supernatant was filtered by vacuum filtration using a Stirred Ultrafiltration Cell (Millipore) with an Ultracel 100 kDa ultrafiltration disc prior to affinity purification. Nickel-Affinity chromatography was performed at room temperature using a HiTrap Talon Crude 5 mL linked to an AKTAPurifier (GE Healthcare)-based imidazole gradient method followed by size-exclusion chromatography using a Superose 6 3.2 /30 column (GE Healthcare) equilibrated in 300 mM sodium chloride, 50 mM sodium phosphate, pH 7.5. The quality of the final NadA3-PorA-Ferritin sample was checked by gel electrophoresis using NuPAGE Novex Bis-Tris 4-12 % gels ran in MES buffer and stained with SimplyBlue SafeStain (ThermoFisher). A Bio-rad Protein Assay Dye assay (Biorad) was performed to determine the protein concentration. Sample was then filtered using a Millex 0.22 µM (Merckmillipore) filter to protect against bacterial contamination. Aliquots of purified sample was then stored at – 20 °C.

2.2.4 Negative stain EM of NadA3-PorA-Ferritin nanoparticles.

3 µL of purified NadA3-PorA-Ferritin sample at 200 ng/µL was loaded onto a copper 300-square mesh grid of carbon/formvar (Agar Scientific) rendered hydrophilic by glow discharge (Quorum Q150). The excess solution was blotted off after 30 seconds using Whatman filter Paper No.1 and then the grid was negatively stained with 1% Uranyl Acetate for 1 minute. This was then blotted using Whatman filter Paper No.1. Observation was made at the Tecnai G2 Spirit Transmission Electron Microscope at 87000x magnification equipped with a CCD 2kx4k camera at the University of Siena.

2.2.5 Cryo-EM sample preparation

Glow discharged Graphene oxide Quantifoil R1.2/1.3 grids (Electron Microscopy Sciences) were charged with 2.5 µL of NadA3-PorA-Ferritin sample at 0.2 mg/mL in a vitrobot blotting robot (ThermoFisher).

2.2.6 Cryo-EM data acquisition

Automated data collection was performed at the Nanoscience Centre, Cambridge on a Titan Krios electron microscope (FEI) operated at 300 kV and equipped with a Falcon III direct detection camera (FEI) using EPU software. Movies comprising 31 frames, 60 second exposure time and a total dose of 30 electrons per $Å^2$ were recorded in counting mode at a magnification of 75000 corresponding to a square pixel size of 1.072 Å.

2.2.7 Cryo-EM data Processing

582 of the collected micrographs were taken through for CTF correction using CTFFIND4 software. Automatic particle picking using RELION-2.1 software allowed

extraction of 60,000 particles in 180x180 pixel boxes. Particles were later classified into 250 2D classes. After performing 2D classification in RELION-2.1, the best-looking 2D class averages, as judged by visual inspection, were selected.

These classes underwent further rounds of 2D classification, comprising a final total of 30,000 NadA3-Ferritin-PorA particles. The refined classes were then combined to generate a preliminary 3D map of the NadA3-PorA-Ferritin and using the electron microscopy density map of the apo-ferritin (PDB ID 4V1W) as a 50 Å reference model for 3D classification and refinement steps. The initial NadA3-PorA-Ferritin 3D map then underwent a further cycle of refinement without using any template. The program Chimera (https://www.cgl.ucsf.edu/chimera/) was then employed to rigid body fitting the apo-ferritin crystallographic coordinates into the electron density map of NadA3-PorA-Ferritin.

2.2.8 Purification of wildtype NadA3 (24-170)-Ferritin

Frozen overexpression *E. coli* cell pellets (deriving from 20 °C overexpressions) were resuspended in binding buffer (300 mM sodium chloride, 50 mM sodium phosphate, pH 8) and lysed by sonication (Qsonica Q700) at 5 cycles of 30 seconds sonication (40% amplitude) interspersed with 1 minute on ice. Cell lysates were clarified by ultracentrifugation at 36,200 x g for 45 minutes at 4 °C and then affinity chromatography was performed at room temperature using a HisTrap HP 5 mL linked to an AKTAPurifier (GE Healthcare), with the protein being eluted by an imidazole gradient. Size-exclusion chromatography was then performed using a Superose 6 10/300 GL column equilibrated in binding buffer. The quality of the final NadA3-Ferritin sample was checked by gel electrophoresis using NuPAGE Novex Bis-Tris 4-12 % gels ran in MES buffer then stained with SimplyBlue SafeStain. Fractions were then pooled and filtered using a Millex 0.22 µM filter. A BCA assay using a Pierce BCA Protein Assay Kit was performed to determine the protein concentration before being concentrated by spin-filtration using a Vivaspin protein concentrator spin column and aliquoted for storage.

2.2.9 Purification of wild type NadA3 (24-170)

Frozen overexpression cell pellets (deriving from 20 °C overexpressions) were resuspended in binding buffer (300 mM sodium chloride, 50 mM sodium phosphate, pH 8) and lysed by sonication (Qsonica Q700) with 5 cycles of 30 seconds of sonication (40% amplitude) interspersed with 1 minute on ice. Cell lysates were clarified by ultracentrifugation at 36200 x g for 45 minutes and then affinity

chromatography was performed at room temperature using a HisTrap HP 5 mL linked to an AKTAPurifier (GE Healthcare), with the protein being eluted by employing an imidazole gradient. Size-exclusion chromatography was then performed using a HiLoad 16/600 superdex 75 pg column (GE Healthcare), equilibrated in binding buffer. The quality of the final NadA3-Ferritin sample was checked by gel electrophoresis using NuPAGE Novex Bis-Tris 4-12 % gels ran in MES buffer then stained with SimplyBlue SafeStain (ThermoFisher). Fractions were then pooled and filtered using a Millex 0.22 µM filter. A BCA assay using a Pierce BCA Protein Assay Kit (ThermoFisher) was performed to determine the protein concentration before being concentrated by spin-filtration and aliquots were stored.

2.2.10 Cloning to obtain a NadA3-PorA encoding expression plasmid vector

The PCR primers used for insertion of the PorA VR2 14 sequence into the NadA3-Ferritin DNA were also used to insert the PorA VR2 14 sequence into NadA3 (24-170) encoding DNA. This DNA was then cloned into a pET-15b expression plasmid vector and then transformed into the BL21 *E. coli* (DE3) expression strain in a similar manner as described in section 2.2.2.

2.2.11 Expression and purification of NadA3-PorA

Following overexpression from the transformed *E. coli* (DE3), cells were then harvested by centrifugation at 6400 x g for 20 minutes at 4°C, and then resuspended in a buffer of 300 mM sodium chloride, 50 mM sodium phosphate, pH 8 and lysed by CelLytic Express (Merck). Cell lysates were then clarified by centrifugation at 16,000 g for 10 minutes. Affinity chromatography was performed at room temperature using a HisGravi trap (GE Healthcare) column followed by size-exclusion chromatography using a HiLoad 16/600 superdex 75 pg (GE Healthcare) equilibrated in PBS. Fractions were then pooled and concentrated, with the concentration checked by a BCA assay using a Pierce BCA Protein Assay kit. The sample was then filtered using a Millex 0.22 µM filter to protect against bacterial contamination.

2.2.12 Purification of wildtype ferritin

Overexpression *E. coli* cell pellets (deriving from 20 °C overexpressions) were resuspended in binding buffer (300 mM sodium chloride, 50 mM sodium phosphate, pH 8) and lysed by sonication (Qsonica Q700) at 5 cycles of 30 seconds sonication (40% amplitude) interspersed with 1 minute on ice. Cell lysates were clarified by

ultracentrifugation at 36,200 x g for 45 minutes at 4 °C and then affinity chromatography was performed at room temperature using a HisTrap HP 5 mL linked to an AKTAPurifier (GE Healthcare), with the protein being eluted by an imidazole gradient. Size-exclusion chromatography was then performed using a Superose 6 10/300 GL column equilibrated in PBS (10 mM, pH 7.4).

2.2.13 Immunogold EM of NadA3-PorA-Ferritin using anti-NadA3 antibodies

3 µL of protein sample containing the desired antigen at 0.2 mg/ml was added to a nickel 300-square mesh grid of carbon/formvar and left for 3 minutes prior to blotting with Whatman filter Paper No.1. A wash with PBS-BSA (1%) was then performed for 30 minutes followed by binding of anti-NadA3 antibody for 1 hour. Grids were then washed again twice using PBS-BSA (1%) before staining with Anti-Human IgG-Gold antibody (Dako) diluted 1:40 in for PBS-BSA (1%) for 1 hour. The grids were washed in distilled water two more times before staining with 3 µL of Uranyless negative stain contrast solution (Electron Microscopy Sciences) for 1 minute. Observation was performed at the Tecnai G2 Spirit Transmission Electron Microscope at 87000x magnification equipped with a CCD 2kx4k camera located at the University of Siena.

2.2.14 SPR of anti-NadA3 antibodies binding to the NadA3-PorA-Ferritin

All SPR measurements were performed using a Biacore T200 instrument (GE Healthcare). For the first experiment (in which antigens were immobilised to a sensor chip NTA (GE Healthcare), the antigens NadA3-PorA-Ferritin and NadA3 (24-170) were diluted to concentrations of 50 µg/mL and 30 µg/mL respectively in HBS-P+ buffer (GE Healthcare). Anti-NadA3 antibodies were diluted in HBS-P+ buffer to starting concentrations of 100 nM. For the second experiment in which antibodies were immobilised to the CM-5 sensor chip (GE Healthcare) via an amine-coupling reaction using a Human Antibody Capture Kit (GE Healthcare), the antigens NadA3-PorA-Ferritin and NadA3 (24-170) were diluted to starting concentrations of 100 nM in HBS-P+ buffer (GE Healthcare). Anti-NadA3 antibodies were diluted in HBS-P+ buffer to concentrations of 50 µg/mL.

2.2.15 Competitive inhibition SBA using anti-NadA3 (24-170) sera

All animal sera used in this SBA assay derived from mouse immunization experiments performed at Novartis Vaccines and Diagnostics S.r.l. in Siena, in compliance with the relevant guidelines (Italian Legislative Decree n° 116 27 January 1992) and consecutive ministerial newsletter (Circolare Ministeriale n.8 del 22 Aprile 1994),

and institutional policies of Novartis. The animal protocol was approved by the Animal Welfare Body of Novartis Vaccines and Diagnostics S.r.l., Siena, Italy, and by the Italian Ministry of Health (approval number AEC/AWB 2013-11 of the 17th December 2013).17.5 µL of sera deriving from mice immunized with NadA3 (24-170) was reacted with 17.5 µL of relevant antigen (at 1 mg/mL) and left rotating overnight at 4 °C on a tube rotator. To a 96 well plate, 25 µL of Dulbecco's PBS containing 1% (w/v) BSA and 0.1% (w/v) glucose was then added to all wells, except those of column 12. which saw 20 µL added to each well. Serial two-fold dilutions of sera were prepared by adding 25 µL of prediluted sera (preincubated with antigens) to 25 µL of buffer previously added to the wells, bringing the volume up to 50 µL with buffer, mixed and then 25 µL transferred in the next well (repeating the procedure from column 2 to 10). 25 µL was discarded from the last well (column 10). Column 12 contained the complement independent control; 5 µL of pre-diluted sera with 12.5 µL of heat inactivated complement and 20 µL of buffer. The wells of Column 11 contained the complement dependent control; 25 µL of buffer, 12.5 µL of active complement, and 12.5 µL of bacteria only. The bacteria were grown until an OD600 nm of 0.23–0.25 and then the bacterial culture was then diluted 1: 10,000 by serial dilution and 12.5 µL of the bacteria added to each well of the 96 well plate. The lyophilized complement was reconstituted in 1 mL of ice-cold water and 12.5 µL of active complement added to the wells in columns 1–11. Bacteria were sampled at time = 0 hour by pipetting the well contents up and down three times and then placing 7 µL from the controls, column 11 and 12, to the top of a square Müller-Hinton (MH) agar plate. The 96-well plate was sealed with Parafilm and incubated for 1 h at 37°C with 5% (v/v) CO_2 in a humidified atmosphere and on a soft orbital rotating shaker. Bacteria were sampled at 60 min using a multichannel pipette by mixing the contents of each well by pipetting up and then transferring 7 µL of and spotting onto square MH agar plates. All the MH agar plates were then incubated overnight at 37°C in a humidified atmosphere with 5% (v/v) CO_2.The following day, the number of colony forming units (CFU) in each spot on each of the plates was recorded. All wells were plated in duplicate and duplicate counts were also recorded. Bactericidal titres were defined as the serum dilution that gives a 50% decrease of CFU after 60 minutes incubation in the reaction mixture, compared with the mean number of CFU in the control reactions at time = 0 hour.

2.2.16 FACS titration assay to investigate specificity of the commercially acquired anti-PorA VR2 14 antibody

48 µL of PBS –BSA (1%) was added per sample to a 96 well plate and 2 µL of the PorA antibody was added to different final concentrations (2 mg/mL, 0.5 mg/mL, 0.05 mg/mL or 0.0005 mg/mL). The MenB bacteria were grown to an OD of 0.25 and then 5 mL of culture pelleted at 140,000 g for 10 minutes and the resulting supernatant discarded. The bacterial pellet was resuspended in 5 mL of PBS-BSA (1%) and 50 µL of this was then added to each well in the 96 well plate. The plate was incubated for 1 hour, then centrifuged at 140,000 g for 5 minutes and the supernatant discarded. The samples were then washed with 150 µL of PBS-BSA (1%) and the plate was centrifuged at 140,000 g for 5 minutes and the supernatant discarded. The pellet was then resuspended in 100 µL of FITC-A-labelled secondary antibody diluted 1:100 in PBS-BSA (1%). The plate was incubated for 30 minutes at room temperature. The plate was then centrifuged at 140,000 g for 5 minutes and the supernatant discarded before being washed washed with 150 µL of PBS-BSA (1%). This step was repeated a further three times. Finally, the pellet was then resuspended in 150 µL of prefiltered 0.5% PFA in PBS and the plate was incubated for 30 minutes, after which the bacteria were checked for inactivation. FACS data collection was performed on a FACS Canto II (BD Biosciences) with 10,000 cells being passed per sample.

2.2.17 Competitive inhibition FACS experiment to analyse PorA VR2 14 epitope presentation by the NadA3-PorA-Ferritin nanoparticle

10 µL of the PorA VR2 14 antibody (at 1 mg/mL) and 10 µL of antigen (at 1 mg/mL) were reacted together for 3 hours at 4 °C on a rotor, and then 4 µL of relevant reaction mix added to each serum sample added to a well of a 96 well plate containing 46 µL of PBS-BSA. The bacteria were grown to an OD of 0.25 and then 5 mL pelleted at 140,000 g for 10 minutes and the resulting supernatant discarded. The bacterial pellet was resuspended in 5 mL of PBS-BSA (1%) and 50 µL of this then added to each well in the 96 well plate. The plate was incubated for 1 hour, then centrifuged at 140,000 g for 5 minutes and the supernatant discarded. Samples were then washed with 150 µL of PBS-BSA (1%). The plate was then centrifuged at 140,000 g for 5 minutes and the supernatant discarded. Sample pellet was resuspended in 100 µL of FITC-A-labelled secondary antibody diluted 1:100 in PBS-BSA (1%). The plate was incubated for 30 minutes at room temperature before being centrifuged again at 140,000 g for 5 minutes and the supernatant discarded. The samples were then washed with 150 µL of PBS-BSA (1%), with this step was then repeated a further three times. Sample pellet was then resuspended in 150 µL of prefiltered 0.5% PFA

in PBS. The plate was incubated at 30 minutes and the bacteria checked for inactivation. FACS data collection was performed on a FACS Canto II (BD Biosciences) with 10,000 cells passed per sample.

2.2.18 SPR to investigate PorA VR2 14 epitope presentation

All SPR measurements were performed using a Biacore T200 instrument (GE Healthcare). The PorA VR2 14 antibody was diluted in HBS-P+ buffer (GE Healthcare) to a concentration of 100 µg/mL and immobilized to a CM-5 sensor chip (GE Healthcare) via an amine-coupling reaction using a Mouse Antibody Capture Kit (GE Healthcare). The antigens NadA3-PorA-Ferritin and NadA3 (24-170) were diluted to starting concentrations of 100 nM in HBS-P+ buffer and injected over the chip.

2.2.19 Immuno-blot to probe PorA VR2 14 epitope presentation

1 µL of antigen (at 0.2 mg/mL) was spotted onto a nitrocellulose membrane, left to dry, and a second 1 µL spot added. Non-specific sites on the membrane were then blocked by soaking in 3% milk PBS-Tween 0.1 % for 1 hour. The membrane was then washed (3 x 5 minute) with PBS-Tween 0.1% before incubation with 1 mL of primary anti-PorA VR2 14 antibody (at 1 ug/mL dissolved in PBS-Tween 0.1%) for 30 minutes at RT. The membrane was washed with PBS-Tween 0.1% (3 x 5 min) before incubation with secondary anti-mouse IgG conjugated to HRP (Dako) at a dilution according to the manufacturer's recommendation. The membrane was then washed in PBS-Tween 0.1 % (4 x 5 minutes) before being incubated with SuperSignal West Pico PLUS Chemiluminescent Substrate (ThermoFisher) for 1 minute. The membrane was visualized using a ChemiDoc Touch Imaging System (Bio-rad).

2.3 Results and discussion

2.3.1 Expression trial of NadA3-PorA-Ferritin

In this rationally designed self-assembling nanoparticle system, monomers of the NadA3-PorA-Ferritin that are expressed in *E. coli* spontaneously self-assemble into the 24-meric ferritin nanoparticle displaying the 8 copies of the NadA3-PorA on its surface. Figure 2-1 is a schematic of the NadA3-PorA-Ferritin monomer protein.

Figure 2-1 Schematic diagram of the NadA3-PorA-Ferritin monomer in terms of amino acid residues. The insertion of the 10 residue long PorA VR2 sees 32 residues removed from a monomer of NadA3 (24-170). The C-terminal of the NadA3 (24-170) monomer is then linked to the ferritin monomer by a 4 residue long linker. The ferritin monomer comprises residues 5-167 of the *Helicobacter pylori* ferritin monomer.

In order to express the NadA3-PorA-Ferritin monomer, it must be encoded by a DNA construct contained within a suitable expression vector which is then transformed into a strain of *E. coli* adapted for heterologous recombinant protein expression. The DNA construct encoding wild type NadA3 (24-170)-Ferritin was already in-house, and so a polymerase incomplete primer extension (PIPE)-based cloning method was devised and performed in order to enable insertion of the PorA VR2 epitope into the NadA3 N-terminal region. Following DNA sequencing to confirm successful PorA VR2 insertion, the NadA3-PorA-Ferritin DNA construct was then cloned into a pET-15b expression plasmid vector. This vector DNA was then transformed into the BL21 *E. coli* (DE3) protein expression strain.

A prior protein overexpression trial at 30 °C (data not shown) had resulted in no NadA3-PorA-Ferritin protein overexpression being detected. To see if temperature may be a factor in the protein expression, a further protein expression trial was attempted using a lower expression temperature of 20 °C. The expression trial was performed using 75 mL of HTMC media inoculated with the BL21 *E. coli* encoding for the NadA3-PorA-Ferrtin, and induced to express with IPTG (isopropyl β-D-thiogalactoside) to a final concentration of 1 mM before being left to express overnight at 20 °C. Samples were taken both before and after IPTG induction so that NadA3-PorA-Ferritin protein overexpression could be identified. Figure 2-2 shows the SDS-PAGE performed on lysed cells following overexpression.

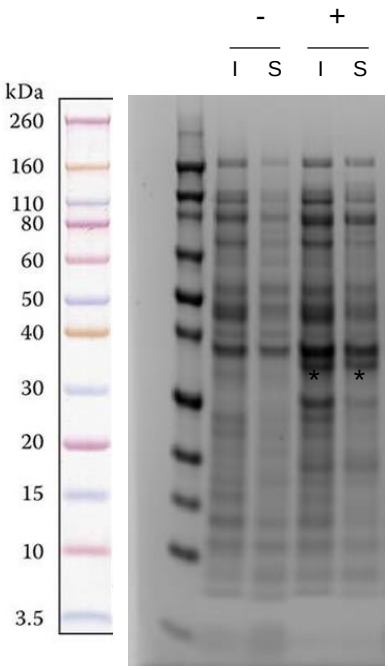

Figure 2-2 SDS-PAGE of NadA3-PorA-Ferritin protein overexpression at 20 °C in *E. coli*. 'I' represents the insoluble fraction while 'S' represents the soluble fraction of the cleared cell lysate. Post-IPTG induction is represented by '+', while '–' represents uninduced samples. * represents the NadA3-PorA-Ferritin monomer at around 34 kDa. On the far left is shown the Novex Sharp Protein Standard.

SDS-PAGE is a denaturing technique (Nowakowski et al., 2014); when NadA3-PorA-Ferritin is treated with SDS, non-covalent interactions are disrupted and the nanoparticle disassembles into its constituent monomers. Therefore, an SDS-treated NadA3-PorA-Ferritin sample when ran on a gel should yield a clear band corresponding to the 34 kDa monomer.

Lowering of the expression temperature results in visibly higher yields of NadA3-PorA-Ferritin monomer expression as represented by the band at around 34 kDa. On self-assembly from the constituent monomers, the NadA3-PorA-Ferritin nanoparticle has a large mass (around 820 kDa) and too high an expression rate in this instance may be toxic to the cell. However, overexpression of recombinant protein at lower temperatures can increase the protein yields obtained, most likely as a result of the decreased rate of protein synthesis giving newly translated proteins time to fold correctly (Rosano and Ceccarelli, 2014). A temperature of 20 °C was therefore selected for future overexpression experiments.

2.3.2 Purification of NadA3-PorA-Ferritin

The NadA3-PorA-Ferritin was expressed again as detailed in section 2.2.2, but this time using an increased cell culture volume to increase the yield of cell mass obtained. To enable the selective purification of the monomer by affinity chromatography, the DNA construct had been designed such that a His-tag would be encoded at the end of the N-terminus of the NadA3-PorA-Ferritin monomer.

The cell mass obtained from the overexpression was sonicated, ultracentrifuged and the resulting protein-containing supernatant was purified by an affinity chromatography procedure that selectively purifies the His-tagged NadA3-PorA-Ferritin from the supernatant. In this procedure, a HiTrap Talon Crude column was used to selectively capture the His-tagged NadA3-PorA-Ferritin from the supernatant and then an imidazole gradient was applied to elute the protein from the column. Following this affinity chromatography step, relevant fractions were pooled, concentrated and then applied to a size exclusion chromatography (SEC) column. Figure 2-3 displays the chromatogram obtained during SEC of the NadA3-PorA-Ferritin nanoparticle.

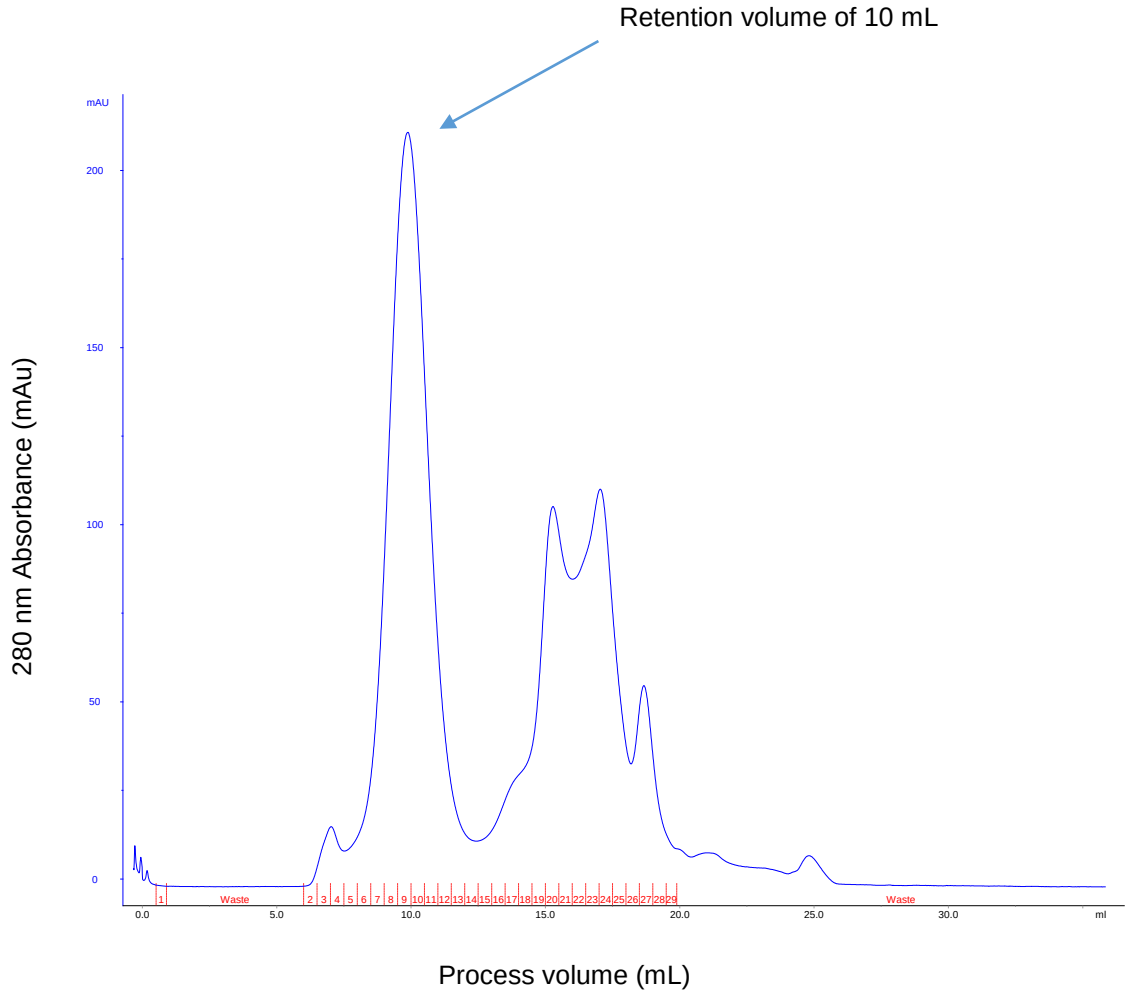

Figure 2-3 Size-exclusion chromatogram obtained during purification of the NadA3-PorA-Ferritin nanoparticle. Size exclusion chromatography was performed using a Superose 6 3.2 /30 column equilibrated in a buffer composed of 300 mM Sodium Chloride, 50 mM Sodium Phosphate, pH 7.5. The large molecular weight of the NadA3-PorA-Ferritin nanoparticle sees it exiting towards the void volume of the column, peaking at around 10 mL. Fractions collected as the run progressed are numbered in red along the x-axis.

The SEC chromatogram in Figure 2-3 shows a peak with a retention volume of around 10 mL. Based on retention volumes for proteins of known molecular weight, this peak can be assumed to correspond to the 820 kDa NadA3-PorA-Ferritin nanoparticle. Following completion of the SEC purification, fractions 8 – 12 corresponding to the putative NadA3-PorA-Ferritin peak were ran alongside other selected fractions on an SDS-PAGE gel to confirm the peak identity. Figure 2-4 shows the SDS-PAGE gel obtained.

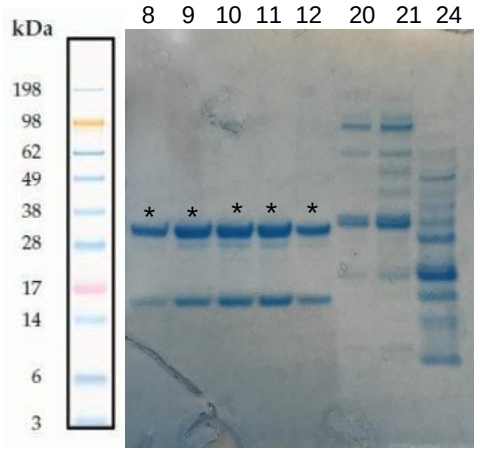

Figure 2-4 SDS-PAGE gel composed of fractions taken from the SEC of NadA3-PorA-Ferritin nanoparticle. The collected SEC fractions are labelled above the gel. Fractions 8 – 12 span the putative NadA3-PorA-Ferritin peak. The band just below the 38 kDa marker represents the NadA3-PorA-Ferritin monomer (*). A band midway between the 17 kDa and 28 kDa markers is as of yet unidentified, however could represent degraded forms of the NadA3-PorA-Ferritin when subjected to the SDS-PAGE process. On the far left is shown the SeeBlue Plus2 Pre-Stained Protein Standard.

In Figure 2-4, thick bands at around 38 kDa corresponding to the NadA3-PorA-Ferritin monomer are present in fractions 8-12 pertaining to the NadA3-PorA-Ferritin peak. The bands seen below at around 17 kD are as of yet unidentified, however as SDS-PAGE is a harsh denaturing process, they could relate to stable degradation products from NadA3-PorA-Ferritin particles. Fractions 20, 21 and 24 are derived from peaks with retention volumes that are too low to contain the large nanoparticle and so the bands visible correspond to other proteins. Fractions 8-12 corresponding to NadA3-PorA-Ferritin were pooled together and a Bradford assay using a Bio-rad Protein Assay Dye (Bio-rad) was performed to determine the protein concentration at an absorbance wavelength of 595 nm, which gave a protein concentration of 0.2 mg/mL.

2.3.3 Negative stain transmission electron microscopy of purified NadA3-PorA-Ferritin

The recombinant protein antigen displayed on the surface of the ferritin was rationally designed such that immunogenic epitopes deriving from both the NadA3 and the PorA VR2 loop epitope could be optimally presented. Many experimental techniques were performed to assess epitope presentation, including cryo electron microscopy (cryo-

EM), which can provide high-resolution structural data on the epitope presentation of NadA3-PorA-Ferritin. Prior to performing cryo-EM analysis, it is customary to perform an initial sample screening procedure using negative stain transmission electron microscopy (TEM). Though negative stain TEM is relatively low resolution analysis, its advantages are that it is comparably quick and easy to perform. Negative stain TEM grids were prepared of the purified NadA3-PorA-Ferritin to assess sample stability and homogeneity as well as provide an initial ultrastructural analysis.

To prepare the negative stain TEM grid, 3 µL of the purified NadA3-PorA-Ferritin at 0.2 mg/mL was added to a charged 300 mesh copper grid, absorbed for 30 seconds and then contrasted with 5 µL of Uranyless stain for 1 minute. These EM grids were prepared from purified NadA3-PorA-Ferritin samples that had been in storage for almost 3 weeks at either 4°C or -20 °C following the purification outlined. Figure 2-5 shows the electron micrographs obtained.

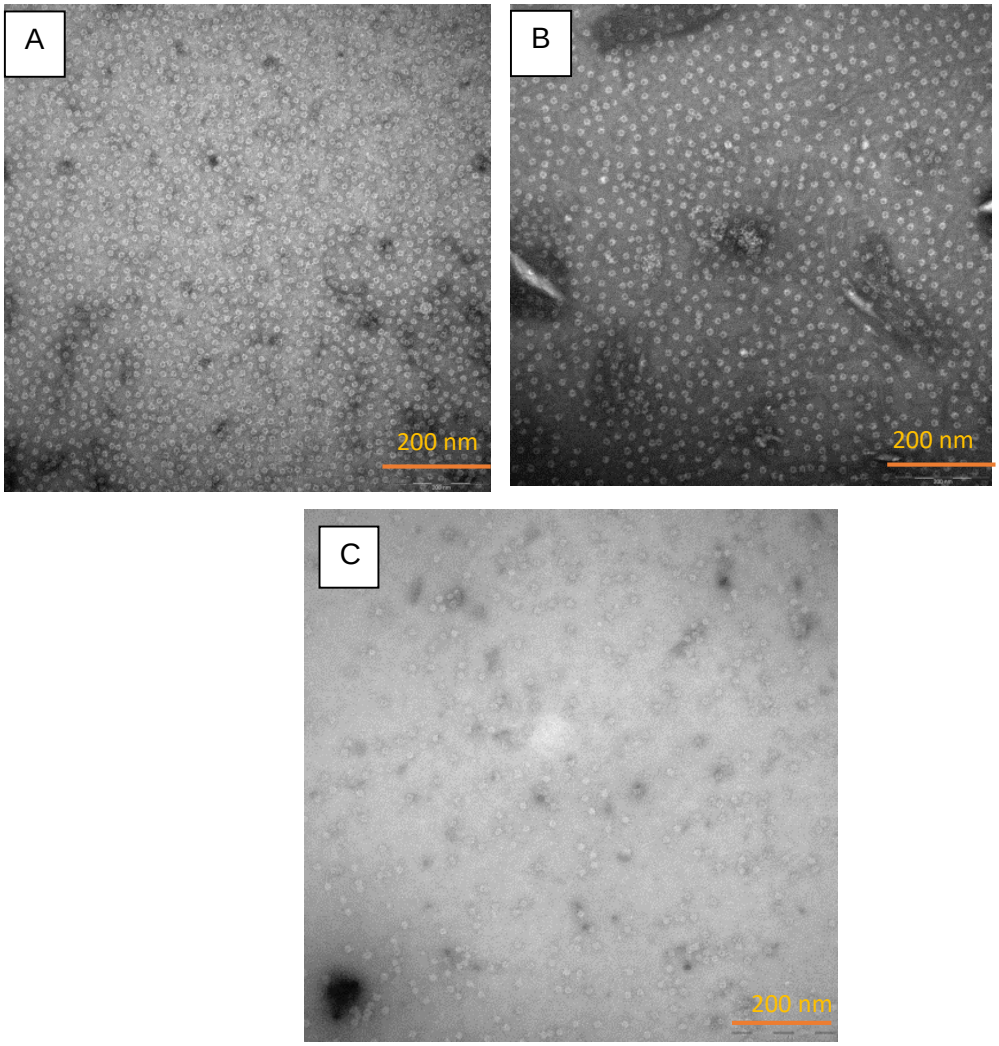

Figure 2-5 Negative stain TEM micrographs of A) Purified NadA3-PorA-Ferritin (stored at 4 °C) B) Purified NadA3-PorA-Ferritin (stored at -20 °C) C) Purified NadA3-PorA-Ferritin stored at -20 °C and made to 20% glycerol. All preparations were stained with Uranyless contrast stain. The bottom right shows the 200 nm scale bar.

In micrograph A showing NadA3-PorA-Ferritin stored at 4 °C, well-formed ferritin nanoparticles with NadA3 stalks are visible, and there does not appear to be any signs of sample degradation. Micrograph B is of the aliquot stored at -20°C, again confirming the presence of stably formed recombinant nanoparticles. These grids were prepared almost 3 weeks after purification and the nanoparticles appear to be stable even when stored at 4 °C.

The concentration of the NadA3-PorA-Ferritin particles on the grids shown in micrographs A and B gives relatively densely packed particles, which could make boxing of particles more difficult if a single particle structural reconstruction analysis

was to be performed directly from this negative stain data. However, this sample concentration would be acceptable to be taken through for cryo-EM grid preparation as this density would likely compensate for particles that usually become lost during the cryo EM grid preparation procedure.

TEM micrograph C is also a preparation of NadA3-PorA-Ferritin stored at -20 °C but this aliquot was also stored by making it up to 20% glycerol. Glycerol is widely used to stabilise proteins; the stabilizing effect is proposed to be due to prevention of protein aggregation by inhibiting protein unfolding and by stabilizing aggregation-prone intermediates (Vagenende et al., 2009). In this case, dilution of the sample due to the addition of glycerol has resulted in particle concentration that would enable better boxing of particles if a single particle reconstruction analysis was to be performed directly from micrographs collected from this grid. However, the addition of glycerol clearly affects the staining contrast making it more difficult to detect electron density arising from the ferritin nanoparticles. Based on these results, NadA3-PorA-Ferritin samples stored at 4°C and -20°C (without the addition of glycerol) were deemed suitable to be taken through for cryo-EM analysis.

Figure 2-6 shows a TEM micrograph of an early preparation of the NadA3-PorA-Ferritin. Though this purification yielded too low a concentration for further downstream assays, it did serve as an early indicator of the correct folding of the NadA3-PorA-Ferritin nanoparticle.

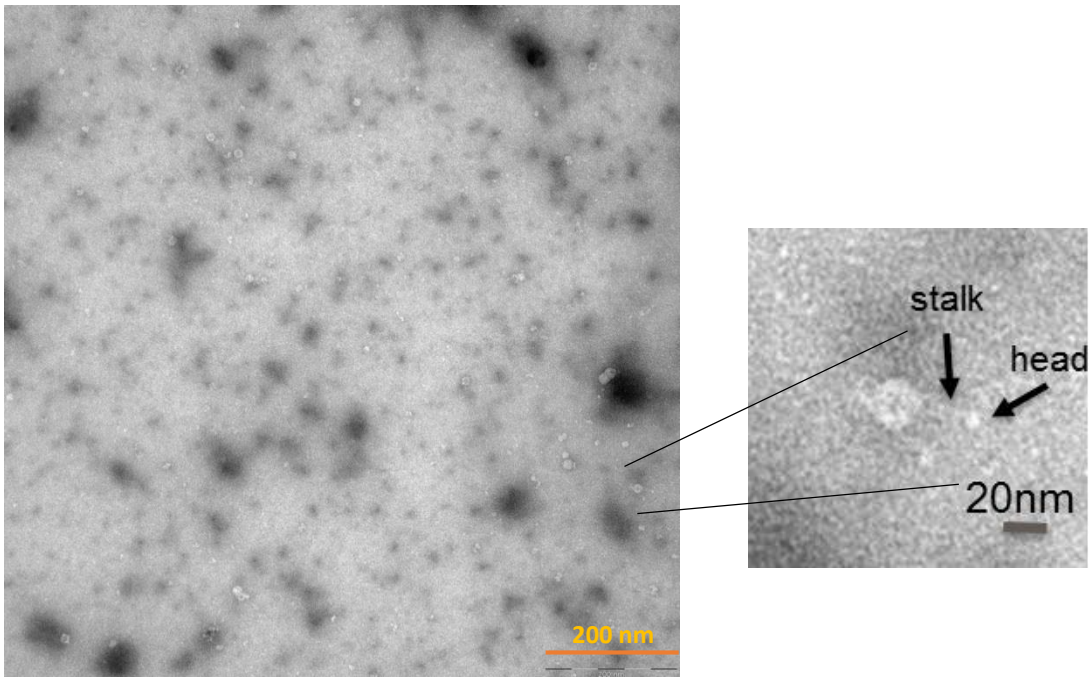

Figure 2-6 A Negative stain TEM micrographs of an early preparation of NadA3-PorA-Ferritin. One of the particles is magnified on the right to show two appendages seen extending from its surface, with electron density originating from the NadA3 stalk and head regions clearly visible.

The prior described size-exclusion chromatography indicated the elution of a protein with the expected molecular weight of the correctly assembled NadA3-PorA-Ferritin nanoparticle. The particle visible here by electron microscopy further agrees with this. It confirms that the NadA3-PorA-Ferritin can successfully self-assemble on expression and with visible appendages coming from the nanoparticle surface, there are early indications that the design allows for correct trimerisation of the NadA3-PorA on self-assembly.

2.3.4 Cryo-EM data acquisition of purified NadA3-PorA-Ferritin

Based on the negative stain TEM described previously, a preparation of the NadA3-PorA-Ferritin nanoparticle was used for data collection performed at the Nanoscience Centre in Cambridge (UK) using a Titan Krios cryo-electron microscope (FEI). Over a data collection period of 48 hours, at least 600 motion-corrected images were collected of the NadA3-PorA-Ferritin preparation on the grid.

The NadA3-PorA-Ferritin sample at a concentration of 0.2 mg/mL was added to Quantifoil R1.2/1.3 grids treated with graphene oxide (GO), which acts as a support layer onto which the molecules can absorb (Cheng et al., 2015). Graphene oxide,

which is a hydrophilic derivative of graphene displays many attributes that makes it superior to amorphous carbon films that are commonly used in electron microscopy (Wilson et al., 2009).

Automated data collection was performed on the Titan Krios electron microscope (FEI) operated at 300 kV and equipped with a Falcon III direct detection camera (FEI) using EPU software. Figure 2-7 Image of and Figure 2-8 Micrograph show a couple of images taken during the data acquisition process for the NadA3-PorA-Ferritin sample grid.

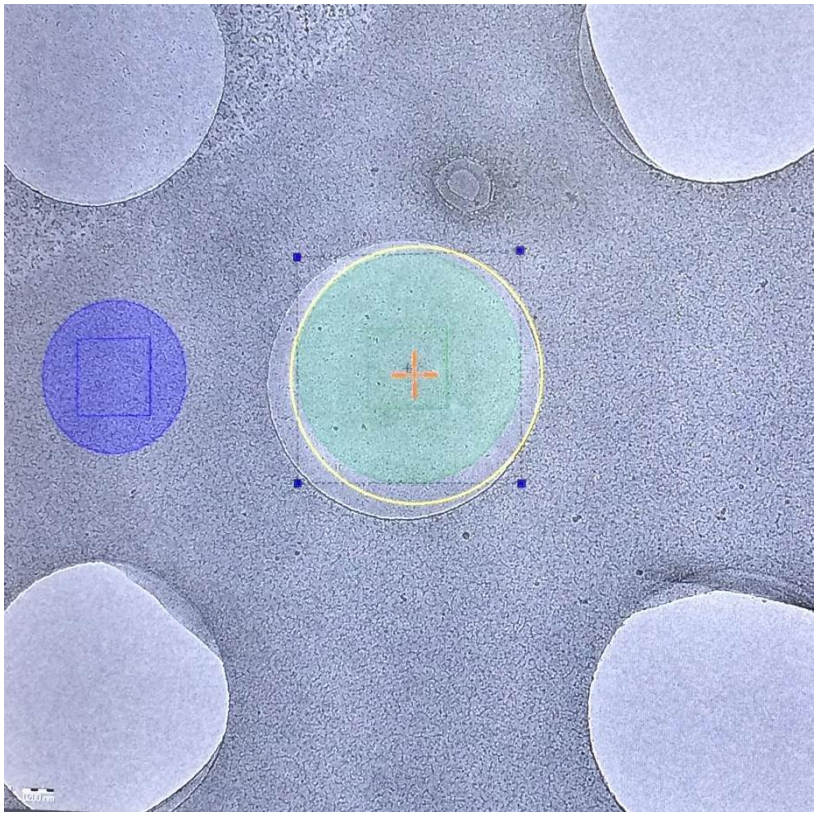

Figure 2-7 Image of the hole picking process during data acquisition of purified NadA3-PorA-Ferritin observed using a Titan Krios electron microscope (FEI) operated at 300 kV and equipped with a Falcon III direct detection camera (FEI) using EPU software. The image captures the selection of holes on that grid that display a good graphene oxide distribution. The selected holes then undergo further analysis.

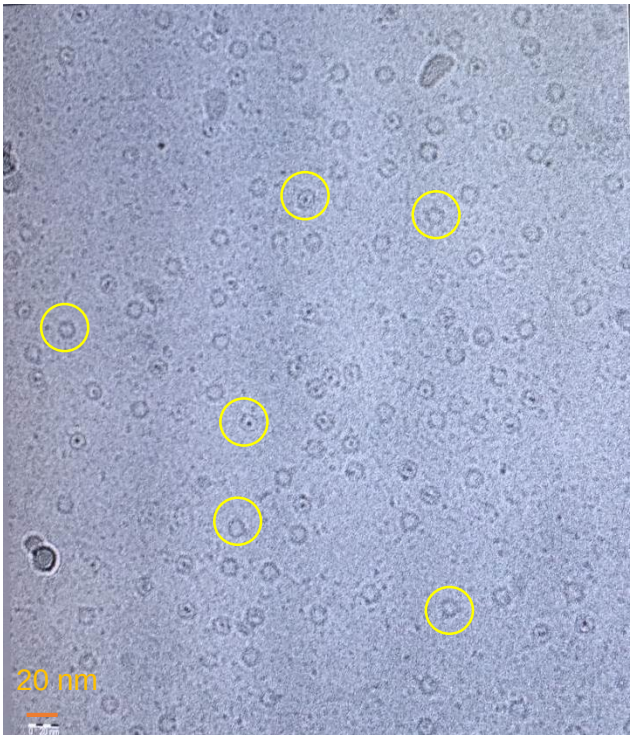

Figure 2-8 Micrograph image obtained during cryo EM data acquisition of purified NadA3-PorA-Ferritin. Magnification was set to 75000 corresponding to a square pixel size of 1.072 Å. In the image, the NadA3-PorA-Ferritin nanoparticles (a selection circled in yellow) can be seen captured in a variety of orientations. The 20 nm scale bar is shown in the bottom left corner.

In Figure 2-7 a grid hole, in which particles of interest are embedded in vitrified ice, is picked based on the fact that this particular grid hole displays an even distribution of graphene oxide. Figure 2-8 shows a micrograph obtained from imaging of a hole on grid selected based on its optimum graphene oxide distribution, such as that one described in Figure 2-7. The purified NadA3-PorA-Ferritin sample concentration of 0.2 mg/mL can be seen to give a good distribution of nanoparticles within the holes of the grid, with the nanoparticles seen captured in a variety of orientations.

In single particle EM, the rationale is to take these 2D projections of the specimen, extract the molecules captured in different orientations and combine them to obtain a 3D model. An ideal situation is one in which the molecules of interest adopt random orientations within the vitreous ice layer, allowing for the capture of a variety of angular projections and leading to a correct electron density map of the structure once all these projections are combined following the single particle reconstruction procedure. However, only a few sample specimens adopt random orientations due to a number of reasons such as interactions at the air-water interface, with neighbouring particles or the support film (Drulyte et al., 2018). This can particularly be a problem for particles with low or no symmetry (though in this case the NadA3-PorA-Ferritin is highly symmetrical) as it leads to a bias in the angular distributions acquired, with missing

views presented as a ‘smearing’ of the electron density, ultimately leading to lower resolution, an inferior or even incorrect electron density map.

2.3.5 Single particle reconstruction of NadA3-PorA-Ferritin from cryo-EM data

Following the cryo-EM data acquisition outlined in section 2.3.4, single particle reconstruction of the NadA3-PorA-Ferritin from the 600 collected micrograph images was performed using RELION 2.1 software (Scheres, 2012). The high symmetry of the nanoparticle aided in the 3D structure determination, with attention focused on obtaining high-resolution structural information of the recombinant NadA3-PorA antigen displayed on the ferritin surface.

The reconstruction process using RELION 2.1 software begins with the import and evaluation of the cryo-EM micrographs of the NadA3-PorA-Ferritin nanoparticle. To obtain high-resolution information from the micrographs, the Contrast Transfer Function (CTF) had to be measured and corrected for each micrograph. The CTF models how the electron microscope captures the specimen of interest as its recorded image on the micrograph and, therefore, allows for an estimation of the distortions present in the micrograph to be made (Jeong et al., 2013). Around 60 individual NadA3-PorA-Ferritin particles were then picked manually from a selection of micrographs by ‘boxing’ them into circles of defined diameter. The quality of the picked particles is crucial towards the reconstruction, otherwise the inclusion of a large number of poor quality particles will preclude final structure determination. Automatic particle picking from the remaining micrographs then allowed for extraction of 60,000 particles which were then classified into 250 2D classes.

2D classification is the step of the process in which the extracted particles are classified into homogenous subsets of particles. Through this process, classes bearing invalid particles, image artefacts or empty fields can be removed which then allows for the identification of high quality classes with high signal-to-noise ratios necessary for the computational determination of 3D structure. These classes were further refined by manual assessment and further rounds of 2D classification, giving a final total of around 30,000 NadA3-Ferritin-PorA particles classified into many 2D classes. The refined classes are then combined to generate a preliminary 3D map of the NadA3-PorA-Ferritin and using the electron microscopy density map of the apo-ferritin as a template in the first cycle of refinement. The initial NadA3-PorA-Ferritin 3D map then undergoes to further cycle of refinement without using any template.

This initial map was then manually fit using Chimera (Pettersen et al., 2004) using the apo-ferritin model.

The particle reconstruction resulted in a high resolution 3.3 Å map of the ferritin scaffold with a measured diameter of 120 Å being obtained (Figure 2-9 A), however the structure of the NadA3-PorA protein antigen on the surface could not be reconstructed due to the high flexibility of the NadA3-PorA antigen in the stalk region. This high flexibility generated structural heterogeneity among the population of NadA3-PorA-Ferritin nanoparticles that results in a detectable cloud of electron density with a diameter of around 400 Å surrounding the ferritin scaffold (Figure 2-9B).

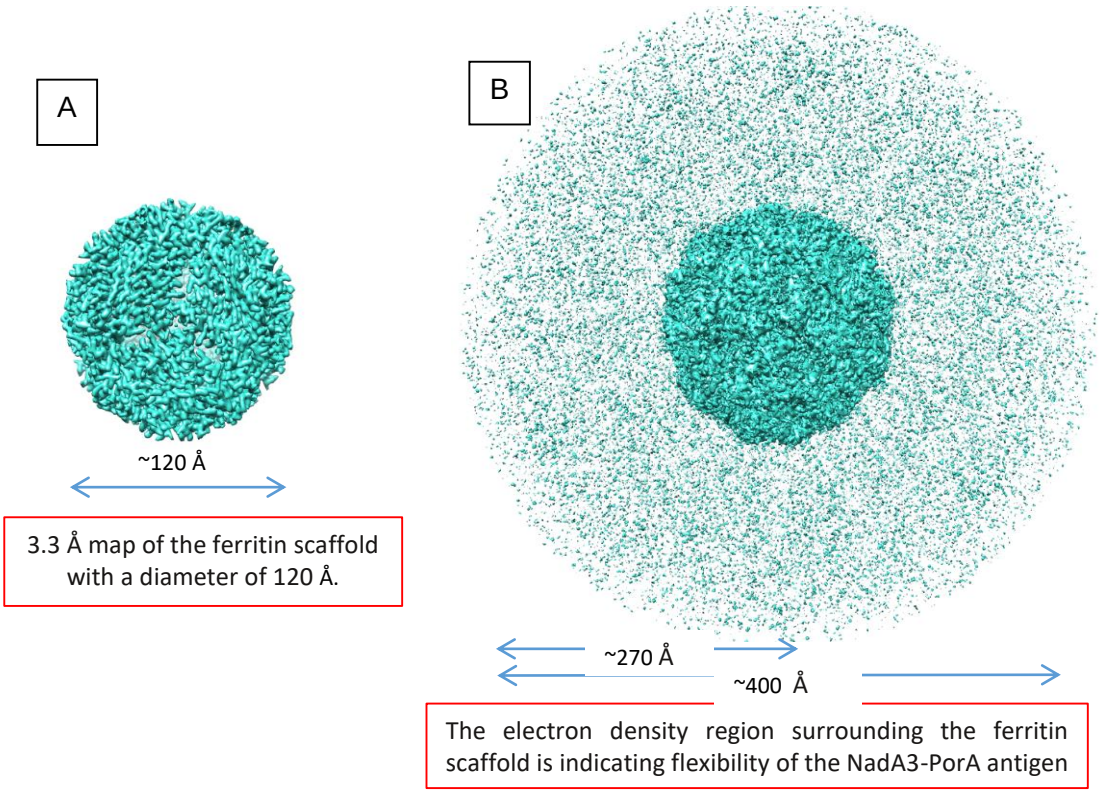

Figure 2-9 NadA3-PorA flexibility detected by Cryo-EM A) The 3.3 Å map of the ferritin scaffold obtained B) A cloud of electron density around the ferritin scaffold is seen due to the inherent flexibility of the NadA-PorA appendages.

Other groups researching similar antigen presentation systems using ferritin also performed cryo-EM analysis for structure elucidation (Kanekiyo et al., 2015; Yassine et al., 2015), with Kanekiyo et al. obtaining a 16 Å map of ferritin presenting an influenza HA antigen. However, differences between the HA antigen and the NadA3-

PorA antigen such as the secondary structure elements present, which may translate into increased flexibility of the NadA3-PorA stalk, can help to explain the added difficulty in reconstructing this antigen. The use of ligand-induced stabilisation to reduce conformational stability is a well-established technique in X-ray crystallography (Vedadi et al., 2006) and so the possibility of using an anti-NadA3 antibody to stabilise a NadA3-PorA appendage was also investigated; however, SEC-purification following an overnight binding reaction to the antibody revealed no detection of an antibody-NadA3-PorA-Ferritin complex to be taken through for electron microscopy analysis.

2.3.6 Structural determination of NadA3-PorA-Ferritin

To determine the recombinant nanoparticle structure, prior collected negative stain EM micrographs (detailed in section 2.3.3) were used. Negative stain EM sample preparation conditions differ to those of cryo-EM in that negative staining tends to induce preferred orientations of molecules on the carbon support film instead of the random orientations adopted in the amorphous ice layer of a cryo-EM grid (Ohi et al., 2004). Having a limited number of preferred orientations is beneficial in the analysis of conformationally heterogeneous samples, and so could be applicable towards solving the structure for NadA-PorA, which exhibits high degrees of structural flexibility that translates into a high conformational heterogeneity throughout the NadA3-PorA-Ferritin particle population.

In a similar process as to that described in section 2.3.4, the process began with the evaluation and importing of good quality negative electron micrographs. Particles were then boxed and picked manually using Boxer software (Figure 2-10 A) and 2D classification of the extracted particles into homogenous subsets was then performed automatically by iMagic software (van Heel and Keegstra, 1981) (Figure 2-10 B) before combination of these 2D classes to generate the 3D map (Figure 2-10 C).

A)

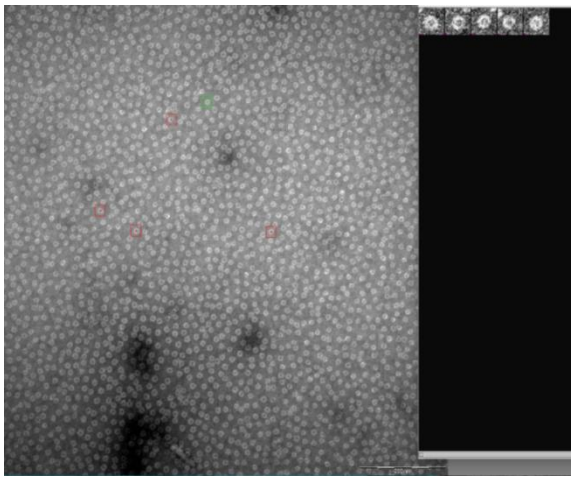

B)

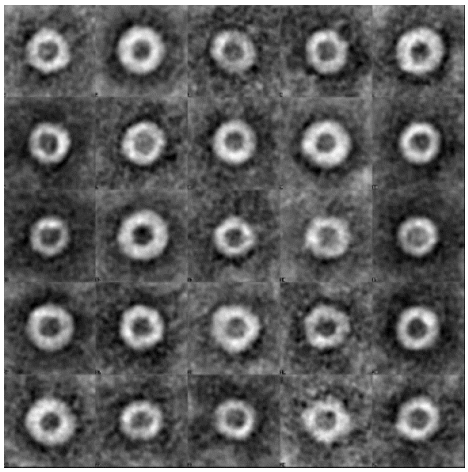

C)

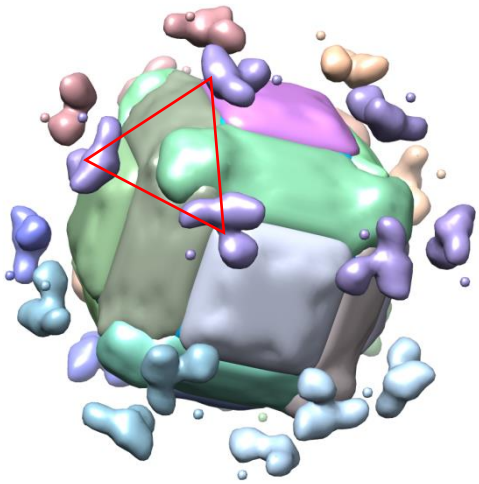

Figure 2-10 An overview of the negative stain EM single particle reconstruction of NadA3-PorA-Ferritin. A) The particle picking process in which Boxer software is used to box NadA3-PorA-Ferritin particles captured in the micrograph into red circles. B) The generated 2D classes using the iMagic software. C) 3D electron density map was generated using iMagic and then segmentation was performed using Chimera. Highlighted by a red triangle is the one of the 8 trimeric interfaces on the surface of the ferritin which form the point where the NadA3-PorA trimerizes.

Figure 2-10 C displays the 3D model of the NadA3-PorA-Ferritin obtained using the negative stain data. The flexibility of the NadA3-PorA still precludes its structural determination; indeed, only a small amount of electron density can be reconstructed at the more stable base of the NadA3-PorA trimer situated at each of the trimeric interfaces on the ferritin surface.

Following this attempt, further electron microscopy approaches were investigated for their potential to overcome the NadA3-PorA flexibility. Single particle electron tomography, also known as subtomogram averaging, is one such technique that can be applied towards solving the structures of molecules that display conformational heterogeneity, asymmetry or high flexibility (Galaz-Montoya and Ludtke, 2017). In single particle electron tomography, a set of images (known as a tilt series) of the desired molecule is collected by tilting the specimen stage through a range of angles, usually about a single axis (over the angular range of +60° to -60° in increments of 1–5°). Each tilt series can then be computationally reconstructed into a 3D tomogram representing the 3D structure of the imaged area (Belnap, 2015). The technique also requires fewer individual single particles for the 3D reconstruction compared to standard electron microscopy. This approach may be able to enable reconstruction of the NadA3-PorA recombinant protein appendage on the surface of the ferritin, albeit at lower resolution achievable by cryo-EM approaches. Iwasaki et al. successfully used single-particle electron tomography to determine the 3D structure of integrin αIIbβ3 in different conformations, a molecule whose structural flexibility had rendered previous single particle reconstruction techniques difficult (Iwasaki et al., 2005).

To prepare a sample for electron tomography, a negatively stained grid loaded with a dilute sample of the NadA3-PorA-Ferritin nanoparticle was prepared before being observed under the electron microscope. Figure 2-11 shows a tomogram obtained from this data collection. In Figure 2-11, a particle with a clear NadA3-PorA stalk on its surface can be seen; however, this preparation of NadA3-PorA-Ferritin did not yield enough particles where the NadA3-PorA were visible for single particle subtomogram averaging and so this approach was also unsuccessful with regards to 3D reconstruction of the NadA3-PorA antigen when presented on the surface of ferritin.

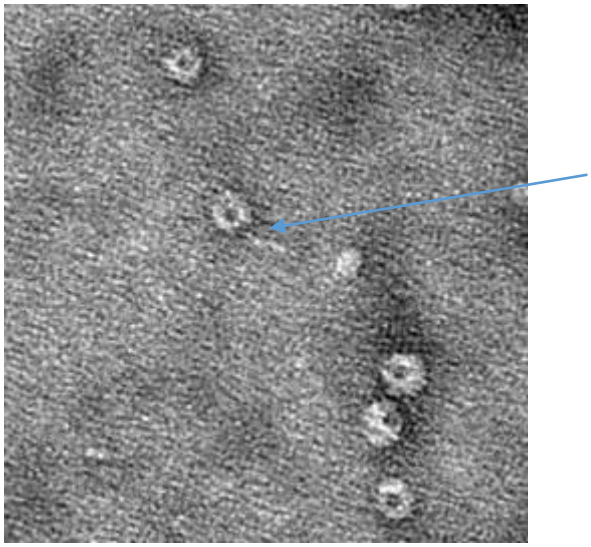

Figure 2-11 An electron tomogram obtained from negative stain electron tomography of the NadA3-PorA-Ferritin nanoparticle. A visible NadA3-PorA appendage is indicated by the arrow.

2.3.7 Purification of wildtype NadA3 (24-170)-Ferritin

To characterise epitope presentation by the NadA3-PorA-Ferritin, a number of other protein constructs must be expressed and purified. One of these protein constructs is the ferritin displaying the wild type NadA3 (24-170), which lacks the PorA VR2 insert. Expression of this construct and then comparing it with the NadA3-PorA-Ferritin can elucidate how insertion of the PorA VR2 loop could affect pre-existing NadA3 epitopes.

The in-house DNA construct encoding NadA3 (24-170)-Ferritin was transformed into BL21 *E. coli* (DE3) expression strain and expressed. Though purification of this construct was initially hampered by low yields and aggregation, a method was optimised that resulted in less aggregation. To purify the wildtype NadA3 (24-170)-Ferritin from an overexpression cell pellet, the cell pellet was first lysed by sonification and then clarified by ultracentrifugation, before undergoing affinity chromatography using a HisTrap HP. Relevant fractions were then pooled and concentrated by spin-filtration and then loaded to a SEC column. Figure 2-12 shows the size-exclusion chromatogram obtained.

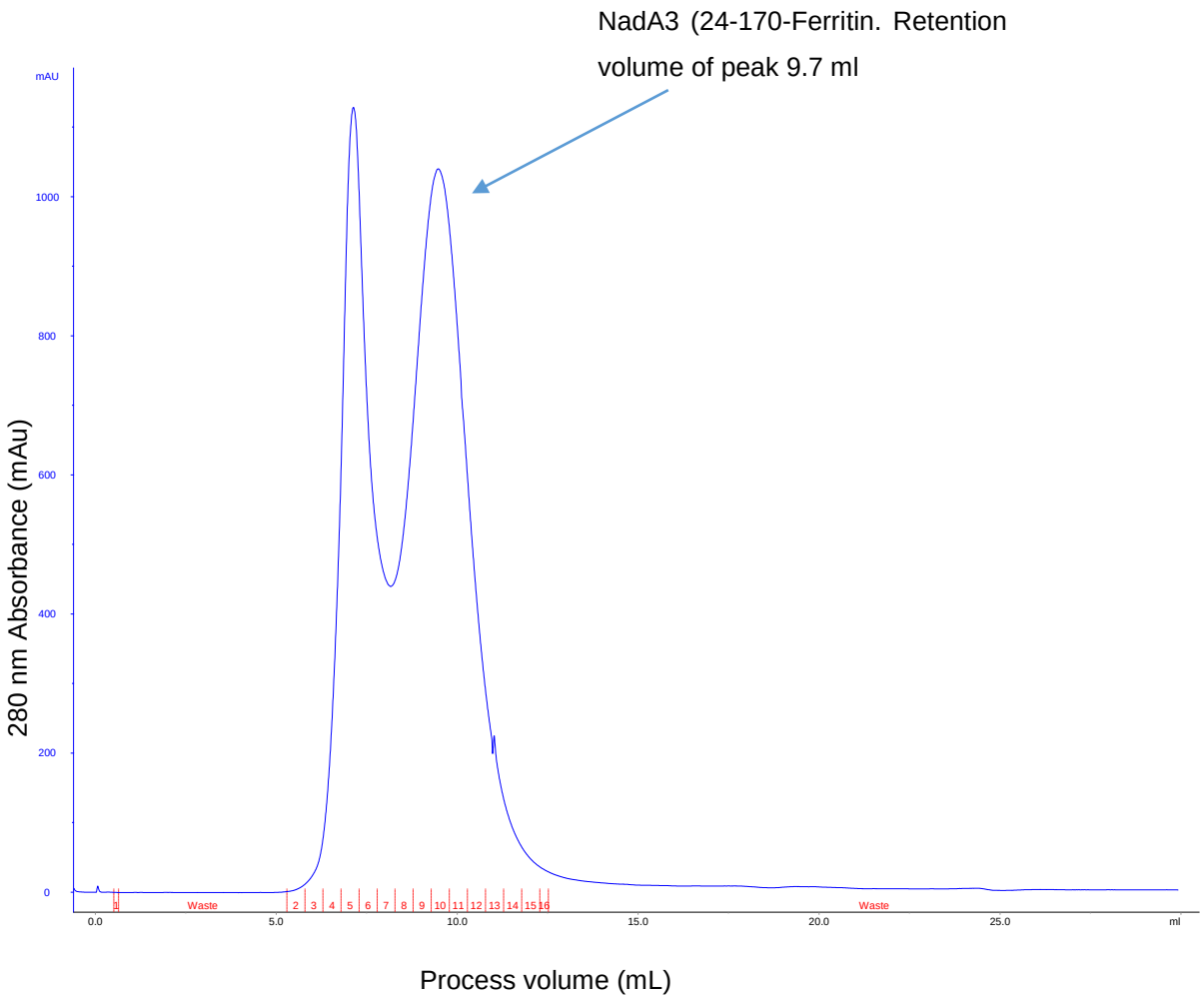

Figure 2-12 SEC chromatogram obtained during purification of wildtype NadA(24-170)-Ferritin. SEC was performed using a Superose 6 10 /300 GL column equilibrated in 300 mM sodium chloride, 50 mM sodium phosphate, pH 8. Fractions collected as the run progressed are numbered in red along the x-axis. The large molecular weight of the NadA3 (24-170) -Ferritin nanoparticle sees it exiting towards the void volume of the column, peaking at around 9.7 mL. The preceding peak at around 6.5 ml is in agreement with the void volume of the column, indicating that this peak contains very large species, which could potentially be aggregates.

The chromatogram shown in Figure 2-12 shows a peak with a retention volume of around 9.7 mL. In comparison to NadA3-PorA-Ferritin, the NadA3 (24-170)-Ferritin nanoparticle has a larger molecular weight closer to 860 kDa, and so it would be expected to exit the column at an earlier retention volume, which is what is observed. The peak with a retention volume of around 6.5 mL is in line with that of the void volume of the column; species exiting the column here are too large (contaminant proteins or aggregates) to enter the pores of the chromatography medium and instead

pass rapidly between the beads, exiting the column earlier (Hong et al., 2012) . A selection of the fractions collected were then ran on an SDS-PAGE gel to confirm peak identities, with Figure 2-13 shows the SDS-PAGE gel obtained.

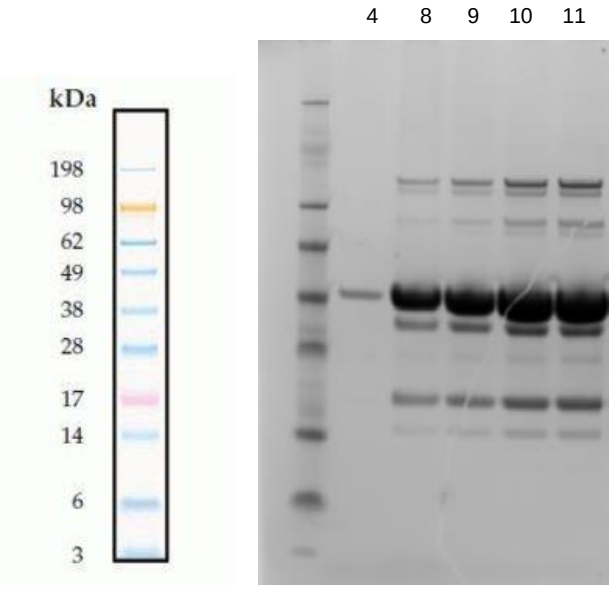

Figure 2-13 SDS-PAGE gel composed of fractions collected from the SEC purification of the NadA3 (24-170)-Ferritin nanoparticle. SEC fractions are labelled above the gel. The band at around 38 kDa marker represents the NadA3 (24-170) - Ferritin monomer. On the far left is the SeeBlue Plus2 Pre-Stained Protein Standard.

From the gel in Figure 2-13 fractions 8 -11 spanning the peak with a retention volume at around 9.7 mL contain large amounts of a protein with a molecular weight around the 38 kDa mark, likely corresponding to the 36 kDa NadA (24-170)-Ferritin monomer. On the other hand, it can also be seen that fraction 4 encompassing the peak eluting at the void volume of around 6.5 mL contains very little of the NadA3 (24-170)-Ferritin monomer and is likely to be composed of contaminant protein. Based on this gel, fractions spanning the peak with a retention volume of 9.7 ml were pooled together and then concentrated for storage.

2.3.8 Purification of wildtype NadA3 (24-170)

A further protein that will enable insight into epitope presentation of the NadA3-PorA-Ferritin antigen is the wild type NadA3 (24-170) trimer. An in-house expression vector encoding this protein already existed, and so could be readily transformed into the appropriate *E. coli* expression strain and then expressed. The cell expression pellet

was lysed and this lysate was then applied to a 5 mL HisTrap HP linked to an AKTAPurifier HPLC system (GE Healthcare), through which the his-tagged NadA3 trimer was progressively eluted from the column using an imidazole gradient. Figure 2-14 shows the chromatogram obtained for this affinity chromatography step.

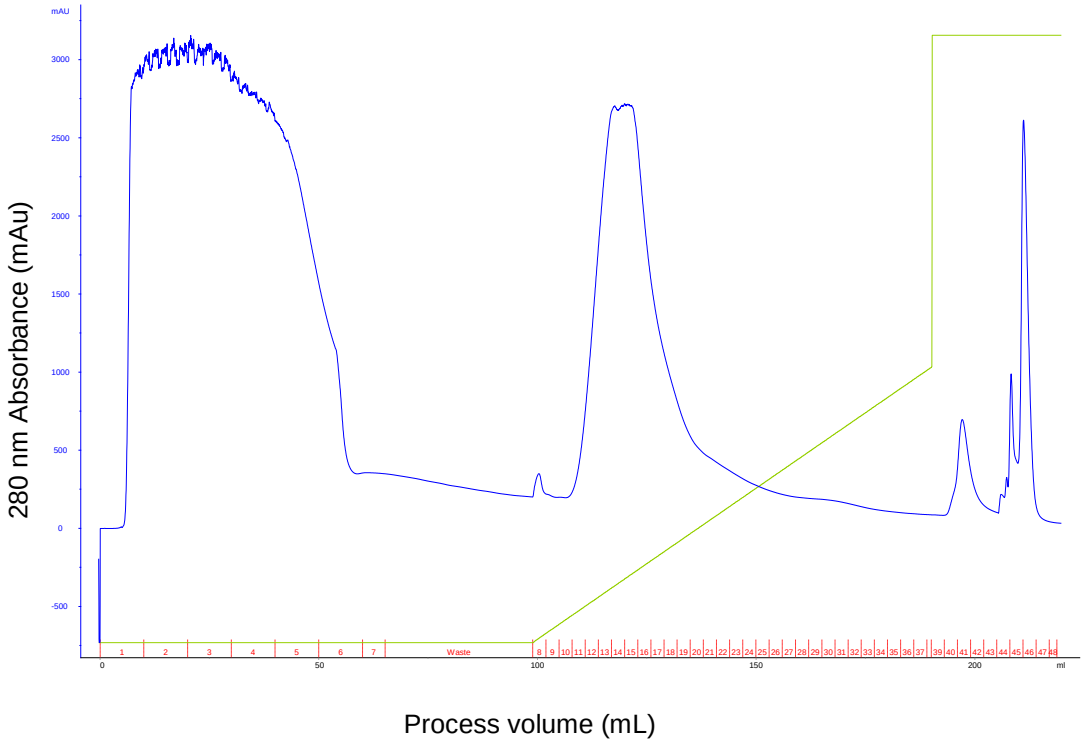

Figure 2-14 Chromatogram for the affinity chromatography purification of NadA3 (24-170). The cell lysate was loaded to a HisTrap HP column and progressively purified by an imidazole gradient, represented by the green line which plateaus at an imidazole concentration of 500 mM. The x-axis shows the volume passed from the point of sample injection and collected fractions are shown in red.

Figure 2-14 demonstrates the selective elution of NadA3 (24-170) using an imidazole gradient (represented by the green line in the chromatogram). When the gradient plateaus, it is equivalent to an imidazole gradient of 500 mM. At this concentration, the high affinity interaction between the his-tagged NadA3 (24-170) and nickel-chelated to the agarose bead support of the column should be displaced by the high imidazole concentration, resulting in the elution of the NadA3 (24-170) trimer from the column. SDS-PAGE performed using collected fractions from this affinity purification revealed fraction 46 to contain a large amount of protein bearing a molecular weight of around 17 kDa (the expected mass of a NadA3 (24-170) monomer). Based on this

gel, the fractions 45 and 46 were pooled, concentrated and loaded to a SEC column with the resulting chromatogram shown in Figure 2-15.

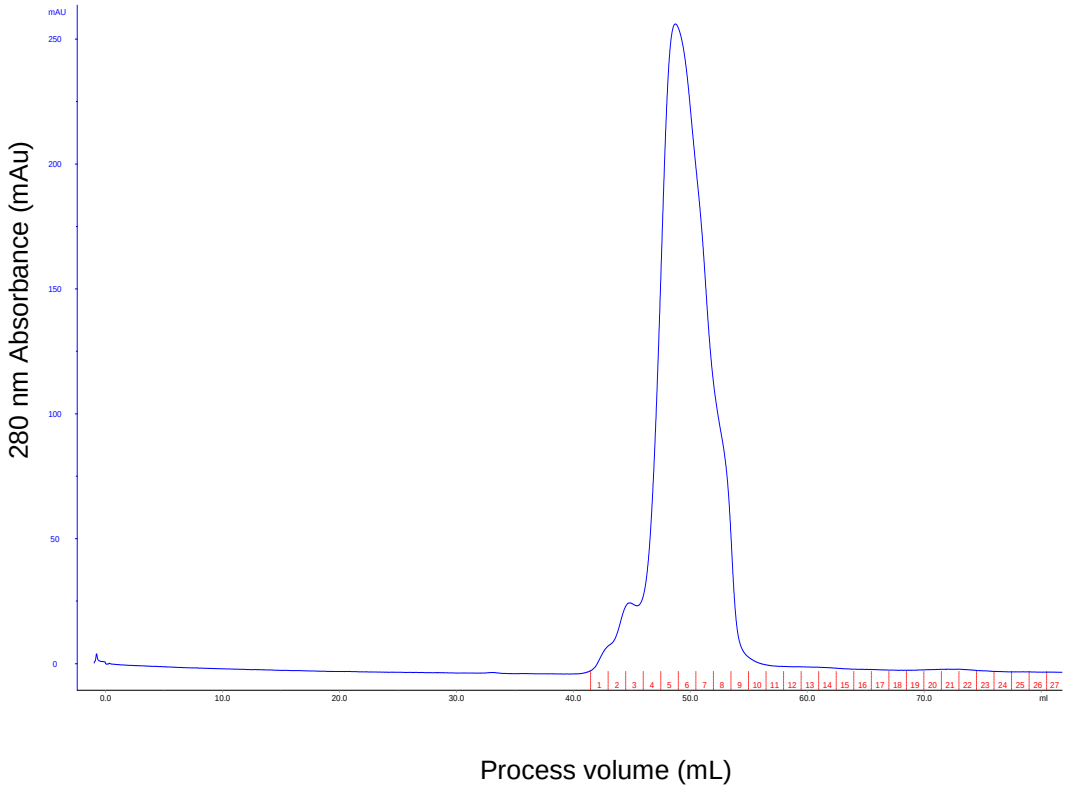

Figure 2-15. SEC chromatogram obtained during purification of the wild type NadA3 (24-170). SEC was performed using a HiLoad 16/600 superdex 75 pg column equilibrated in a buffer composed of 300 mM Sodium Chloride, 50 mM sodium phosphate, pH 8. The x-axis shows the volume passed from the point of sample injection and collected fractions are shown in red.

The chromatogram obtained for the size-exclusion purification of NadA3 (24-170) shows a large peak with a retention volume of around 50 mL. To confirm that this peak corresponds to the NadA3 (24-170) trimer, fractions from the SEC purification were loaded to an SDS-PAGE gel, which is shown in Figure 2-16.

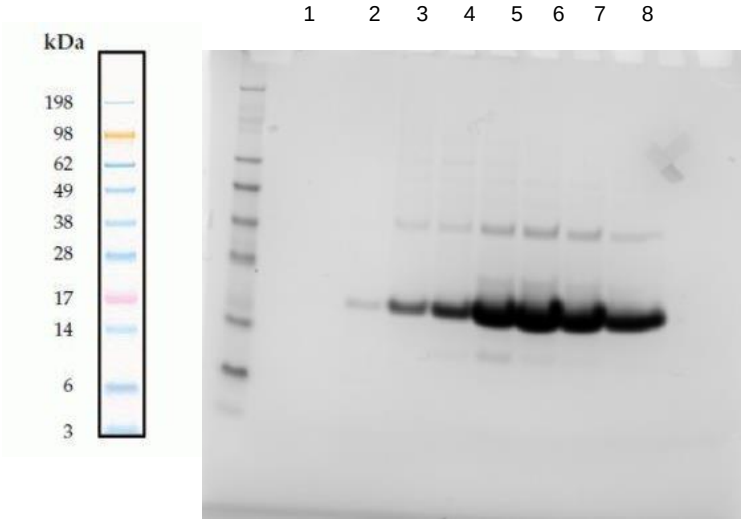

Figure 2-16 SDS-PAGE gel composed of fractions taken from the SEC of NadA3 (24-170) protein. The collected SEC fractions are labelled above the gel. The band at 17 kDa likely represents the monomer, while the bands that can be seen at around the 38 kDa are possibly undenatured dimers of the NadA3. On the far left is shown the SeeBlue Plus2 Pre-Stained Protein Standard.

The SDS-PAGE in Figure 2-16 shows a clear band at around the 17 kDa mark for the fractions that derive from the postulated NadA3 (24-170) trimer peak. As SDS-PAGE is a denaturing technique, the NadA3 trimer would be expected to appear on the gel predominantly in its monomeric 17 kDa form. The peak seen on the SEC above can therefore be confirmed to contain the NadA3 (24-170) trimer, and so the fractions spanning this peak were pooled and concentrated for storage. The bands seen around the 38 kDa marker in these same fractions likely correspond to partially denatured NadA3 (24-170) in its dimeric form, as the molecular weight of the monomer is 17 kDa and a dimer would therefore be around 34 kDa.

2.3.9 Cloning and purification of the NadA3-PorA chimeric protein antigen

In this nanoparticle system, ferritin is used as a vehicle to enhance the immunogenicity of the chimeric subunit protein antigen NadA3-PorA. In order to assess the impact of surface presentation on the ferritin, *in vivo* studies are envisioned in which the immunogenicity arising from administration of the subunit antigen alone NadA3-PorA is compared to that when it is presented as part of the rationally designed NadA3-PorA-Ferritin. Therefore, it was also necessary to obtain the purified NadA3-PorA protein antigen alone without the ferritin. To do this, a PIPE-based cloning mutagenesis method was devised in which the PCR primers that had been previously

used for insertion of the PorA VR2 sequence into the NadA3 (24-170) Ferritin DNA were used instead to insert the PorA VR2 sequence into NadA3 (24-170) encoding pET-15b expression vector DNA. The PCR reaction mix was prepared and the PCR reaction was performed with three different annealing temperatures (65/70/75 °C) tested to find the optimum temperature. Table 2-1 details the PCR mix prepared and the thermocycler parameters for the PCR mutagenesis reactions.

Table 2-1 Reagent conditions and parameters of the PCR mutagenesis for insertion of the PorA VR2 14 sequence into the NadA3 (24-170) pET-15b expression vector DNA. A) PCR reaction mix composition B) Thermocylcer parameters for the PCR reaction.

A

Reagent (final concentration)	**Volume**
MilliQ water	Made to 50 µL
Forward primer (10 µM)	1.5 µL
RbS2 2A Reverse primer (10 µM)	1.5 µL
NadA3 (24-170) pET-15b expression vector DNA (0.2 ng/µL)	2 µL
KAPA HiFi Hot Start Ready Mix (2X stock)	25 µL

B

Thermocycle stage	Number of cycles, Temperature, Time
1	X 1, 95 °C, 2 mins
2	X 30: 98 °C, 20 seconds, 65/70/75 °C, 20 seconds 72°C, 11 mins
3	X 1, 72°C, 11 mins 4 °C, Indefinite

Following the PCR mutagenesis reaction, a 2% agarose gel was then prepared to confirm a successful PCR reaction and separation of the PCR products and confirm. This gel is shown in Figure 2-17.

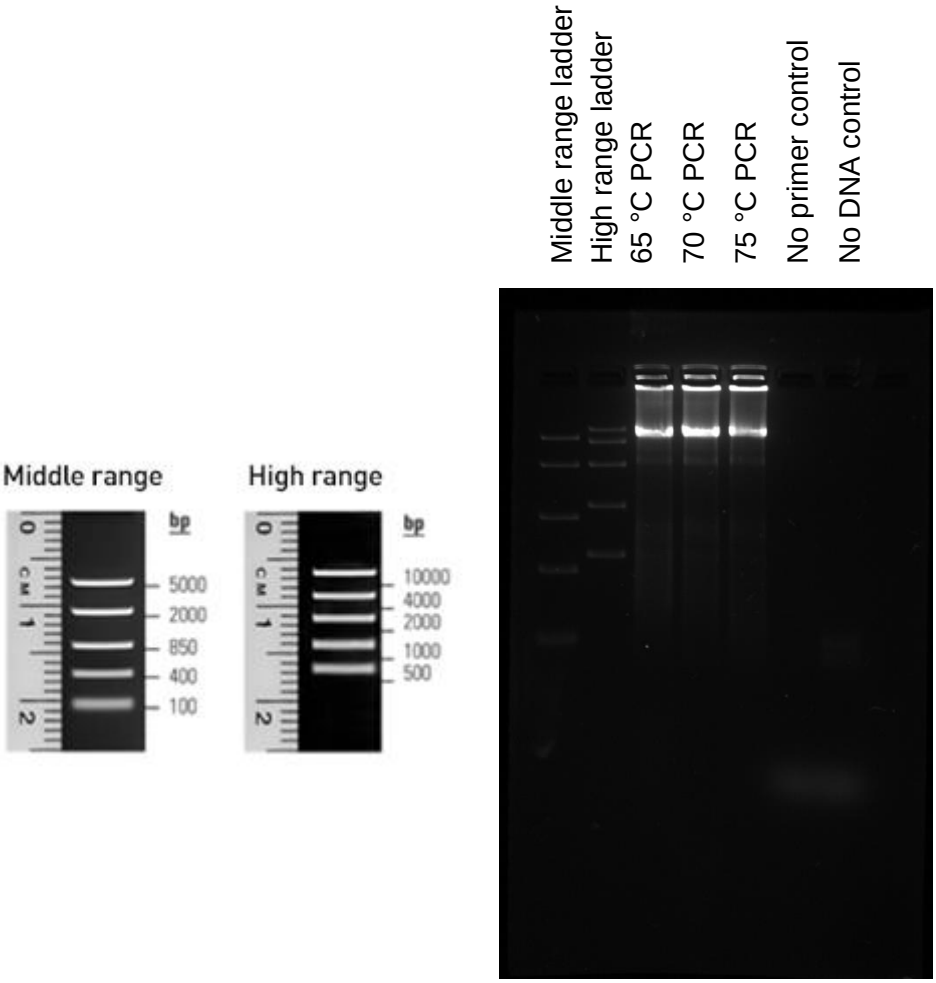

Figure 2-17 2% Agarose gel of the PCR mutagenesis reactions for insertion of the PorA VR2 14 sequence into the NadA3 (24-170) pET-15b expression vector DNA. Two DNA base pair (bp) ladders are used; Middle and High range (ThermoFisher). Loaded to the gel are three reaction mixes tested at different annealing temperatures (65, 70 and 75 °C), as well as two control samples. DNA is visualised using SYBR Safe stain (ThermoFisher).

From Figure 2-17, it can be seen that all three annealing temperatures result in a high yield of DNA, with a dominant PCR product of around 6000 base pairs. The NadA3 (24-170)-encoding pET-15b vector template is around 6000 base pairs; however, the difference between the NadA3 (24-170)-encoding template vector DNA and a vector that has undergone mutagenesis for insertion of the PorA VR2 14 is not great enough to differentiate on this gel. The 70 °C annealing temperature mix was taken through for enzymatic digestion to remove methylated template DNA, leaving just PCR-amplified DNA. This DNA was then transformed into MACH1 *E. Coli*, which resulted

in a good amount of colonies on the transformation plate. Two of these colonies (arbitrarily named colony 1 and 2) were PCR-screened to identify transformation with the pET-15b vector encoding for NadA3-PorA. The resulting 2% agarose gel is shown in Figure 2-18.

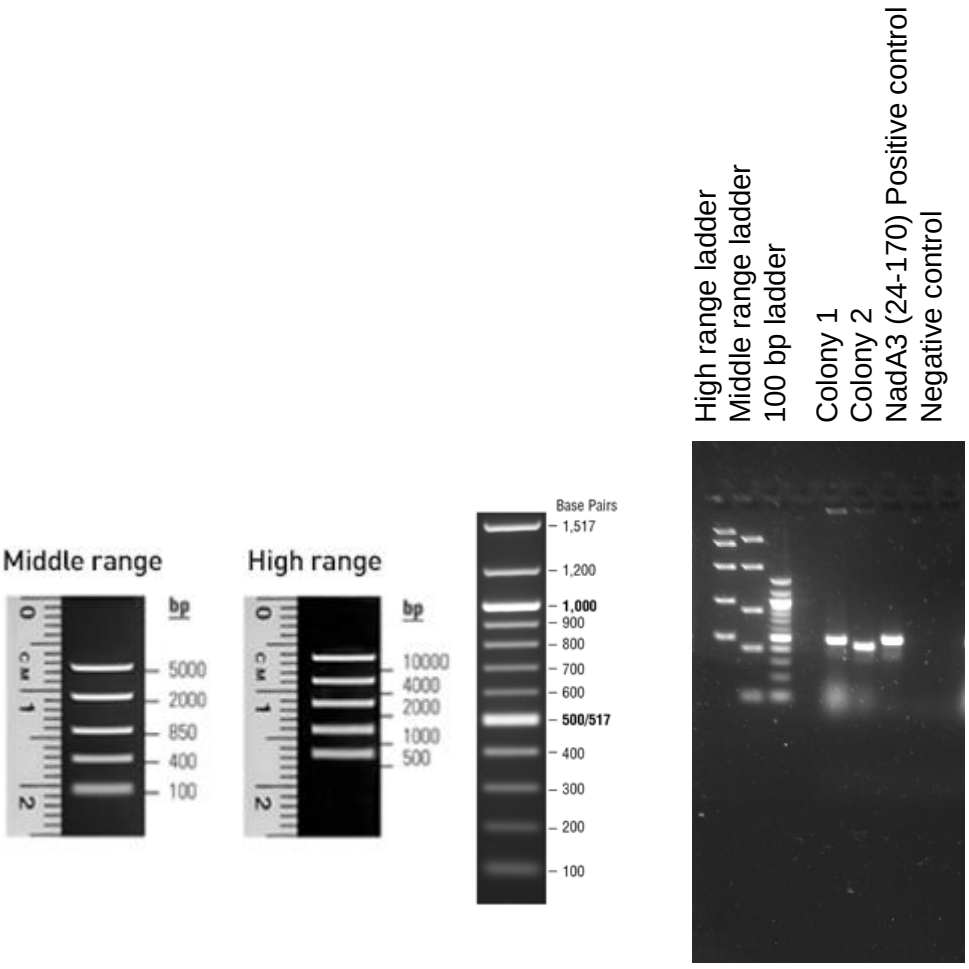

Figure 2-18 2% Agarose gel of the PCR screening reaction to identify colonies transformed with the pET-15b vector encoding for NadA3-PorA. Three DNA base pair (bp) ladders are used; Middle and High range (ThermoFisher) and a 100 base pair ladder (New England Biolabs). Loaded to the gel are DNA from transformation colonies 1 and 2, as well as two control DNA samples; the positive control NadA3 (24-170)-encoding pET-15b vector template and a negative PCR control. DNA is visualised using SYBR Safe stain (ThermoFisher).

From Figure 2-18, the expected base pair length of the NadA3 (24-170) DNA sequence is correctly detected in the positive control sample. If colony 2 and the NadA3 (24-170) positive control are compared, colony 2 shows a prominent band with a lower mass. A lower mass would result from a shorter DNA sequence, which is what

would be expected following mutagenesis for insertion of the PorA VR2 14 loop. As a result of the mutagenesis for insertion of the PorA VR2 14, a DNA sequence is obtained that encodes for the NadA3-PorA protein. The NadA3-PorA differs from NadA3 (24-170) in that 33 amino acid residues have been removed and replaced by the 10 amino acids residues the PorA VR2 14 loop. Colony 1 shows a DNA band with similar mass to that positive control, and therefore is unlikely to contain the PorA VR2 insert. Colony 2 can be confirmed to have been transformed with the pET-15b vector encoding for NadA3-PorA and was therefore selected to have its DNA harvested for transformation into the BL21 *E. coli* protein expressions strain.

A 100 mL expression culture of the BL21 *E. coli* using HTMC media was performed and the resulting cell pellet was lysed using CelLytic Express. This lysate was then applied to a HisGraviTrap to capture the His-tagged NadA3-PorA protein, which was then progressively eluted from the column using an imidazole gradient. Figure 2-19 shows the SDS-PAGE obtained from this affinity purification step.

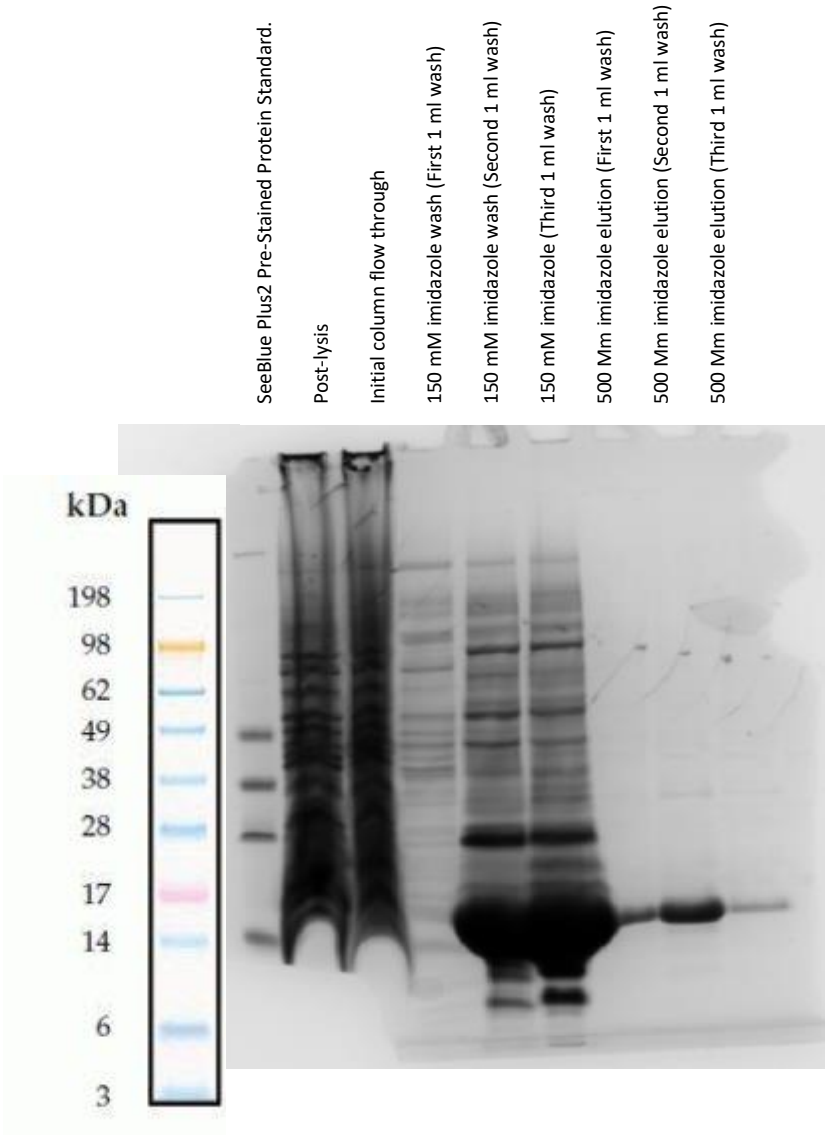

Figure 2-19 SDS-PAGE gel showing samples taken from the affinity purification of the recombinant NadA-PorA protein. On the far left is shown the SeeBlue Plus2 Pre-Stained Protein Standard. 150 mM and 500 mM refer to the concentrations of the successive imidazole elutions used to elute protein from the column.

From the gel displayed in Figure 2-19 , it can be seen that a large amount of a protein with a mass of around15 kDa (in accordance to that of the NadA3-PorA) is observed being eluted off the column early following the washing step with the 150 mM imidazole solution. This is unexpected as the His-tagged NadA-PorA would be expected to be eluted following the higher 500 mM imidazole elution. The apparent elution of the NadA-PorA after the application of the 150 mM imidazole wash could be

explained due to the large amount of protein present challenging the protein retention limit of the HisGraviTrap column.

Following this step, the 1 mL fractions originating from the 150 mM imidazole washes believed to contain large amounts of NadA3-PorA were pooled and concentrated, and then further purified by loading to a HiLoad 16/600 superdex 75 pg size -exclusion column (GE Healthcare). Figure 2-20 shows the size-exclusion chromatogram obtained.

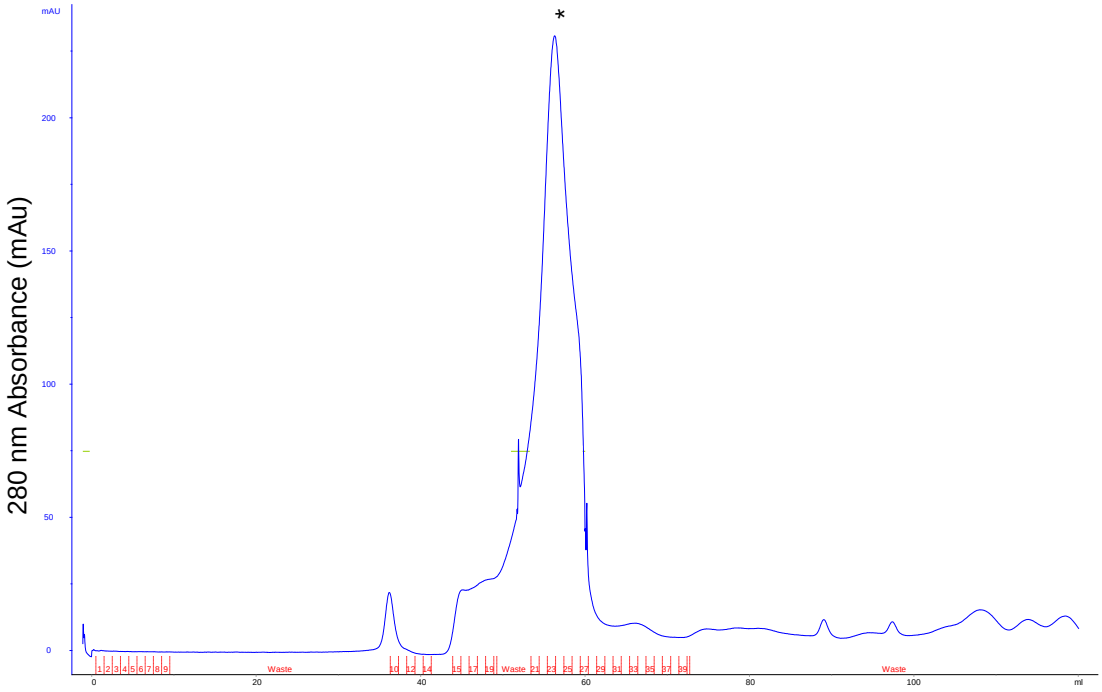

Figure 2-20 SEC Chromatogram obtained during purification of the subunit protein antigen NadA3-PorA. SEC was performed using a HiLoad 16/600 superdex 75 pg column equilibrated in PBS. The peak corresponding to the NadA3-PorA monomer is labelled with *. The x-axis shows the volume passed from the point of sample injection and collected fractions are shown in red.

Comparing the chromatogram obtained for NadA3 (24-170) shown in Figure 2-15 to that obtained here for NadA3-PorA, the dominant peak here has a lower retention volume. This is as expected, as the NadA3-PorA trimer has a mass 9 kDa less than that of the NadA3 (24-170) and so would be expected to have exited the column at a higher retention volume. An SDS-PAGE gel performed following this SEC purification identified fractions 21– 27 as containing the NadA3-PorA protein. These fractions were pooled, concentrated and a BCA assay was performed to confirm the

concentration. A stability gel was performed on the purified NadA3-PorA to compare effect of storage temperature following one month of storage. Samples from the pooled 150 mM wash steps and the SEC-purified NadA3-PorA were loaded to the gel (shown in Figure 2-21).

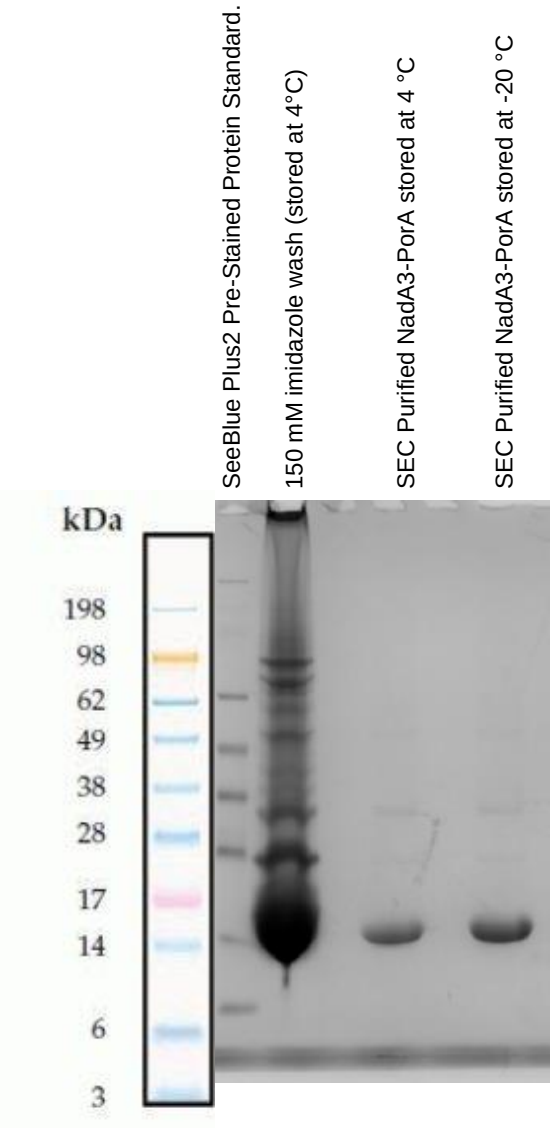

Figure 2-21 SDS-PAGE gel to compare purified NadA3-PorA samples stored at 4 °C or -20 °C for one month. The samples loaded are labelled above the gel.

From the gel shown in Figure 2-21, both the purified NadA3-PorA samples stored at either 4 °C or -20 °C for one month are comparable with no signs of protein degradation; however, protein aliquots used in future assays were derived from -20 °C storage to ensure stability. Optimal storage temperatures are dependent on the

protein being studied, and so performing an SDS-PAGE gel as shown here is one of the practical examples of identifying suitable storage conditions (Raynal et al., 2014).

2.3.10 Purification of the wild-type Ferritin

Another useful control protein is the *H. pylori* ferritin scaffold alone, without the NadA3-PorA appendages. Kanekiyo et al. examined the immunological consequences of deploying a ferritin scaffold for the presentation of influenza hemagglutinin antigens in the nanoparticle system described in the introduction chapter (Kanekiyo et al., 2013). With at least half of the world's population estimated to be infected with *Helicobacter pylori* (Ansari and Yamaoka, 2018), one obvious concern was that pre-existing *anti-H. pylori* antibodies would compromise subsequent immunisations with the hemagglutinin-ferritin nanoparticles. In response to this, studies were performed in which mice were pre-immunised with the *H. pylori* ferritin, where it was found that pre-existing immunity to the ferritin did not result in diminished anti-hemagglutinin responses. Furthermore, in response to concerns that immunisation with a *H. pylori* ferritin scaffold might override immune tolerance and promote autoimmunity, studies in immunised mice found no increase in intracellular staining of $CD4^+$ or $CD8^+$ T-cells in response to murine ferritin peptide stimulation, nor were anti-murine ferritin antibodies found in the sera.

Purified *H. pylori* ferritin in the context of this study would act as a useful tool and control protein for the comprehensive characterisation of the NadA3-PorA-Ferritin nanoparticle, both at an immunological and structural level. An already available in-house construct encoding for the *H. pylori* ferritin scaffold modified to present the surface exposed glycine-serine rich amino acid linkers (that are presented at the surface-trimeric interfaces of the ferritin and form the point of attachment of the NadA3 C-termini) was subsequently expressed and purified. Though the linkers present were a six-residue long linker variant, rather than the four-residue long linker used in the NadA3-PorA-Ferritin, this ferritin scaffold construct was still deemed as an acceptable control. Detailed in this section are two attempts to purify the ferritin scaffold following expression in *E. coli.*

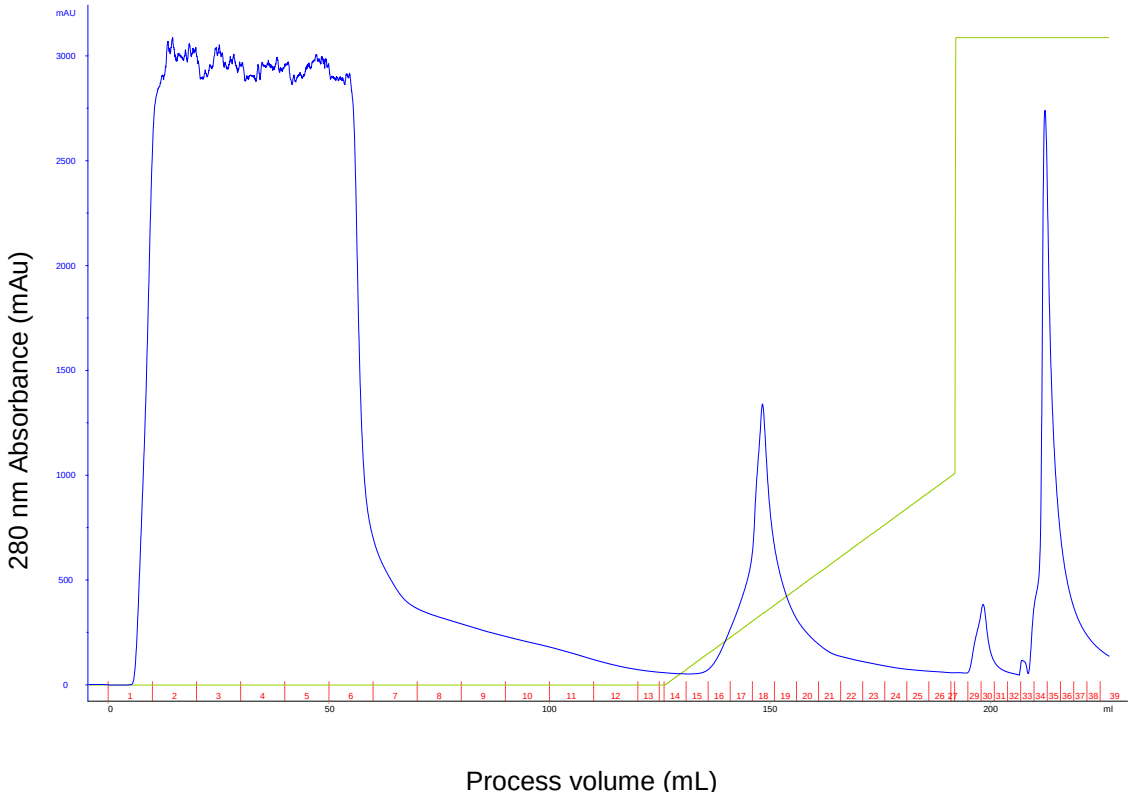

Figure 2-22 Chromatogram for the affinity chromatography purification of wildtype Ferritin. The cell lysate was loaded to a HisTrap HP column and progressively purified by an imidazole gradient, represented by the green line which plateaus at an imidazole concentration of 500 mM. The x-axis shows the volume passed from the point of sample injection and collected fractions are shown in red.

The affinity chromatography purification of the first attempt at purifying wild type ferritin is shown in Figure 2-22, while Figure 2-23 shows the SDS-PAGE performed using collected fractions from the purification. The expected molecular weight of the wild type ferritin monomer is 20 kDa; a band with this size is seen clearly in fractions 34 – 37 which spanned the 500 mM imidazole elution peak. Based on this gel, the fractions were pooled, and concentrated, with this pooled sample represented by the ‘post-IMAC’ sample shown on the gel.

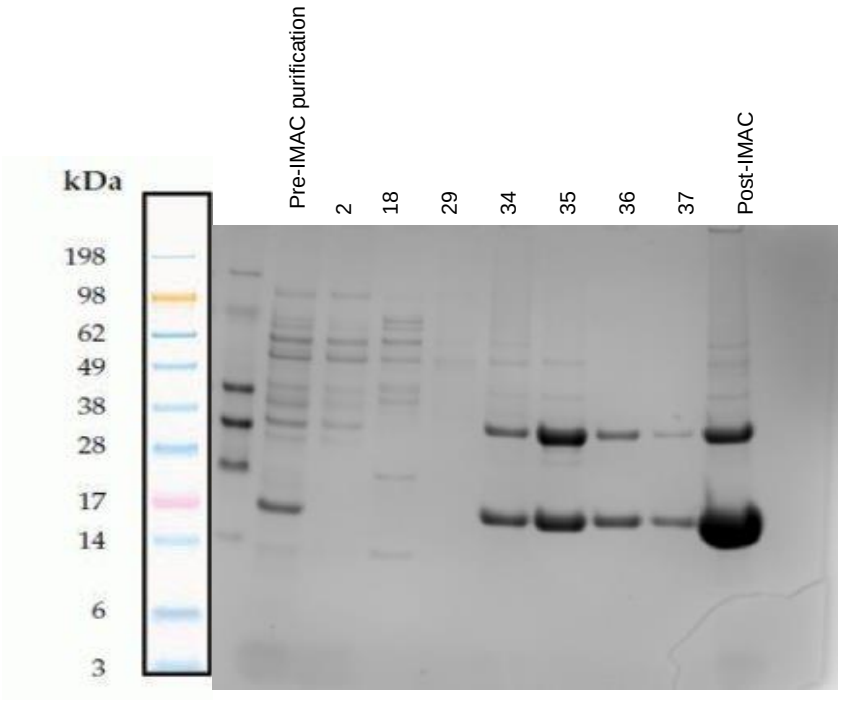

Figure 2-23 SDS-PAGE gel composed of fractions collected from the affinity purification of the wildtype Ferritin nanoparticle. Affinity purification fractions are labelled above the gel. The band at around 20 kDa clearly detected in fractions represents the wildtype ferritin monomer. On the far left of the gel is the SeeBlue Plus2 Pre-Stained Protein Standard.

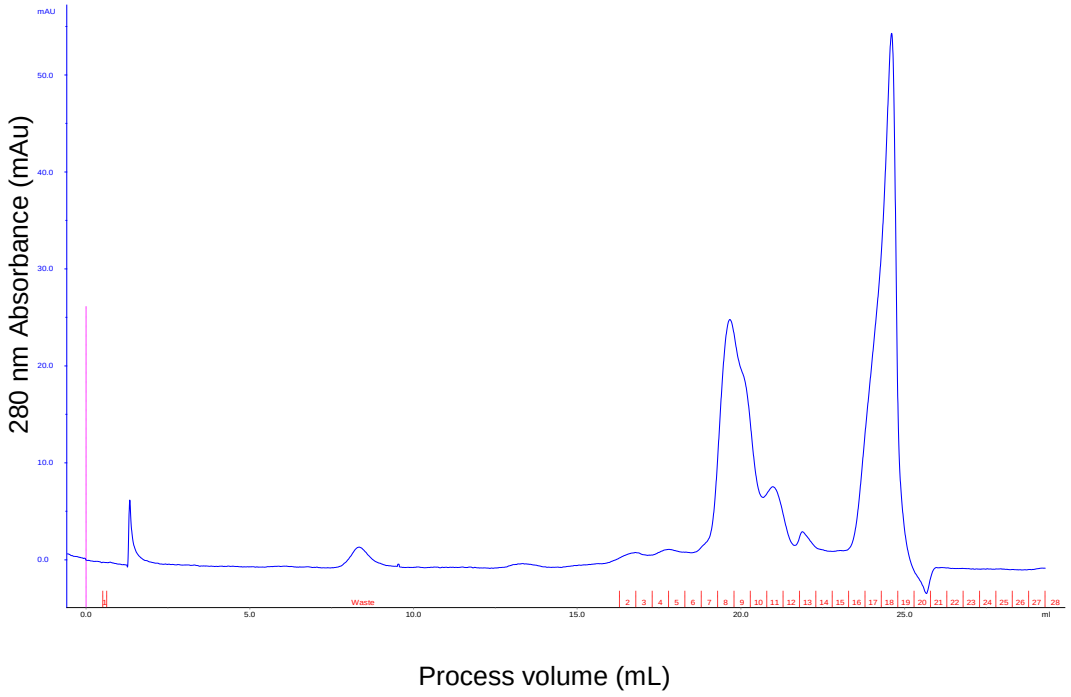

Figure 2-24 SEC chromatogram obtained during purification of the wildtype Ferritin. SEC was performed using a Superose 6 10 /300 GL column equilibrated in PBS (10 mM, pH 7.4). Fractions collected as the run progressed are numbered in red along the x-axis.

From the size-exclusion chromatogram shown in Figure 2-24, no peak with the expected retention time for the ~ 450 kDa ferritin nanoparticle can be seen. The expected retention time would be around 15 mL, however only two main peaks around 20 and 25 mL are seen for smaller species. Indeed, precipitation of the sample was noted during spin-concentration of the sample prior to sample injection. Expression and purification of the ferritin was repeated again and the results are shown in Figure 2-25 and Figure 2-26.

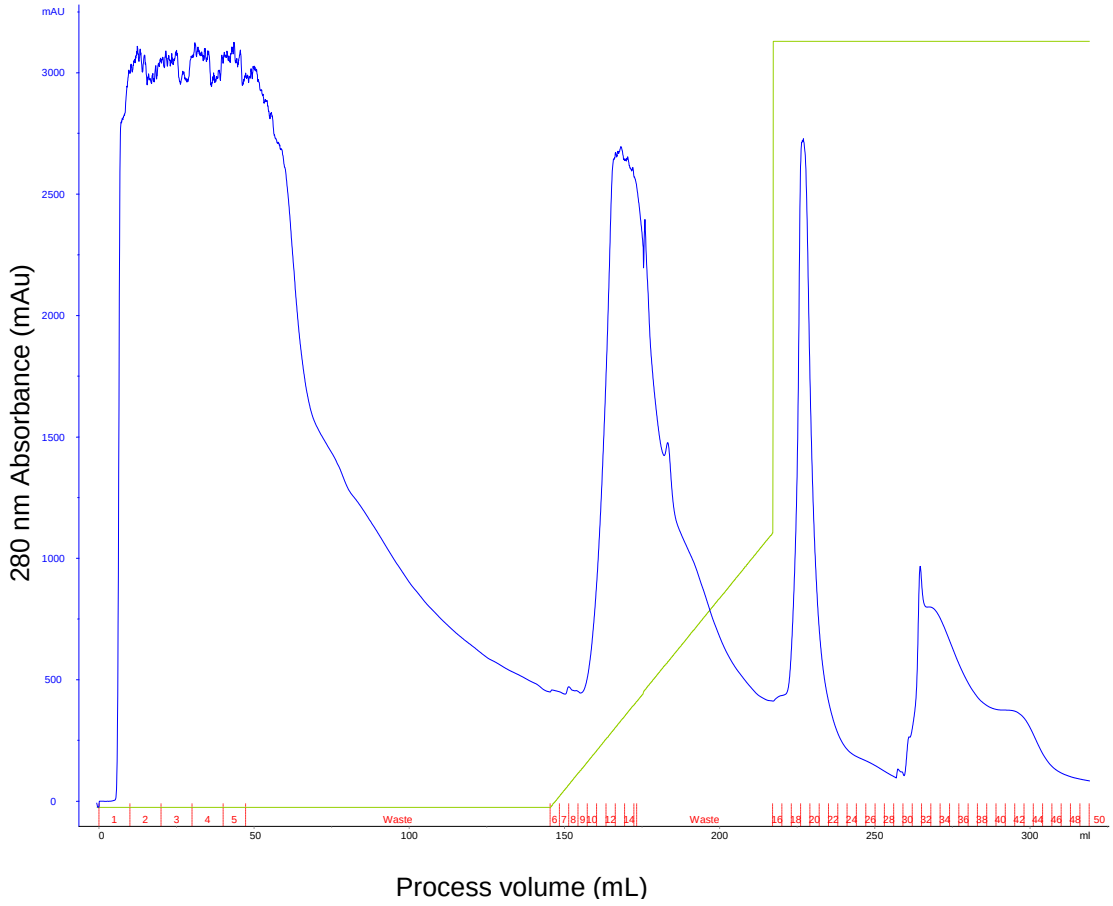

Figure 2-25 Chromatogram for the affinity chromatography purification of wildtype Ferritin. The cell lysate was loaded to a HisTrap HP column and progressively purified by an imidazole gradient, represented by the green line which plateaus at an imidazole concentration of 500 mM. The x-axis shows the volume passed from the point of sample injection and collected fractions are shown in red.

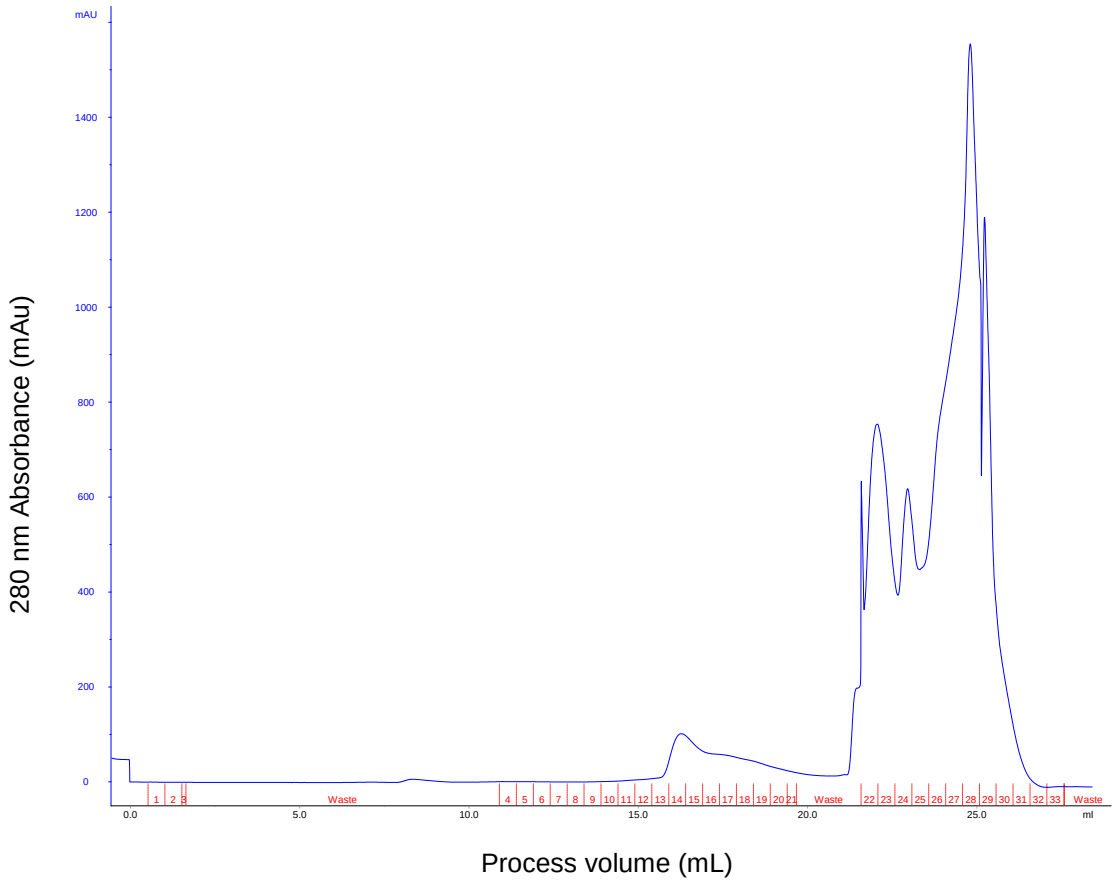

Figure 2-26 SEC chromatogram obtained during purification of the wildtype Ferritin. SEC was performed using a Superose 6 10 /300 GL column equilibrated in 10 mM PBS. Fractions collected as the run progressed are numbered in red along the x-axis.

Figure 2-25 displays the affinity-purification of for the repeated ferritin purification attempt, from which fractions 31-44 were identified by an SDS-PAGE gel as containing a band corresponding to a 20 kDa ferritin monomer. These fractions collected, concentrated and loaded to a size-exclusion column, the resulting chromatogram shown in Figure 2-26. As noted in the previous purification attempt, precipitation was again seen in the spin column during protein concentration for SEC. Again, no major peak with a retention time corresponding to an assembled ferritin nanoparticle is present, but there are peaks again at later retention volumes suggesting smaller, degradative protein species.

Recombinant proteins can be extremely sensitive to solution conditions and can frequently aggregate during the concentration process (Bondos and Bicknell, 2003). Successful purification of *Helicobacteri pylori* ferritin has been reported (Cho et al.,

2009); however, in addition to purification parameter differences, the ferritin attempted to be purified in this work differs in that it is a mutated version (presenting the six residue amino acid residue linkers on its surface), and so may also be a factor in its aggregation potential on concentration.

2.3.11 Insertion of the PorA VR2 loop may impact on NadA3 epitopes as revealed by immunogold negative stain electron microscopy

This recombinant NadA3-PorA antigen displayed on the ferritin surface contains immunogenic epitopes deriving from both the NadA3 and the PorA VR2 loop epitope. To understand how these epitopes are presented when displayed as part of this nanoparticle system, a series of antibody-based experiments was performed.

Human monoclonal antibodies elicited from vaccination with the Bexsero vaccine have been isolated and their epitopes characterised (Giuliani et al., 2018). In the experiments that follow, a selection of these monoclonal antibodies was used. Figure 2-27 shows the epitopes on the NadA3 recognized by these antibodies.

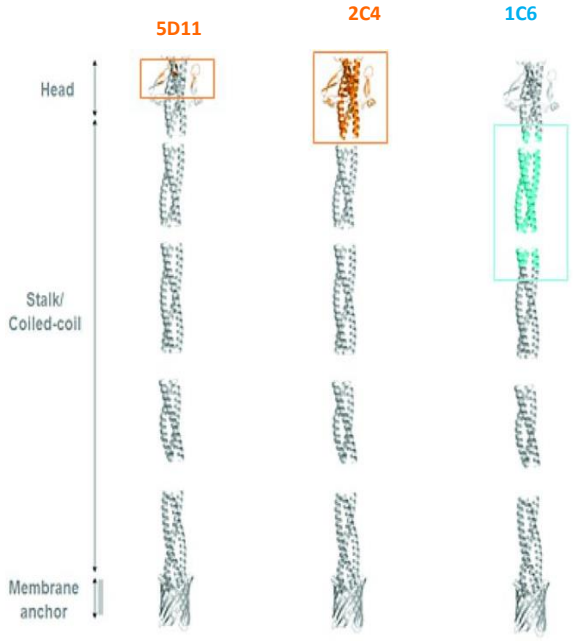

Figure 2-27 Diagram showing the mapped epitopes for the anti-NadA3 antibodies 5D11, 2C4 and 1C6. In this diagram, the full length NadA3 is displayed however in this thesis only the truncated NadA3 (24-170) is considered. Orange is used to highlight epitopes predominately mapped to the NadA3 N-terminal head region recognised by the antibodies 5D11 and 2C4, whereas blue is used for predominantly stalk epitopes. It should be noted that 1C6 recognizes an epitope mapped to the coiled-coil stalk, but also part of the N-terminal head region. This diagram is adapted from Giuliani et al. 2018.

The epitope of antibody 5D11 has been mapped predominantly to the wing-like folds in the NadA3 N-terminal head, whereas the antibody 2C4 which recognises an epitope mapped to both the head region and part of the stalk (mapped residues 16-107). Antibody 1C6 on the other hand recognises an epitope that has been mapped predominantly to the stalk (mapped residues 100 – 170 (Giuliani et al., 2018).

Immunogold negative stain electron microscopy was performed to analyse the presentation of NadA3 epitopes on the NadA3-PorA-Ferritin nanoparticle. In this immunolabelling technique, gold-labelled secondary antibodies are used for detection of primary antibody binding to epitopes. In a series of experiments, binding by the primary antibodies 1C6 and 2C4 was detected by a gold-labelled anti-human IgG secondary antibody. Figure 2-28 and Figure 2-29 display a selection of the micrographs obtained from these immunogold EM experiments.

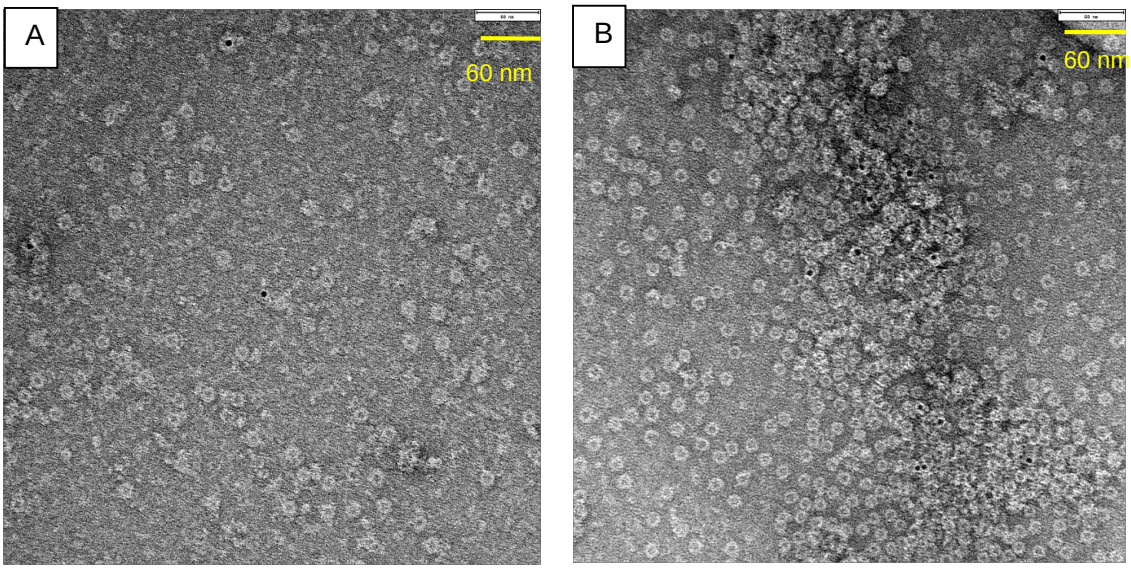

Figure 2-28 Immunogold EM micrographs for the detection of the anti-NadA3 antibody 1C6 binding to **A)** Wild type NadA3 (24-170) -Ferritin **B)** NadA3-PorA-Ferritin nanoparticle. Binding by the 5 nm gold-labelled anti-human secondary antibody can be seen as black dots on the micrographs. A 60 nm scale bar is shown in the top right corner of each micrograph.

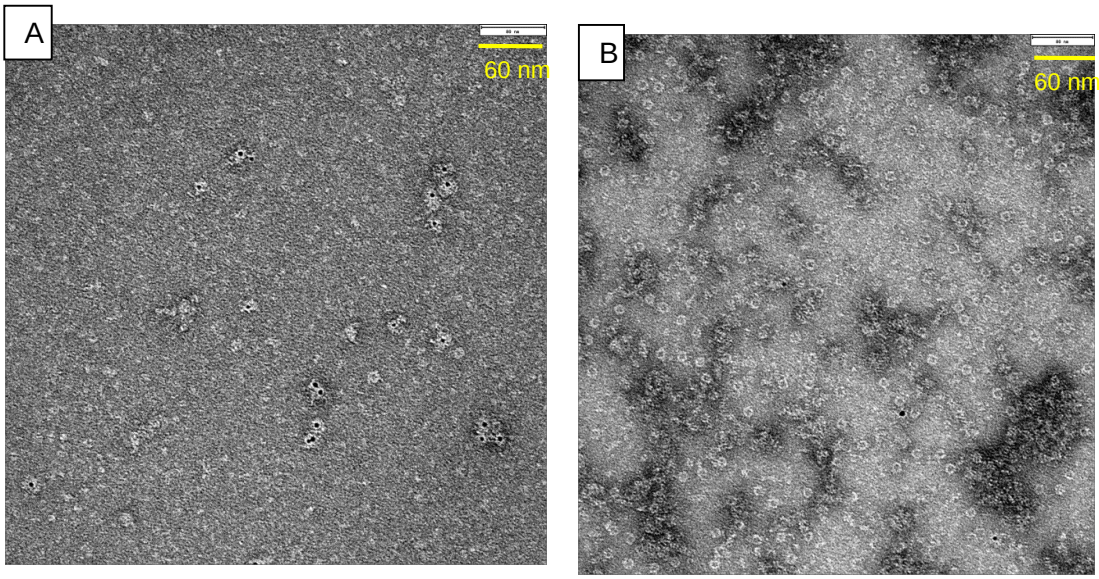

Figure 2-29 Immunogold EM micrographs for the detection of anti-NadA3 antibody 2C4 binding to **A)** Wild type NadA3 (24-170) -Ferritin **B)** NadA3-PorA-Ferritin nanoparticle. Binding by the 5 nm gold-labelled anti-human secondary antibody can be seen as black dots on the micrographs. A 60 nm scale bar is shown in the top right corner of each micrograph.

In the micrographs, the black dots represent electron density deriving from the gold particles conjugated to the secondary antibodies. From Figure 2-28, for both NadA3 (24-170)–Ferritin and NadA3-PorA-Ferritin minimal binding by the 1C6 antibody is

observed. For antibody 2C4, shown in Figure 2-29, there is more detection of antibody binding for the NadA3 (24-170)-Ferritin compared to NadA3-PorA-Ferritin.

If the binding by the antibodies to their NadA3 (24-170)-Ferritin is considered, the lack of detectable binding by the antibody 1C6 compared to 2C4 could be due to steric constraints. The secondary antibody 2C4 recognises an epitope mapped to the NadA3 head, whereas 1C6 recognises epitopes predominantly mapped to the NadA3 stalk (Giuliani et al., 2018). Detection of antibody binding requires that the secondary antibody (labelled with the 5 nm gold particle) binds to the primary antibody. Based on the NadA3 (24-170)-Ferritin structure, the NadA3 head is far more accessible to binding by the primary antibody than the NadA3 stalk. The secondary antibody is therefore also less sterically hindered in binding to the primary antibody bound to the NadA3 head. This could explain why in the case of NadA3 (24-170)-Ferritin, the degree of detection of antibody 2C4 binding to its epitope is far greater than the binding detected for the antibody 1C6.

In the case of minimal recognition of binding by 2C4 to NadA3-PorA-Ferritin compared to NadA3 (24-170)-Ferritin, the creation of the NadA3-PorA-Ferritin saw removal of residues from the NadA3 wing-like folds in its N-terminal head region to accommodate the PorA VR2 14 epitope. Since 2C4 recognises an epitope mapped to the head region, it's likely that changes made to insert the PorA VR2 have an impact on the exposure and/or proper folding of the epitope.

2.3.12 Investigating NadA3 epitope presentation by SPR

As a further method to investigate epitope presentation, Surface Plasmon Resonance (SPR) experiments were performed in which a panel of anti-NadA3 antibodies were assayed for binding against a range of NadA3 epitope-containing protein antigens. The panel of antibodies used includes those described in 2.3.11, with the addition of an extra antibody 7F11 (which has been mapped to recognise residues 95–170 predominantly in the NadA3 stalk region) (Giuliani et al., 2018). In the same paper, SPR was a key technique used to measure the binding affinities of the isolated human monoclonal antibodies.

SPR is an optical technique suited for detecting binding interactions between two different proteins. One of the proteins, also known as the flow-through analyte, is injected and flows over the sensor chip which has the second protein of interest

immobilized on its surface. Any binding interactions will produce a small change in the refractive index at the gold surface (Drescher et al., 2009). Response units (RU) describe this change in refractive index and plotting the RU versus time produces a sensogram from which binding affinities can be calculated following fitting to an appropriate kinetic model (Nguyen et al., 2015).

A Biacore T200 SPR instrument was used to measure antibody binding to the antigens NadA3-PorA-Ferritin, NadA3 (24-170) -Ferritin and NadA3 (24-170). In the first experiment, the antigen NadA3-PorA-Ferritin or NadA3 (24-170) was immobilized onto a nitrilotriacetic acid (NTA) sensor chip (GE Healthcare); the surface of this chip is adapted to bind his-tagged proteins through chelation to Ni2+, which itself is chelated to the surface of the chip by the NTA. Following confirmation of antigen immobilsation to the surface of the chip, the antibodies were injected over the surface of the chip and binding interactions were measured. The sensorgrams obtained for these two antigens after injection with the antibodies are displayed in Figure 2-30.

A)

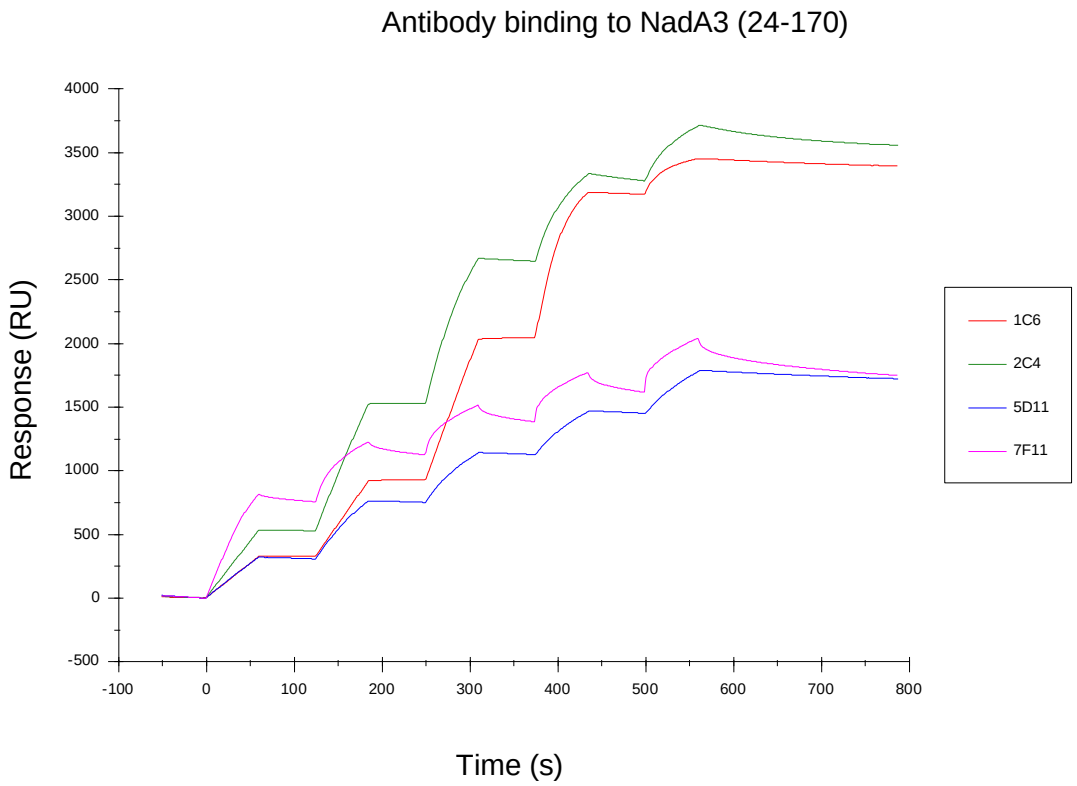

B)

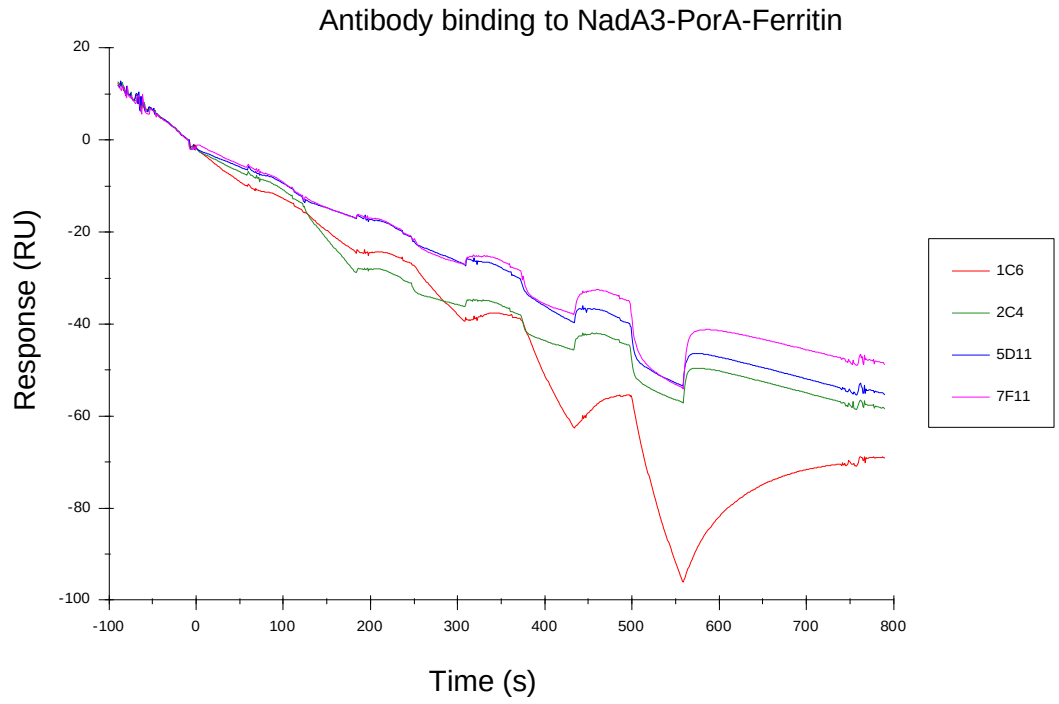

Figure 2-30 Sensorgram profiles of the SPR analysis performed for a panel anti-NadA3 antibodies binding to NadA3-epitope containing antigens immobilised to the surface of the sensor chip. In **A)** NadA3 (24-170) is immobilised and in **B)** NadA3-PorA-Ferritin is immobilised to chip surface. To the right of each sensorgrams is the panel of antibodies used, with each colour coded.

Figure 2-30 shows that though binding to the NadA3 (24-170) trimer by all the tested antibodies was detected as indicated by the positive signals obtained, no binding by the same antibodies is detected in the case of the NadA3-PorA-Ferritin antigen (a negative change in RU is obtained for all the antibodies). This was postulated as a result of steric hindrance on the chip surface arising from the ferritin nanoparticle, which would prevent adequate epitope presentation to antibodies.

To circumvent this potential steric hindrance, a second SPR experiment was performed in which the antibodies, rather than the antigen, were immobilized to the surface of the chip. For the second SPR experiment, the antibodies 1C6, 2C4 and 5D11 were immobilised to a CM-5 sensor chip (GE Healthcare) via an amine-coupling reaction using a Human Antibody Capture Kit (GE Healthcare) and the antigens NadA3-PorA-Ferritin, NadA3 (24-170)-Ferritin and NadA3 (24-170) were injected over the chip. Figure 2-31 shows the SPR sensorgrams obtained.

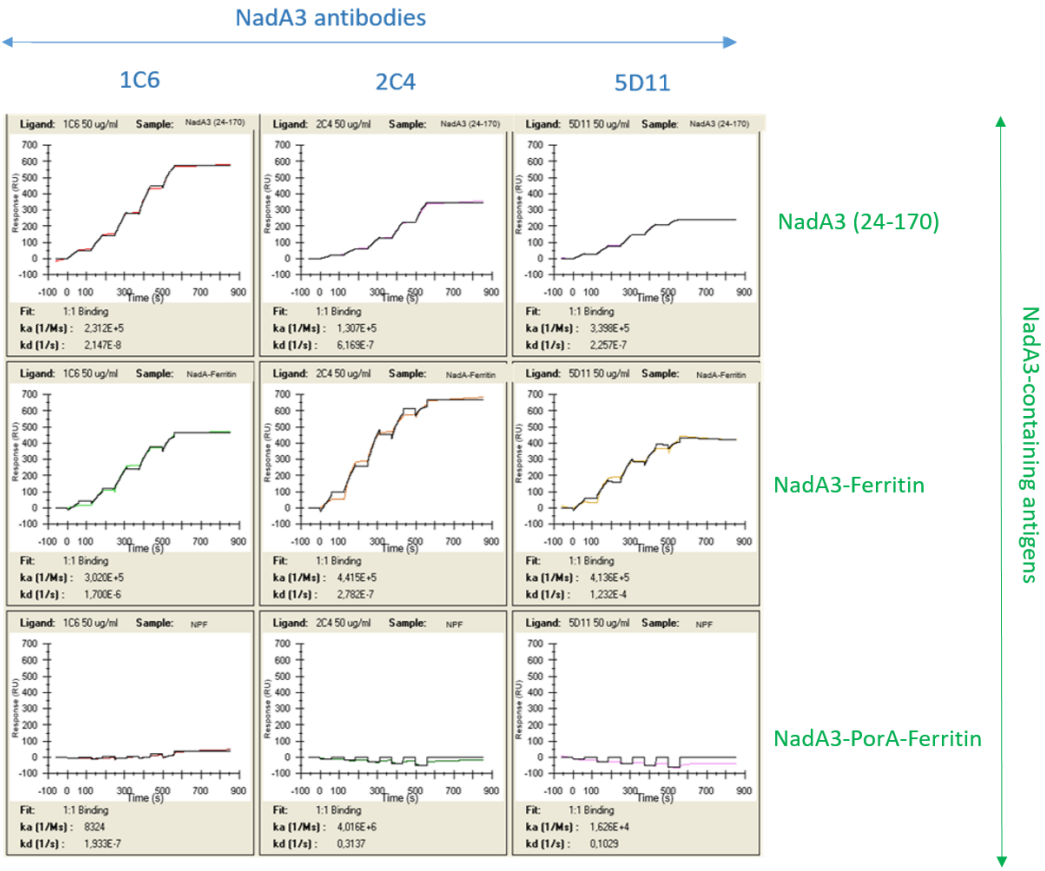

Figure 2-31 Sensorgram profiles of the SPR analysis performed using a panel of anti-NadA3 antibodies. The antibodies 1C6, 2C4 and 5D11 are across the columns as shown by the blue arrow and the antigens NadA3 (24-170), NadA3-Ferritin and NadA3-PorA-Ferritin go down in rows as shown by the green arrow. In the sensorgrams, the black line represents the response obtained and the red, green, orange or purple lines are for fitting to a with the 1:1 Langmuir binding model in order to obtain the individual association (k_a) and dissociation ($k_{d)}$ kinetic rate constants (shown in the grey legends beneath each sensorgram).

As shown in Figure 2-31, binding by NadA3-Ferritin and wildtype-NadA3 (24-170) is observed for all the antibodies. However, very little binding is observed by NadA3-PorA-Ferritin to any of the antibodies recognizing NadA3; 1C6 (an antibody mapping to the stalk of NadA3) shows the higher affinity compared to the two anti-NadA3 head antibodies 2C4 and 5D11. The lack of binding by antibodies 2C4 and 5D11 is unsurprising, as insertion of the PorA VR2 epitope into the NadA3 N-terminal head would be expected to abrogate epitope presentation in this region. The lack of detectable binding for 1C6 can be explained by the discovery that the epitope for this antibody has been characterized to map to residues in the region 100-170 of the NadA3 stalk (Giuliani et al., 2018), very close to the base of the NadA3 head region (as confirmed by its solved crystal structure (Liguori et al., 2018)) – thus there is the

possibility that the PorA insertion can affect the epitope conformation and lead to less recognition by the antibody 1C6.

2.3.13 Presented NadA3 epitopes on NadA3-PorA-Ferritin bind polyclonal anti-NadA3 antibodies

The SPR results in section 2.3.12 revealed that insertion of the PorA VR2 epitope had an impact on epitopes recognised by a panel of anti-NadA3 monoclonal antibodies. Though these epitopes were negatively affected by the PorA VR2 insertion, the possibility remained that other NadA3 epitopes on the NadA3-PorA-Ferritin retained their ability to bind their cognate antibodies. To examine this possibility, an SBA (Serum Bactericidal Assay) was performed which would in theory expand the pool of anti- NadA3 (24-170) antibodies available to assay.

The SBA assay measures the ability of circulating antibodies to lyse meningococci in the presence of complement, via the classical pathway of complement activation. Licensure of meningococcal vaccines, including Bexsero, has been based on the results obtained from the SBA assay as a surrogate of vaccine efficacy, where bactericidal titres obtained from immunisation sera are used to define the correlate of protection (McIntosh et al., 2015). The assay requires active complement, either intrinsic to the serum being tested or added in from an exogenous source. Due to sourcing issues associated with human complement, baby rabbit complement is often used as an approved source of complement.

As an indirect way to assess NadA3 (24-170) epitope presentation on the NadA3-PorA-Ferritin nanoparticle, a competitive inhibition SBA assay was performed. In this assay, sera obtained from mice immunized with NadA3 (24-170) was pre-reacted separately with a range of NadA3 (24-170) containing antigens, including the NadA3-PorA-Ferritin. A source of baby rabbit complement was then added and then the reaction mixture reacted with a MenB stain, BZ83, which highly expresses NadA3 on its surface.

The rationale for this competitive inhibition SBA is that addition into the sera of an antigen optimally presenting NadA3 epitopes will see the ‘sequestering away’ of anti-NadA3 antibodies present in the sera. This will result in a reduction in the bactericidal titre as there are less bactericidal antibodies present in the sera to engage in

complement-mediated killing of meningococci. Table 2-2 shows the results of the competitive inhibition SBA.

Table 2-2 Results of a competitive inhibition SBA assay in which sera obtained from mice immunized with NadA3 (24-170) was pre-reacted with a range of antigens and the resulting bactericidal titre measured. A titre of <4 is negative for bactericidal killing, whereas a titre >4 is an established correlate of protection. * signifies a bacteriostatic titre, defined as a titre that results in a colony count >50% of the negative control. The obtained titre for the NadA3-PorA-Ferritin is indicative of anti-NadA3 antibodies being sequestered away by binding to NadA3 epitopes optimally presented on the NadA3-PorA-Ferritin nanoparticle.

Antigen	SBA titre
Sera alone	128
NHBA (negative control protein)	512
Wild type Ferritin	256*
NadA3	<4
NadA3-Ferritin	<4
NadA3-PorA-Ferritin	<4

The results in Table 2-2 show that the negative control antigens (immunized sera alone, NHBA and wild type ferritin - obtained from the 'post-IMAC' sample detailed in Figure 2-23.) all resulted in high bactericidal titres (>4) as expected. This is because the anti-NadA3 antibodies are still available in the sera to engage in complement-mediated killing.

When the sera are pre-reacted with antigens containing NadA3 epitopes, in all cases the bactericidal titre becomes negative (a titre of <4 is negative for bactericidal killing) in this SBA. This is as expected and is indicative of anti-NadA3 (24-170) antibodies being sequestered away by binding to optimally presented NadA3 (24-170) epitopes

and so becoming unavailable to engage in the killing of meningococci. The fact that pre-reaction with NadA3-PorA-Ferritin gives a negative titre is a useful result, as the SPR data presented in section 2.3.11 suggested that NadA3 (24-170) epitope presentation on the NadA3-PorA-Ferritin was compromised by the insertion of the PorA VR2. However, that assay made use of a very limited antibody panel, whereas in comparison the sera here is polyclonal and so contains a wider pool of anti-NadA3 antibodies. The results obtained here suggest that other NadA3 epitopes are optimally presented by the NadA3-PorA-Ferritin particle.

In addition, a FACS assay was also performed to confirm that the polyclonal mouse anti-NadA3 (24-170) serum used in the competitive FACS contains anti-NadA3 antibodies. In order to do this, two NadA3 expressing MenB strains BZ83 and 5/99, as well as a NadA3 knockout version of strain 5/99, were tested for their ability to bind anti-NadA3 (24-170) antibodies present in the sera. Figure 2-32 displays the result of this assay.

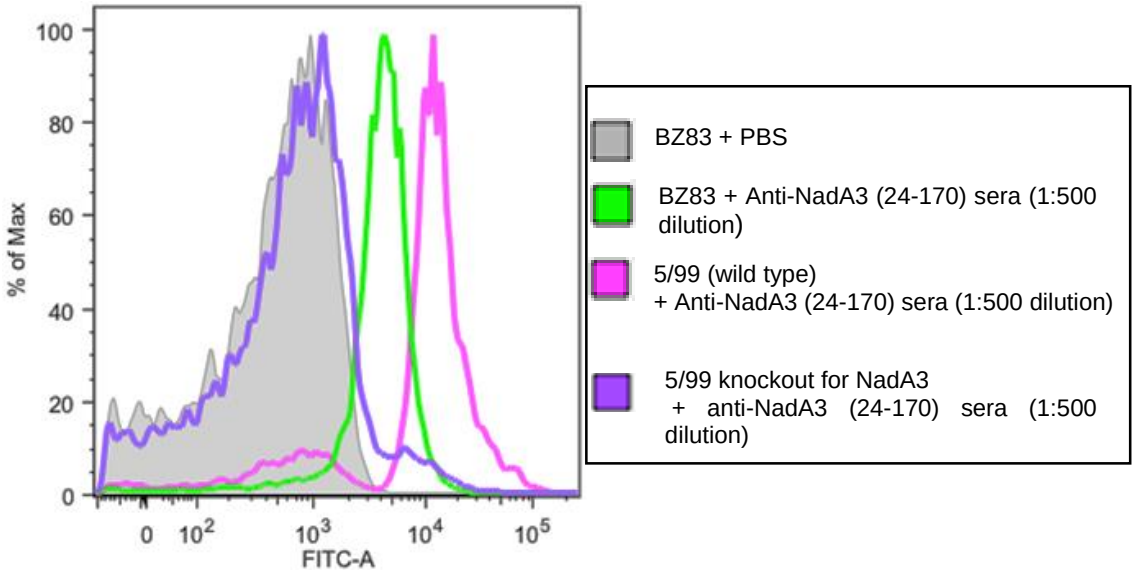

Figure 2-32 Histogram depicting polyclonal anit-NadA3 (24-17) immunisation sera binding to surface exposed NadA3 on three different MenB strains. Four reaction mixes were assayed (shown color-coded in the legend to the right), including one control reaction (using PBS in place of sera) with the other three comprising three different strains of MenB challenged with the polyclonal sera. Primary antibody binding to NadA3 was detected by binding of a FITC-labelled secondary antibody. The FITC-A fluorescence intensity (x-axis) is plotted against the % of maximum number of cells counted (y-axis).

From the Figure 2-32 , the anti-NadA3 (24-170) antibodies can be seen to bind to only the NadA3-expressing MenB strains BZ83 and wildtype 5/99. Confirmation of anti-NadA3 antibodies in the sera can be ascertained based on the fact that the NadA3-

knockout of the 5/99 strain results in a large decrease in the detection of antibody binding. The use of flow cytometry to identify antibody binding has been used previously, with Giuliani et al. using flow cytometry to confirm vaccine-induced human antibody binding to native NadA3 on the surface of MenB bacteria (Giuliani et al., 2018).

2.3.14 FACS titration assay to investigate specificity of the commercially acquired anti-PorA VR2 14 antibody

The NadA3-PorA recombinant antigen on the surface of the ferritin nanoparticle contains epitopes from two immunogenic antigens expressed on the surface of MenB. Experiments described thus far focused on examining how NadA3 epitopes are presented in this nanoparticle system. Attention now focuses on the small 10 residue loop derived from the VR2 epitope of the porin protein PorA.

A series of experiments were planned to examine antibody recognition of this epitope. However, in this case an antibody recognizing the PorA VR2 14 variant was not available in-house, therefore a commercially available antibody was sourced from NIBSC ('Anti-Meningococcal Serosubtype P1.14 Monoclonal Antibody', NIBSC code: 03/142').

To confirm the specificity of this commercially acquired PorA antibody, a FACS titration assay was performed. The titration FACS assay tested the ability of the PorA VR2 14 antibody to recognize PorA VR2 epitopes expressed on a panel of MenB strains; these selected strains are displayed in Table 2-3. These strains were selected based on their PorA VR2 sequences; beginning with strain UK320 that expresses a PorA with the desired VR2 14, then moving onto strains with diverging sequence similarity to the VR2 14, with strain NZ98/254 effectively a knockout (based on its lack of sequence similarity) and functioning as the negative control in this experiment.

The failure to validate the specificity of commercially-acquired antibodies has been cited has one reason for irreproducibility in the life sciences (Schonbrunn, 2014). The use of knockout controls for a specific antigen is regarded as one of the more stringent controls to assess antibody specificity.

Table 2-3 - The panel of MenB strains tested in the FACS titration assay. The VR2 type expressed by each strain is shown alongside their respective amino acid sequences.

Tested MenB Strain	PorA VR2 type	VR2 amino acid sequence
UK320	14	YVDEKKMVHA
M07-0240852	14-6	YVDEKQVSHA
NM117	9	YVDEQSKYHA
NZ98/254	4	HVVVNNKVATHVP

This plate-based assay was performed by challenging the above bacteria with the PorA VR2 14 antibody (titrated over a range of final concentrations ranging from 1 µg/mL to 40 µg/mL) and then a FITC-A secondary antibody was used to detect this interaction by flow cytometry. Figure 2-33 shows the flow cytometry results obtained for each MenB strain.

UK320:

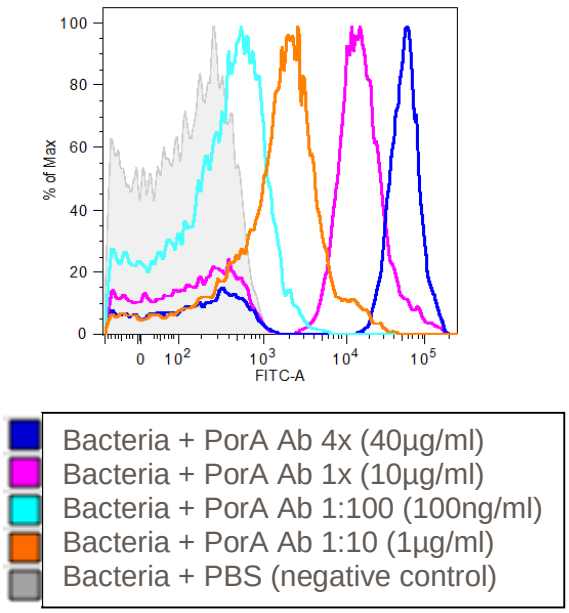

M07-0240852:

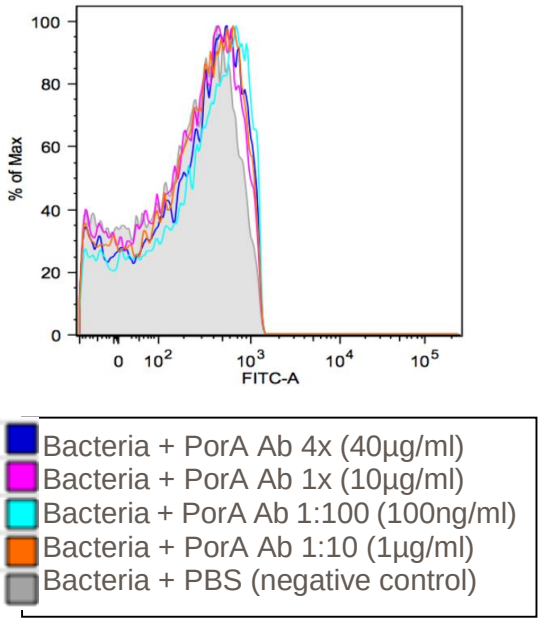

NZ98/254:

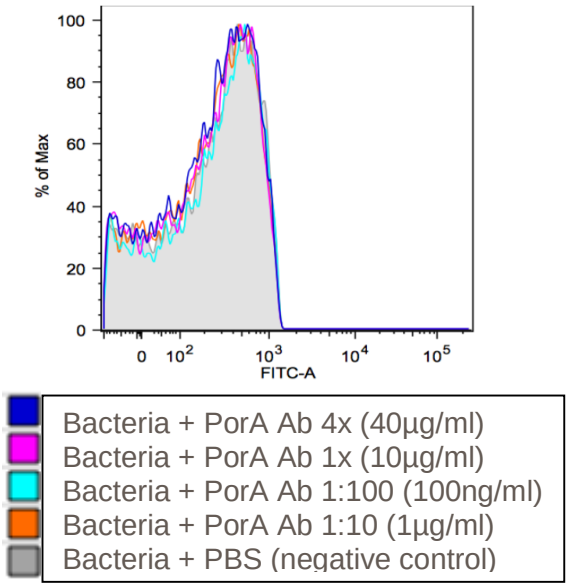

NM117:

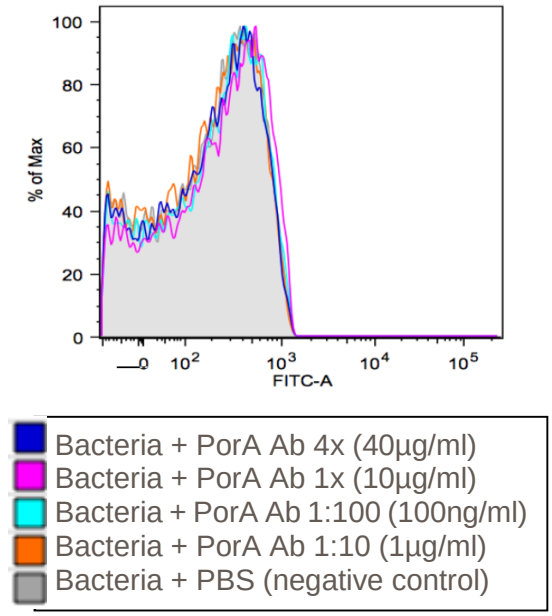

Figure 2-33 - Histograms obtained from the FACS titration experiment for PorA VR2 14 antibody against a panel of MenB strains. The FITC-A fluorescence intensity (x-axis) is plotted against the maximum number of cells counted (y-axis). The MenB strain assayed is indicated in the top left corner above each plot. The boxed legend below each histogram describes each colour coded reaction mix (each of which contains the PorA antibody (Ab) to a different final concentration).

From the FACS results shown in Figure 2-33, it is clear that the only strain that the anti-PorA antibody binds to is strain UK320 (the strain expressing the PorA with the VR2 14 epitope). As the tested concentration of the antibody increases, there is an increase in detected fluorescence as compared to the background (the PBS control) as expected. It is noted that even at the highest tested antibody concentration (40

µg/mL), there is a population of cells (towards the left side of the histogram) that are not bound by antibody. Though this population of cells decreases as the antibody concentration increases, saturating conditions with the antibody concentrations assayed are not reached – this is important to consider for an assay to be detailed in 2.3.15. For all the other MenB strains that are negative for expression of the PorA VR2 14 epitope, no binding by the PorA antibody to the bacteria is detected. Binding to strain M07-0240852 for example, which bears a PorA VR2 sequence that differs by just three amino acids shows complete abolishment of the PorA VR2 14 antibody binding. Similar VR2 analyses have been performed in the past, one example being by Martin et al who investigated the PorA specificity of SBA responses. In that study, they found that deletion of amino acids within the VR2 epitope or replacement of the epitope though genetic exchange enabled strains to resist complement-mediated lysis by vaccine-induced antibodies (Martin et al., 2006). From these results, the specificity of the commercially-acquired PorA antibody for the VR2 14 epitope can be confirmed.

2.3.15 Competitive inhibition FACS experiment to assess PorA VR2 14 epitope presentation by the NadA3-PorA-Ferritin nanoparticle

Following on from the confirmation of the PorA antibody specificity as demonstrated by the experiment in section 2.3.14, assays to examine the PorA epitope presentation on the NadA3-PorA-Ferritin could be performed. A competitive inhibition FACS assay was performed using a similar rationale as described for the competitive inhibition SBA assay in section 2.3.13. In this experiment, MenB bacteria were challenged with a mixture of the PorA antibody pre-reacted with PorA VR2 14-containing antigens. The PorA antibody would bind to presented VR2 epitopes and therefore be unavailable for binding to the bacteria, and so a reduction in the fluorescence would be seen.

Table 2-4 shows the two MenB strains selected, both of which were used in the FACS titration assay described in section 2.3.14. The strain UK320 was selected on the basis that the antibody recognizes the PorA VR2 expressed by this strain, while the VR2 expressed by NZ98/254 was shown to be negative for antibody recognition and so therefore acts as a negative control in the experiment.

Table 2-4 – The panel of MenB strains tested in the competitive inhibition FACS titration assay using the anti-PorA 14 antibody. The variable region 2 (VR2) sequence of each strain is shown.

Tested MenB Strain	PorA VR2 epitope	VR2 amino acid sequence
UK320	14	YVDEKKMVHA
NZ98/254	4	HVVVNNKVATHVP

In this plate-based experiment, the bacteria were added to reaction mixtures containing the PorA antibody that had been pre-reacted overnight with the antigens. The final antibody concentration of the reaction was selected based on the result obtained in FACS titration assay (section 2.3.14) and was equivalent to a 10 µg/mL concentration. The samples were then analysed by FACS, with Figure 2-34 showing the histograms obtained.

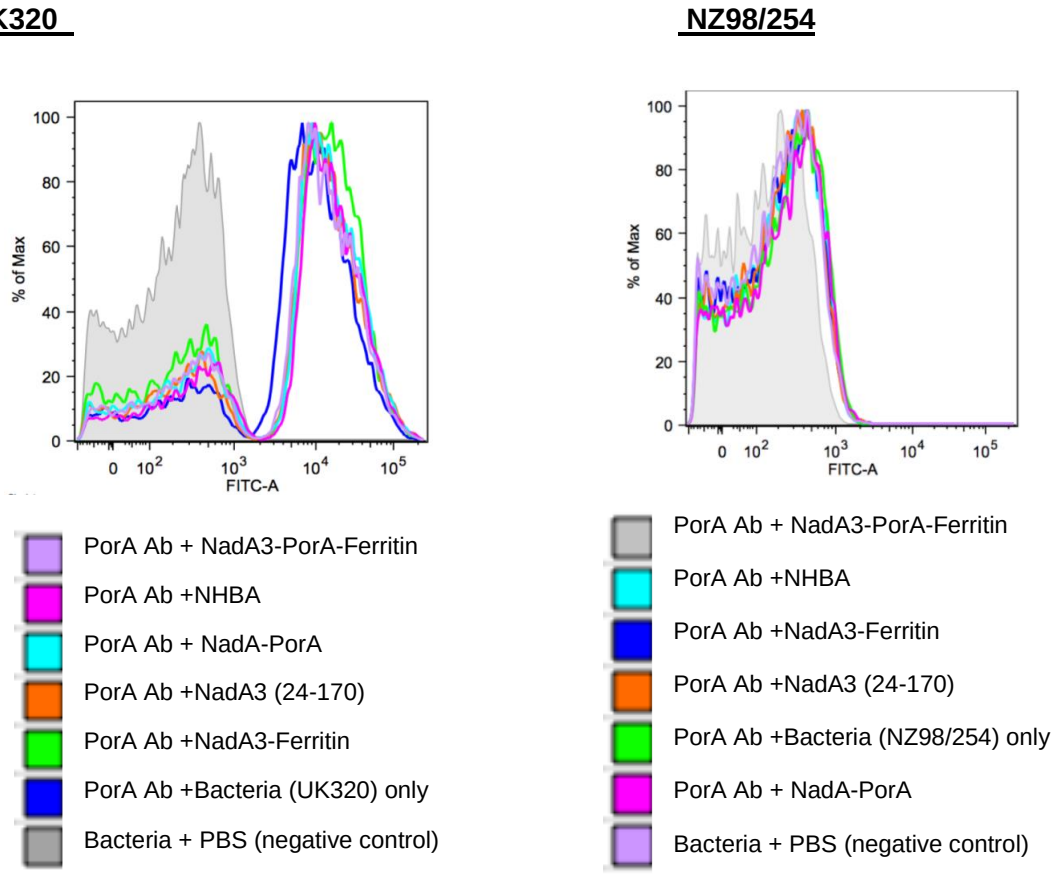

Figure 2-34 Histograms obtained for competitive inhibition FACS experiment to assess PorA VR2 14 epitope presentation by the NadA3-PorA-Ferritin nanoparticle. The FITC-A fluorescence intensity (x-axis) is plotted against the % of the maximum number of cells counted (y-axis). The MenB strain assayed is indicated in the top left corner above each plot. The boxed legend to the right of each histogram describes each colour coded reaction mix. NHBA is acting as a negative control protein.

shows the two histograms obtained for reactions using either the UK320 or NZ98/254 strain. For the NZ98/254 strain acting as a negative control, no binding by the anti-PorA antibody to the bacteria is detected, as expected. For the UK320 strain, the reaction in which the bacteria are reacted alone with the PorA antibody acts as the baseline from which any shift in fluorescence detected due to sequestering away of the antibody by binding to antigen should be seen. If antibody is being sequestered by competing antigen, then a decreasing shift in fluorescence from this baseline should be seen. However, no observable shift in fluorescence when using any antigens bearing the PorA epitope (both the PorA-NadA3 and NadA3-PorA-Ferritin antigens) is seen. Assessing epitope presentation by this method is difficult as many reaction variables need to be optimized (such as working at saturating concentration of antibody - the inability to reach saturating concentrations of antibody was noted in

the titration in section 2.3.14) to reach a conclusive result. Therefore, a more straightforward method to assess PorA epitope presentation was instead performed by immunoblot and SPR.

2.3.16 SPR confirms presentation of the PorA VR2 14 epitope on the nanoparticle

SPR was performed as an alternative to investigate the PorA VR2 14 epitope presentation on the NadA3-PorA-Ferritin nanoparticle. The PorA VR2 14 antibody was immobilized to a CM-5 sensor chip (GE Healthcare) via an amine-coupling reaction using a Mouse Antibody Capture Kit (GE Healthcare) and the antigens NadA3-PorA-Ferritin, NadA3-PorA and NadA3 (24-170) were injected over the chip. The sensorgrams obtained for the SPR experiments using these three antigens are shown in Figure 2-35.

A) **NadA3 (24-170)**

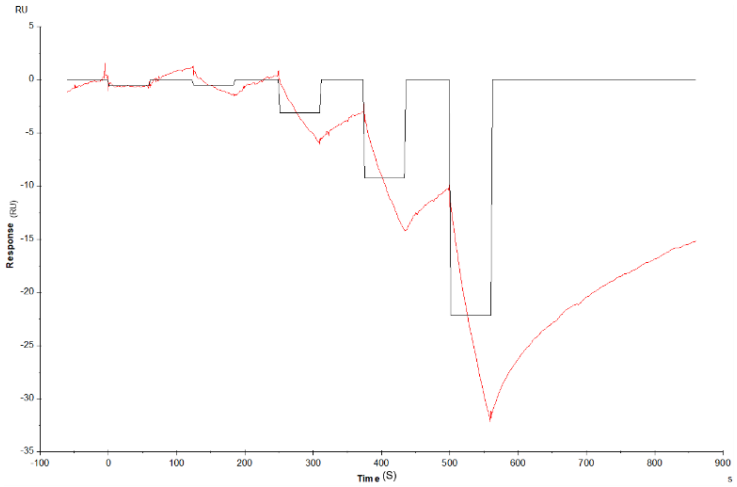

B) **NadA3-PorA-Ferritin**

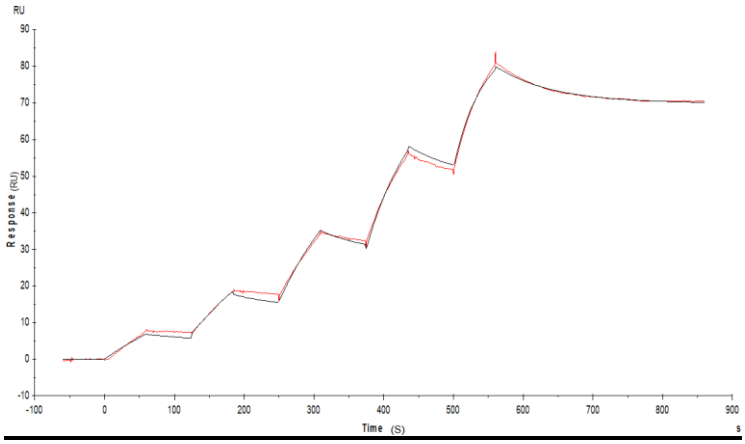

C) **NadA3-PorA**

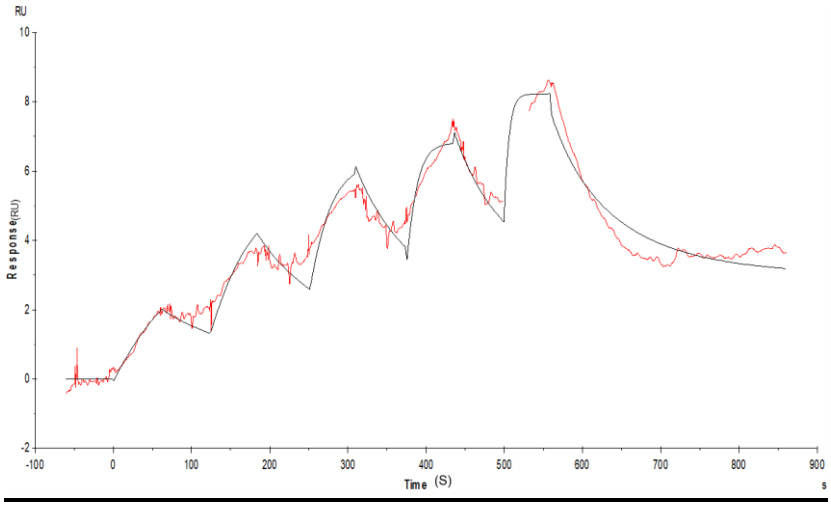

Figure 2-35 - Sensorgram profiles of the SPR analysis performed using the PorA VR2 14 antibody against the antigens A) NadA3 (24-170) B) NadA3-PorA-Ferritin C) NadA3-PorA. In the sensorgrams, the black represents the response obtained and the red line is the calculated curve for two state reaction kinetic model. Obtained responses fitted better to a two-state reaction kinetic model rather than a 1:1 binding kinetic model (curve not shown).

For the sensorgram of the negative control, NadA3 (24-170) shown in Figure 2-35A, a negative signal with no detectable affinity is obtained as expected. For both the NadA3-PorA-Ferritin and NadA3-PorA sensorgrams (Figure 2-35B and C respectively), positive signals with high affinity interactions (molar kd of 18 pM and 142 pM respectively) were detected, therefore suggesting that on both antigens the PorA VR2 14 epitope is accessible for specific antibody recognition.

2.3.17 Immunodot blot to confirm PorA VR2 14 epitope presentation on the NadA3-PorA-Nanoparticle

In addition to the SPR result, an immunodot blot was also deemed as a more straightforward method to confirm PorA VR2 14 epitope presentation on the NadA3-PorA-Ferritin. In this assay, small quantities of the antigens NadA3-PorA-Ferritin, NadA3-Ferritin and wildtype NadA3 (24-170) were dotted onto a nitrocellulose membrane and then tested against the PorA VR2 14 antibody, with antibody binding detected using a HRP-conjugated secondary anti-mouse IgG antibody. The developed immunoblot is shown in Figure 2-36.

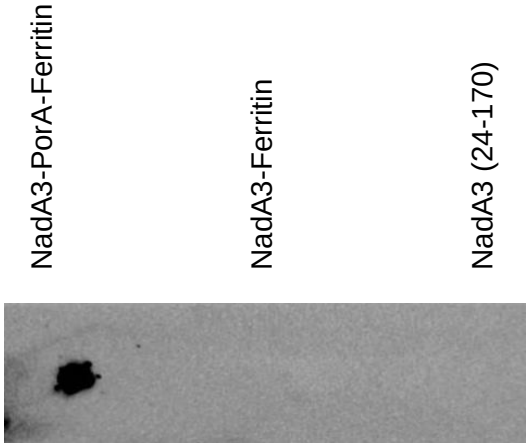

Figure 2-36 – Immunodot blot to probe PorA VR2 14 epitope presentation. Anti-PorA VR2 14 antibody was tested against the antigens NadA3-PorA-Ferritin, NadA3-Ferritin and wildtype NadA3 (24-170). Binding of the primary anti-PorA antibody was detected by incubation with secondary anti-mouse IgG conjugated to HRP.

Binding by the antibody is detected for the NadA3-PorA-Ferritin, the only antigen present on the blot containing the PorA VR2 14 epitope, confirming that the PorA VR2 loop is presented in an optimum conformation for recognition by its cognate antibody.

2.4 Conclusion

In this chapter, the expression, purification and structural characterisation of the rationally-designed Nada3-PorA-Ferritin was described. Beginning with the rational design of the nanoparticle system based on X-ray crystallography data, a genetic construct was then designed to enable successful expression of the protein nanoparticle in *E. coli*. Many approaches were then performed to validate that the NadA3-PorA-Ferrin could present immunogenic epitopes as had been envisioned.

An initial structural analysis by TEM gave an initial indication that NadA3-PorA trimerisation was successful on self-assembly of the nanoparticle. Moving on from this, cryo-EM was performed with the aim of obtaining a high-resolution structure of the NadA3-PorA antigen when presented on the ferritin. Initial single particle reconstruction from both negative stain and cryo-EM data clearly indicates a high flexibility of the NadA3-PorA appendage in the stalk region of the NadA3 homotrimeric protein. Other electron microscopy approaches, including cryo- tomography, gave the same indication of flexibility in the region of the NadA3 stalk.

Alongside the ultrastructural analyses, a variety of antibody-based experiments were performed to characterise epitope presentation on the NadA3-PorA-Ferritin. Initially, immunogold EM demonstrated that insertion of the PorA VR2 loop may impact on the NadA3 epitope presentation in the N-terminal head region. Epitope presentation on the NadA3 stalk as detected by immunogold EM was more difficult to assess, potentially due to steric hindrance of the antibody, and so SPR was performed as an alternative analysis of NadA3 epitope presentation. Using a limited pool of anti-NadA3 antibodies, the SPR data suggested that modifications made to accommodate the PorA VR2 loop had induced structural changes in the NadA3, effecting epitopes both in the N-terminal head region as well as in the stalk.

A fundamental aspect of the NadA3-PorA chimeric antigen design is that it should be able to elicit anti-NadA3 responses, and so further assays needed to be performed to ensure that native NadA3 epitopes were still present. In the competitive SBA, sera containing a wider pool of polyclonal anit-NadA3 antibodies could confirm that NadA3 epitopes were optimally presented. In a similar manner, the PorA VR2 epitope was also investigated to confirm its optimal presentation when displayed as the NadA3-PorA-Ferritin nanoparticle. The specificity of a commercially acquired PorA VR2 antibody was first confirmed by FACS before antibody-based assays including SPR

and immunoblots showed that the PorA VR2 epitope was presented by the nanoparticle.

The work described in this chapter is a validation of the rational structure-based design process, showing that a novel antigen can be feasibly produced and presents its immunogenic epitopes optimally for the potential induction of an immune response. Following on from this *in vitro* characterisation, the next stage is to evaluate the immunogenicity of the NadA3-PorA-Ferritin *in vivo*.

3. Chapter 3

in vivo immunogenicity of a rationally-designed nanoparticle antigen

3.1 Introduction

The previous chapter described the purification and epitope characterisation of the NadA3-PorA-Ferritin nanoparticle system. The rationally-designed nanoparticle was able to be purified and a series of experiments confirmed that epitopes deriving from both the NadA3 and the PorA VR2 components were optimally presented by the system. In order to investigate whether the NadA3-PorA could confer broad strain protection and if presentation of the subunit NadA3-PorA in this multi-copy format could enhance the immunogenicity compared to when the subunit is administered alone, it was necessary to perform *in vivo* immunisation studies.

Following a pilot study acting as an initial assessment of the humoral response to NadA3-PorA-Ferritin immunisation, a larger *in vivo* study to enable a more comprehensive study of the immunogenic potential of the multi-array antigen presentation was performed. In addition to characterising the humoral response by IgG ELISA, experiments derived from this study attempted to measure cellular response to immunisation, the B cell components in lymphoid organs and the bactericidal activity of induced antibodies.

In host defence against meningococcal bacteria, specific IgG antibodies present in sera and the complement system are considered crucial (Goldschneider et al., 1969). Indeed, licensure of meningococcal vaccines, including Bexsero has been based on the results obtained from the serum bactericidal assay (SBA) assay as a surrogate of vaccine efficacy, in which bactericidal antibody titres obtained from immunized sera are widely accepted as a correlate of protection (McIntosh et al., 2015).

Analysis derived from the large *in vivo* study will seek to characterise the Th1-Th2 balance in response to vaccination with the nanoparticle by analysing IgG subclasses. The immune response's Th1-Th2 balance against a vaccine antigen can vary dependent on the vaccine formulation - the choice of adjuvant for example is particularly influential (Lefeber et al., 2003). In mice, a Th1 response is associated with production of IgG2a, IgG2b and IgG3 antibodies whereas IgG1 is more associated with a Th2-like response (Germann et al., 1995).

In addition to the bactericidal capability of functional antibodies, $CD4^+$T cells are also important in that they are able to provide Th2 cytokine-mediated help to antigen-specific B cells by stimulating immunoglobulin class switching, affinity maturation, and increasing the magnitude of the antibody response, ultimately leading to an improved

immune response (Oftung et al., 2016). Furthermore, these T-cells are also able to induce immunological memory while also indirectly aiding the phagocytic uptake and destruction of bacteria by other innate immune cells. Therefore, to evaluate T cell responses to a vaccine formulation, it is necessary to characterise the cytokine response.

Another aspect of the rational design of the NadA3-PorA-Ferritin that can be assessed is its ability to present T-cell epitopes. The protective immune function of T-cells depends on their ability to recognise cells presenting specific peptides (T-cell epitopes) derived from antigens. Identification of such peptides can be crucial for vaccine development and since the rational design of the NadA3-PorA chimeric antigen may have resulted in loss or gain of T-cell epitopes, this was also investigated.

3.1.1 Aim and objectives

There are two key immunological aspects to consider for the NadA3-PorA-Ferritin nanoparticle system. The first is that presentation of subunit antigens, in a multi-copy format using self-assembling proteins such as ferritin, has been demonstrated to improve immunogenicity. The second aspect is the chimeric nature of the NadA3-PorA antigen, composed of epitopes from two MenB proteins to confer a broad strain coverage against MenB and to also simplify the vaccine formulation. To sufficiently characterise the immunogenic potential of the NadA3-PorA-Ferritin, the objectives were:

1. The completion of a pilot study as an initial assessment of the humoral response to immunisation with the NadA3-PorA-Ferritin and optimisation of ELISA parameters for future assays.
2. A large *in vivo* study to investigate the immunogenicity of the NadA3-PorA-Ferritin both at a humoral (though ELISA and SBA assays) and cell-mediated level (cytokine titres).
3. Further characterisation of the rationally designed system by analysing T-cell epitopes.

3.2 Materials and methods

3.2.1 Materials

Reagent	Supplier
Addavax	Invivogen, San Diego
Ammonium Chloride	Sigma, Dorset, UK
Anti-GL7-FITC antibody	Biolegend, UK
Anti-IgD-PerCp-Cy5.5 antibody	Biolegend, UK
Anti-CD38-PE-Cy7 antibody	Biolegend, UK
Anti-B220-APC antibody	Biolegend, UK
Anti-mouse IFN-γ antibody	BD Biosciences, Wokingham, UK
Biotin-conjugated anti-mouse IFN-γ antibody	eBioscience
Anti-Mouse IgG –Peroxidase antibody	Sigma, Dorset, UK
BSA	Sigma, Dorset, UK
Color Prestained Protein Standard, Broad Range	Neb, US
ConA	Sigma, Dorset, UK
FBS for cell culture	Sigma, Dorset, UK
Goat anti-mouse IgG1-HRP	Bio-rad, UK
IRDye 680RD Donkey anti-mouse secondary antibody	Li-cor, UK
LEAF purified anti-mouse CD16/32 Fc block	Biolegend, UK
LEGENDplex mouse inflammation panel (13-plex) flow cytometry kit	Biolegend, UK
Nitrocellulose membrane	Sigma, Dorset, UK
Nunclon Delta 96-Well plate Thermo	ThermoFisher, Waltham, MA
Nunc MaxiSorp flat-bottom plate	ThermoFisher, Waltham, MA
OptEIA Set for mouse IL-5	BD Biosciences, Wokingham, UK
OVA	Sigma, Dorset, UK
PBS	In-house
Pen-Strep	Sigma, Dorset, UK,

Rat anti-mouse IgG2a	ThermoFisher, Waltham, MA
RPMI-1640	Sigma, Dorset, UK
Skimmed milk powder	Sigma, Dorset, UK
Sodium chloride	Sigma, Dorset, UK
Sodium phosphate	Sigma, Dorset, UK
streptavidin-conjugated HRP	BD Biosciences, Wokingham, UK
Sulphuric acid	Sigma, Dorset, UK
TMB ELISA Substrate High Sensitivity	Abcam, Cambridge, USA
Tris Ultra Pure	ICN Biomedicals, Aurora, USA
Trypan Blue	Sigma, Dorset, UK
Tween 20	Sigma, Dorset, UK
Zombie NIR Fixable Viability Kit	Biolegend, UK

3.2.2 Dot-blot to probe PorA VR2 14 antibody binding to NadA3-PorA-Ferritin

1 µL of antigen (at 0.1 mg/mL diluted in PBS) was spotted onto a nitrocellulose membrane, left to dry, and a second 1 µL spot added. Non-specific sites on the membrane were then blocked by soaking in 5% BSA-PBS-Tween 20 (0.05%) for 45 minutes. The membrane was then incubated with 8 mL of anti-NadA3 (24-170) immunisation sera (diluted at 1:10,000 in PBS-Tween 20 (0.05%)) overnight at 4 °C. The membrane was then washed with PBS-Tween 20 0.05% (3 x 5 minutes) before incubation with 10 mL of IRDye 680RD Donkey anti-mouse secondary antibody (diluted 1: 10,000 in PBS-Tween20 (0.05%)) for 45 minutes. The membrane was then washed with PBS-Tween20 0.05% (3 x 5 minutes) and visualised by fluorescence detection.

3.2.3 SEC-HPLC of antigens for immunisation

A BioSep-SEC-S 4000 column (Phenomenex) was equilibrated in a mobile phase composed of 300 mM sodium chloride, 100 mM sodium phosphate, pH 7. For the subunit antigens, 50 µL of NadA3 (24-170) or NadA3-PorA at a final concentration of 0.25 mg/mL (diluted in mobile phase) was injected at a flow rate of 1 mL/min. For the

nanoparticle NadA-PorA3-Ferritin, a 50 µL sample was injected at a final concentration of 0.5 mg/mL with a flow rate of 1 mL/min.

3.2.4 NadA3-PorA-Ferritin pilot study immunisation

All animal studies were ethically reviewed and carried out in accordance with European Directive 2010/63/EEC. All protocols were subjected to ethical review and were carried out in a designated establishment. Three female BALB/c mice (7-9 weeks old) were housed in study groups and allowed free access to food and water. Each was immunised at three different time-points (day 1, 14 and 28). Each immunisation dose consisted of 25 µL Addavax (Invivogen) and 25 µL of 10 mM PBS containing the 10 µg of NadA3-PorA-Ferritin. The 50 µL immunisation dose was administered intramuscularly into the thigh. Blood was collected by tail bleeds (except on the day of the cull, where it was obtained by heart puncture) and left to coagulate at RT for 30 minutes before sera was collected by centrifugation at 10,000 g for 10 minutes at 4 °C. Collected sera was then stored at -20 °C.

3.2.5 Checkerboard titration ELISA (stages one and two)

The checkerboard titration was composed of two stages. In stage 1, all wells except column 1 of a Nunc MaxiSorp flat-bottom plate were coated with 50 µL of 1X PBS, pH 7.4. 100 µL of NadA3 (24-170) at 2 µg/mL diluted in 1X PBS was added into column 1 and then 50 µL of this was added into column 2 and mixed. This serial dilution was continued across the plate up until column 11. Column 12 was left as a blank. The plate was then covered with Clingfilm and left to incubate at 4°C overnight. The following morning, the plate was washed three times with wash buffer (1 X PBS, Tween-20 0.05%, pH 7.4) and then blocked by the addition of 200 µL of blocking buffer (5% BSA in 1X PBS, Tween-20 0.05%, pH 7.4) to all wells of the plate, followed by incubation for 1 hour at 37 °C. The plate was then washed three times in wash buffer before the addition of 50 µL of 1X PBS, pH 7.4 to all rows except those of row A. To row A, 100 µL of immunisation sera was added at a dilution of 1:500 (diluted in blocking buffer). 50 µL of this was added into row B, mixed, and the serial dilution continued up until row H. Row G saw no addition of sera. The plate was covered as before with Clingfilm and incubated for 2 hours at 37 °C. The plate was then washed three times with wash solution before the addition of 100 µL of Anti-Mouse IgG–Peroxidase antibody diluted to 1:10,000 in blocking buffer was added to all the wells of the plate. The plate was covered as before and incubated for 1 hour at 37 °C before washing three in was buffer. This was followed by the addition of 50 µL of substrate

to all wells and the plate was then covered with foil for 30 minutes. After the 30 minutes had elapsed, 10 µL of 10% sulphuric acid was added to all wells to stop the reaction and the absorbance was read at 450 nm.

In stage 2, 50 µL of NadA3 (24-170) at 0.125 µg/µL (diluted in 1X PBS, pH 7.4) was added to all wells of a Nunc MaxiSorp flat-bottom plate. The plate was then covered with Clingfilm and left to incubate at 4°C overnight. The following morning, the plate was washed three times with wash buffer (1 X PBS, Tween-20 0.05%, pH 7.4) and then blocked by the addition of 200 µL of blocking buffer (5% BSA in 1X PBS, Tween-20 0.05%, pH 7.4) to all wells of the plate, followed by incubation for 1 hour at 37 °C. The plate was then washed three times in wash buffer before the addition of 50 µL of 1X PBS, pH 7.4 to all rows except those of column 1. To column 1, 100 µL of immunisation sera was added at a dilution of 1:500 (diluted in blocking buffer). 50 µL of this was added into row B, mixed, and the serial dilution continued up until row H. Column 12 saw no addition of sera and was left as a blank. The plate was covered as before with Clingfilm and incubated for 2 hours at 37 °C. The plate was then washed three times with wash solution. 100 µL of blocking buffer was then added to all wells except those of row A. 100 µL of anti-mouse IgG–peroxidase antibody diluted to 1:2000 in blocking buffer was added to row A and 50 µL of this added into row B, and a serial dilution made down to row H. Row G saw no addition of secondary antibody. The plate was covered as before and incubated for 1 hour at 37 °C before washing three times in wash buffer. This was followed by the addition of 50 µL of substrate to all wells and the plate was then covered with foil for 30 minutes. After the 30 minutes had elapsed, 10 µL of 10% sulphuric acid was added to all wells to stop the reaction and the absorbance was read at 450 nm.

3.2.6 Total serum IgG ELISA for NadA3-PorA-Ferritin pilot study

All the wells of a Nunc MaxiSorp flat-bottom plate were coated with 100 µL of NadA3 (24-170) at 2 µg/µL diluted in 1X PBS, pH 7.4 The plate was then covered with Clingfilm and left to incubate at 4°C overnight. The following morning, the plate was washed three times with wash buffer (1 X PBS, Tween-20 0.05%, pH 7.4) and then blocked by the addition of 200 µL of blocking buffer (2% skimmed 0.1% fat milk in 1X PBS, Tween-20 0.05%, pH 7.4) to all wells of the plate, followed by incaution for 1 hour at 37 °C. The plate was then washed three times in wash buffer before the addition of 100 µL of blocking buffer to all wells except those of column 1. To column 1, 200 µL of immunisation sera was added at a dilution of 1:500 (diluted in blocking buffer). 100 µL of this was added into column 2, mixed, and the serial dilution

continued up until column 11. Column 12 saw no addition of sera. The plate was covered as before with Clingfilm and incubated for 2 hours at 37 °C. The plate was then washed three times with wash solution before the addition of 100 µL of Anti-Mouse IgG –Peroxidase antibody diluted to 1:10,000 in blocking buffer was added to all the wells of the plate. The plate was covered as before and incubated for 1 hour at 37 °C before washing three in was buffer. This was followed by the addition of 100 µL of substrate to all wells and the plate was then covered with foil for 30 minutes. After the 30 minutes had elapsed, 20 µL of 10% sulphuric acid was added to all wells to stop the reaction and the absorbance was read at 450 nm.

3.2.7 Large *in vivo* immunisation study

All animal studies were ethically reviewed and carried out in accordance with European Directive 2010/63/EEC. Six female BALB/c mice (7-9 weeks old) per group were housed in study groups and allowed free access to food and water. Each was immunised at three different timepoints (day 1, 21 and 35). Each immunisation dose consisted of 12.5 µL Addavax (Invivogen) and 37.5 µL of 10 mM PBS containing the relevant antigen. The 50 µL immunisation dose was administered intramuscularly into the thigh. Blood was collected by tail bleeds (except on the day of the cull, where it was obtained by heart puncture) and left to coagulate at RT for 30 minutes before sera collection by centrifugation at 10,000 g for 10 minutes at 4 °C. Collected sera was then stored at -20 °C. On termination, spleens and inguinal lymph nodes were also isolated.

3.2.8 Isolation of splenocytes

Isolated spleens were processed by forcing though a metal mesh cell strainer followed by washing with RPMI 1640 supplemented with 10% FBS and 1% Pen Strep. Erythrocytes were removed by resuspension in Boyle's solution (composed of 0.17 M Tris and 0.16 M ammonium chloride mixed at a ratio of 1:9). The splenocytes were washed again in complete RPMI 1640 before viable cell numbers were measured using Trypan Blue exclusion. 100 µL of splenocytes at concentration of $5x10^6$ cells/mL was added into wells of a Nunclon Delta 96-Well plate and the wells were then stimulated with either; mapped peptides to a final concentration of 5 µg/mL, relevant antigen to a final concentration of 5 µg/mL, ConA to a final concentration 5 µg/mL or complete RPMI for 72 hours at 37°C, 5% CO_2. The supernatants were then harvested and stored at -20°C.

3.2.9 Total serum IgG ELISA to detect anti-NadA3 (24-170) antibodies

The wells of a Nunc MaxiSorp flat-bottom plate were coated with 100 µL of NadA3 (24-170) at 2 ug/µL diluted in 1X PBS, pH 7.4 The plate was then covered with Clingfilm and left to incubate at 4°C overnight. The following morning, the plate was washed three times with wash buffer (1 X PBS, Tween-20 0.05%, pH 7.4) and then blocked by the addition of 200 µL of blocking buffer (2% skimmed 0.1% fat milk in 1X PBS, Tween-20 0.05%, pH 7.4) to all wells of the plate, followed by incubation for 1 hour at 37 °C. The plate was then washed three times in wash buffer before the addition of 100 µL of blocking buffer to all wells except those of column 1. To column 1, 200 µL of immunisation sera was added at a dilution of 1:500 (diluted in blocking buffer). A serial dilution series on the plate was then initiated by taking 100 µL from each well in column 1 and then adding it into column 2, mixing by pipetting up and down 5 times, and the serial dilution continued as per for the successive columns up to until column 11. Column 12 saw no addition of sera. The plate was covered as before with Clingfilm and incubated for 2 hours at 37 °C. The plate was then washed three times with wash solution before the addition of 100 µL of Anti-Mouse IgG–Peroxidase antibody diluted to 1:10,000 in blocking buffer was added to all the wells of the plate. The plate was covered as before and incubated for 1 hour at 37 °C before washing three times with wash buffer. This was followed by the addition of 100 µL of substrate to all wells and the plate was then covered with foil for 30 minutes. After the 30 minutes had elapsed, 20 µL of 0.2 M sulphuric acid was added to all wells to stop the reaction and the absorbance was read at 450 nm.

3.2.10 Analysis of anti-NadA3 (24-170) IgG1 and IgG2a antibody titres by ELISA

All the wells of a Nunc MaxiSorp flat-bottom plate were coated with 100 µL of NadA3 (24-170) at 2 µg/µL diluted in 1X PBS, pH 7.4 The plate was then covered with Clingfilm and left to incubate at 4°C overnight. The following morning, the plate was washed three times with wash buffer (1 X PBS, Tween-20 0.05%, pH 7.4) and then blocked by the addition of 200 µL of blocking buffer (2% skimmed 0.1% fat milk in 1X PBS, Tween-20 0.05%, pH 7.4) to all wells of the plate, followed by incubation for 1 hour at 37 °C. The plate was then washed three times in wash buffer before the addition of 100 µL of blocking buffer to all wells except those of column 1. To column 1, 200 µL of immunisation sera was added at a dilution of 1:500 (diluted in blocking buffer). A serial dilutions series on the plate was then initiated by taking 100 µL of this

was then added into column 2, mixed by pipetting up and down 5 times, and the serial dilution continued as per for the successive columns up to until column 11. Column 12 saw no addition of sera. The plate was covered as before with Clingfilm and incubated for 2 hours at 37 °C. The plate was then washed three times with wash solution before the addition of 100 µL of goat anti-mouse IgG1-HRP or rat anti-mouse IgG2a, HRP antibody (diluted to 1: 20,000 or 1:5000 in blocking buffer, respectively) was added to all the wells of the plate. The plate was covered as before and incubated for 1 hour at 37 °C before washing three times with wash buffer. This was followed by the addition of 100 µL of substrate to all wells and the plate was then covered with foil for 30 minutes. After the 30 minutes had elapsed, 20 µL of 0.2 M sulphuric acid was added to all wells to stop the reaction and the absorbance was read at 450 nm.

3.2.11 Multiplex cytokine analysis of cellular immune response

Supernatants from stimulated splenocytes were measured using the LEGENDplex mouse inflammation panel (13-plex) flow cytometry kit in conjunction with BD FACSCanto system.

3.2.12 IFNγ ELISA for T-cell epitope mapping

The levels of IFNγ in the stimulated splenocyte supernatants were determined by ELISA. Briefly, Nunc-Immuno Maxisorp 96-well plates were coated overnight at 4°C with an anti-mouse IFNγ antibody in carbonate buffer (0.05 M, pH 9.6), followed by a blocking step with 2% skimmed milk in 1X PBS for 1.5 hours at RT. The supernatants were diluted 3.3X on the plate in 2% BSA in 1X PBS, and the plates were incubated at RT for 2 hours, followed by 1 h incubation with biotin-conjugated anti-mouse IFNγ antibody. This was followed by a 30 minutes incubation with streptavidin-conjugated HRP. The plates were developed by the addition of substrate and the reaction was stopped with 0.2 M sulphuric acid after 5 minutes. The plates were read at 450 nm.

3.2.13 IL-5 ELISA for T-cell epitope mapping

The levels of IL-5 in the stimulated splenocyte supernatants were determined by using the OptEIA Set for mouse IL-5 as according to the manufacturer's instructions.

3.2.14 Germinal centre analysis

Harvested inguinal lymph nodes spleens were processed by forcing though a metal mesh cell strainer followed centrifugation at 250 g for 5 minutes and washing with RPMI 1640 supplemented with 10 % FBS and 1% Pen Strep. Viable cell numbers

were measured using Trypan Blue exclusion. 200 µL of the cells were aliquoted into relevant wells on a round-bottom 96 well plate and the plate was then span at 500 g for 3 minutes and the supernatant removed. The cell pellet was resuspended in 10 µL LEAF purified anti-mouse CD16/32 Fc block for 10 minutes in the dark. Samples were then stained with anti-GL7-FITC, anti-IgD-PerCp-Cy5.5, anti-CD38-PE-Cy7, anti-B220-APC antibodies in 1X PBS-1% BSA at 4 °C for 30 minutes in the dark. Samples were then washed with 1X PBS before staining with the Zombie NIR Fixable Viability Kit in 1 X PBS and incubated 4 °C for 30 minutes in the dark. Following further washes with 1X PBS-1% BSA, the plate was stored at 4 °C in the dark until analysis on the BD FACSCanto II system.

3.2.15 Serum bactericidal activity of immunisation sera

The serum bactericidal activity (SBA) of immunisation sera against *N. meningitidis* strains was evaluated using baby rabbit complement at 25% of the total volume of the reaction (12.5 µL of complement in 50 µL of the reaction volume). SBA titres were defined as the serum dilution that resulted in a 50% decrease in colony-forming units (CFUs) per ml after a 60 minute incubation of the *N. meningitidis* bacteria with the reaction mixture compared to the control CFU per mL at time 0.

3.2.16 Statistical analysis

Statistical analysis of data was calculated by one-way analysis of variance (ANOVA). Where significant differences are indicated, differences between means were determined by the Tukey Simultaneous Tests for Differences of Means. All the calculations were made using Minitab 17 statistical software.

3.3 Results & Discussion

3.3.1 Immunodot blot for confirmation of NadA3 epitope presentation on the NadA3-PorA recombinant protein

An *in vivo* study will be performed comparing the immune response following administration of the subunit antigen NadA3-PorA to that induced when it is presented as the NadA3-PorA-Ferritin nanoparticle. This NadA3-PorA antigen was expressed and purified from a *de novo* constructed DNA sequence, which saw insertion of the PorA VR2 14 sequence into the NadA3 (24-170) encoding DNA via a PCR-based

method. Following purification of the NadA3-PorA subunit antigen, SPR and immunoblots were performed to confirm presentation of the PorA VR2 14 epitope, however a similar assay is required to confirm presentation of NadA3 epitopes prior to performing *in vivo* studies. In this assay, small quantities of the antigens NadA3-PorA, NadA3 (24-170) and NadA3-Ferritin were added onto a nitrocellulose membrane and then tested against anti-NadA3 (24-170) immunisation sera. Figure 3-1 shows the immunoblot obtained.

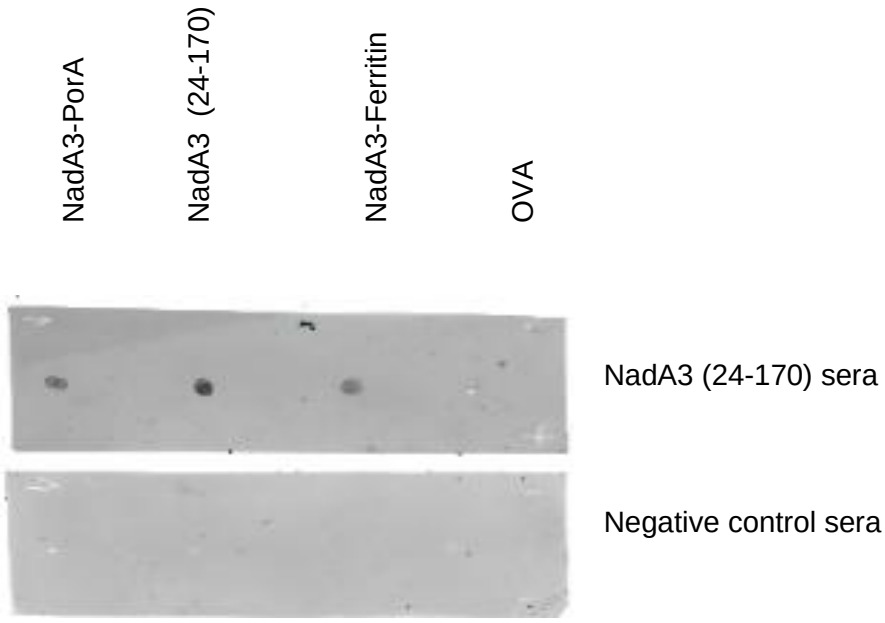

Figure 3-1 Immunoblot to probe NadA3 (24-170) epitope presentation on the NadA3-PorA subunit antigen. Binding of anti-NadA3 (24-170) antibodies present in the immunisation sera was tested against the antigens NadA3-PorA, NadA3 (24-170) and NadA3-ferritin and OVA (acting as a negative control). Negative control serum was obtained from a non-immunised BALB/c mouse. Antibody binding was detected by incubation with a IRDye 680RD Donkey anti-mouse secondary antibody (Li-cor).

From the immunoblot in Figure 3-1, a positive signal for binding of anti-NadA3 (24-170) antibodies is detected only for the NadA3 epitope-containing antigens NadA3-PorA, NadA3 (24-170) and NadA3-Ferritin. There is no detectable binding by antibodies present in the anti-NadA3 (24-170) to OVA. Presentation of NadA3 (24-170) epitopes on the NadA3-PorA antigen can therefore be conferred from this result.

3.3.2 SEC-HPLC to assess stability of the purified antigens prior to immunisation

Prior to immunisation, the structural integrity of the purified antigens NadA3 (24-170), NadA3-PorA and the NadA3-PorA-Ferritin nanoparticle after several months of storage at -20 °C was checked by SEC-HPLC. Though SDS-PAGE can detect signs of protein degradation, it is however a denaturing technique that results in the disassembly of the trimeric antigens (and the nanoparticle) into its constituent monomers, and therefore is unable to determine if the antigens are present in their native assemblies. Samples of the purified antigens were loaded to a BioSep-SEC-S 4000 column (Phenomenex) resulting in the chromatograms shown in Figure 3-2.

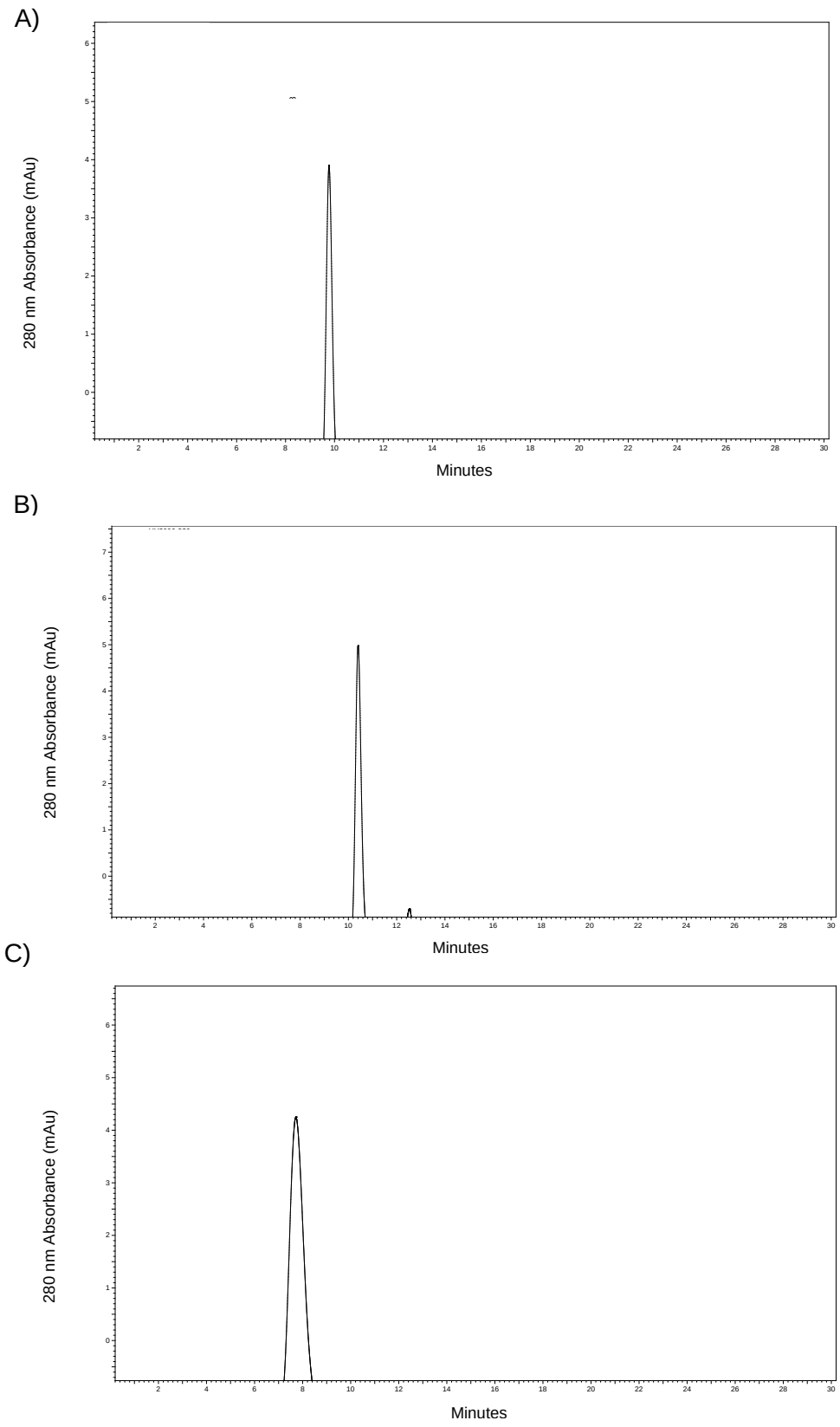

Figure 3-2 Analytical size-exclusion chromatograms obtained for the antigens A) NadA3 (24-170) B) NadA3-PorA C) NadA3-PorA-Ferritin. Performed using a BioSep-SEC-S 4000 column equilibrated in a mobile phase of 300 mM sodium chloride, 100 mM sodium phosphate, pH 7 and the flow rate set to 1 mL/min. The dominant peaks in each chromatogram with retention times of 9.5, 10.5 and 7.6 minutes are consistent with the molecular weights for each respective antigen.

From the chromatograms shown in Figure 3-2, the dominant peaks seen in each are consistent with retention times for NadA3 (24-170), NadA3-PorA and NadA3-PorA-Ferritin respectively based on their molecular weights. Apart from the chromatogram for NadA3-PorA which shows a second minor peak (which could be a small sign of degradation), these chromatograms show a single dominant peak, suggesting that all antigens are in their native conformations. Scarselli et al. simarly used SEC-HPLC to show that a panel of rationally designed meningococcal proteins based on the Bexsero antigen fHbp were present as monodisperse monomers and had not aggregated or degraded (Scarselli et al., 2011).

An SDS-PAGE gel shown in Figure 3-3 was also performed to detect obvious instances of protein degradation within the purified antigen samples. From these results, it can be seen that all the antigens retain the denaturation patterns obtained directly following their purification and no indication of degradation can be seen in any of the samples. In the structural characterisation of a Chlamydia antigen based on the porin protein PorB, Madico et al. used SDS-PAGE to identify protein constructs that were more prone to aggregation and destabilisation (Madico et al., 2017) while another study used SDS-PAGE as a form of quality control to monitor for protein degradation of a purified malarial protein antigen candidate (Jin et al., 2018).

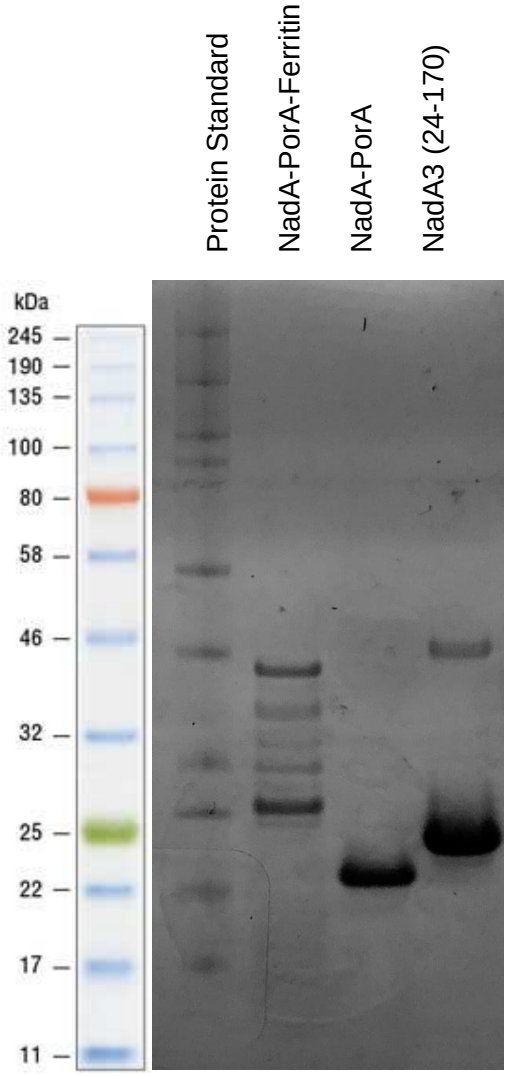

Figure 3-3 SDS-PAGE of the purified antigens to be used for immunisation. The antigens are labelled above each lane of the gel and the molecular weight ladder (Color Prestained Protein Standard, Broad Range) is shown to the left of the gel.

3.3.3 Pilot NadA3-PorA-Ferritin immunisation study

Prior to beginning a large *in vivo* study, a smaller pilot study was performed to confirm that immunisation with the NadA3-PorA-Ferritin was able to induce an immune response. The work performed in the pilot study also enabled optimisation of the ELISA procedure to take through to the larger study.

Three female BALB/c mice (7-9 weeks old) were immunised with NadA3-PorA-Ferritin to assess its ability to raise an antigen-specific immune response. Each immunisation dose was administered intramuscularly into the thigh and contained 10 µg of the

NadA3-PorA-Ferritin nanoparticle adjuvanted with the adjuvant AddaVax. The immunisation schedule consisted of three doses, administered on day 1, 14 and 28, with mice terminated at day 42.

The adjuvant AddaVax is a squalene-based oil-in-water nano-emulsion based on the formulation of MF59, an adjuvant that has been shown to enhance both quality and quantity of antigen-specific immune responses (O'Hagan et al., 2013). Other studies in the literature have also selected either the AddaVax or MF59 as adjuvants for delivery of their self-assembling protein nanoparticle systems (Kanekiyo et al., 2013; Kim et al., 2018; Marcandalli et al., 2019). Its primary mechanism of action seems to be in its ability to generate an immunocompetent environment at the site of injection (Lofano et al., 2015); in a comparison study with alum, Calabro et al. showed that MF59 was able to more effectively promote neutrophil recruitment and antigen translocation to the lymph nodes (Calabro et al., 2011). Research has shown that MF59 strongly affects T-cell dependent B-cell responses, with one study demonstrating through adult murine IgG responses to the influenza hemagglutinin that MF59 was able to promote a potent T follicular helper cell (T_{FH}) response, which subsequently helps control the magnitude of the germinal centre in the primary lymph organ (Mastelic Gavillet et al., 2015). The formation of the germinal centre is an essential determinant of the magnitude and quality of the humoral response and memory, being where the expansion, selection, and affinity maturation of antigen-specific B cells takes place during primary responses to an antigen (Lofano et al., 2015).

Following sera collection, total IgG against NadA3 (24-170) was assessed by ELISA. In order to optimise reagent concentrations for the ELISA, a series of checkerboard titration (CBT) plates were performed. In the first stage of the CBT, coating antigen (in this case NadA3 (24-170)) was titrated against immunisation sera while anti-mouse IgG secondary antibody remained constant. In the second stage of the CBT process, the coating antigen concentration remained constant and the secondary antibody concentration was titrated against the sera.

Figure 3-4 describes CBT stages one and two for sera obtained on day 21 (one week after the second immunisation dose) from a single mouse.

A)

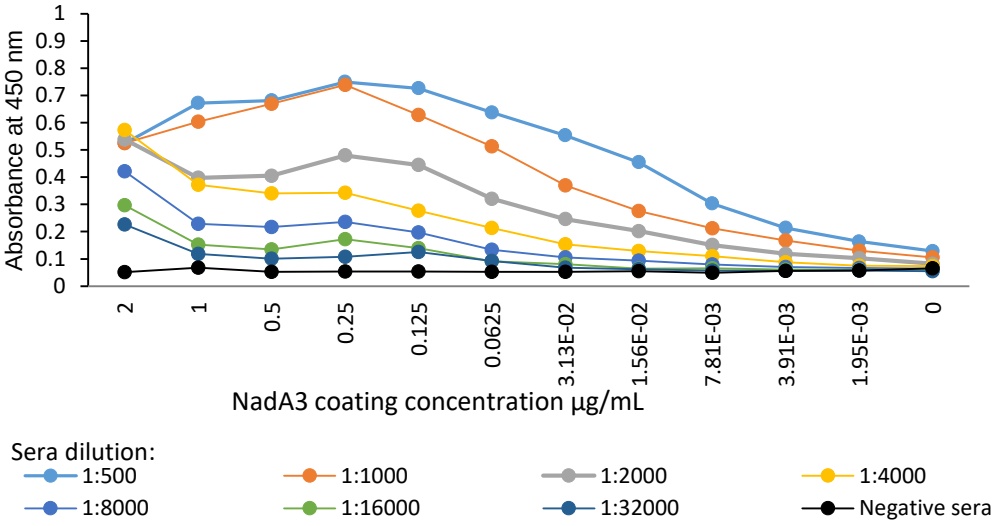

B)

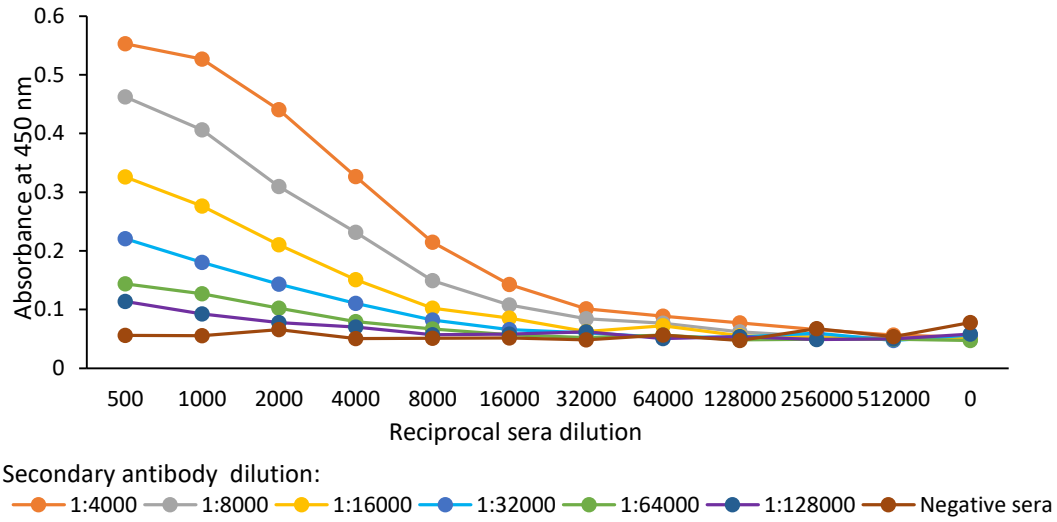

Figure 3-4 CBT ELISA results obtained for a single mouse at the day 21 time-point (1 week after the second dose) of the NadA3-PorA-Ferritin pilot study. Plates were coated with the antigen NadA3 (24-170). A) Results of stage 1 of the CBT process, in which the concentration of coating antigen NadA3 (24-170) is titrated against sera B) Results of stage 2 of the CBT process, in which sera is titrated against the concetration of the secondary IgG antibody.

The first stage of the CBT, which seeks to determine an optimal coating antigen concentration, is shown in Figure 3-4A. At a sera dilution of 1:500, a plateau in absorbance was reached at around 0.125 µg/mL coating antigen concentration, which means that at this sera dilution antigen above this concentration was in excess. Based on this, the second stage of the CBT (shown in B) was coated with NadA3 (24-

170) at a concentration of 0.125 µg/mL. A sigmoidal curve with an absorbance plateau was only reached for more concentrated dilutions of the secondary antibody.

As the quantity of secondary antibody available was limiting, increasing the coating antigen concentration and the volume of coating antigen were deemed as preferable options to optimize the ELISA. Sera obtained from all three mice across all timepoints of the study were then titrated on ELISA plates coated with an increased volume of NadA3 (24-170) at a higher concentration of 2 µg/mL. Figure 3-5 shows the results of this ELISA.

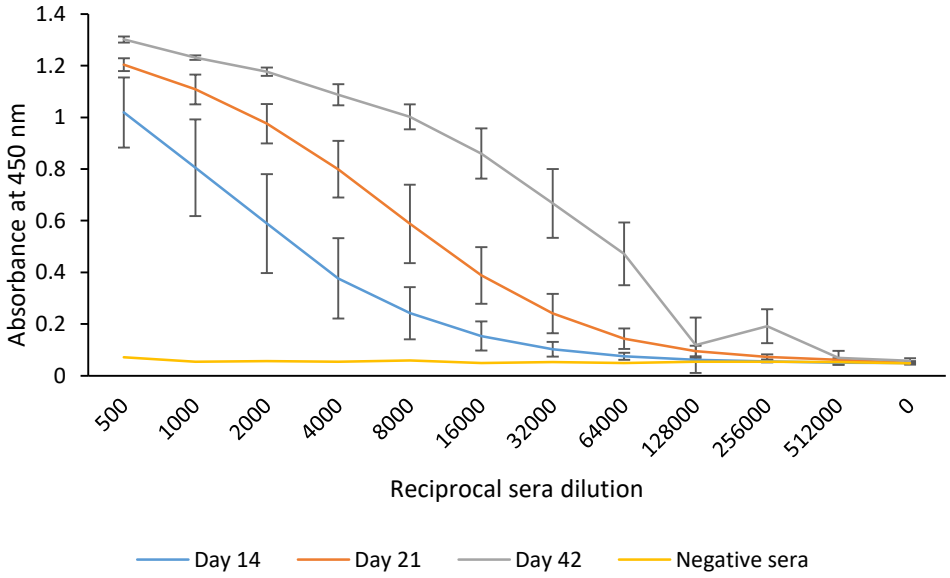

Figure 3-5 Total IgG ELISA across all three time-points for the NadA3-PorA-Ferritin pilot study. NadA3 (24-170) antigen coated the wells of the plate at 2 µg/mL, while the anti-IgG secondary HRP-labelled antibody was used at a 1: 10,000 dilution as according to the manufacturer's instructions. Day 14 represents sera obtained 2 weeks after 1st dose, Day 21 is sera obtained 1 week after the second dose and Day 42 sera was obtained 2 weeks after third dose. Results represent the mean ± SD (n=3 mice). Negative serum was obtained from a single non-immunised BALB/c mouse.

As can be seen from Figure 3-5, coating the plate at an increased concentration of NadA3 (24-170) has enabled much higher OD values to be obtained while sparing on the amount of secondary antibody used. For both day 21 and day 42 timepoints, the obtained optical densities began to plateau, indicating sera is becoming saturating and the maximum achievable OD is being reached. The sera dilution range also

enables the endpoint titres to be calculated for all the time-points. The calculated anti-NadA3 (24-170) IgG endpoint titres are shown in Figure 3-6.

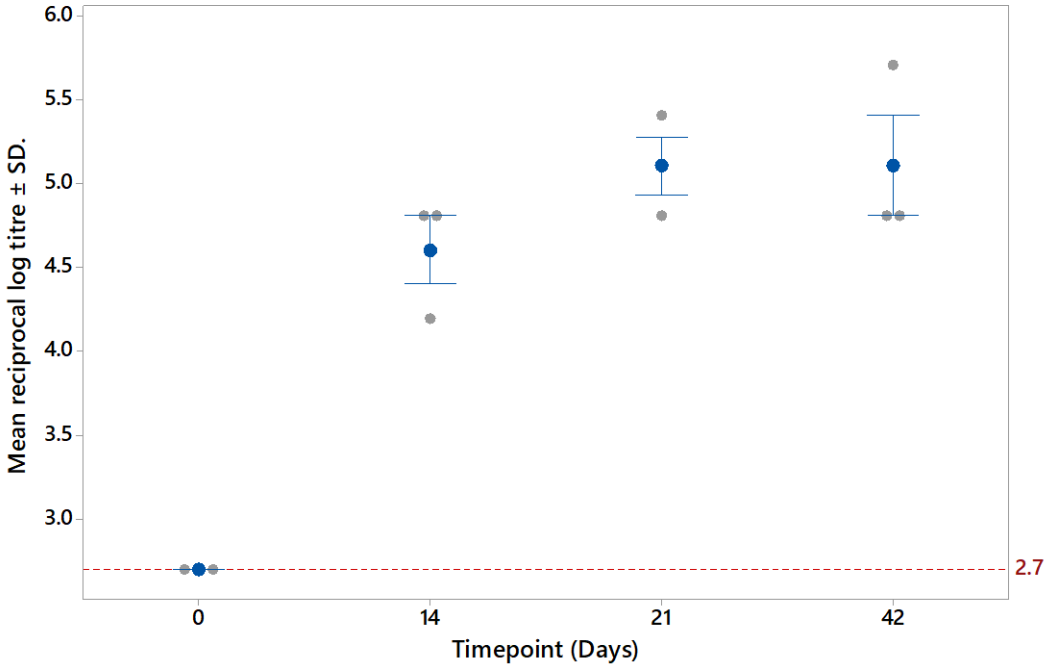

Figure 3-6 Endpoint serum IgG titres across all three time-points of the NadA3-PorA-Ferritin pilot study. NadA3 (24-170) antigen coated the wells of the plate at 2 µg/mL, while the anti-IgG secondary HRP-labelled antibody was used at a 1:10,000 dilution as according the manufacturer's instructions. The dashed red line at a titre of 2.7 represents the titre obtained at the starting sera dilution. Results represent the reciprocal endpoint log titres for each of the three mice. Each mouse is represented by ●, the mean reciprocal endpoint titre per time-point is represented by ● ± SD.

From Figure 3-6, an increase in the endpoint titres are seen post-second dose relative to the first dose, though this was found to not be significant. Though endpoint titres reached are similar post second and third doses (a non-significant difference was noted) a third immunization may still be deemed necessary during future *in vivo* studies. In another similar structural vaccinology study for the development of novel meningococcal vaccine antigens, each mouse was immunised three times, though no comparison of the bactericidal titre obtained following each immunisation was performed (Scarselli et al., 2011). A study in which another Bexsero antigen, fHbp, was used as a scaffold present PorA VR2 epitopes also performed three immunisations but did not assess the immune response at different timepoints (Hollingshead et al., 2018).

3.3.4 *in vivo* immunisation: Study design and overview

Following the pilot study, a larger *in vivo* study was performed in which groups of six female BALB/c mice (7 – 9 weeks old) were immunised with the antigens NadA3-PorA, NadA3-PorA-Ferritin and NadA3 (24-170). The study was split into two identical studies i.e. three mice per group per study, equalling a total of six mice per group once both were combined. The study was designed in order to investigate the fundamental hypothesis; presentation of the subunit antigen NadA3-PorA in a multi-copy format on the surface of ferritin can enhance the immune response. The study's immunisation groups and the rationale for their inclusion are detailed in Table 3-1.

Table 3-1 The immunisation groups that comprise the *in vivo* immunisation study. The mass of NadA3 antigen (NadA3-PorA or NadA3 (24-170) contained within each dose is shown for each group.

Immunisation groups (Mass of NadA3 antigen administered per dose)	Group number	Dose group	Further detail
NadA3-PorA (1 µg)	1	Low	
NadA3-PorA-Ferritin (1 µg)	2	Low	Contains the equivalent of 1 µg of NadA3-PorA.
NadA3-PorA (10 µg)	3	High	Equivalent to 650 pmol of NadA3-PorA.
NadA3-PorA-Ferritin (10 µg)	4	High	Contains the equivalent of 10 µg of NadA3-PorA.
NadA3 (24-170) (11.5 µg)	5	-	Equivalent to 650 pmol of NadA3 (24-170).

Groups 1 -4 were split into two dose groups. The 'low' dose group consists of groups 1 and 2, where an equivalent of 1 µg of NadA3-PorA antigen was administered, whereas the 'high' dose group contains groups 3 and 4, which see a higher equivalent dose of 10 µg NadA3-PorA administered per dose.

To assess the design of the chimeric NadA3-PorA, it is necessary to understand how the modifications made to the NadA3 (24-170) in order to accommodate the PorA VR2 14 epitope may affect the anti-NadA3 protective response. Therefore, group 5 in which the wild-type NadA3 (24-170) is administered has also been included. Again, in order to make comparisons with the NadA3-PorA (subunit or when presented on the ferritin), an equivalent molar quantity of NadA3 (24-170) has been selected. 10 µg of NadA3-PorA is equal to 650 pmol which is equivalent to 11.5 µg of the wildtype

NadA3 (24-170). The immunisation schedule is depicted in Figure 3-7 and consisted of three doses administered intramuscularly in the presence of AddaVax adjuvant.

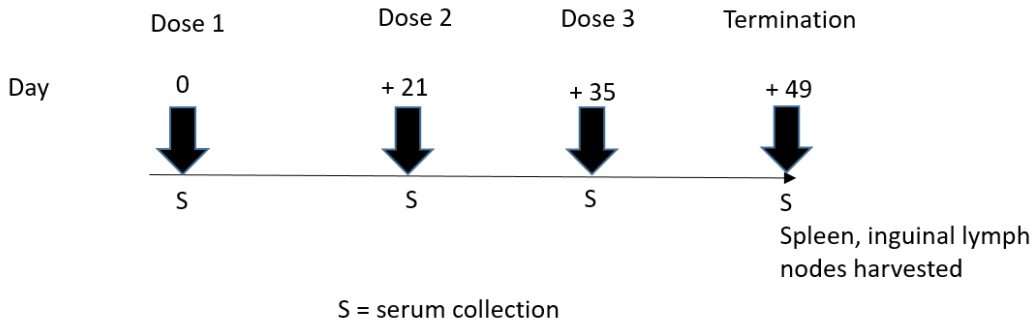

Figure 3-7 A diagram of the *in vivo* study immunisation schedule

3.3.5 Nanoparticle immunization results in higher anti-NadA3 total IgG titres

The IgG antibody isotype is involved in a range of protective functions, from interaction with C1q which leads to complement-mediated cell lysis through to initiating cellular effector functions including phagocytosis and respiratory burst (Vidarsson et al., 2001). Serum bactericidal activity is a crucial component of host defense against meningococcal disease, and is mediated by antigen-specific IgG antibodies and a functional complement system (Goldschneider et al., 1969). In addition, opsonic antibodies may also be important in protection, whereby IgG antibodies directly facilitate phagocytosis though binding to Fc receptors (FcR) present on most myeloid cells (Vidarsson and van de Winkel, 1998) (Lehmann et al., 1999).

The NadA3-PorA chimeric antigen contains epitopes derived from two MenB antigens; the trimeric NadA3 (24-170) and the VR2 epitope from the porin protein PorA. One way to measure the humoral response to immunisation is to measure the raised antibody titres by ELISA.

In the Bexsero vaccine, the PorA serosubtype 1.4 membrane protein is delivered in its native membrane environment via outer membrane vesicles (OMVs). OMVs are a complex mixture of periplasmic, cytoplasmic and outer membrane proteins (Vipond et al., 2006), though OMVs can be used to coat ELISAs in evaluating OMV-based MenB vaccines (Findlow et al., 2006). In this project however, the PorA VR2 loop epitope is derived from a PorA of a different serosubtype to the one found in Bexsero and so there exists no purified outer membrane vesicles bearing the PorA of this

serosubtype in-house. Therefore, detection by ELISA of antibodies raised against the PorA VR2 14 loop has not been possible. Serum bactericidal assays will instead provide information about the anti-PorA VR2 14 antibodies raised by immunisation with NadA3-PorA-Ferritin. However, NadA3 (24-170) specific antibodies can be detected by ELISA since the purified NadA3 (24-170) antigen is suitable for coating of ELISA plates. Sera collected at the various timepoints (shown in Figure 3-7) was assayed for total anti-NadA3 (24-170) IgG antibodies by ELISA. Figure 3-8 shows the anti-NadA3 (24-170) total IgG endpoint titres for sera collected on the day 21 and day 35.

A)

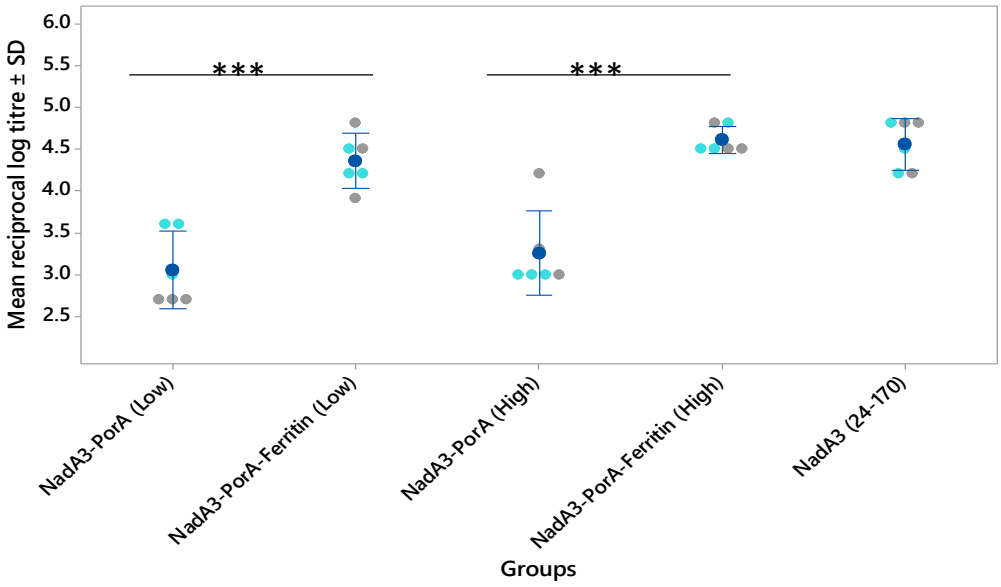

B)

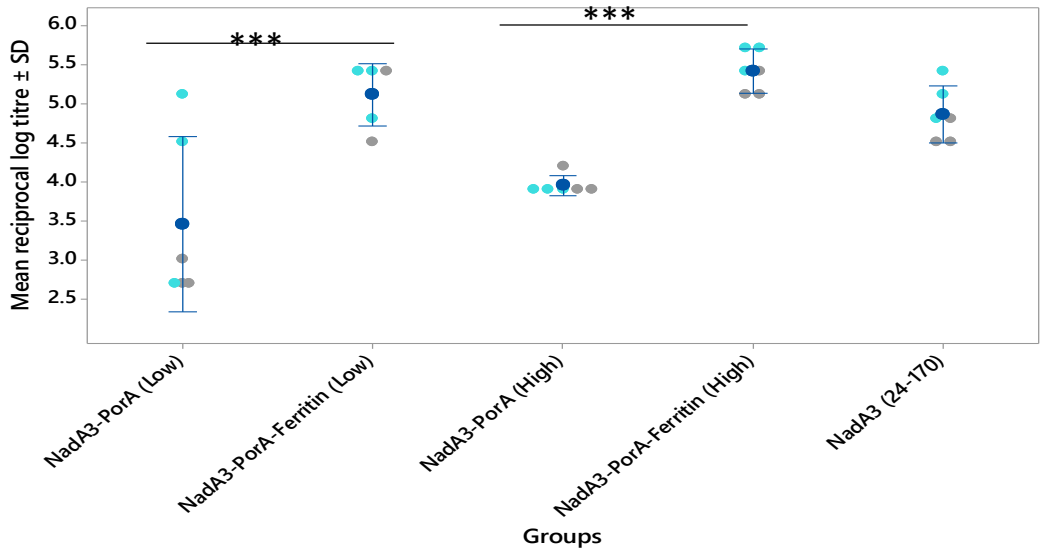

Figure 3-8 Anti-NadA3 (24-170) total IgG titres showing that NadA3-PorA-Ferritin immunisation mediates a more potent humoral immune responses over the subunit antigen NadA3-PorA alone. Titres displayed derive from sera collected A) 21 days after immunisation with the first dose B) Day 35 timepoint, 2 weeks after the second dose. The study was split into two studies, initiated 2 weeks apart; light blue ● indicate the endpoint titres from mice of the first study, grey dots ● those from the second study. The dark blue dot ● represents the mean reciprocal endpoint log titre ± SD. Significant differences between means were determined by the Tukey Simultaneous Tests for Differences of Means, with significance denoted as ***$p < 0.001$.

Figure 3-8A displays the anti-NadA3 (24-170) total IgG titres for sera collected 21 days after immunisation. For both dose comparisons, the increase in titres obtained following nanoparticle immunisation was found to be statistically significant ($p < 0.001$) over those of the subunit NadA3-PorA antigen administration alone. If the 'low dose' groups are compared, then an increase in total IgG titres to levels comparable to that of the wildtype NadA3 (24-170) is seen following immunisation with the NadA3-PorA-Ferritin nanoparticle over the subunit NadA3-PorA alone. This is also seen when the 'high dose' groups are compared, allowing for potential dose sparing as the differences between the titres obtained for the 'low' and 'high' doses of the NadA-PorA-Ferritin are non-significant.

In comparing groups 3 and 5, which are equivalent molar doses of the subunit antigens NadA3-PorA and NadA3 (24-170), immunisation with the wild type NadA3 (24-170) results in significantly higher titres ($p<0.001$). This would indicate that the modifications made to NadA3 to accommodate the PorA VR2 14 loop may have resulted in a loss or compromised immunogenic epitopes within the NadA3 N-terminal head region. This observation is not surprising, as analysis of the human humoral response to vaccination with Bexsero revealed that NadA3 contains multiple protective epitopes located through its structure; from its N-terminal region through to its coiled-coil stalk (Giuliani et al., 2018). However, when this NadA3-PorA subunit is presented in a multi-copy format on the surface of the ferritin, these titres are in a sense 'rescued' and raised to comparable levels of the wild type NadA3. Whether the population of antibodies raised still results in comparable bactericidal killing of MenB as to that elicited by wild type NadA3, however, can only be assessed by future SBA assays.

Anti-NadA3 (24-170) total IgG titres were then analysed for sera collected at the day 35 time-point, 2 week post-second dose, for which the results are shown in Figure 3-8B. From Figure 3-8B, it can be seen that the total IgG titres obtained post-second dose have increased, but the general trend observed is the same as for titres obtained post-first dose. One difference is that the anti-NadA3 titres raised by the wildtype NadA3 (24-170) are no longer significantly higher than those induced by immunisation with an equivalent molar amount of the subunit NadA3-PorA antigen. This may be due to NadA3 (24-170) immunisation antibody titres approaching a plateau before those induced by NadA3-PorA immunisation, which is possible by a day 35 timeframe (Leenaars and Hendriksen, 2005).

As discussed in the introduction chapter, the more robust humoral immune responses seen when an antigen is presented in a multicopy, repetitive array compared to the 'soluble' single antigen has been mainly attributed to stronger germinal centre B-cell activation due to multiple simultaneous engagements with B-cell receptors, which sees more antigen processed and stronger interactions with T_{FH} cells (Rappuoli and Serruto, 2019). Furthermore, effects relating to particulate antigen trafficking and immune organ localisation have also been proposed to contribute (Irvine et al., 2013). There are numerous examples of high density particulate antigenic arrays successfully exploiting this immunological mechanism in order to enhance vaccine immune responses. Ferritin as a scaffold to display influenza HA antigen, which resulted in antibody titres tenfold higher than those of a licensed inactivated vaccine remains a pertinent example (Kanekiyo et al., 2013). In a significant step forward from self-assembling natural protein particles such as ferritin, Marcandalli et al. were able to computationally design from scratch a self-assembling protein nanoparticle presenting 20 stable copies of the RSV fusion protein in its prefusion conformation, which again was able to elicit far higher neutralising antibody titres compared to the soluble protein alone (Marcandalli et al., 2019).

An example using a synthetic-based nanoparticle include a study by Ding et al., who conjugated the porcine circovirus Cap protein from PCV2 in an orientationally defined manner to the surface of gold nanoparticles, which promoted phagocytosis and enhanced both cellular and humoral immunity (Ding et al., 2017). Similarly, a candidate malaria antigen was conjugated to lipid-enveloped poly(lactide-co-glycolide) acid (PLGA) nanoparticles, resulting in enhanced promotion of germinal centre formation and higher titre, durable antigen-specific antibodies (Moon et al., 2012).

3.3.6 Analysis of anti-NadA3 IgG1 and IgG2a antibody titres

The humoral response to immunisation was further investigated by analysing the IgG1 and IgG2a subclass titres. IgG can be further divided into four subclasses, IgG1, IgG2, IgG3 and IgG4, named according to their decreasing abundance within the body (Schur, 1988). At an amino acid sequence level, they are highly conserved however they differ in regions that are involved in both binding both to Fc receptors and C1q (Vidarsson et al., 2014). These differences are reflected in the ability of a subclass to activate complement or bind to FcR-expressing cells, which leads to phagocytosis. In humans, IgG1 has been found to activate complement effectively (Bindon et al., 1988), whereas IgG2 is more effective when the antigen is presented

at higher surface densities (Michaelsen et al., 1991). Furthermore, IgG1 has also been shown to be regularly highly effective at inducing phagocytosis mediated by FcR binding (Naess et al., 1999).

The antigen type, its route of administration, and secondary immune signals a B cell receives can all influence the skewing of antibody subclass response (Vidarsson et al., 2014). Whereas antibody responses to soluble protein antigens tend to be primarily IgG1 (Vidarsson et al., 2014), responses to bacterial capsular polysaccharides in the absence of T-cell help can be almost completely IgG2 (Barrett and Ayoub, 1986). Th1 and Th2 subsets of CD4+ T-cells upon stimulation with the antigen can also help to influence differentiation of the B-cell, with the Th1 subset able to enhance production of the IgG2a antibody and Th2 the production of IgG1 (Bretscher, 2014; Mosmann and Coffman, 1989). Adjuvants too can affect the Th1-Th2 balance; in a head-to-head study, Knudsen et al. demonstrated that each adjuvant had its own immunological signature, independent of the antigen, with MF59 found to exhibit a Th2 bias, resulting in a tendency towards IgG1 (Knudsen et al., 2016). Figure 3-9 (IgG1) and (IgG2a) display titres obtained for both timepoints day 21 and 35.

A)

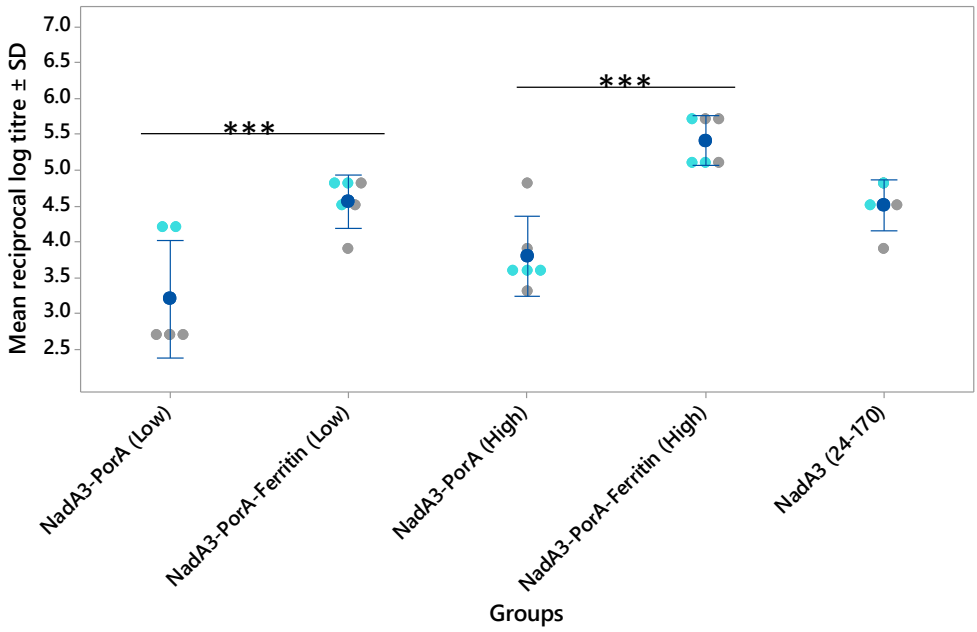

B)

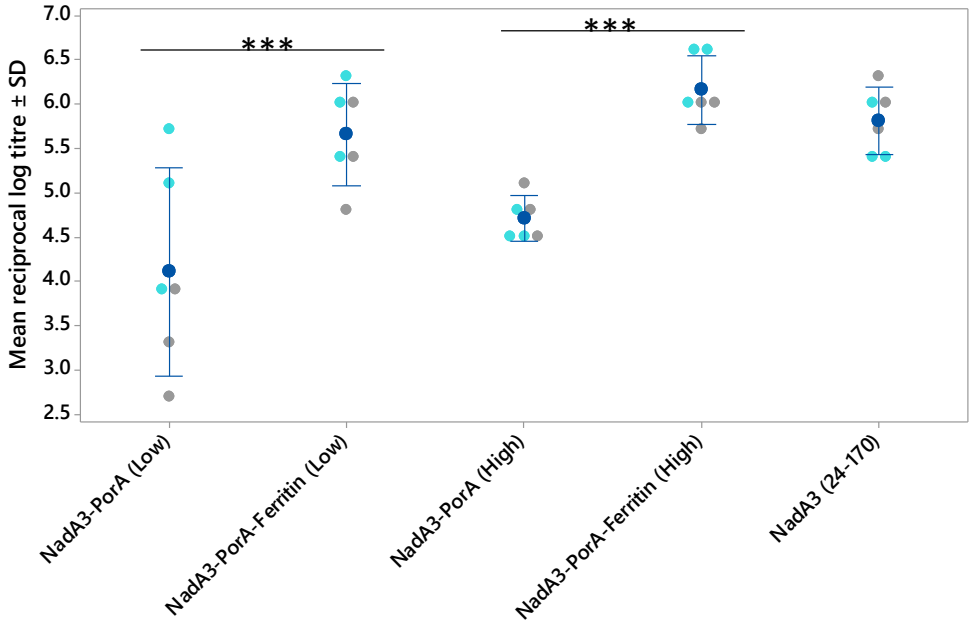

Figure 3-9 Anti-NadA3 (24-170) IgG1 titres showing that NadA3-PorA-Ferritin immunisation mediates a more potent humoral immune response over the subunit antigen NadA3-PorA alone. Titres displayed derive from sera collected either A) 21 days after immunisation with the first dose or B) At the day 35 time-point, 2 weeks after the second dose. Sera was assayed for anti-NadA3 (24-170) endpoint IgG1 titres by ELISA. The study was split into two studies, initiated 2 weeks apart; light blue ● indicate the endpoint titres from mice of the first study, grey dots ● those from the second study. The dark blue dot ● represents the mean reciprocal endpoint log titre ± SD. Significant differences between means were determined by the Tukey Simultaneous Tests for Differences of Means, with significance denoted as ***$p < 0.001$.

From the day 21 IgG1 titres displayed in Figure 3-9A, the titres follow the same general trend as those for the total IgG, with the nanoparticle immunisations achieving significance over those with the subunit antigen NadA3-PorA ($p< 0.001$). Furthermore, rather than equalling the titres of the wild type NadA3 (24-170), the titres for higher dose group of NadA3-PorA-Ferritin surpass those of the wild type ($p<0.05$). As for the total IgG, the IgG1titres obtained with immunisation with the subunit NadA3-PorA compared to the wild type NadA3 (24-170) follow a similar trend as for the total IgG but are no longer significantly different. IgG1 titres obtained for day 35 (shown in Figure 3-9B) have increased for all groups while still following a similar trend as seen for day 21. However, the higher dose group of the NadA3-PorA-Ferritin is no longer significantly higher than the wild type NadA3 (24-170), and the titres obtained for the wild type NadA3 (24-170) are now significantly higher than both those for the NadA3-PorA subunit antigen ($p<0.005$).

A)

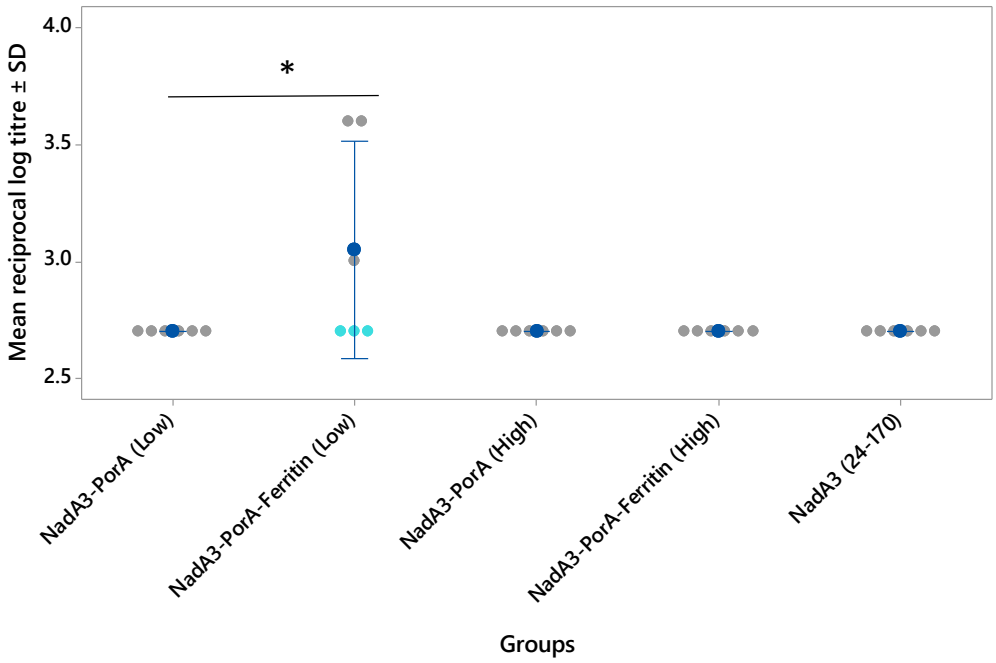

B)

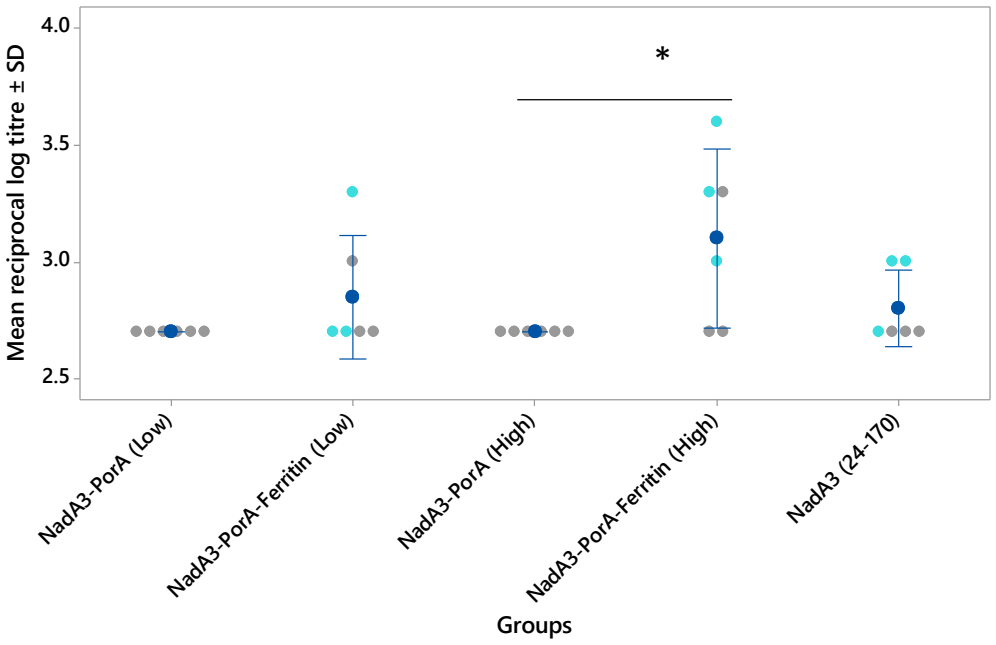

Figure 3-10 Anti-NadA3 (24-170) IgG2a titres. Titres displayed derive from sera collected either A) 21 days after immunisation with the first dose or B) At the day 35 time-point, 2 weeks after the second dose. Sera was assayed for anti-NadA3 (24-170) endpoint IgG2a titres by ELISA. Along the x-axis the immunisation groups are displayed. The study was split into two studies, initiated 2 weeks apart; light blue ● indicate the endpoint titres from mice of the first study, grey dots ● those from the second study. The dark blue dot ● represents the mean reciprocal endpoint log titre ± SD. Significant differences between means were determined by the Tukey Simultaneous Tests for Differences of Means, with significance denoted as *p < 0.05.

Figure 3-10 shows the IgG2a titres obtained at the day 21 and 35 timepoints. At the day 21 time-point, IgG2a titres are at background throughout apart from the lower dose NadA3-PorA-Ferritin group, which reaches significance ($p<0.05$) whilst still remaining low. Titres remain low at the day 35 timepoint, with only the higher dose NadA3-PorA-Ferritin group inducing IgG2a titres significantly higher only than when compared to the subunit NadA3-PorA immunisation groups ($p <0.05$).

In comparing the IgG1 and IgG2a titres overall, the antibody responses induced are strongly skewed towards a Th2-type response, though nanoparticle immunisation does appear to slightly shift the Th1-Th2 balance towards a more mixed response in comparison to subunit NadA3-PorA antigen immunisation. The NadA3-PorA antigen comprises the epitopes from the Bexsero vaccine proteins NadA3 and the PorA membrane protein. As part of the multicomponent vaccine, NadA3 was selected for inclusion based on its ability to help induce a broad protection against a diverse collection of MenB strains, as assessed by SBA or the ability of anti-NadA3 antibodies to confer passive protection in rat or mouse models (Serruto et al., 2012). However, the relative contribution of each anti-NadA3 IgG subclass to host immunity against MenB is lacking in the literature. Each of the IgG subclasses can aid in the clearance of encapsulated bacteria, such as MenB, by different mechanisms, however an immune response showing a broad distribution of subclasses may be beneficial (Lefeber et al., 2003). Given that in mice it has been observed that IgG2a has a greater ability than IgG1 to activate the classical pathway of complement mediated killing (Michaelsen et al., 2004), the fact that immunisation with NadA3-PorA-Ferritin induces higher IgG2a titres could positively impact the SBA titres obtained.

The overall Th2-type response seen for all the immunisation groups could be explained by the observation that soluble proteins primarily induce IgG1 (Vidarsson et al., 2014). Another factor that could contribute is the MF59-based adjuvant used. MF59, as mentioned previously, was found to induce an IgG1 bias when used to adjuvant a panel of different protein antigens (Knudsen et al., 2016).

Nanoparticle immunisation resulting in a shift towards a more balanced Th1-Th2 response compared to soluble subunit antigen was observed for a malarial protein surface displayed on lipid-enveloped PLGA nanoparticles, however the absolute IgG2 titres and increase in significance was far greater than seen here (Moon et al., 2012). The type of nanoparticle in that study, a lipid-enveloped PLGA nanoparticle, is also a hugely different system to the protein-based ferritin and so this could explain the differences in the Th1-Th2 balance seen.

Though only the anti-NadA3 humoral response is discussed in this section, it is also worth considering what has been observed with regards to the PorA component. The PorA (serosubtype P1.4) component of the Bexsero vaccine is contained in OMVs derived from MenB strain NZ98/254; these OMVs had already been successfully deployed as a vaccine to control a MenB epidemic in New Zealand. The protection conferred by OMVs of wild type circulating invasive strains is largely attributed to their ability to induce bactericidal antibodies against PorA (Holst et al., 2005). One study found that IgG1 dominated the IgG subclass response after vaccination with one such type of OMV (Naess et al., 1999). Another study using the Bexsero antigen fHbp as a scaffold to present the PorA VR2 loop found that adjuvanting with alum induced a predominantly Th2 response with higher IgG1 titres, while the adjuvant monophospholipid A (MPLA) enhanced Th1 responses, enhancing the levels of IgG2a antibody directed against the PorA VR2 loop epitope (Hollingshead et al., 2018).

3.3.7 Cellular immune response to vaccination with NadA3-PorA-Ferritin

T-cell epitopes are short peptides that are presented by the membrane-histocompatibility complex (MHC) proteins, of which there are two classes; class I and II. The two classes of MHC molecules are recognised by distinct subsets of T cells, with class I MHC molecules recognised by CD8+ T-cells and class II by CD4+ T- cells. Specific T-cell activation by binding to MHC molecules can only happen following enzymatic degradation of antigen and its presentation as an MHC-peptide complex (Naess et al., 2001).

Nearly all nucleated cells express MHC class I molecules (Hewitt, 2003). CD8+ T-cells become cytotoxic T-cells on recognition of the peptide-MHC class I complex and are primarily responsible for pathogen surveillance and cytolysis of somatic cells presenting endogenously derived antigenic peptides (i.e. from viruses or other intracellular pathogens) on their MHC class I molecules. MHC class II molecules however are expressed primarily only on cells of the immune system, particularly by professional APCs such as dendritic cells, macrophages, and B-cells. Therefore, extracellular bacteria such as MenB are presented to CD4+ T cells by way of peptide-MHC class II complexes, following their uptake of the bacterium by the aforementioned APCs. Naïve CD4+ T-cells are primed by the interaction with APCs

in peripheral lymphoid tissue and once primed, these CD4+ T-cells then differentiate into helper T-cells (Th), which help to amplify the immune response, or regulatory (Treg) T-cells (Sanchez-Trincado et al., 2017). There are three main classes of Th cells: Th1 (help promote cell-mediated immunity against intracellular pathogens), Th2 (antibody-mediated immunity), and Th17 (inflammatory response and defence against extracellular bacteria) (Sun and Zhang, 2014).

The Th1 or Th2 classes of CD4 T-cells can be classified according to the cytokines they produce (Abbas et al., 1996). Intracellular microbes tend to induce a Th1-skewed response, with these cells producing important inducers of cellular immunity in response, such as IFN-ɣ and TNF-α. Extracellular pathogens and parasites on the other hand tend to trigger Th2 responses, which sees these cells producing cytokine factors such as IL-4, IL-5, IL-6, and IL-13, which are Important for the induction and regulation of B-cell responses.

With protective immunity against MenB relying on humoral effector functions such as complement mediated killing and opsonophagocytosis (Vermont and van den Dobbelsteen, 2002), Th2 helper cells play an important immuno regulatory role by helping to stimulate B-cells to produce antibodies both at a systemic and mucosal level (Ada, 1990). This Th2 cytokine-mediated help towards antigen-specific B cells ultimately leads to an improved immune response by stimulating immunoglobulin class switching, affinity maturation, and increasing the magnitude of the antibody response (Oftung et al., 2016). Furthermore, T cells are also able to induce immunological memory while also indirectly aiding the phagocytic uptake and destruction of bacteria by promoting the activation of phagocytic cells. Indeed, enhancing of the immunogenicity of polysaccharide antigens by conjugating them to carrier proteins bearing T-cell epitopes (in the case of conjugate meningococcal vaccines for example) is one demonstration of the power of T-cell activation (MacDonald et al., 1998).

Given the importance of cell-mediated immunity in the form of CD4+ T-cell activation, antigen-specific T cell cytokine secretion in response to immunisation with NadA3-PorA-Ferritin versus the subunit antigen NadA3-PorA was investigated. Splenocytes were isolated from the immunisation groups 1-4 described in section 3.3.4 and these were then stimulated with the homologous subunit antigen NadA3-PorA for 72 hours. The NadA3 (24-170) immunisation group 5 was instead stimulated with its homologous antigen NadA3 (24-170). After the 72-hour stimulation period, cytokine

levels in the culture supernatant were measured using the LEGENDplex mouse inflammation panel flow cytometry kit.

In this bead-based multiplex assay, the panel used allowed for the simultaneous quantification of 13 mouse cytokines, including IL-2, 4, 5, 6, 9, 10, 13, 17A, 17F, 21, 22, IFNγ and TNFα, which are collectively secreted by Th1, Th2, Th9, Th17, Th22 and T_{FH} cells. Compared to a traditional cytokine ELISA method, this multiplex assay enables higher sensitivities and a broader dynamic range. Figure 3-11 through to Figure 3-14 detail the cytokine responses as classified by T-cell helper subsets. In this assay, control groups were also included; 'NadA-PorA control' and 'NadA3 control' groups are non-immunised spleens stimulated with their homologous antigens. The RPMI negative control group consists of immunised splenocytes from each group stimulated with no antigen.

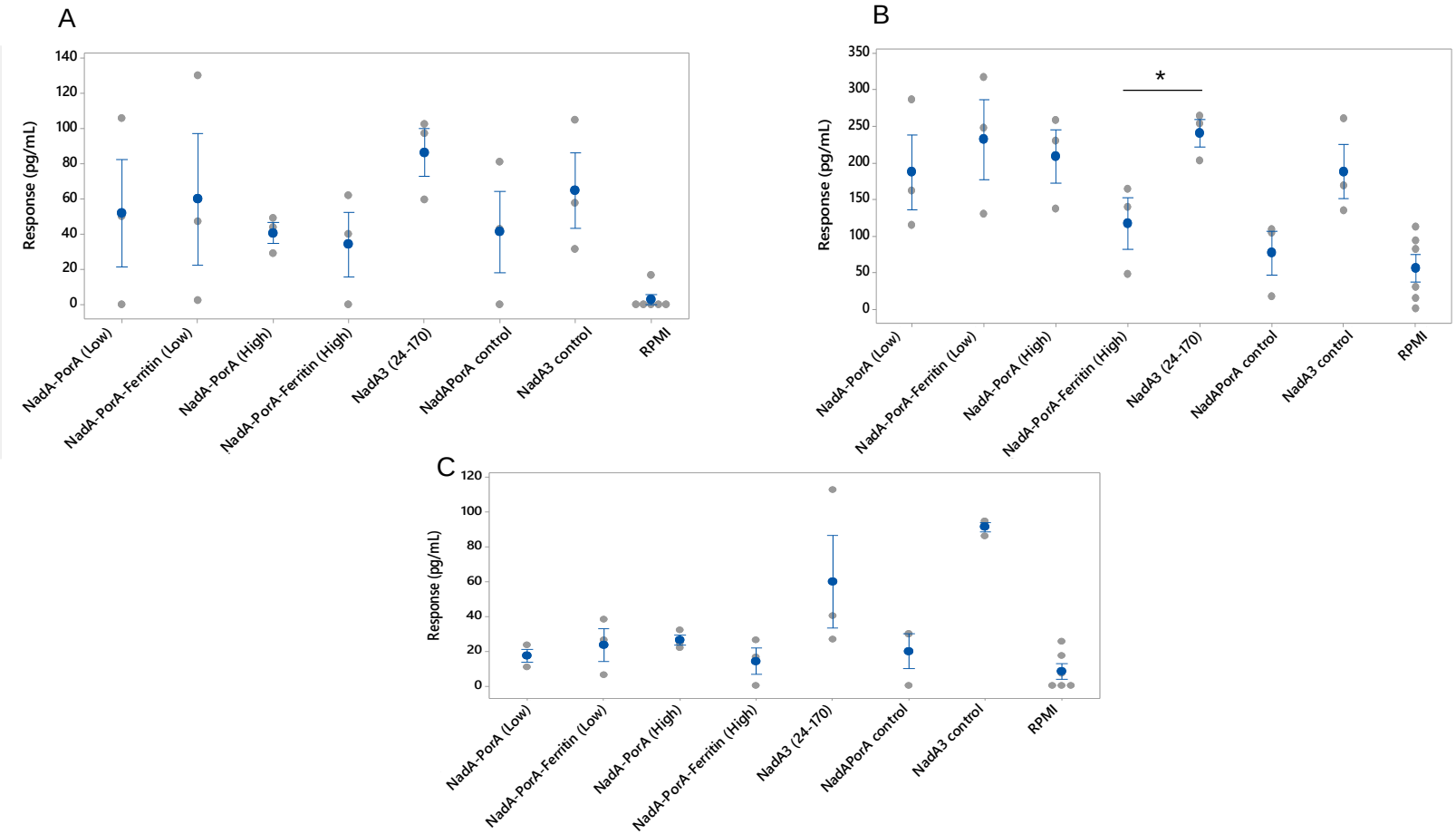

Figure 3-11 Cellular immune responses in terms of Th1 cytokines A) IFNγ B) IL-2. C) TNF-α. After 72 hours of stimulation with either NadA3-PorA or NadA3 (24-170) the supernatants were assayed for the presence of cytokines using the LEGENDplex mouse inflammation kit. Grey dots ● represent individual mice and the dark blue dot ● represents the group mean, with the interval bar representing the standard error of the mean. Three mice per group were analysed, except for the RPMI group where n=6. Statistical analysis of data was calculated by one-way analysis of variance (ANOVA). Significant differences between means were determined by the Tukey Simultaneous Tests for Differences of Means, with significance denoted as *p < 0.05.

Figure 3-11 shows the Th1 cytokine response to immunisation. Both IFNγ and IL-2 have been classed as cytokines expressed by Th1 cells, while TNF-α is produced by both Th1 and Th2 cells (Zhu et al., 2010). In comparing the responses obtained for immunisation with the nanoparticle to the subunit NadA3-PorA, there are no significant differences between them.

If the NadA3 (24-170) immunised group is examined, in the case of TNF-α a significant difference ($p < 0.05$) in the response over the rest of the immunisation groups is found. This holds true also for the control group naïve splenocytes stimulated with NadA3 (24-170). Though in these two groups, the stimulating antigen is NadA3 (24-170) rather than NadA3-PorA, these differences in responses could be indicative of the wild type NadA3 (24-170) retaining different T-cell epitopes compared to the modified NadA3-PorA.

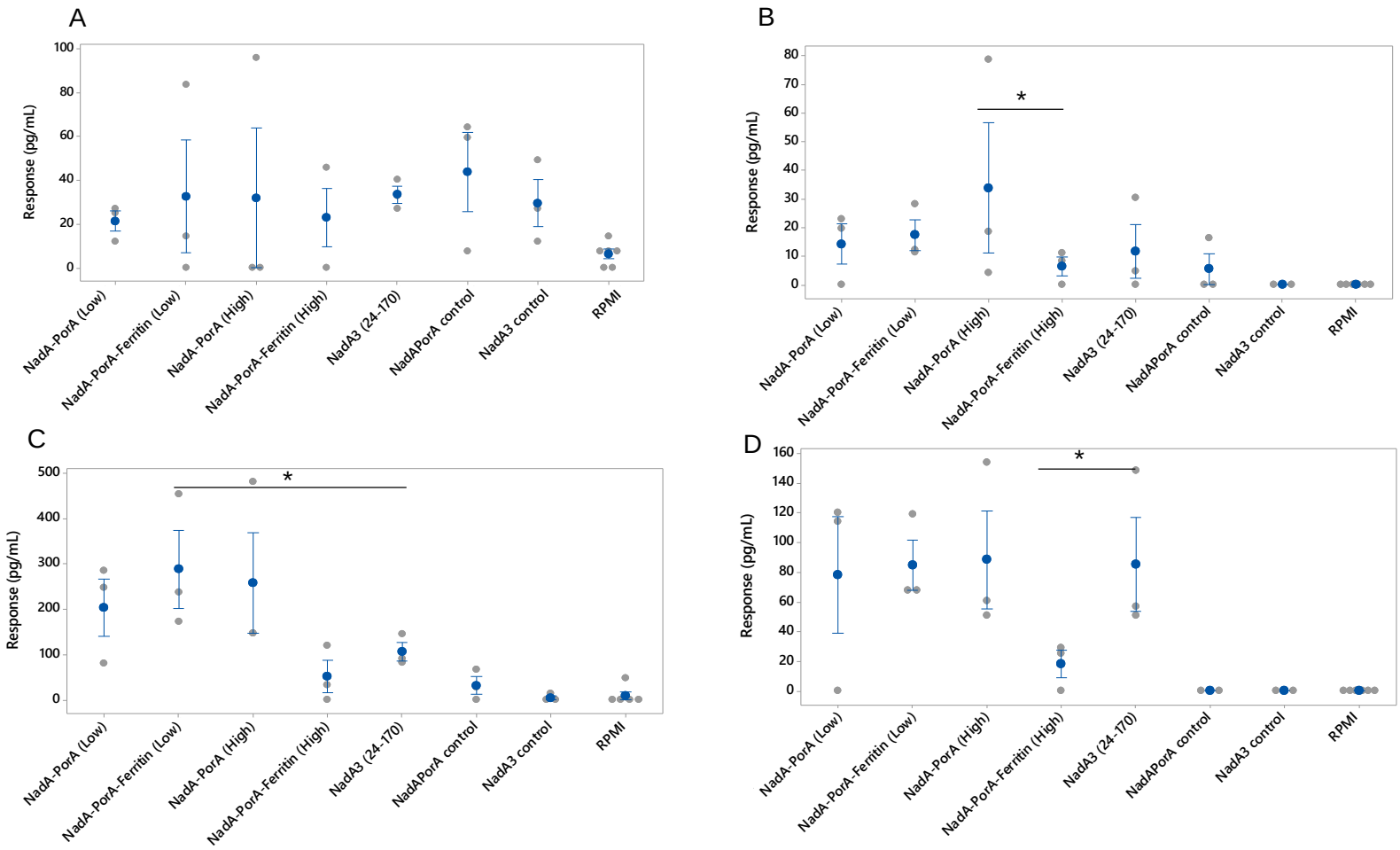

Figure 3-12 Cellular immune responses in terms of Th2 cytokines A) IL-10 B) IL-4 C) IL-5 D) IL-13. After 72 hours of stimulation with either NadA3-PorA or NadA3 (24-170) the supernatants were assayed for the presence of cytokines using the LEGENDplex mouse inflammation kit. Grey dots ● represent individual mice and the dark blue dot ● represents the group mean, with the interval bar representing the standard error of the mean. Three mice per group were analysed, except for the RPMI group where n=6. Statistical analysis of data was calculated by one-way analysis of variance (ANOVA). Significant differences between means were determined by the Tukey Simultaneous Tests for Differences of Means, with significance denoted as *p < 0.05.

The Th2 cytokine responses are shown in Figure 3-12. IL-4, -5 and -13 are signature cytokines of the Th2 lineage, with IL-10 also being classed alongside (Zhu et al., 2010). In comparing the responses obtained for immunisation with the nanoparticle to the subunit NadA3-PorA, there are no significant differences between them in the case of IL-10. However, for the rest of the cytokines, the higher dose NadA3-PorA-Ferritin group registers responses significantly lower (ranging from $*p < 0.05$ to $**p < 0.01$). Yet, this is countered by the fact that lower dose NadA3-PorA-Ferritin group shows responses comparable to those of both subunit NadA3-PorA groups. If responses by the NadA3 (24-170) immunised group are examined, it is seen that the IL-5 response is significantly lower ($*p < 0.05$) compared to the NadA3-PorA-Ferritn lower dose group.

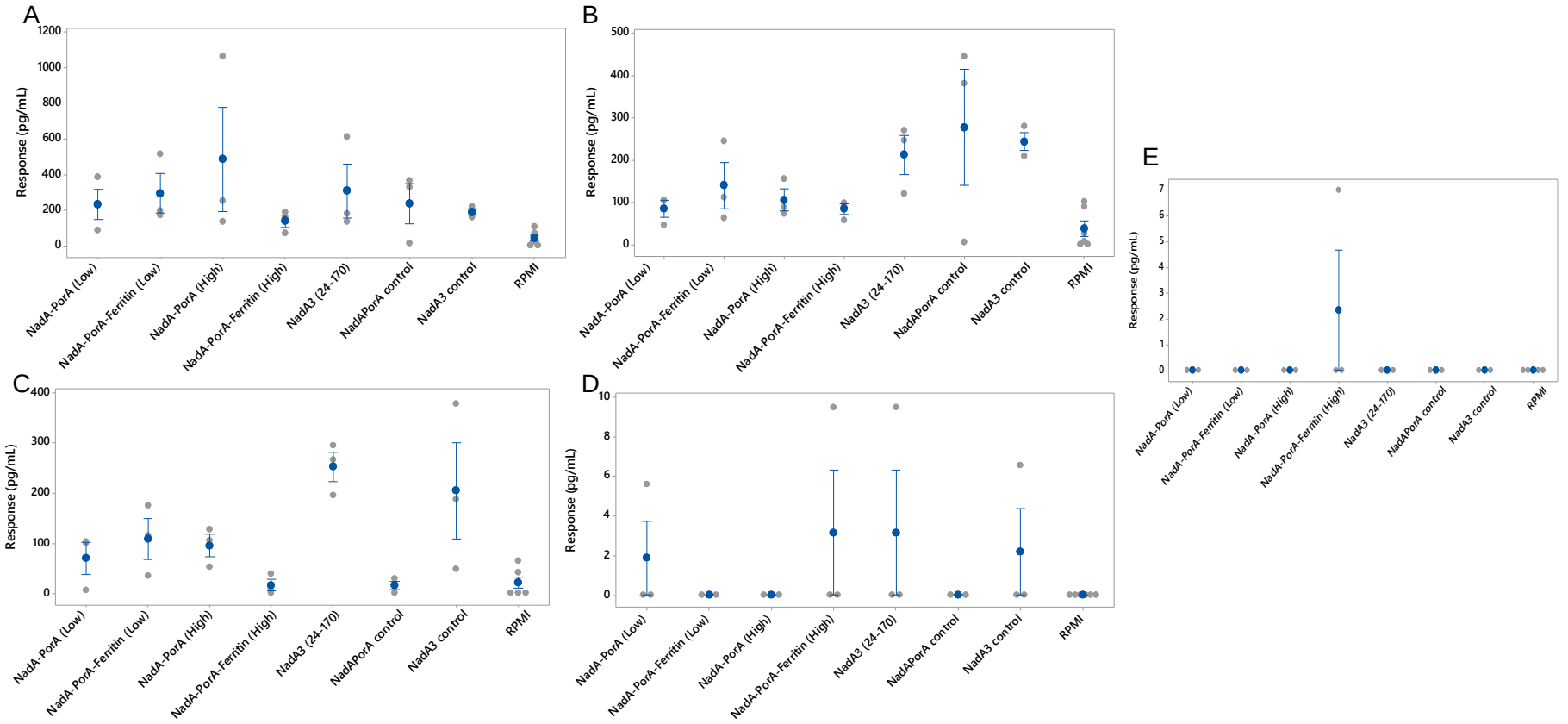

Figure 3-13 Cellular immune responses in terms of Th17, Th22 and T_{FH} cytokines A) IL-6 B) IL-22 C) IL-17A D) IL-17F E) IL-21. After 72 hours of stimulation with either NadA3-PorA or NadA3 (24-170) the supernatants were assayed for the presence of cytokines using the LEGENDplex mouse inflammation kit. Grey dots ● represent individual mice and the dark blue dot ● represents the group mean, with the interval bar representing the standard error of the mean. Three mice per group were analysed, except for the RPMI group where n=6.

In Figure 3-13, an attempt has been made to group cytokines of the Th17, Th22 and T_{FH} lineages, though as per Th1 and Th2, many of these cytokines not specific and are shared between the lineages. Th17 cells are generally considered to act as positive regulators of immune responses (Wu et al., 2018) recognised as having IL-17A, IL-17F, and IL-22 signature cytokines, as well as being good producers of IL-21 and IL-6 (Zhu et al., 2010). Th22 cells, playing a significant role in inflammatory and autoimmune disorders, are characterised on the other hand by production of IL-22 and TNF-α (Scheiblhofer et al., 2017). T_{FH} cells are specialised in providing help to B cells, and are essential for germinal centre formation, affinity maturation and development of memory B cells (Crotty, 2014). IL-21 can be classed as a cytokine secreted by T_{FH} cells (Jandl et al., 2017). In comparing the responses obtained for immunisation with the nanoparticle to the subunit NadA-PorA, again, there are no significant differences between them. Notable is that immunisation with NadA3 (24-170) (and subsequent stimulation with said antigen) results in significant increases in IL-17A responses (ranging from *p < 0.05 to ***p < 0.001).

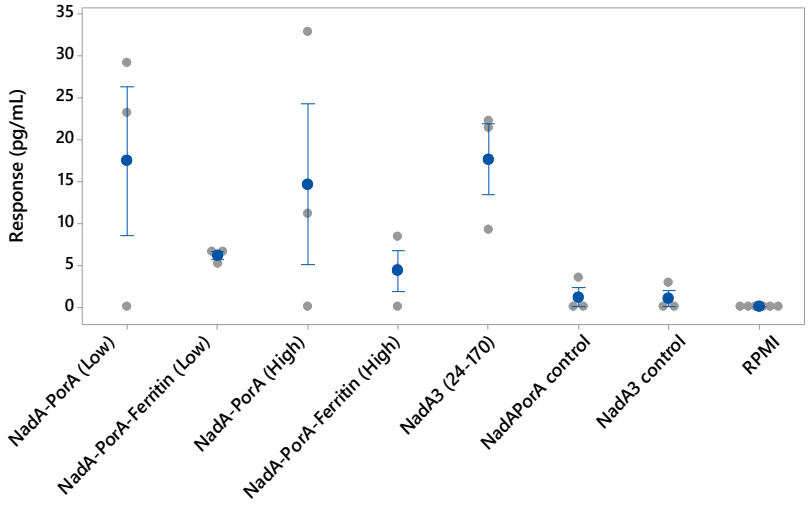

Figure 3-14 Cellular immune responses in in terms of Th9 lineage A) IL-9. After 72 hours of stimulation with either NadA3-PorA or NadA3 (24-170) the supernatants were assayed for the presence of cytokines using the LEGENDplex mouse inflammation kit. Grey dots ● represent individual mice and the dark blue dot ● represents the group mean, with the interval bar representing the standard error of the mean. Three mice per group were analysed, except for the RPMI group where n=6.

The final cytokine to be discussed is IL-9, recognised as being produced by cells of the Th9 lineage, which are implicated in allergic inflammation, and immunity to

extracellular pathogens, amongst others (Roy and Awasthi, 2019). Figure 3-14 shows the responses obtained. No significant differences are found between the nanoparticle and the subunit immunised groups.

The IgG1/IgG2a titres presented in section 3.3.6 showed a slight shift toward a more mixed Th1/Th2 balance following immunisation with the nanoparticle NadA3-PorA-Ferritin. This however is not reflected in the cytokine responses presented here, with no clear significant differences seen between the nanoparticle and subunit immunisations for any of the cytokines seen. Using a quite different nanoparticle system (lipid-enveloped PLGA nanoparticles) to surface present a malarial protein, Moon et al. found a more balanced Th1/Th2 antibody response due to nanoparticle immunisation, however this too was not reflected in the cytokine analysis of reticulated splenocytes, which gave no statistically significant differences nanoparticle or subunit immunisation (Moon et al., 2012).

3.3.8 T-cell epitope mapping of the NadA3-PorA chimeric antigen

The protective immune function of T-cells depends on their ability to recognise cells presenting specific peptides derived from antigens. Identification of such peptides (T-cell epitopes) can be crucial for vaccine development, especially in an era of rational epitope-based vaccine design, which foresees the potential of identifying and incorporating multiple immunoprotective epitopes into single, chimeric molecules to confer broadly protective and efficacious vaccines. In this respect, mapping of T cell epitopes can be defined as the identification of antigen-derived peptides recognised by either CD4 or CD8 T cells (Li Pira et al., 2010).

In the rational design of the NadA3-PorA chimeric antigen, residues were removed from the native NadA3, which may then have an impact on the T-cell epitopes that remain and the ability of the antigen to elicit an immune response. In the case of MenB, an antibody-mediated response is particularly important therefore focus is given to identifying CD4 T-cell epitopes (rather than CD8 T-cell epitopes) of the NadA3-PorA chimeric antigen.

The recognition of T-cell epitopes is accomplished through binding of the CD4 T-cell receptor (TCR) expressed on the surface of the T-cell, which makes contacts with both the MHC molecule and the presented peptide. A key determinant of each TCR's specificity for a particular peptide is a hypervariable region within the genes of each of the α and β subunits of the TCR. These hypervariable encoded form the primary region of direct engagement with peptides presented by the MHC class II molecules (Sharma and Holt, 2014). Figure 3-15 depicts the interactions between the CD4 TCR and antigen presenting cells.

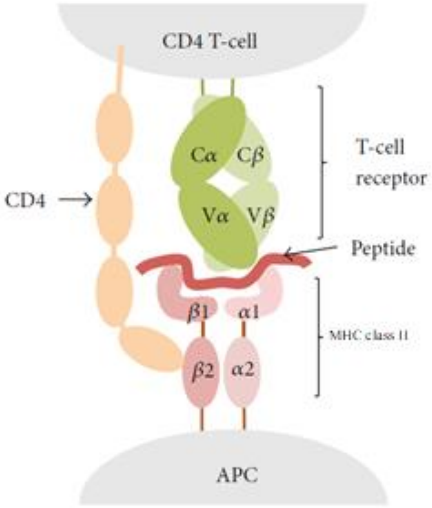

Figure 3-15 TCR recognition of T-cell epitopes presented by MHC class II molecules on the cell surface of APCs. The variable (represented by 'V') domains of each of the α and β subunits of the TCRs are where the aforementioned hypervariable regions are found. Diagram adapted from (Sanchez-Trincado et al., 2017).

To map immunogenic peptides, one could produce a complete panel of peptides, each of given length and a predetermined overlapping sequence that together span the entire length of the candidate antigen. Though comprehensive, this approach is prohibitive in terms of cost and labour time. *In silico* epitope prediction methods offer a way to overcome these limitations.

The potential of a peptide to stimulate T-cells is dependent on three basic steps: (i) antigen processing (that is, the generation of peptides from the antigen) (ii) peptide binding to MHC molecules and (iii) recognition of a peptide by its cognate TCR (Sanchez-Trincado et al., 2017). Of these, peptide binding to MHCs is the most selective for determination of T-cell epitopes. Numerous tools and databases are available to predict the level of binding of a peptide to a given MHC allele. Using such

tools, peptide panels can be restricted by deleting those peptides that have been predicted as unlikely binders to MHC molecules.

Though epitope predicting tools show good performance in identifying MHC class I peptides, the prediction of MHC II binding epitopes is more limited (Lin et al., 2008). This lower predictive binding accuracy can be assigned to a number of factors, such as the shallower peptide binding pocket of the MHC II molecule, which renders it more permissive to a wider range of peptide sequences than MHC class I binding pockets (Sanchez-Trincado et al., 2017). Figure 3-16 illustrates these differences.

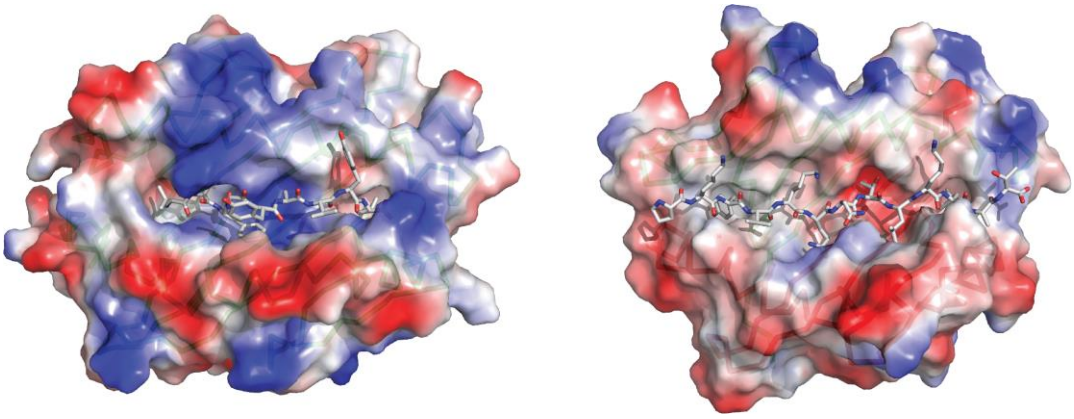

MHC class I binding pocket surface MHC class II binding pocket surface

Figure 3-16 The molecular surface from the point of view of the interacting TCR for both MHC I and II molecules. Both diagrams show the linear peptide within their respective binding pockets. Whereas the binding pocket for the MHC I is more closed, that of the MHC II is more shallow and open. As a result of this, MHC I molecules bind shorter peptides of 8–11 amino acids whereas MHC II molecules bind longer peptides of 9–22 amino acids. Image adapted from (Sanchez-Trincado et al., 2017).

There are numerous *in silico* methods that can be used to predict MHC-binding peptides and can be generally divided into the following two categories: data-driven and structure-based methods. By modelling the molecular dynamic simulations of binding, the structure-based approaches are advantaged in that experimental data is not required (Esther and Pedro, 2009). However, this approach is more computationally intensive and less successful in T-cell epitope prediction (Patronov and Doytchinova). The data-driven approach instead predicts MHC-binding peptides based on experimentally identified MHC-binding sequences.

An *in silico* approach was performed to predict NadA3-PorA derived peptides that could bind to MHC class II molecules and these peptides were then synthesised. For this work, the IEDB (Immune Epitope DataBase) was used to predict T-cell epitopes within the NadA3-PorA antigen (Vita et al., 2019). Epitope prediction using the IEDB

MHC-II binding predictor tool begins with the input of a protein sequence and as the binding core of an MHC class II molecule is reasoned to be 9 residues long, redundancy of predicated sequences (due to predicted sequences bearing the same 9-mer binding core) was reduced by splitting the protein sequence of NadA3-PorA into a series of 15-mers each with an overlap of 10 residues (Fleri et al., 2017).

These peptides were then fed into the IEDB MHC class II predictor, with predictions made for binding to the mouse H2-IAd and H2-IEd MHC class II haplotype antigens (Sellers et al., 2011). MHC molecules are highly polymorphic, however each laboratory mouse strain is homozygous and has a unique MHC haplotype designated by a small letter. In the case of BALB/c mice the MHC class II haplotype antigens are H2-IA d and H2-IE d.

Figure 3-17 shows a screenshot of the IEDB MHC class II predictor input.

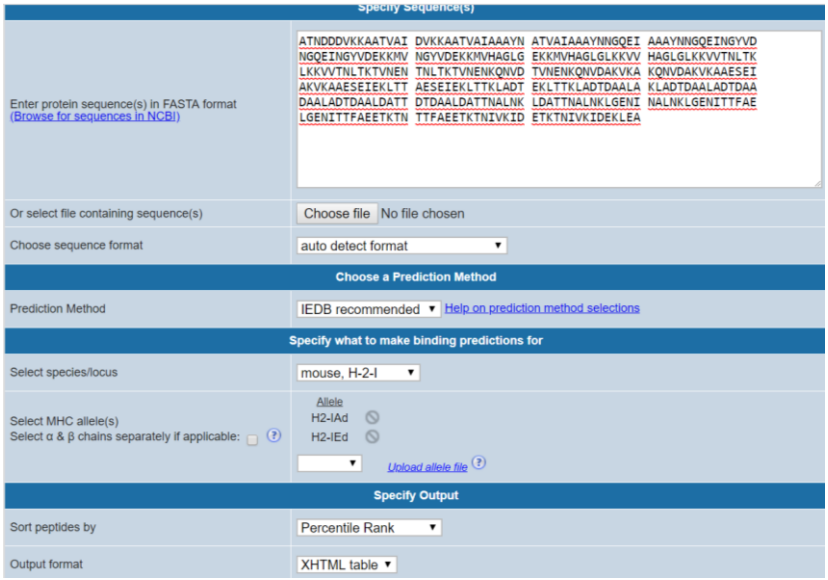

Figure 3-17 – A screenshot of the input form of IEDB MHC class II predictor for predicting NadA3-PorA peptides.

The output then gives a list of predicted binding sequences, from which the two peptides demonstrating the greatest predicted binding (represented by a lower percentile score on the output) were selected. A peptide, designated ‘NadA3 specific peptide’, mapped to a region removed on insertion of the PorA VR2 14 epitope. As means to validate this approach to peptide prediction, a negative control peptide was designed using a random sequence generator and was similarly entered into the

IEDB, with the output file predicting a low binding to MHC class II molecules for this peptide. A NadA3 specific peptide derived from a region removed in the NadA3-PorA construct would not be expected to stimulate splenocytes primed by NadA3-PorA-Ferritin immunisation. Table 3-2 shows the final set of peptides that were synthesised.

Table 3-2 List of peptides synthesised for splenocyte stimulation experiments. The 'MHC binders' are those predicted to bind to MHC class II molecules. The 'negative control' peptide is not predicted to bind to the MHC class II. The NadA3 specific peptide is derived from a region removed in the NadA3-PorA construct and would therefore not be expected to stimulate splenocytes primed by NadA3-PorA-Ferritin immunisation.

Peptide	Amino acid sequence
MHC binder 1	DVKKAATVAIAAAYN
MHC binder 2	AESEIEKLTTKLADT
Negative control	AAAYNNGQEINGFKA
NadA3 specific peptide	GTITKKDATAADVEA

In order to evaluate the immunogenicity of these peptides, mice that had been immunised with the NadA3-PorA-Ferritin had their splenocytes isolated and then the ability of the identified T-cell epitope peptides to stimulate CD4+ T-cells assessed by cytokine ELISA. It was also necessary to analyse the cytokine response to stimulation by these peptides in spleens that had been immunised with the wild-type NadA3 (24-170). This acted as a positive control, as stimulation by both MHC binder 1 & 2, as well as with the NadA3 specific peptide, would be expected to result in some level of cytokine response. Cytokine ELISAs were performed in order to detect the IFNγ (Figure 3-18) and IL-5 (Figure 3-19) responses for stimulated splenocytes deriving from either NadA3-PorA-Ferritin or NadA3 (24-170) immunisations.

A)

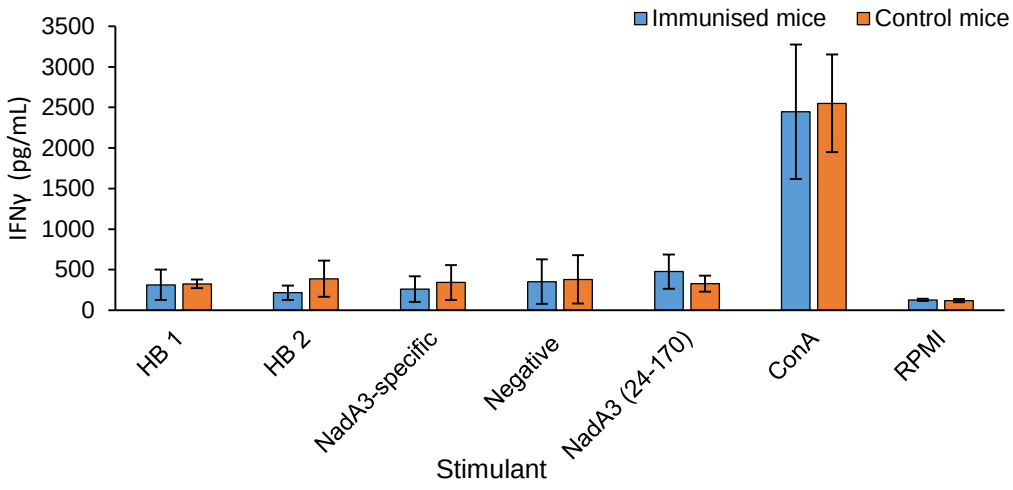

B)

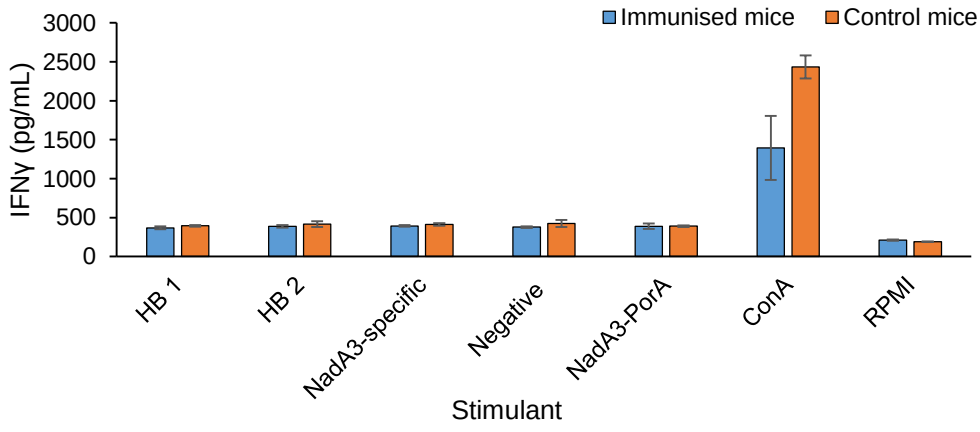

Figure 3-18 The IFNγ cytokine response measured for stimulated splenocytes deriving from immunisation with either with A) NadA3-PorA-Ferritin or B) NadA3 (24-170). For both immunised mice (blue) or control mice (orange), n=3 mice per group. Responses are represented as the group mean ±SD.

The IFNγ response for the NadA3 (24-170) immunisation group is shown in Figure 3-18A. There is not a significant difference in responses when the antigen NadA3 (24-170) is used to stimulate immunised or control splenocytes, with IFNγ responses low in both cases. It is therefore unsurprising that stimulation with any of the peptides

derived from NadA3 (24-170) predicted binders of the MHC class II, binders I and II, as well as the NadA3-specific also result in similarly low IFNγ responses. Indeed, IFNγ responses for immunised spleens when stimulated by these peptides fail to induce a response that surpasses that seen even for the control, non-immunised spleens. Only stimulation with the mitogen Concanavalin A (ConA) acting as a positive control for stimulation results in significantly high IFNγ responses for both immunised and control mice ($p<0.001$). For splenocytes derived from immunisation with NadA3-PorA-Ferritin, shown in Figure 3-18B, the IFNγ responses are similarly low, both when peptide or antigen NadA3-PorA is used to stimulate.

A)

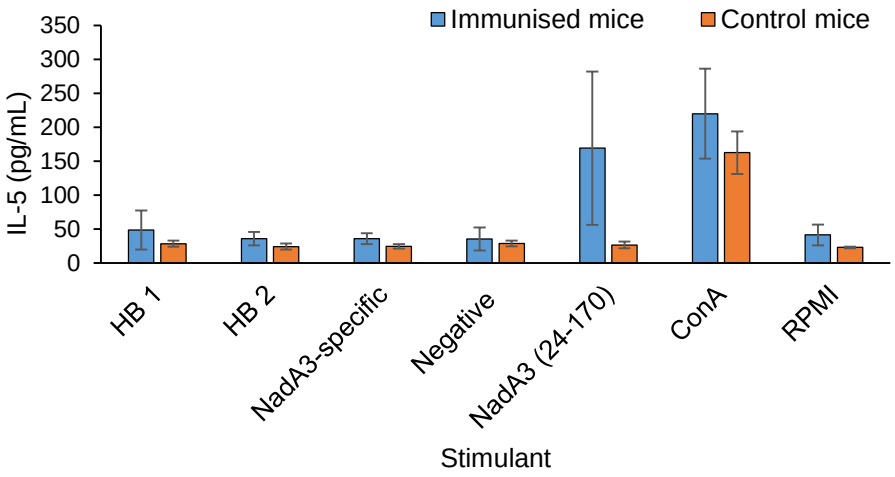

B)

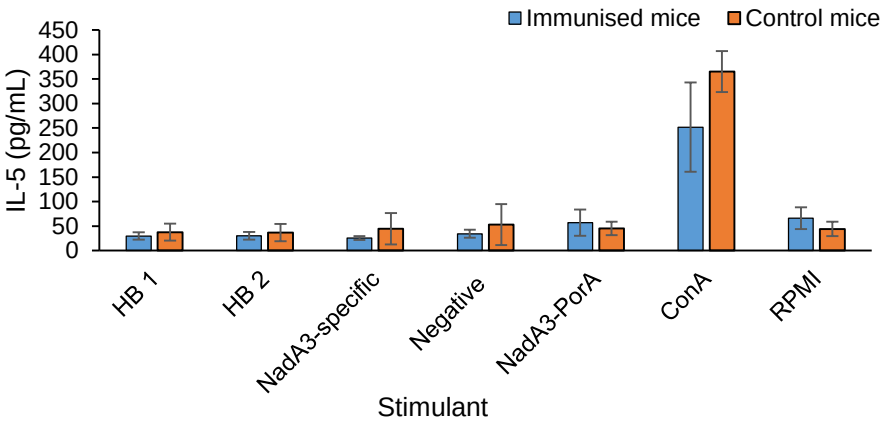

Figure 3-19 The IL-5 cytokine response measured for stimulated splenocytes deriving from immunisation with either with A) NadA3-PorA-Ferritin or B) NadA3 (24-170). For both immunised mice (blue) or control mice (orange), n=3 mice per group. Responses are represented as the group mean ±SD.

Figure 3-19A displaying results for the NadA3 (24-170) immunisation group shows that stimulation with NadA3 (24-170) results in a low IL-5 response that is not significantly greater than the IL-5 responses obtained for any other synthesised peptides. Stimulation with the synthesized peptides gives greater mean IL-5 responses over those of the control splenocytes, though not significantly so.

For splenocytes derived from immunisation with NadA3-PorA-Ferritin (Figure 3-19B), stimulation with the NadA3-PorA antigen does not result in a significant IL-5 response over any that induced by any of synthesised peptides. In addition, stimulation by any

of the synthesised peptides results too in a low IL-5 response that fails to surpass that produced by the control, non-immunised spleens.

Analysis of both the IFNγ and IL-5 response revealed that stimulation with the NadA3 (24-170) wildtype peptide was unable to induce significantly different responses in immunised splenocytes compared to control splenocytes. Since the native NadA3 (24-170) antigen is unable to induce responses, it is not surprising that the mapped peptides are also unable to induce potent responses.

As none of the predicted peptides can sufficiently stimulate splenocytes in the NadA3-immunsed group, it is not possible to confirm whether T-cell epitopes have been mapped. A number of reasons could explain the failure of the 'predicted' peptides to stimulate splenocytes. It could be that the peptides predicted by the Immune Epitope DataBase are not as capable in their ability to bind MHC class II molecules as predicted. Perhaps a more comprehensive (but expensive) screen composed of overlapping peptides encompassing the entire antigen could more conclusively identify T-cell epitopes.

3.3.9 Analysis of germinal centre formation promoted by NadA3-PorA-Ferritin immunisation

The longer-lived and higher titre humoral responses elicited by immunisation with nanoparticles suggest that they may promote the formation of germinal centers within lymphoid organs. To investigate this, splenocytes and lymphocytes (from inguinal draining lymph nodes) from the *in vivo* study (detailed in section 3.3.4) were isolated and germinal centre B cells were stained with an antibody panel before being quantified by flow cytometry.

The antibody panel consisted of four fluorescently-labelled antibodies, each specific for a certain marker. The markers were: B220, recognised as a pan B-cell marker in mice (Rodig et al., 2005), IgD, as it has been observed that the majority of germinal centre B cells are negative for this marker (Shinall et al., 2000), GL-7 as a positive marker for germinal centre B cells (Naito et al., 2007) and CD38 which is down-regulated on germinal centre B cells (Oliver et al., 1997). The germinal centre B cells were identified by flow cytometry according to the expression pattern B220+, IgD-, CD38 low, GL7+, with Figure 3-20 showing the gating straetgy and Figure 3-21 showing the results.

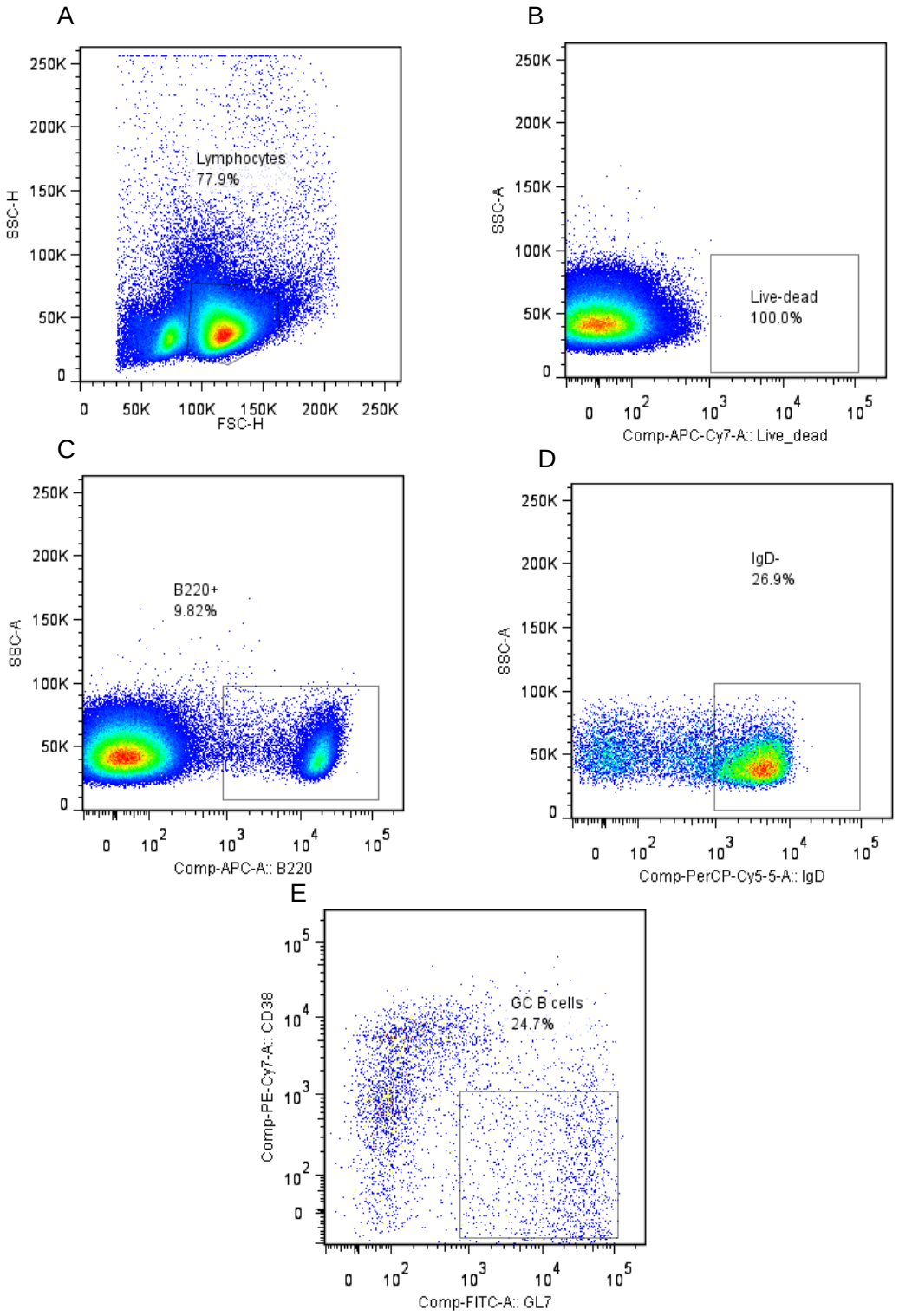

Figure 3-20 Flow cytometry gating strategy for germinal centre B cells. A) Lymphocytes were separated on the basis of forward-scatter height (FSC-H) and side-scatter height (SSC-H). B) Live cells were identified C) B220 expressing cells were gated D) IgD- cells were identified by excluding IgD+ cells E) GC B cells were defined based on high GL7 expression and low expression of CD38.

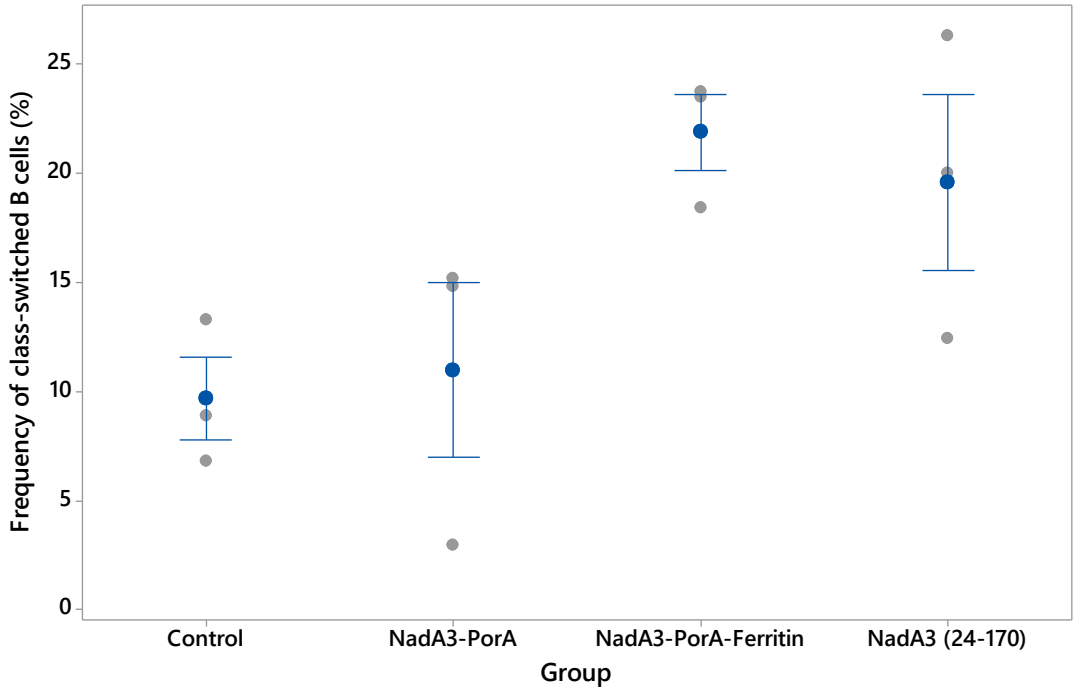

Figure 3-21 Analysis of germinal centre formation due to nanoparticle immunisation. Mice derived from the NadA3-PorA, NadA3-PorA-Ferritin high dose groups and the wild type NadA3 (24-170) group had their inguinal draining lymph nodes isolated and analysed for germinal centre formation. The number of isotype-switched germinal centre B cells (GL-7^{+}CD38 low, gated on B220^{+}IgD^{-} populations) in draining inguinal lymph nodes was measured by flow cytometric analysis. Grey dots ● indicate individual mice (n=3 per group). The dark blue dot ● represents the mean frequency of class-switched B-cells ± SD.

Figure 3-21 shows the frequency of the germinal centre (GC) B cells from inguinal lymph node lymphocytes isolated from control non-immunised mice and the immunisation groups NadA3-PorA, NadA3-PorA-Ferrtin (high dose groups) and NadA3 (24-170) (corresponding groups 3, 4 and 5 respectively detailed in Table 3-1). Immunisation with the subunit antigen NadA3-PorA induces GC formation to levels comparable to the control, non-immunised group. In comparison, the wildtype NadA3 (24-170) results in higher germinal centre formation compared to the subunit NadA3-PorA, though not significantly so.

As detailed in section 3.3.5, there were significant differences ($p< 0.001$) in the anti-NadA3 total IgG titres obtained in response to immunisation with NadA3-PorA and the NadA3 (24-170). Immunisation with protein antigens will usually result in both cellular and humoral responses, with B cells recognizing their cognate antigen in its native form (Heesters et al., 2016) whereas T cells recognize digested peptides as mentioned previously. As the interaction between GC B cells and T_{FH} cells is under

normal circumstances essential for GC response (Nutt and Tarlinton, 2011), the loss of either B cell or T cell epitopes may explain the differences seen both here and in the anti-NadA3 IgG responses.

The NadA3-PorA antigen is not technically deficient in terms of epitopes however, as though resides were lost from the NadA3, these were replaced by PorA VR2 14 loop epitope, which has also been shown to be highly immunogenic in terms of evoking bactericidal antibodies (Rouppe van der Voort et al., 1997). The induction and maintenance of anti-PorA are typically T-cell dependent (Meiring et al., 2005), with one such study that sought to map PorA-specific T cell epitopes identifying peptides corresponding to the surface exposed loops on the PorA, some of which were identical to B-cell epitopes on the protein (Wiertz et al., 1991).

When the levels of germinal centre formation induced by the administration of the NadA3-PorA-Ferritin is compared to that induced by the NadA3-PorA, it can be seen that the NadA3-PorA-Ferritin is able to raise GC formation to levels of the wildtype NadA3 (24-170). However, the difference observed between the NadA3-PorA and NadA3-PorA-Ferritin again is not statistically significant. Though a trend can be seen of increasing germinal centre following immunisation with the nanoparticle compared to the subunit NadA3-PorA, it should be acknowledged that the data presented in this present experiment is also limited due to the small sample size (n=3).

Tokatlian et al. showed that displaying the HIV gp140 trimeric subunit antigen on the surface of ferritin resulted in significantly higher GC B cells over immunisation with the subunit trimer alone (Tokatlian et al., 2019). Similarly, another study using lipid-enveloped PLGA nanoparticles to surface-display a malarial protein subunit antigen also found nanoparticle-display also enhanced germinal centre formation in respect to the subunit antigen (Moon et al., 2012).

3.3.10 Serum bactericidal activity of antibodies raised by nanoparticle immunisation

Both the NadA3 and PorA VR2 components of the NadA3-PorA chimeric antigen are able to elicit bactericidal antibodies that are crucial in mediating protection against MenB. The total IgG ELISA assays detailed in section 3.3.5 revealed that immunisation with the NadA3-PorA-Ferritin nanoparticle induced significantly higher anti-NadA3 antibody titres than those elicited by immunisation with the NadA3-PorA subunit antigen alone. However, an SBA assay is necessary to determine the

bactericidal titre of these elicited antibodies and to fully assess the efficacy of multi-copy antigen presentation. Comparing the bactericidal titres to those obtained by wild-type NadA3 (24-170) will also inform to what degree the modifications made in creating the chimeric antigen can affect the subsequent bactericidal response raised.

An SBA assay with the appropriate MenB strain also offers the possibility to confirm for the first time that the rational design enables the induction of antibodies against the PorA VR2 epitope and the bactericidal capacity of these elicited antibodies. To do this, sera obtained from the *in vivo study* (groups described in section 3.3.4) will be tested in an SBA against three different MenB strains. The selected strains are detailed in Table 3-3.

Table 3-3 The MenB panel used in the SBA to assess bactericidal antibodies raised by NadA3-PorA-Ferritin immunisation.

MenB strain	Details
5/99	Overexpressing NadA3. Expresses a PorA with a different VR2 epitope.
M08-02 40104	A NadA3 knockout, expressing a PorA with the VR2 14 epitope.
M14933	Expressing both NadA3 and PorA with the VR2 14.

The 5/99 strain contains a PorA VR2 epitope that differs from the one used in NadA3-PorA-Ferritin (PorA VR2 14) and so this strain effectively acts to detect for NadA3 antibodies only. This is based on the fact that OMV-based vaccines have been shown to offer limited or no-cross protection against strains bearing PorA molecules with a different VR2 (Holst et al., 2009), in addition to the worked detailed in the previous chapter where a mismatched PorA VR2 epitope was used to confirm the specificity of the commercially acquired PorA antibody. In the case of strain M08-02 40104, it is a NadA3 knockout and expresses a PorA bearing the VR2 14 epitope, so therefore can be considered as a suitable means for measuring bactericidal killing elicited by anti-PorA VR2 14 antibodies only. The final strain, M14933, expresses both NadA3 and the PorA with VR2 14. In Table 3-4 are shown the results for the day 35 immunisation sera assayed against these three MenB strains.

Table 3-4 SBA of sera taken from day 35 to assess bactericidal titres elicited by immunisation with the NadA3-PorA-Ferritin. Assay was performed in the presence of baby rabbit complement. * Group numbers are derived from Table 3-1.

Immunisation sera	Group number *	MenB strain		
		5/99	M08-0240104	M14933
NadA3-PorA (Low)	1	<64	<64	<64
NadA3-PorA-Ferritin (Low)	2	<64	<64	<64
NadA3-PorA (High)	3	<64	<64	<64
NadA3-PorA-Ferritin (High)	4	64	<64	<64
NadA3 (24-170)	5	<64	<64	<64
Non-immunised BALB/c control sera	-	<64	<64	<64
Internal control NadA3 clinical lot	-	>=32768	-	4096

As can be seen from Table 3-4, none of the immunisation groups 1-5 are able induce bactericidal titres; a titre of 64 or less is classed as being negative for bactericidal activity. The NadA3 clinical lot, acting as a positive control in this assay, is the only group able to elicit bactericidal titres against all MenB strains except from the M08-0240104 strain, which lacks the NadA3.

To see if sera from another timepoint might elicit improved bactericidal titres, sera deriving from day 49, collected 2 weeks following the third dose was used in a repeat SBA assay against the same strains. Only three mice per group, all deriving from the same study, were used to supply sera in this assay. Figure 3-22 shows the anti-NadA3 titres antibody (total IgG, IgG1 and IgG2a) for this time-point.

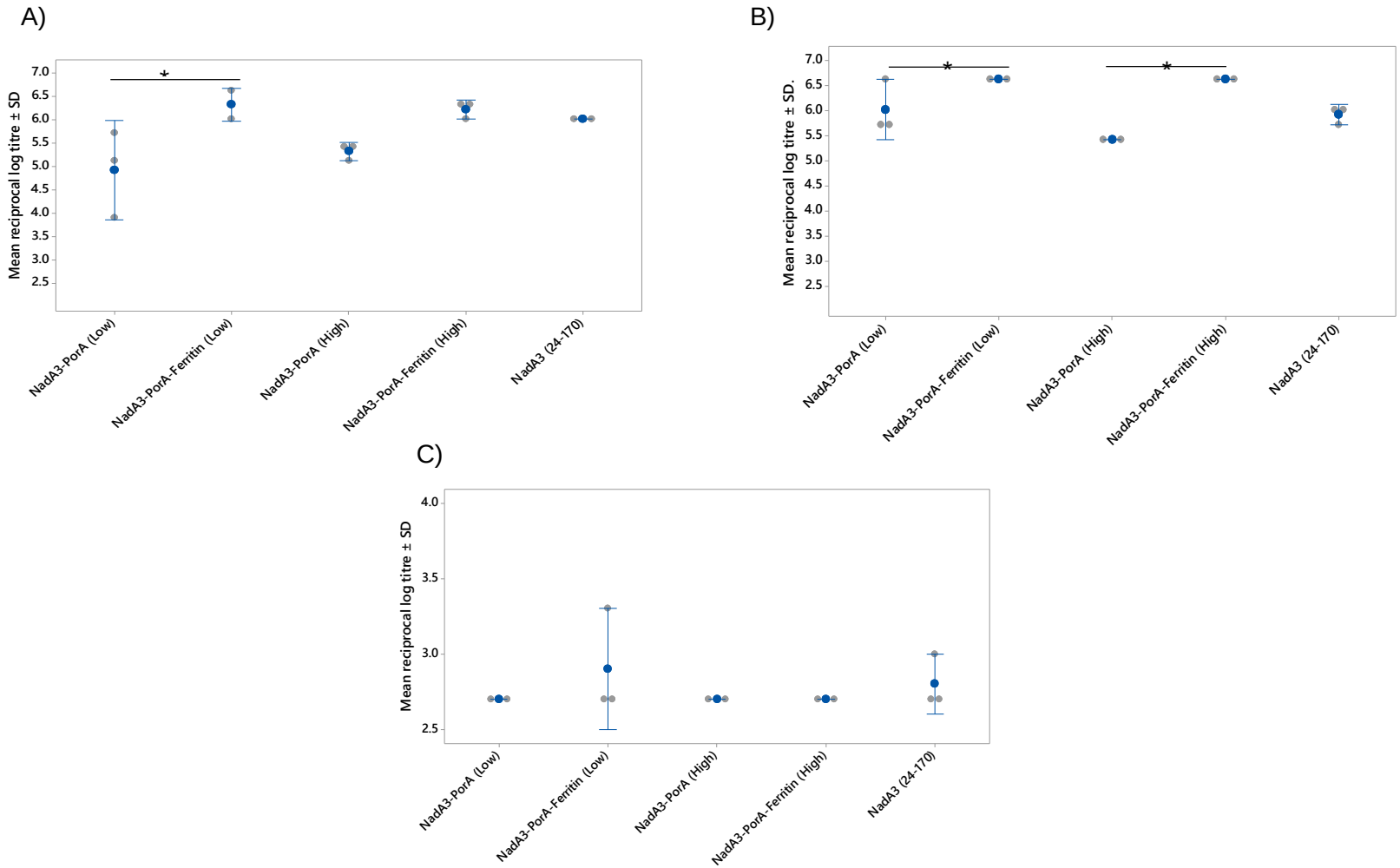

Figure 3-22 Anti-NadA3 (24-170) antibody titres collected at day 49, 2 weeks following the third dose. A) Total IgG B) IgG1 C) IgG2a. Mice were taken from study 1 only and each individual mouse is represented by a grey dot ●, the dark blue dot ● represents the mean reciprocal endpoint log titre ± SD. Significant differences between means were determined by the Tukey Simultaneous Tests for Differences of Means, with significance denoted as *p < 0.05.

Figure 3-22 shows the day 49 anti-NadA3 (24-170) antibody titres obtained measured by total IgG, IgG1 and IgG2a. Total IgG follows a similar trend as for day 35, with significant ($p<0.05$) differences between the nanoparticle and subunit 'low' dose groups. The 'high' dose groups however no longer show significant differences, though the smaller sample size of three mice means that significance between groups is more difficult to establish. The IgG1 also follows a similar trend as day 35, with both significant differences ($p<0.05$) between the nanoparticle and subunit antigen administrations for both dosage groups. The IgG1 titres obtained for the wildtype NadA3 (24-170) are now significantly lower ($p<0.05$) than those obtained for both NadA3-PorA-Ferritin dose groups. IgG2a again fits the same trend, with all titres remaining low and non-significance between the groups. Table 3-5 shows the SBA bactericidal titres obtained using these day 49 sera.

Table 3-5 SBA of sera taken from day 49 to assess bactericidal titres elicited by immunisation with the NadA3-PorA-Ferritin. Assay was performed in the presence of baby rabbit complement. * Group numbers are derived from Table 3-1

Immunisation sera	Group number *	MenB strain		
		5/99	M08-0240104	M14933
NadA3-PorA (Low)	1	<16	<16	16
NadA3-PorA-Ferritin (Low)	2	32	<16	64
NadA3-PorA (High)	3	<16	<16	16
NadA3-PorA-Ferritin (High)	4	64	<16	16
NadA3 (24-170)	5	64	<16	64
Non-immunised BALB/c control sera	-	<16	<16	<16
Internal control NadA3 clinical lot	-	>4096	<16	4096

As can be seen from Table 3-5Table 3-4, the obtained bactericidal titres are similar to those obtained for day 35, with none of the immunisation groups 1-5 being able to

elicit titres that can be classed as bactericidal. Again, the NadA3 clinical lot is the only sera able to result in bactericidal killing of the NadA3-expressing strains 5/99 and M14933.

The total IgG ELISA titres indicate that all the immunisation groups 1 - 5 can induce antibodies against the NadA3 (24-170). In groups 1-4, the immune response is targeted towards the NadA3-PorA antigen, which has seen modifications made to the NadA3 (24-170) N-terminal head region to accommodate the PorA VR2 epitope, raising the possibility that bactericidal epitopes may have been lost. For example, an analysis of a panel of human monoclonal antibodies (mAbs) isolated from human vaccinees of the Bexsero vaccine demonstrated that all mAbs targeting the N-terminal head region of NadA3 were found to be bactericidal whereas a lesser proportion of those targeting the stalk displayed bactericidal activity (Giuliani et al., 2018). Though this observation is confounded by group 5, which is immunisation with NadA3 (24-170), an antigen bearing an intact, unmodified N-terminal head region. However, the clinical lot of NadA3, which is the full-length version of NadA3, is the only sample that is bactericidal positive. This could also suggest that in the truncated NadA3 (24-170) bactericidal epitopes may also be destabilised and no longer optimally presented.

All the sera tested is also bactericidal negative against strain M08-0240104, which is used here to detect for bactericidal PorA VR2 14 antibodies. There is a possibility that the PorA VR2 14 epitope on the NadA3-PorA chimeric antigen may not be presented optimally *in vivo*, even though prior *in vitro* SPR assays were positive for recognition by a PorA VR 14 antibody. In the literature, one study found that recombinant PorA protein could be immunogenic in mice, though only when it was reconstituted in liposomes was it able to induce a good bactericidal response, suggesting that the PorA (and its immunodominant epitopes such as VR2) needs to be in its correct conformation in order to elicit a bactericidal response (Arigita et al., 2003). Hollingshead et al. designed a series of novel MenB protein antigens in which the Bexsero antigen fHbp was used as a scaffold for the display of a range of PorA VR2 epitopes, and found that while all the chimeric fHbp-PorA antigens could produce antibodies that detected PorA on the surface of the *N. meningitidis* bacterium, not all these antigens could induce bactericidal antibodies (Hollingshead et al., 2018). In that study, the anti-PorA bactericidal response raised by the chimeric fHbp-PorA depended on the PorA VR2 peptide chosen, its position in the fHbp scaffold and the adjuvant used.

3.4 Conclusion

Following the purification and epitope characterisation of the NadA3-PorA-Ferritin nanoparticle, an *in vivo* investigation into the efficacy of this system was conducted. Prior to initiation of the study, the stability of the antigens was checked by both SEC-HPLC and SDS-PAGE to confirm that all were still in their native form. A pilot study was conducted as an initial assessment of the capability of the NadA3-PorA-Ferritin nanoparticle to induce antibodies against the NadA3 component as well as to optimise the ELISA procedure for future assays.

From the pilot study, the nanoparticle was shown to be able to induce an antibody response against NadA3 epitopes presented by the NadA3-PorA chimeric antigen. A larger *in vivo* study was then begun to assess how multicopy presentation can enhance the immune response over the administration of subunit antigen alone. The inclusion of the wildtype NadA3 also could reveal how the modifications made in the design of the NadA3-PorA could affect the immune response raised against the NadA3 epitopes present. From the total IgG and IgG1 anti-NadA3 titres, the NadA3-PorA-Ferritin could induce significantly higher titres than the subunit antigen, whereas IgG2a did reach significance but titres remained very low. In comparing the subunit antigen NadA3-PorA to the wildtype NadA3, titres were significantly lower in most cases for the chimeric NadA3-PorA, suggesting that modifications made modified some immunogenic epitopes. However, presentation of the chimeric antigen on the surface of the ferritin could raise these titres to comparable levels to the wildtype NadA3.

As shown by the antibody ELISA experiments, nanoparticle immunisation did significantly alter the Th1/Th2 balance, but this was not reflected in the cytokine multiplex assay which showed no real differences between subunit and nanoparticle immunisations in terms of the cytokine responses of stimulated splenocytes. Analysis of the germinal centre B cells revealed a trend of the nanoparticle immunisation inducing increased germinal formation in comparison to the subunit NadA3-PorA immunisation, though the differences were not statistically significant. An attempt to map T-cell epitopes of the NadA3 was unsuccessful, as none of the stimulants (both mapped peptides and complete antigens NadA3, NadA3-PorA) could induce significantly different cytokine responses

All immunisation groups were SBA negative against a panel of MenB strains, suggesting that bactericidal antibodies are not raised *in vivo*, perhaps due to sub

optimal presentation of epitopes that elicit bactericidal antibodies. A negative titre obtained also for the NadA3 (24-170) immunisation sera but a positive one for the NadA3 (full-length) clinical lot suggests that bactericidal epitopes may be modified in the truncated NadA3 (24-170).

Alternative assays may be required to assess the antibodies raised by both the NadA3 and PorA VR2 14 components of the NadA3-PorA antigen. One such assay is a FACS-based assay to detect anti-NadA3 and PorA antibodies binding to the surface of MenB bacteria.

4. Chapter 4

Formulation of a cationic liposome adjuvant by microfluidics

4.1 Introduction

In the previous chapter, an *in vivo* study was described in which the primary goal was to assess the immunogenicity of the NadA3-PorA antigen when presented in a multi-copy format on the self-assembling ferritin nanoparticle. In that study, all the antigens were adjuvanted with MF59-like adjuvant AddaVax. Delivery of the NadA3-PorA subunit antigen on the surface of a ferritin nanoparticle was found to enhance the immune response over that induced by the NadA3-PorA subunit antigen alone.

In the introduction chapter, the potency of cationic liposomes as vaccine adjuvants was discussed. To further explore how the immune response can be modulated, a cationic liposome adjuvant made by a novel microfluidic process was formulated to deliver the NadA3-PorA-Ferritin. This would form the basis for a head-to-head study to compare vaccine efficacy when NadA3-PorA-Ferritin is adjuvanted with AddaVax versus cationic liposomes.

In this chapter, the development of a cationic liposome formulation produced by a microfluidic process is described. In order to enable co-delivery of antigen and adjuvant, there are several possible methods available in order to associate protein antigens to liposome formulations, one example being the surface absorption of antigen to the cationic liposomes. This is dependent on electrostatic forces, with antigens bearing isoelectric points below 7 being able to be absorbed onto the surface of cationic liposomes at physiological pH (Henriksen-Lacey et al., 2010b). The NadA3-PorA-Ferritin with a theoretical isoelectric point of 5.3 would therefore be suitable for surface adsorption to the cationic liposomal surface.

An automated mixer platform (NanoAssemblr, Precision NanoSystems Inc.) was used for controlled, bottom-up, molecular self-assembly of liposomes via custom-engineered microfluidic mixing cartridges which allow for millisecond mixing of nanoparticle components at the nanometer scale. The chip comprises of two inlet streams; an organic phase and aqueous phases, leads to a nanoprecipitation of liposomes and rapid mixing (Zhigaltsev et al., 2012). The chip employs a staggered herringbone structure which stirs the solution with chaotic advection, enabling the reproducible formulation of liposomes displaying uniform size distributions (Dimov et al., 2017).

To begin with, the neutral lipids 1,2-distearoyl-sn-glycero-3-phosphocholine (DSPC) and cholesterol, along with the cationic lipid 1,2-dioleoyl-3-trimethylammonium-

propane (DOTAP) were selected as the basis for the formulation and subsequent microfluidic process parameter optimisation. Figure 4-1 shows the structures of these three lipids.

A)

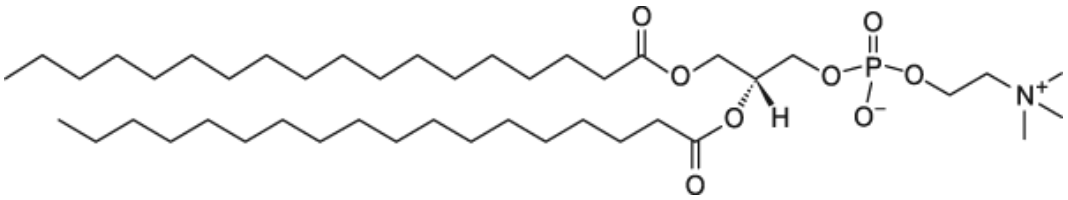

B)

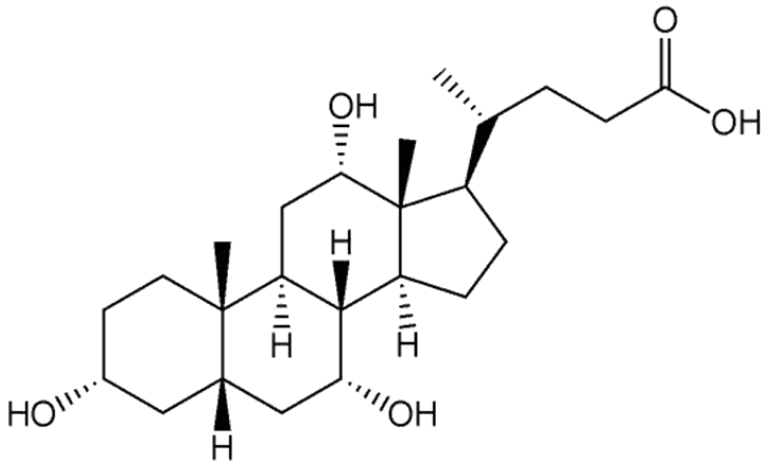

C)

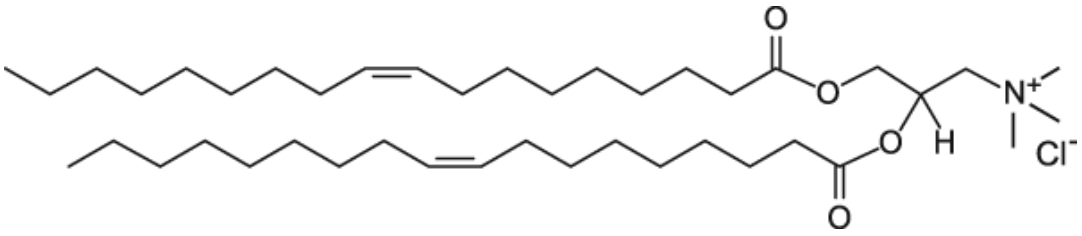

Figure 4-1The structures of the three initial lipids used for the development of a cationic liposome formulation, A) DSPC, B) Cholesterol, and C) DOTAP.

DSPC and cholesterol formed the neutral components of the formulation. The inclusion of a high transition temperature lipid, such as DSPC, can increase the liposome stability, leading to reduced clearance rates from the body circulation

(McNeil et al., 2011). Cholesterol incorporation into the liposome membranes leads to improved lipid packing which can reduce or even eliminate the main phase gel to liquid phase transition temperature (Ohtake et al., 2005). This leads to increased bilayer fluidity, with liposomes showing improved stability *in vivo* and a reduction in the susceptibility to serum degradation (Kirby et al., 1980). The cationic lipid DOTAP is a quaternary ammonium compound coupled via an ester linkage to two unsaturated acyl chains. One study comparing different cationic lipids recorded differing immune responses depending on the cationic lipid, thus suggesting different underlying mechanisms for their action (Henriksen-Lacey et al., 2011a). In the case of DOTAP-based liposomes, they have been demonstrated to increase the humoral immune response and shift the T-cell response towards a Th1-biased direction compared to when antigen is administered alone (Brgles et al., 2009).

4.1.1 Aim and objectives

The main aim of the work presented in this chapter was to use microfluidics for the reproducible and rapid production of a cationic liposome adjuvant for the delivery of NadA3-PorA-Ferritin nanoparticle. This would form the basis for a head-to-head study comparing adjuvantation with the MF59-like adjuvant AddaVax. To achieve this aim, the objectives were to:

1. Identify the ideal lipid composition of the cationic liposome formulation.
2. Optimise the microfluidic process parameters for production of the cationic formulation.
3. Successfully adsorb the NadA3-PorA-Ferritin to cationic liposomes.

4.2 Materials and methods

4.2.1 Materials

Reagent	Supplier
1,1′-Dioctadecyl-3,3,3′,3′-tetramethylindocarbocyanine perchlorate (DilC)	Sigma, Dorset, UK
1,2-distearoyl-sn-glycero-3-phosphocholine (DSPC)	Avanti Polar Lipids, Alabaster, USA
1,2-dimyristoyl-rac-glycero-3-methoxy-PEG2000 (DSPE-PEG2000)	Avanti Polar Lipids, Alabaster, USA
1,2-dioleoyl-3-trimethylammonium-propane (DOTAP)	Avanti Polar Lipids, Alabaster, USA
Cholesterol	Sigma, Dorset, UK
Dimethyldioctadecylammonium (DDA)	Avanti Polar Lipids, Alabaster, USA
Dialysis tubing cellulose membrane (Typical molecular weight cut-off of 14,000, flat width 25 mm)	Sigma, Dorset, UK
Distearoylphosphatidylethanolamine- PEG2000 (DMG-PEG2000)	Avanti Polar Lipids, Alabaster, USA
Ethanol	Fisher Scientific, Loughborough, UK
13 mm membrane diameter, 0.22 µm pore size, KX Syringe Filter, Mixed Cellulose	Cole-Parmer, UK
Millex®-GP 0.22 µm, polyethersulfone, 33 mm	Merck, Germany
modified polyethersulfone (mPES) 750 KDa MWCO hollow fibre column	Spectrum labs, UK
Ovalbumin	Sigma
Tris Ultra Pure	ICN Biomedicals, Aurora, USA

4.2.2 Production of liposomes using microfluidics

Lipids at various molar ratios (depending on the formulation) were dissolved in ethanol to create a lipid stock. Liposomes were manufactured using a NanoAssemblr (Precision NanoSystems Inc) by injecting the ethanol-solubilised lipids and aqueous

buffer (Tris 10 mM, pH 7.4) into separate chamber inlets of the NanoAssemblr chip. The flow rate ratio (FRR) (ratio between solvent and aqueous stream) as well as the total flow rate (TFR) of both streams were controlled by syringe pumps, calibrated to the syringe inner diameter. The liposome formulation was collected from the chamber outlet and solvent removed by either dialysis at room temperature against Tris buffer (10 mM, pH 7.4) under magnetic stirring or by Tangential flow filtration (TFF) using a KR2i TFF System (Spectrum labs) with a modified polyethersulfone (mPES) 750 KDa MWCO hollow fibre column (Spectrum labs).

4.2.3 Quantification of lipid recovery

To assess lipid recovery through the liposome production and purification process, the lyophilic tracer 1,1′-Dioctadecyl-3,3,3′,3′-tetramethylindocarbocyanine perchlorate (DilC) (Sigma) was incorporated by adding it at 0.2 mol% to the lipid stock for each formulation prior to liposome formulation on the NanoAssemblr. Samples were added into a 96 well black flat bottom plate and the plate was read on a POLARstar Omega plate reader using an excitation wavelength of 482 nm and emission wavelength of 520 nm.

4.2.4 Measurement of particle characteristics by DLS

Characterisation of the liposomes was performed using dynamic light scattering (DLS) (Malvern NanoZS, Malvern Instruments, Worcestershire, UK). Particle size was reported as the z-average (intensity based mean particle diameter) and the zeta potential using particle electrophoresis Polydispersity index (PDI) measurements were used to assess particle distribution. Liposome formulations were diluted 1:10 in diluted buffer (10 mM Tris or 1X PBS diluted 1:300 in water) and measurements took place at 25 °C with the refractive index (RI) set to 1.50.

4.2.5 Adsorption of NadA3-PorA-Ferritin to DDA-based liposomes

A concentrated solution of the NadA3-PorA-Ferritin antigen was added slowly to the liposome 10% DDA formulation such that the final protein concentration was 0.44 mg/mL and the final lipid concentration was 5 mg/mL. The solution was vortexed for 5 seconds and allowed to equilibrate for 10 minutes prior to characterisation by DLS.

4.2.6 Statistical analysis

Statistical analysis of data was calculated by one-way analysis of variance (ANOVA). Where significant differences are indicated, differences between means were determined by the Tukey Simultaneous Tests for Differences of Means. All the calculations were made using Minitab 17 statistical software.

4.3 Results & Discussion

4.3.1 Determination of the cationic lipid content for the liposome formulation

To begin the process development for the liposome adjuvant, a series of increasingly cationic formulations were prepared via a microfluidic method using the NanoAssemblr. The impact of increasing the content of the cationic lipid DOTAP was analysed with a Zetasizer Nano ZS (Malvern, UK), which was used to analyse liposome size and polydispersity index by dynamic light scattering (DLS) and the zeta potential by particle electrophoresis.

Table 4-1 shows the composition of the lipid formulation stocks prepared in ethanol. In the table, lipids are represented as their molar ratios. Moving across the formulation series 1-5, the cationic lipid DOTAP content increases.

Table 4-1 Composition of the lipid formulation stocks used to investigate the effect of increasing cationic lipid content on the resulting liposome formulations. Lipids are represented in molar ratios.

Lipid	Formulation 1	Formulation 2	Formulation 3	Formulation 4	Formulation 5
DSPC	66	63	60	50	10
Cholesterol	34	32	30	30	40
DOTAP	0	5	10	20	50

Following preparation of the lipid stocks, liposomes were produced using the NanoAssemblr. Table 4-2 displays the microfluidic parameters used to produce this series of cationic liposome formulations.

Table 4-2 NanoAssemblr parameters used for the production of the series of cationic liposome formulations.

Microfluidic parameter	Value
Lipid solvent	Ethanol
Lipid stock concentration	2 mg/mL
Aqueous phase	Tris (10 mM, pH 7.4)
Flow rate ratio	3:1
Total flow rate ratio	12 mL/min

Following production on the NanoAssemblr, liposomes were purified by buffer exchange dialysis (into Tris, 10 mM, pH 7.4) to remove the ethanol solvent and the physiochemical attributes of the liposomes were then analysed by DLS using the Zetasizer Nano ZS. Figure 4-2 shows the results obtained.

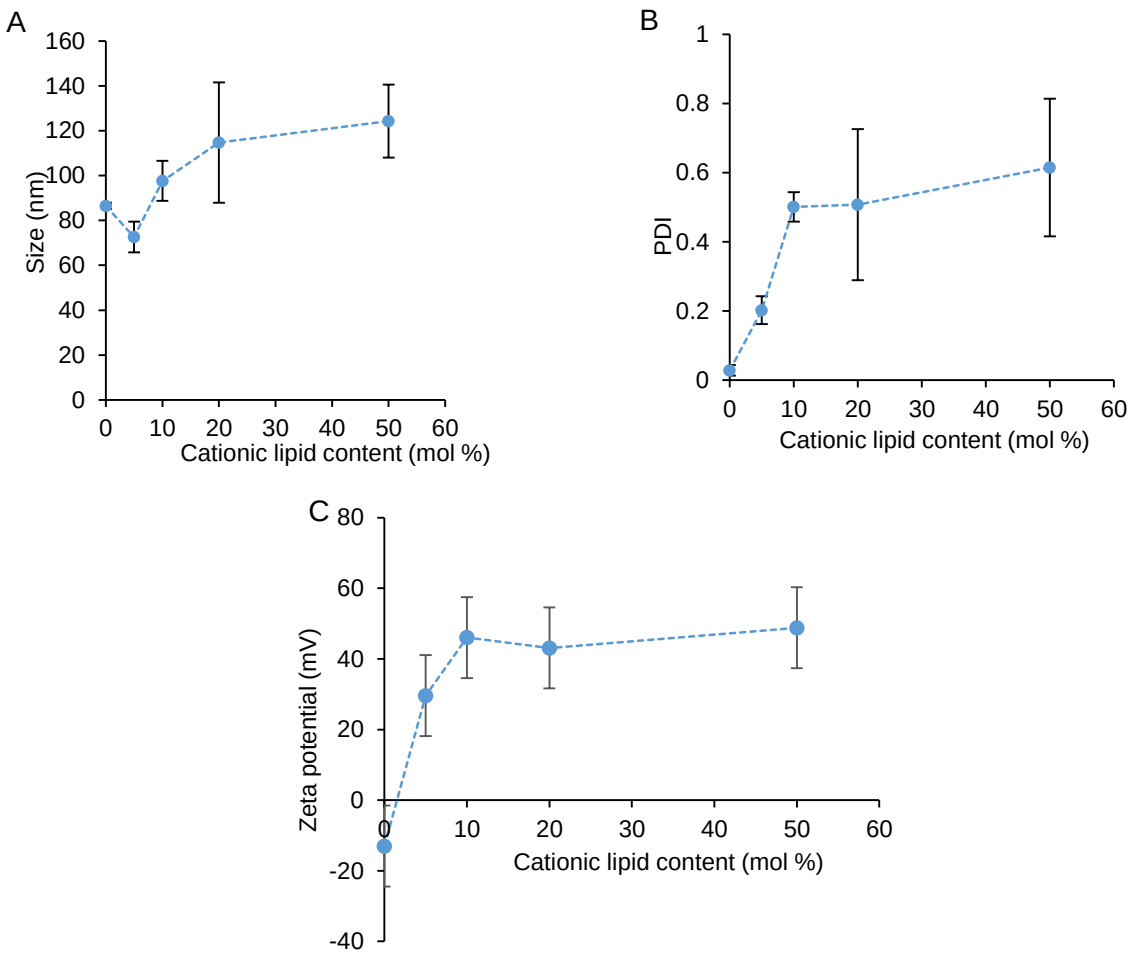

Figure 4-2 The effect of the cationic lipid DOTAP content on the physiochemical characteristic of liposomes. Formulations were characterised in terms of A) Size B) PDI C) Zeta potential (measured in 10 mM Tris, pH 7.4 diluted 1:300 in water). Results are presented as the mean ± SD of three independent experiments.

From the results in Figure 4-2 it can be seen that increasing the DOTAP content of the liposomes resulted in a trend of increasing vesicle size (Figure 4-2A) with 50% DOTAP content resulting in significantly larger ($p<0.05$) liposomes than those at 5% DOTAP content. However, as the DOTAP content is increased the formulations also become more heterogeneous as measured by the PDI (Figure 4-2B)

Therefore, the size value measured at 50% DOTAP content represents a very heterogeneous formulation. There is a concomitant increase in zeta potential as would be expected, with a maximum of approximately 40 mV being reached for liposomes containing 10 % or more DOTAP (Figure 4-2C).

Campbell observed the opposite, with the inclusion of DOTAP found to reduce the mean vesicle diameter and the PDI of DSPC:DOTAP liposomes (Campbell et al., 2001), while another study found that adjusting the molar ratio of DOTAP to the

neutral lipid DOPC had little effect on the size of the liposome formulations (Ma et al., 2011). However, neither of these studies manufactured their liposomes by microfluidics, which may also contribute towards the observations in the present study.

To enable the design of improved vaccine formulations, a large amount of research has been performed to understand the implications of these liposomal physiochemical characteristics. The adjuvant effect of liposomes is linked to several mechanisms, including the formation of an antigen depot at the site of injection, induction of local inflammation and increased antigen uptake by APCs (Soema et al., 2015). This is in addition to the fact that liposomes deliver subunit antigens (which are generally too small to be taken up by dendritic cells efficiently) in a more particulate format of a comparable size to a pathogen, which can help to enhance endocytic uptake by dendritic cells (Brewer et al., 1998).

Both the size and surface charge are key parameters influencing the cellular uptake and biodistribution of liposomes (Lou et al., 2019). Regarding cationic liposome size, it had been previously reported that vesicle size for cationic liposomes within a size range of 200 to >2000 nm had no significant impact on their drainage from the injection site, though an impact on the cell-mediated immune response was noted (Henriksen-Lacey et al., 2011b). This non-dependence on vesicle size can be explained by the importance of electrostatic interactions with extracellular matrix proteins, which results in cationic liposome aggregation at the site of injection (Kaur et al., 2012b). More recently, however, different pharmacokinetic profiles were seen for smaller liposomes at 40 nm compared to larger cationic liposomes of 500 nm (Lou et al., 2019). In that study, the smaller liposomes were shown to drain more rapidly to the lymph nodes. Similar observations with cationic chitosan nanoparticles suggested that a combination of free- and cell-mediated transport to lymph nodes could explain the biodistribution of these smaller cationic liposomes (Cordeiro et al., 2019).

In addition to this size component, the liposome surface charge also is an important factor in dendritic cell uptake. As the cellular membrane is anionic, cationic liposomes are well-placed to interact electrostatically with dendritic cells (Christensen et al., 2011). Regarding the cationic lipid content of a liposome formulation, one study found that a higher surface charge density was able to better promote the antigen uptake and maturation of dendritic cells, resulting in a more potent antigen-specific immune response (Ma et al., 2011).

The accumulation of a nanoparticle in target tissue depends on a number of physiochemical characteristics, including the particle size distribution of the formulation as indicated by its PDI (Danaei et al., 2018). The safe, stable and efficient formulation of nanoparticles therefore requires monodisperse nanoparticle populations of a certain size. PDI values at around 0.05 indicate highly monodisperse formulations, while moving towards a PDI of 0.7 suggest a broader particle size distribution.

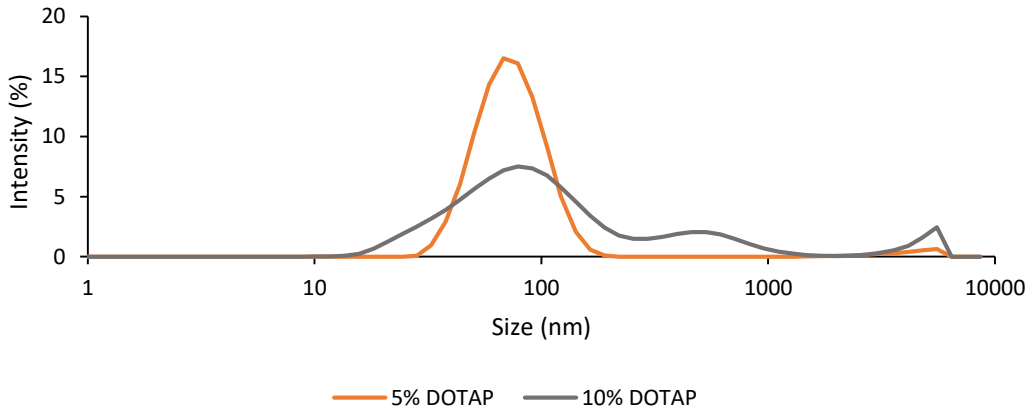

Figure 4-3 DLS size intensity plots illustrating the shift towards a more polydisperse formulation as the DOTAP content is raised from 5% to 10% for the liposome formulations.

At a DOTAP content of 5% (Formulation 2), highly cationic liposomes can still be produced while maintaining an ideally low PDI (<0.2). However, increasing the DOTAP molar ratio beyond 5% results in more polydisperse formulations as can be seen for the 10% DOTAP formulation. The shift towards polydispersity in formulations with a DOTAP content greater than 5% is reflected in the size intensity chart shown in Figure 4-3. Based on the results, formulation 2 with a 5% DOTAP content was selected to take through for further optimisation of the microfluidic process parameters.

4.3.2 Analysis of lipid recovery following liposome purification and sterilization.

In the data presented in 4.3.1, removal of residual ethanol solvent following microfluidic liposome production was accomplished by dialysis purification. In addition, however, purification of these liposome formulations was also investigated using Tangential Flow Filtration (TFF) as an alternative purification method to dialysis.

Following purification, sterilisation of these liposomes by syringe filtration was also attempted.

TFF has been demonstrated to be an effective, scalable purification method in the liposome manufacturing process (Forbes et al., 2019). Purification by TFF occurs via diafiltration, which sees the continuous removal of permeable molecules from a solution by pumping it over a ultrafiltration membrane (Correa et al., 2016). The retentate then re-circulates through the system until purification is complete. Replacement buffer introduced at the same rate as the waste removal ensures that sample volume remains constant and purification continues unimpaired.

In order to quantitate lipid recovery at each stage of the process, liposomes were fluorescently-labelled with the lipophilic marker 1,1′-Dioctadecyl-3,3,3′,3′-tetramethylindocarbocyanine perchlorate (DilC). To quantify the lipid recovery, it was first necessary to prepare a DilC fluorescence standard curve. This standard curve was prepared from a DilC-incorporated formulation 1 (formulation composition detailed in Table 4-1). Figure 4-4 shows the mean standard curve obtained.

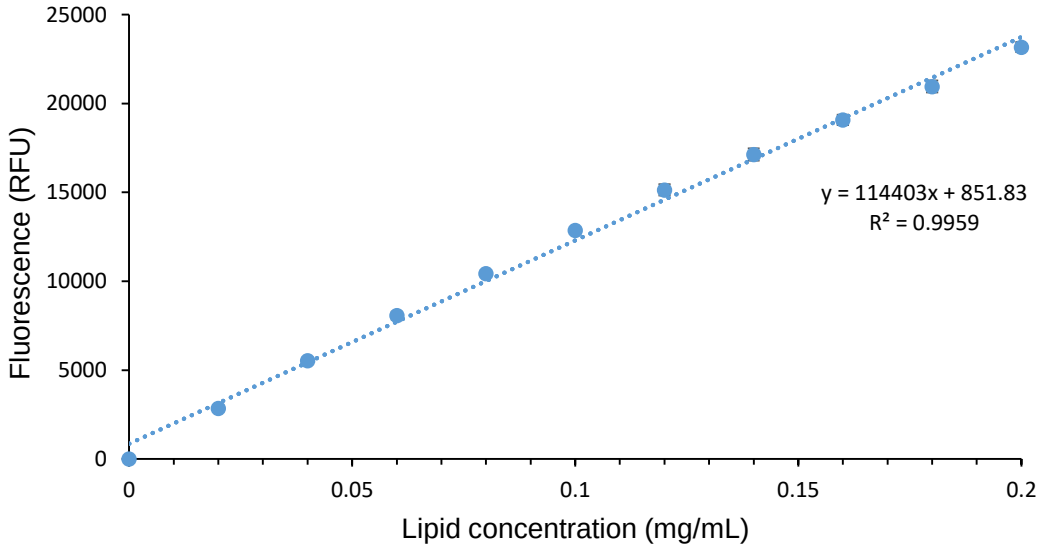

Figure 4-4 Mean fluorescence standard curve used to calculate lipid recovery throughout the liposome purification and production process. The curve was prepared using formulation 1 labelled with DilC (at 0.2 mol%). Results represent the mean of nine measurements performed over three days ± SD. A linear regression analysis was used to determine both the LOD and LOQ from the standard curve, which were calculated to be 0.008 mg/mL and 0.025 mg/mL respectively.

Following preparation of this standard curve, lipid recovery following purification and sterilisation was performed for each of the five formulations detailed in section 4.3.1. Figure 4-4 shows the results of the lipid recovery following purification by either dialysis or TFF for each of the five formulations. The final column in the table displays the lipid recovery following dialysis and then sterilisation using Millex-GP filters.

Table 4-3 Lipid recovery (%) following purification by either dialysis or TFF and then post-syringe sterilisation (after dialysis). Results are presented as the mean ± standard deviation of three independent experiments.

Formulation	DOTAP content (mol %)	Lipid recovery (%)		
		Post-dialysis	Post-TFF	Post syringe sterilisation (following dialysis)
1	0	100 ± 1	76 ± 11	95 ± 7
2	5	100 ± 15	74 ± 29	0 ± 0
3	10	100 ± 10	0 ± 0	0 ± 0
4	20	89 ± 8	0 ± 0	0 ± 0
5	50	94 ± 3	0 ± 0	0 ± 0

From the results presented in Table 4-3, it can be seen that whilst high DOTAP-content liposomes can be purified by dialysis, purification by TFF was difficult for liposomes containing over 5% molar ratio of DOTAP. In addition to this, syringe filtration was challenging for all the cationic formulations, with each showing poor recovery post-syringe filtration.

These observations could be due to catatonic lipids binding electrostatically to components of the TFF and syringe filters. TFF had previously been used to successfully purify neutral and anionic liposomes with high lipid recovery using the same modified polyethersulfone (mPES) 750 kDa MWCO hollow fibre column as used here (Forbes et al., 2019). However, Dimov et al describe the application of a custom-built TFF device that was able to also purify cationic liposome formulations using polyethersulfone ultrafiltration membrane discs (300 kDa cut off, pore size 0.45 Biomax) rather than a mPES column, as well as reporting similar using Ultrafiltration regenerated cellulose membranes (10 kDa, with a pore size 0.22 µm from Sigma)

(Dimov et al., 2017). Regarding syringe filter sterilisation, the 0.22 µm Millex-GP filters used are also composed of PES. Given the poor lipid recovery described for TFF purification and syringe filtration of cationic liposomes, dialysis was therefore adopted as method of choice for their purification and alternative sterilisation methods would be investigated if appropriate.

Sterilisation of liposomes was also attempted using syringe filters composed of mixed cellulose (Cole-Parmer) using an anionic, cationic and neutral liposome formulation. As for the PES filters, these syringe filters too were unable to sterilise any of the formulations, with the lipid recovery also measured as 0%.

4.3.3 DOTAP-formulation microfluidic process development: Flow rate ratio optimisation

Microfluidic flow parameters such as the Flow Rate Ratio (FRR, the ratio of the aqueous and organic solution flow rates) and the Total Flow Rate (TFF, the total rate at which the solutions pass through the chip) can impact the physical characteristics of the resulting liposomes and so both can be fine-tuned for a given formulation to achieve the desired liposomal attributes (Kastner et al., 2014). Following on from the selection of formulation 2 based on its observed favourable physiochemical characteristics as described in 4.3.1, a microfluidic process development was initiated to optimise the process parameters FRR and TFR for the formulation. The first parameter to be investigated was the FRR. Formulation 2 was produced on the NanoAssemblr over a series of different FRRs, purified by dialysis and then its physiochemical characteristics analysed. Figure 4-5 shows the physiochemical characteristics of the liposomes obtained over this FRR series.

A

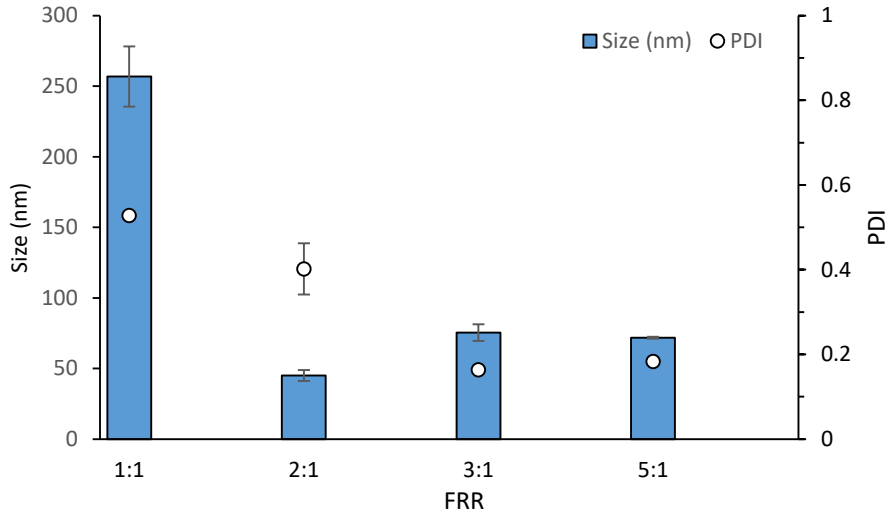

B

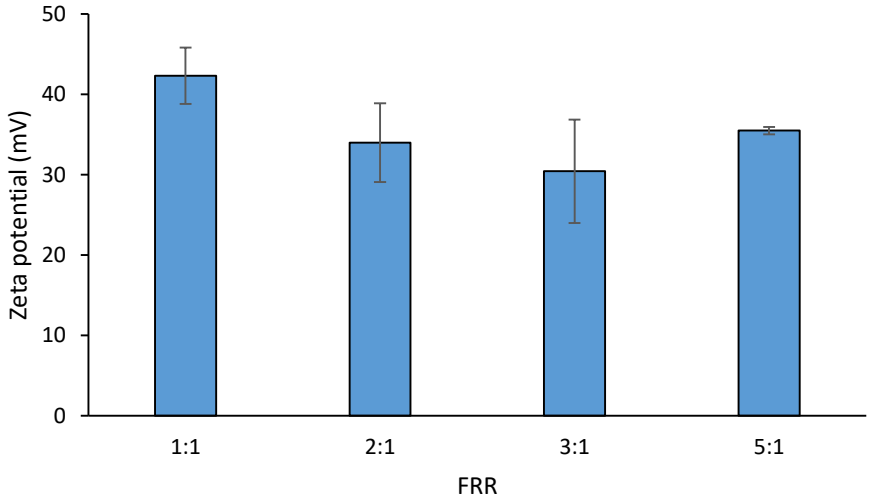

Figure 4-5 Physiochemical characteristics of the 5% DOTAP formulation prepared with the NanoAssemblr over a series of FRRs. Initial lipid concentration was 2 mg/mL and the TFR was fixed at 12 mL/min. Formulations were characterised in terms of A) Size & PDI B) Zeta potential (measured in 10 mM Tris, pH 7.4 diluted 1:300 in water). Results are presented as mean ± SD of three independent experiments. Statistical analysis of data was calculated by one-way analysis of variance (ANOVA).

The results show that a FRR of 1:1 results in particles of the largest size and PDI. Moving from a FRR of 1:1 to 2:1, there was a significant decrease in both the size and PDI ($p<0.05$ and $p<0.001$ respectively). At a FRR of 3:1, there is a significant increase in the size over that obtained for the FRR of 2:1 ($p<0.001$). However, the FRR of 3:1 does result in a significantly reduced PDI ($p<0.001$), giving the smallest PDI (≤ 0.2) of the entire series. In terms of the zeta potential, it remains at around 30

mV with only the difference between FRR 1:1 and 3:1 calculated as being significant ($p<0.05$).

The decrease in liposome size moving from a FRR of 1:1 has been observed in other studies (Forbes et al., 2019; Jahn et al., 2007). Microfluidic mixing of the organic and aqueous phase causes lipid nanoprecipitation and self-assembly into planar lipid bilayers that exhibit bending to reduce unfavourable interactions between the hydrophobic acyl chains and the aqueous phase, leading to formation of spherical vesicles. As the FRR increases, the alcohol concentration decreases more rapidly and lessens the time for lipid discs to stabilise, ultimately resulting in the formation of smaller liposomes (Zizzari et al., 2017).

4.3.4 DOTAP-formulation microfluidic process development: The total flow rate optimisation

The second microfluidic flow parameter to be investigated was the TFR. Based on the FRR optimisation results presented in section 4.3.3, the FRR was then kept fixed at 3:1 and the TFR was then altered over a series of different rates. The physiochemical characteristics of the liposomes obtained over this TFR series are shown in Figure 4-6.

.

A

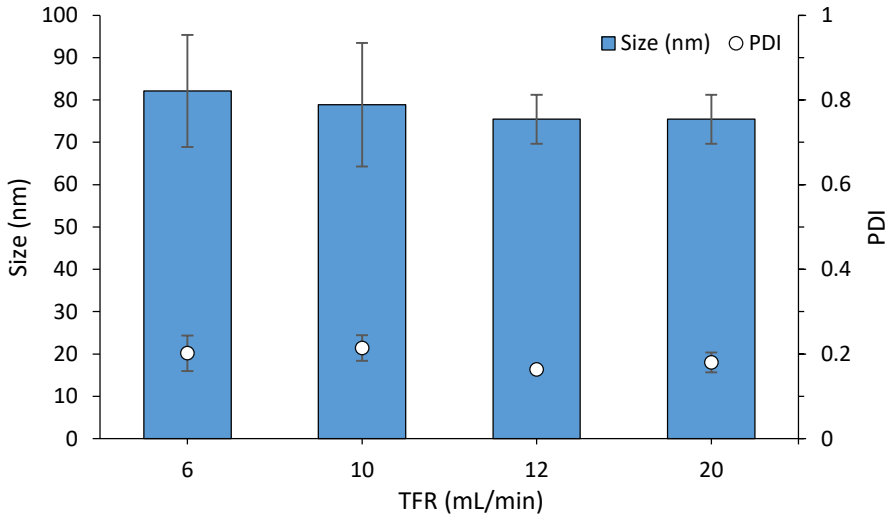

B

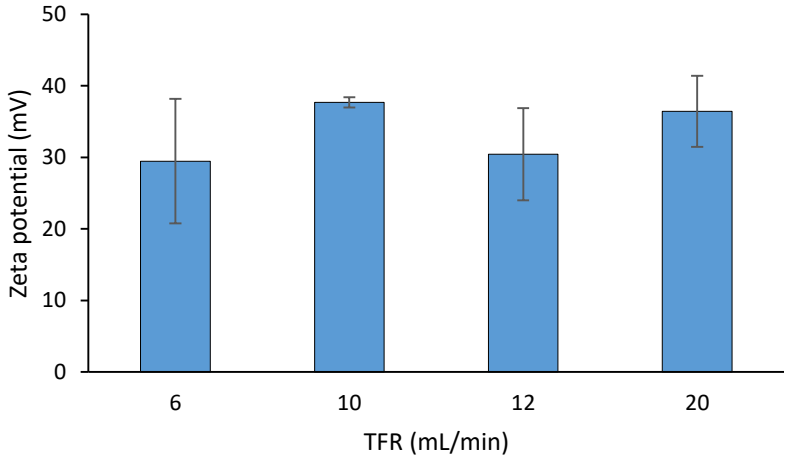

Figure 4-6 Impact of the TFR on the physiochemical characteristics of the 5% DOTAP formulation. Initial lipid concentration was 2 mg/mL and FRR was kept fixed 3:1. Formulations were characterised in terms of A) Size & PDI B) Zeta potential (measured in 10 mM Tris, pH 7.4 diluted 1:300 in water). Results are presented as mean ± SD of three independent experiments.

From Figure 4-6 it can be seen that both the liposome size and PDI is independent of the total flow rate with no significant change across the series (Figure 4-6A). Similarly, the zeta potential does not significantly change (Figure 4-6B).

Other studies (Joshi et al., 2016; Kastner et al., 2015) also reported little effect of the TFR on physiochemical characteristics of the liposomes produced. Such results

support the applicability of microfluidic manufacture, as it means liposome characteristics can be maintained while increasing the total flow rate through the system i.e. the rate of liposome formulation manufacture. Another study reported liposomes made at 20 mL/min to be smaller than those obtained at 1 mL/min, an effect they attributed to the greater shear forces on mixing at higher flow rates, which leads to smaller particles being produced (Guimarães Sá Correia et al., 2017). No significant difference in the zeta potential in response to changing TFF was reported in that study.

4.3.5 PEGylation of liposome formulation

The microfluidic development described in sections 4.3.3 and 4.3.4 established a FRR of 3:1 and a TFR of 12 mL/min for the microfluidic production of the 5% DOTAP formulation. Moving on from this, the potential to stabilise the formulation by addition of polyethylene glycol (PEG), a widely used hydrophilic polymer for this purpose, was investigated.

Pegylation of a liposome surface leads to the formation of a hydrated shell that can prevent aggregation of vesicles (Needham et al., 1992) and protects against destruction from plasma proteins *in vivo*, while also reducing adsorption of opsonins. This increase in stability and circulatory time led to PEGylated liposomes being deemed ‘Stealth liposomes’ on account of their ability to evade the immune system (Immordino et al., 2006). In addition to this, PEG also has the favourable attributes of low immunogenicity and antigenicity (Dreborg and Akerblom, 1990). Pegylation has been shown to influence both the liposomal vaccine biodistribution and interaction with innate immune cells. One study investigating the effect of varying the pegylation content of a cationic liposomal formulation found a composition of 10 mol% PEGylation could influence the CAF01 (Cationic adjuvant formulation 01) liposome formulation retention at the site of injection and a shift towards a Th2 bias, whilst higher levels (25 mol%) of PEG blocked the formation of a depot and promoted clearance to the draining lymph nodes (Kaur et al., 2012a). To further elucidate whether a depot effect at the site of injection or lymphatic-targeting of liposomes results in greater vaccine efficacy, another study found that PEGylation at 1-5 %mol of DOTAP liposomes promoted trafficking to draining lymph nodes and enhanced vaccine-induced antibody responses (Wang et al., 2014).

Though a number of methods are available to incorporate PEG onto a liposome surface, the most widely used of these methods is the use of a lipid cross-linked to a PEG moiety, with distearoylphosphatidylethanolamine- PEG being one such example

of this (DSPE-PEG) (Allen et al., 1991). To investigate the effect of PEGylation on the liposomes produced, a series of formulations were made using the NanoAssemblr in which the 5% DOTAP formulation was PEGylated to different degrees. Two different PEGylated lipids were tested which differ by the length of their saturated alkyl chains; the first being the aforementioned DSPE-PEG2000 and the second 1,2-dimyristoyl-rac-glycero-3-methoxy-PEG2000 (DMG-PEG2000), a variant of which is a component of the lipid nanoparticle used to deliver the therapeutic agent of Patisiran, a first of its kind RNA interference therapy approved in the US and Europe (Zhang et al., 2019). Both of these PEGylated lipids are shown in Figure 4-7, while Table 4-4 details the formulations prepared.

A)

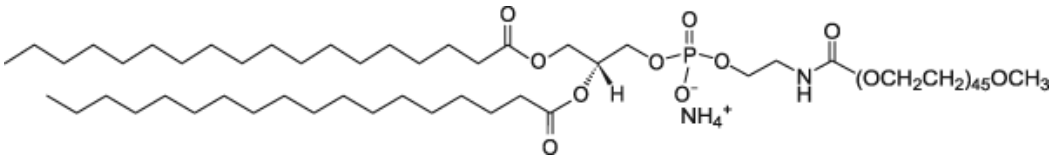

B)

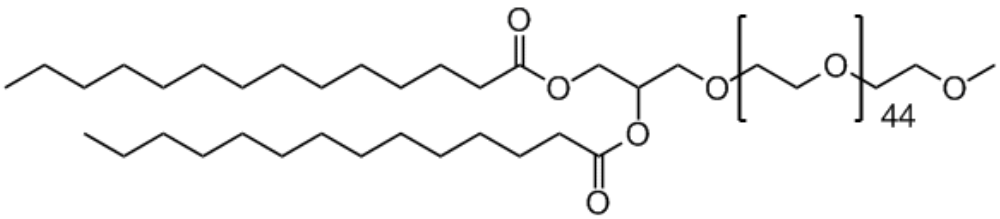

Figure 4-7 The structures of the two PEGylated lipids A) DSPE-PEG2000 B) DMG-PEG2000

Table 4-4 Composition of the liposome formulations prepared to investigate the effect of PEGylation. All lipids are presented as molar ratios.

Lipid	2% PEG formulation	10% PEG formulation	20% PEG formulation
DSPC	63	63	63
Cholesterol	30	22	12
DOTAP	5	5	5
DMG-PEG 2000 or DSPE-PEG 2000	2	10	20

The liposome formulations detailed in Table 4-4 were prepared on the NanoAssemblr and purified by dialysis. The physiochemical attributes of these formulations post-dialysis are shown in

Figure 4-8.

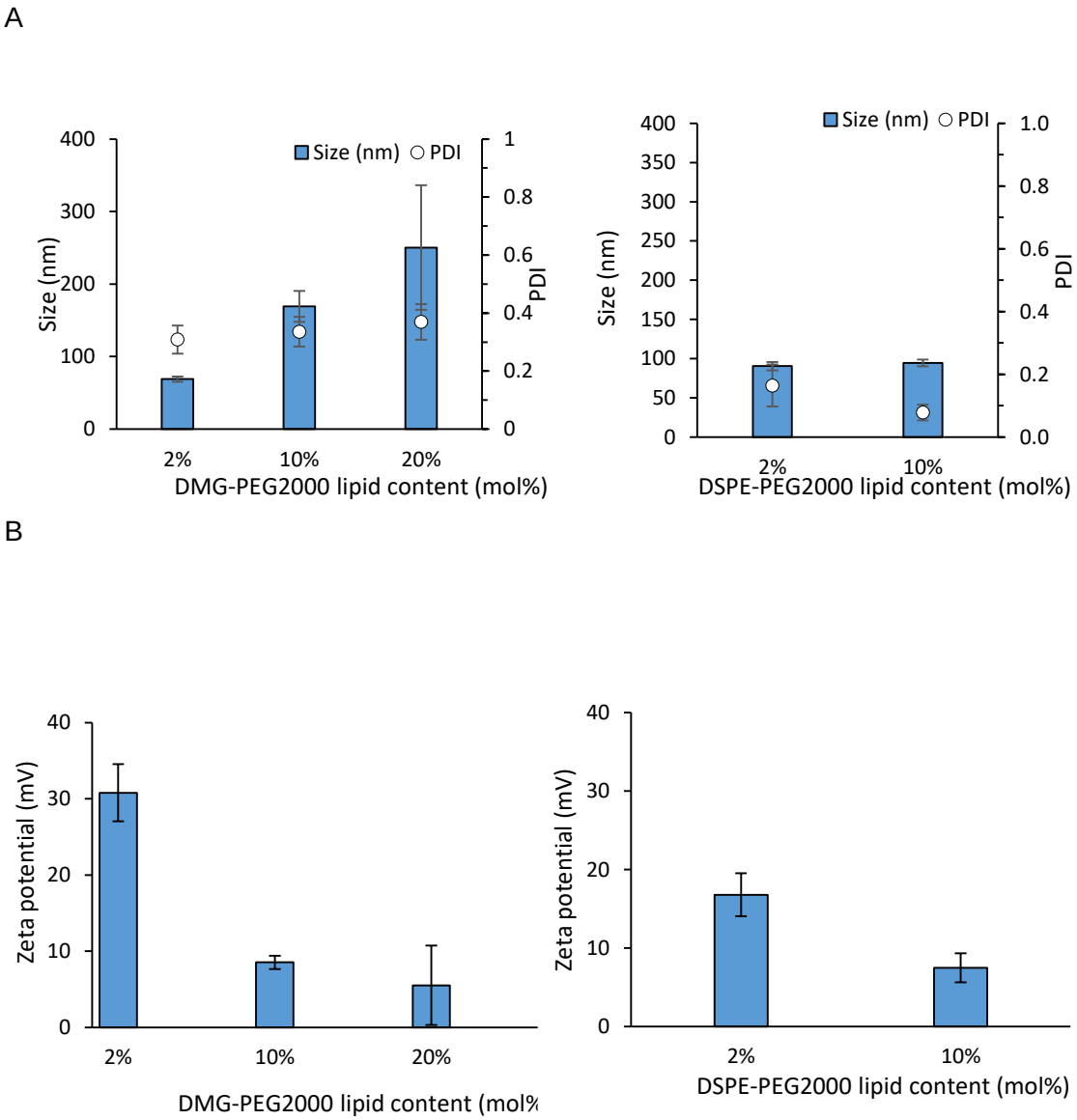

Figure 4-8 Physiochemical characterisation of liposomes PEGylated using the lipids DMG-PEG2000 and DSPE-PEG2000. Initial lipid concentration was 2 mg/mL, FRR set to 3:1 and the TFR was fixed at 12 mL/min Formulations were characterised in terms of A) Size & PDI B) zeta potential (measured in 10 mM Tris, pH 7.4 diluted 1:300 in water). Results are presented as mean ± SD of three independent experiments.

Figure 4-8A displays the vesicle size and PDI obtained for each formulation PEGylated with either DMG-PEG2000 or DSPE-PEG2000. For formulations containing DMG-PEG2000, vesicle size increases as the amount of the PEGylated lipid increases, and its inclusion results in more polydisperse formulations with the PDI rising above 0.3 throughout the series. Compared to DMG-PEGylated liposomes, the formulations obtained using DPSE-PEG2000 demonstrate less polydispersity with PDI values < 0.2, whereas vesicle size remains constant at around 90 nm moving between both 2% and 10% DSPE-PEG2000 content formulations, which is a small increase from the 75 nm obtained for non-PEGylated liposomes. The zeta potentials obtained for these PEGylated formulations are shown in

Figure 4-8B. Prior to pegylation, the zeta potential of the formulation was ~ 30 mV. Barring the formulation at 2% DMG-PEG2000, the rest of the formulations all display a reduction in zeta potential from that of the unpegylated formulation.

This is a demonstration of the masking of the cationic charge due to the hydrophilic PEG chains extending out from the surface of the liposome (Kaur et al., 2012b). Reduction in the zeta potential due to PEGylation can reduce the antigen retention on the liposomal surface – this would have impaired the electrostatic association of the NadA3-PorA-Ferritin to the liposomal formulation, and so the formulation development continued without pegylation of the formulation.

4.3.6 Development and characterisation of a DDA-based cationic liposomes formulation

Following this DOTAP-based liposome formulation development and characterisation, the cationic lipid component was exchanged for the cationic lipid Dimethyldioctadecylammonium (DDA). Gall in 1966 first identified DDA as being a potent cationic lipid adjuvant in 1966 (Gall, 1966) and today it is present as part of a binary mixture with the immunopotentiator α,α′-trehalose 6,6′-dibehenate (TDB) in the cationic liposomal adjuvant CAF01 (Davidsen et al., 2005). CAF01 is a promising adjuvant that has been to shown induce strong CD4+ T-cell response characterized by a mixed Th1/Th17 (Henriksen-Lacey et al., 2010a; Kamath et al., 2012) and has recently been tested in a phase I clinical trial for a chlamydia vaccine (Abraham et al., 2019). The structure of DDA is a quaternary ammonium salt consisting of a nitrogen atom bound by two methyl groups and two octadecyl groups (Figure 4-9).

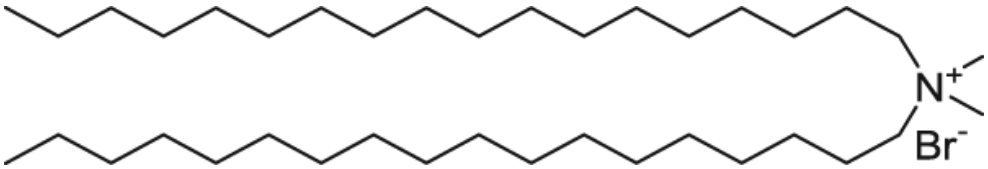

Figure 4-9 The structure of the bromide salt of Dimethyldioctadecylammonium (DDA).

In a similar manner as described for the DOTAP-based formulations in 4.3.1, the microfluidic process optimisation began by preparing formulations to varying cationic lipid content and selecting the most suitable for further development. Two different formulations were prepared to 5% and 10% (molar ratio) of DDA using the NanoAssemblr and the impact of the DDA content assessed. Table 4-5 shows the composition of the two lipid formulation stocks prepared in ethanol.

Table 4-5 Composition of the lipid formulation stocks used to investigate the effect of increasing cationic DDA lipid content on the resulting liposome formulations. Lipids are represented as molar ratios.

Lipid	Formulation 1	Formulation 2
DSPC	63	60
Cholesterol	32	30
DDA	5	10

Following preparation of the lipid stocks, liposomes were produced using the NanoAssemblr. Table 4-6 displays the microfluidic parameters used for the production of the two DDA liposome formulations.

Table 4-6 NanoAssemblr parameters used for the production of the series of cationic liposome formulations.

Microfluidic parameter	Value
Lipid solvent	Ethanol
Lipid stock concentration	40 mg/mL
Aqueous phase	Tris (10 mM, pH 7.4)
Flow rate ratio	3:1
Total flow rate ratio	12 mL/min

Following production on the NanoAssemblr (FRR set to 3:1 and TFR 12 mL/min), liposomes were purified by dialysis to remove the ethanol solvent as before. The physiochemical attributes of the liposomes were then analysed using the Zetasizer Nano ZS. Table 4-7 shows the results obtained.

Table 4-7 The effect of the cationic lipid DDA content on the physiochemical characteristics of liposomes. Formulations were characterised in terms of size, PDI and zeta potential. Results are presented as mean ± SD of three independent experiments.

Molar ratio of DDA	Size (nm)	PDI	Zeta potential (mV)
5%	104 ± 1	0.15 ± 0.01	56 ± 1
10%	93 ± 1	0.06 ± 0.01	51 ± 5

Table 4-7 shows the physiochemical characteristics of the two formulations prepared. There are no significant differences between either of the formulations in terms of their size, PDI or zeta potential. Formulation 2 (10 % DDA content) was taken through for further microfluidic process development in a similar manner as described for the DOTAP-based formulation, beginning with optimisation of the FRR and then the TFR. For FRR optimisation (Figure 4-10), the TFR was kept constant at 12 mL/min, which established a FRR of 3:1 to be then be taken through to the TFR optimisation (Figure 4-11).

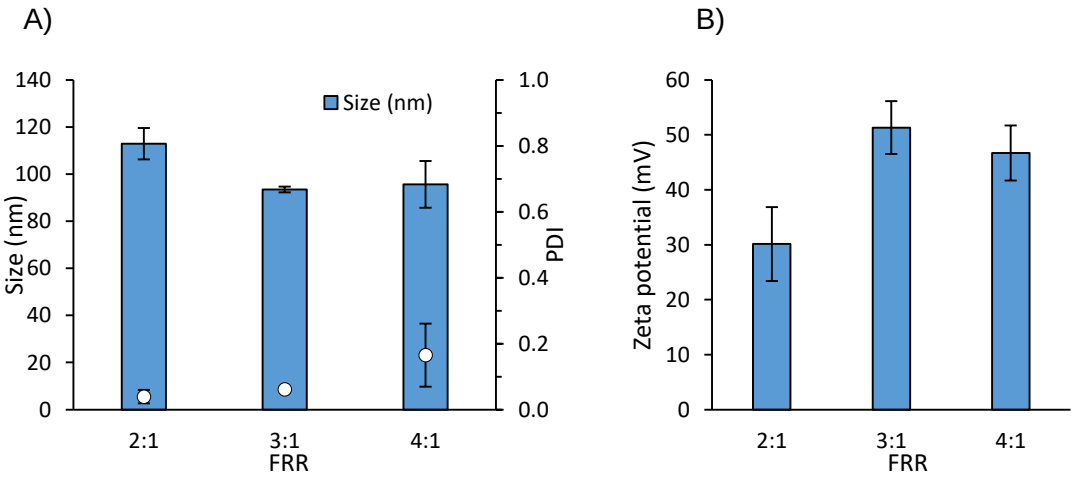

Figure 4-10 Physiochemical characteristics of the 10% DDA formulation prepared with the NanoAssemblr over a series of FRRs. Initial lipid concentration was 40 mg/mL and TFR was 12 mL/min. Formulations were characterised in terms of A) Size and PDI and B) Zeta potential (measured in 10 mM Tris, pH 7.4 diluted 1:300 in water). Results are presented as mean ± SD of three independent experiments.

From Figure 4-10, it can be seen that all FRRs tested result in formulations optimum PDIs (<0.2), however the FRR of 2:1 results in liposomes that are significantly larger ($p<0.05$). For the zeta potential, the FRR of 3:1 produces significantly more positive liposomes than the 2:1 FRR ($p<0.05$). Since the NadA3-PorA-Ferritin is to be electrostatically associated to the liposome surface, a FRR 3:1 resulting in liposomes with a greater cationic charge is the preferred choice.

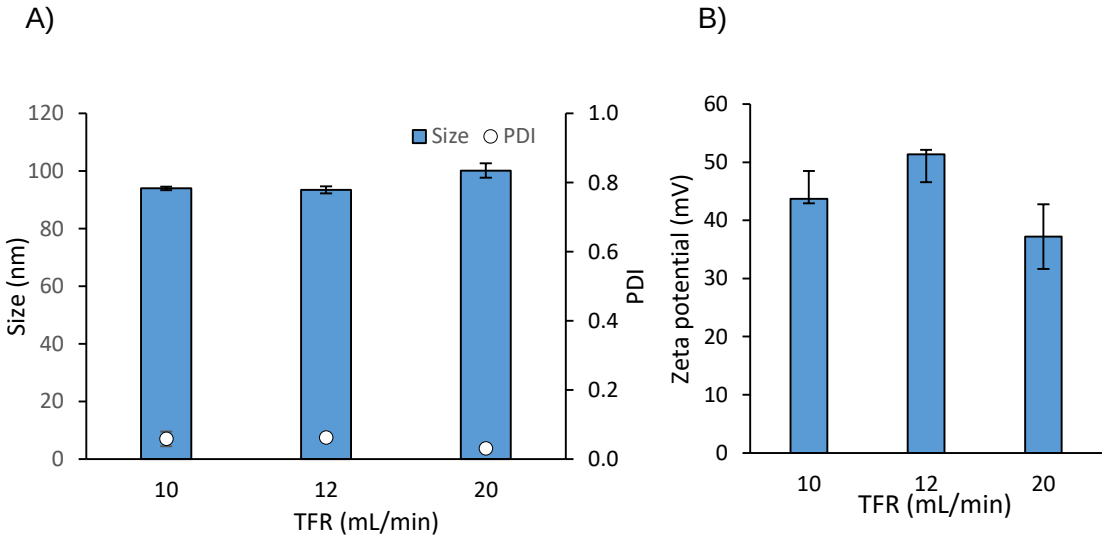

Figure 4-11 Impact of the TFR on the physiochemical characteristics of the 10% DOTAP formulation. Initial lipid concentration was 2 mg/mL and FRR was 3:1. Formulations were characterised in terms of A) Size & PDI B) Zeta potential (measured in 10 mM Tris, pH 7.4 diluted 1:300 in water). Results are presented as mean ± SD of three independent experiments.

For the TFR optimisation shown in Figure 4-11, no significant differences in the liposomal physiochemical characterises are observed, with the PDI remaining very low (<0.1) throughout the series. The zeta potential remains high throughout the series, in a range of 37 – 50 mV, which are in agreement with Kastner et al. who showed that zeta potentials of DOTAP:DOPE liposomes maintained zeta potentials despite changes in the total flow rate (Kastner et al., 2014).

4.3.7 Stability of the DDA-based liposome formulation

Section 4.3.6 established a FRR of 3:1 and TFR of 12 mL/min for the microfluidic production of the DDA formulation. To check the stability of this formulation, a fresh batch was prepared and its stability was measured over thirteen days of storage at 4 °C to confirm that a potential vaccine could be used within this practical timeframe from formulation. The results shown in Figure 4-12.

A)

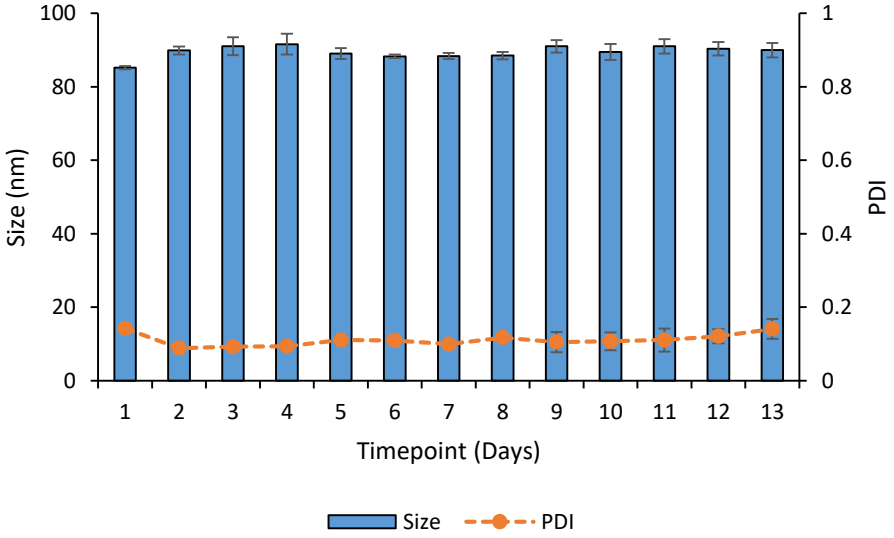

B)

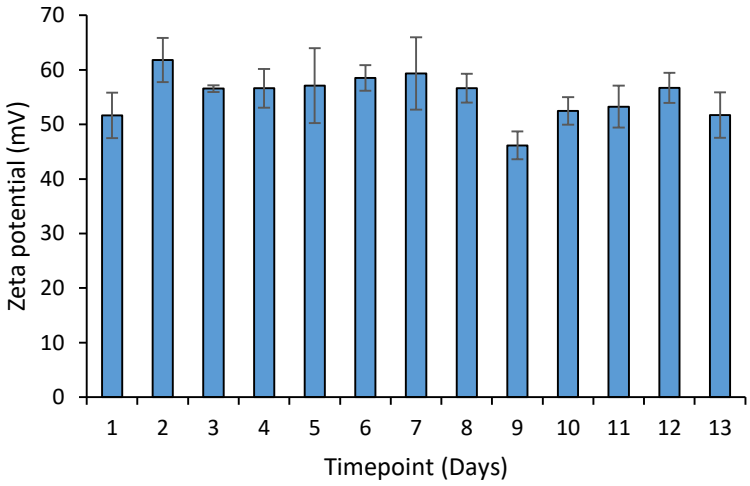

Figure 4-12 Stability study of the DDA formulations stored at 4 °C over a period of thirteen days. Formulations were characterised in terms of A) Size & PDI B) Zeta potential (measured in 10 mM Tris, pH 7.4 diluted 1:300 in water). Results are presented as mean ± SD of three technical replicates.

From the results presented in Figure 4-12, the DDA formulation is stable over the thirteen days tested when stored at 4 °C in terms of size, PDI and zeta potential, with none of these attributes changing significantly over the measured time period. Though a cationic formulation could be expected to be more stable with respect to a neutral formulation in solution, based on the fact that charged liposomes repel each other and so can prevent against aggregation in solution (Bozzuto and Molinari, 2015) this is not always the case. Indeed, the literature reports that liposomes formed solely

from DDA are found to be unstable and aggregate in the presence of small amounts of salt, and the same is observed even in pure water over time (Davidsen et al., 2005).

4.3.8 Investigating protein antigen adsorption to the DDA-liposome formulation

With a DDA-based liposome formulation established, the adsorption of the NadA3-PorA-Ferritin to the liposomal surface was then investigated. One study using the DDA:TDB CAF01 formulation observed that alongside the cationic charge, an antigen adsorption of >50% to the liposomal surface were important factors to ensure efficient deposition of antigen at the site of injection, which led to increased presentation to APCs that influenced the ability of the vaccine to induce potent cell-mediated responses (Henriksen-Lacey et al., 2010b). Another study with the DDA:TDB formulation also showed that a high degree of antigen surface adsorption was important in being able to induce Th1/Th17 responses (though was not necessarily a prerequisite to stimulate Th2 and antibody responses) (Kamath et al., 2012).

In the head-to-head *in vivo* study, the protein antigen NadA3-PorA-Ferritin will be administered at a final concentration of 0.44 mg/mL. Initial attempts at antigen adsorption had the DDA formulation at a lipid concentration of 1 mg/mL and small volumes of concentrated ovalbumin (OVA) acting as a model protein or NadA3-PorA-Ferritin added carefully to the side of vial before being mixed instantaneously by vortexing. This was equal to a protein-to-lipid weight ratio of 0.4. DLS measurements revealed aggregation of the liposomes at this ratio, and so a decreased protein-to-lipid ratio was investigated.

This time, the NadA3-PorA-Ferritin or OVA antigen was added to a more concentrated solution of the DDA liposome formulation such that the final protein concentration was 0.44 mg/mL and the final lipid concentration was 5 mg/mL. The protein-to-lipid ratio was now reduced to 0.09. The solutions were vortexed as before for 5 seconds and allowed to equilibrate for 10 minutes prior to characterisation by DLS, the results of which are shown in Table 4-8.

Table 4-8 The physiochemical characteristics of the DDA liposome formulation before and after protein antigen (OVA or NadA3-PorA-Ferritin) adsorption. Protein-to-lipid ratio was 0.09. Results are presented as the mean ± SD of three independent experiments.

Formulation	Size (nm)	PDI	Zeta potential (mV)
DDA liposomes alone	105 ± 1	0.07 ±0.02	50 ± 10
DDA liposomes: OVA	1870 ± 2258	0.66 ±0.5	21 ± 5
DDA liposomes: NadA3-PorA-Ferritin	131 ± 20	0.24 ±0.09	21 ± 3

The results displayed in Table 4-8 show that association of the OVA results in a large increase in the liposome size and PDI as measured by DLS, indicating aggregation of the liposomes. Association of the NadA3-PorA-Ferritin, however, at the same protein-to-lipid ratio results in an increase of size by ~ 25 nm and a raised PDI to an acceptable 0.25. For both proteins, the zeta potential of the formulations decreases on antigen adsorption, though still remains positive. Figure 4-13 compares the size intensity plots obtained for the DDA liposomes and the DDA:NadA3-PorA-Ferritin formulation.

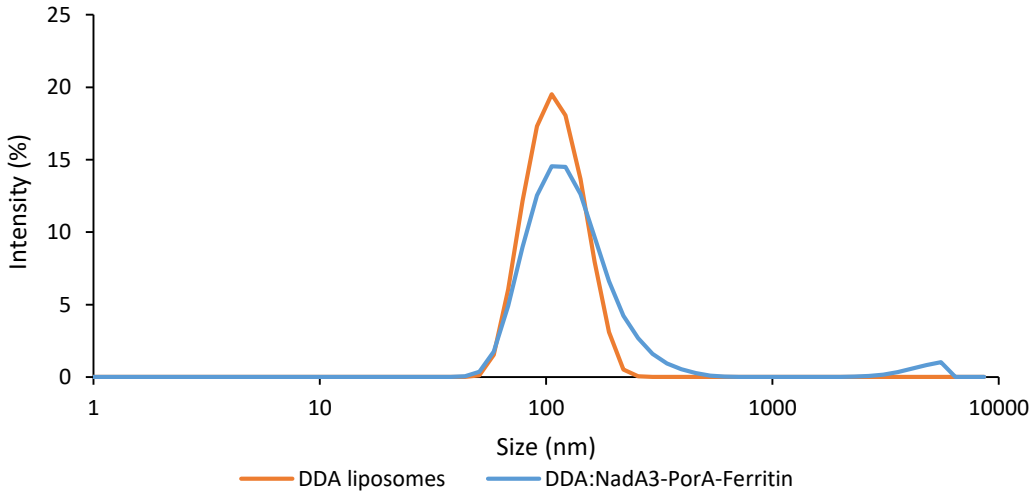

Figure 4-13 DLS size intensity comparing the DDA liposomes before and after association with the NadA3-PorA-Ferritin nanoparticle. There is a slight shift towards polydispersity following association with the nanoparticle.

A study by Hamborg et al. found distinct differences in a DDA:TDB formulation's liposomal colloidal stability depending on the protein antigen-to-lipid mass ratios

(Hamborg et al., 2013) and can help to explain the size distribution obtained here. They proposed a number of scenarios to explain the physical state of a liposome formulation based on the protein-to-lipid mass ratio. Below a certain protein antigen-to-lipid mass ratio, where the entire amount of the added negatively charged antigen is adsorbed to the liposome surface, the size of the liposomes remains largely unchanged, though a small fraction may aggregate on addition of the protein. This scenario most likely represented a vaccine formulation administered clinically. However, at higher protein antigen-to-lipid mass ratios, the increased concentration of negatively charged antigen induces liposomal aggregation because of excessive electrostatic attractions between liposomes and absorbed/ excess bulk antigen. They also noted different aggregative and stabilising effects depending on the antigen used. Differences in the surface coverage of the antigens when adsorbed to the liposomes could explain this, and may also explain the differences seen here between the OVA and NadA3-PorA-Ferritin adsorptions.

4.4 Conclusion

In this chapter, the aim was to develop and characterise a cationic liposome adjuvant formulation for the delivery of the NadA3-PorA-Ferritin. This would form the basis of a comparative study looking at the differences in immunogenicity induced by the AddaVax MF59-like emulsion versus cationic liposomes. Microfluidics, representing a rapid and scalable process to produce homogenous liposome formulations, was used to prepare initially a DOTAP-based formulation.

The composition and microfluidic process parameters for this formulation were optimised, and the lipid recovery tracked throughout the process to ensure a valid method for the production of these liposomes. PEGylation of the liposomes was also investigated, though saw too large a reduction in zeta potential to enable surface adoption of the NadA3-PorA-Ferritin antigen. The cationic lipid component was then exchanged for well-characterised DDA lipid and the formulation process optimised as before. Antigen adsorption studies showed that a stable liposome formulation could be obtained by adjusting the protein-to-lipid mass ratio.

As eluded to in this chapter, the immunogenicity of a liposome formulation is complex and is dependent on a number of factors, from lipid composition to liposome size and charge. The next chapter will compare the response seen by AddaVax adjuvant and will characterise the immune response induced by adjuvantation with this liposome formulation.

5. Chapter 5

Adjuvant head-to-head study and biodistribution

5.1 Introduction

One objective of the *in vivo* study is to assess how the presentation of the NadA3-PorA subunit antigen in a multicopy on the surface of a ferritin nanoparticle can enhance the immune response. Comparison to the antibody titres and the cellular immune response obtained with immunisation using the wild-type NadA3 (24-170) can also elucidate the extent to which the rational insertion of the PorA VR2 14 epitope can affect the immunogenicity of remaining protective NadA3 epitopes. To ensure a sufficient immune response is raised, all these groups are adjuvanted with the MF59-like adjuvant AddaVax. In the previous chapter, the optimisation of a benchtop microfluidic process for the production of a DDA-based cationic liposome adjuvant was described. This adjuvant will form the basis of a head-to-head comparison study to examine how the use of adjuvant can affect the immune response elicited by immunisation with the NadA3-PorA-Ferritin.

5.1.1 Aim and objectives

The main aim of the work presented in this chapter is to compare the immune responses for when the NadA3-PorA-Ferritin nanoparticle is administered with a DDA-based cationic liposome adjuvant, manufactured by a reproducible and rapid benchtop microfluidic process, versus the MF59-like AddaVax emulsion. To achieve this aim, the objectives were to:

1. Compare the humoral response (total IgG, IgG1, IgG2a) obtained for when NadA3-PorA-Ferritin is delivered with either AddaVax or DDA liposomes.
2. Analyse the cellular immune response induced by both adjuvants using a multiplex assay.
3. Assess the protective bactericidal capacity of the antibodies raised by performing an SBA.

5.2 Materials and methods

5.2.1 Materials

Reagent	Supplier
1,1'-Dioctadecyl-3,3,3',3'-Tetramethylindodicarbocyanine (DiD)	ThermoFisher, Waltham, MA
1,2-distearoyl-sn-glycero-3-phosphocholine (DSPC)	Avanti Polar Lipids, Alabaster, USA
Addavax	Invivogen, San Diego
Alexa Fluor 790 Antibody Labelling Kit	ThermoFisher, Waltham, MA
Ammonium chloride	Sigma, Dorset, UK
Anti-Mouse IgG –Peroxidase antibody	Sigma, Dorset, UK
ConA	Sigma, Dorset, UK
Cholesterol	Sigma, Dorset, UK
Dialysis tubing cellulose membrane (Typical molecular weight cut-off of 14,000, flat width 25 mm)	Sigma, Dorset, UK
Dimethyldioctadecylammonium (DDA)	Avanti Polar Lipids, Alabaster, USA
Ethanol	Fisher Scientific, Loughborough, UK
FBS for cell culture	Sigma, Dorset, UK
Goat anti-mouse IgG1-HRP	
LEGENDplexTM mouse inflammation panel (13-plex) flow cytometry kit	Biolegend, UK
Nunclon Delta 96-Well plate Thermo	ThermoFisher, Waltham, MA

Nunc MaxiSorp flat-bottom plate	ThermoFisher, Waltham, MA
PBS	In-house
Pen-Strep	Sigma, Dorset, UK,
Rat anti-mouse IgG2a	
RPMI-1640	Sigma, Dorset, UK
Skimmed milk powder	Sigma, Dorset, UK
Sodium chloride	Sigma, Dorset, UK
Sodium phosphate	Sigma, Dorset, UK
Sulphuric acid	Sigma, Dorset, UK
TMB ELISA Substrate High Sensitivity	Abcam, Cambridge, USA
Trypan Blue	Sigma, Dorset, UK
Tris Ultra Pure	ICN Biomedicals, Aurora, USA
Tween 20	Sigma, Dorset, UK

5.2.2 Preparation of DDA liposome: NadA3-PorA-Ferritin formulation for immunisation

Liposomes were manufactured using a NanoAssemblr (Precision NanoSystems Inc) by injecting the ethanol-solubilised lipids and aqueous buffer (Tris 10 mM, pH 7.4) into separate chamber inlets of the NanoAssemblr chip. All liposomes were formulated at 40 mg/mL initial lipid concentration, 3:1 flow rate ratio and 12 mL/min total flow rate. The DDA-based liposome formulation was collected from the chamber outlet and the ethanol solvent removed by dialysis at room temperature against Tris buffer (10 mM, pH 7.4) under magnetic stirring for 2 hours. Characterisation of the liposomes was performed using dynamic light scattering (DLS) (Malvern NanoZS, Malvern Instruments, Worcestershire, UK). Particle size was reported as the z-average (intensity based mean particle diameter) and the zeta potential using particle

electrophoresis. Polydispersity index (PDI) measurements were used to assess particle distribution. Liposome formulations were diluted 1:10 in diluted buffer (10 mM Tris or 1X PBS diluted 1:300 in water) and measurements took place at 25 °C with the RI set to 1.50. A concentrated solution of the NadA3-PorA-Ferritin antigen was added slowly to the DDA liposome formulation such that the final protein concentration was 0.44 mg/mL and the final lipid concentration was 5 mg/mL. The solution was vortexed for 5 seconds and allowed to equilibrate for 10 minutes prior to characterisation by DLS.

5.2.3 *in vivo* immunisation study

All animal studies were ethically reviewed and carried out in accordance with European Directive 2010/63/EEC. All *in vivo* studies were conducted under the regulations of the animals (scientific procedures) act 1986. All protocols were subjected to ethical review and were carried out in a designated establishment. The immunisation of the AddaVax immunised mice is detailed in section 3.2.7. For the liposome adjuvanted group, five female BALB/c mice (7-9 weeks old) were housed together and allowed free access to food and water. Each mouse was immunised at three different timepoints (day 1, 21 and 35) The 50 µL immunisation dose was administered intramuscularly into the thigh and contained a dose of NadA3-PorA-Ferritin equivalent to 10 µg of NadA3-PorA in DDA-liposomes at a final concentration of 5 mg/mL. The adjuvant free group consisted of a mass of NadA3-PorA-Ferritin equivalent to 10 µg of NadA3-PorA in 10 mM PBS. The 50 µL immunisation dose was administered intramuscularly into the thigh. Blood was collected by tail bleeds (except on the day of the cull, where it was obtained by heart puncture) and left to coagulate at RT for 30 mins before sera collection by centrifugation at 10,000 g for 10 mins at 4 °C. Collected sera was then stored at -20 °C. On termination, spleens and inguinal lymph nodes were also isolated.

5.2.4 Isolation of splenocytes

Isolated spleens were processed by forcing though a metal mesh cell strainer followed by washing with RPMI 1640 supplemented with 10% FBS and 1% Pen Strep Erythrocytes were removed by resuspension in Boyle's solution (composed of 0.17M Tris and 0.16M ammonium chloride mixed at a ratio of 1:9). The splenocytes were washed again in complete RPMI 1640 before viable cell numbers were measured using Trypan Blue exclusion. 100 µL of splenocytes at a concentration of $5x10^6$ cells/mL was added into wells of a Nunclon Delta 96-Well plate and the wells were then stimulated with either; mapped peptides to a final concentration of 5 µg/mL, relevant antigen to a final concentration of 5 µg/mL, ConA to a final concentration 5

µg/mL or complete RPMI for 72 hours at 37°C, 5% CO_2. The supernatants were then harvested and stored at -20°C.

5.2.5 Total serum IgG indirect ELISA to detect anti-NadA3 (24-170) antibodies

The wells of a Nunc MaxiSorp flat-bottom plate were coated with 100 µL of NadA3 (24-170) at 2 ug/µL diluted in 1X PBS, pH 7.4. The plate was then covered with Clingfilm and left to incubate at 4°C overnight. The following morning, the plate was washed three times with wash buffer (1 X PBS, Tween-20 0.05%, pH 7.4) and then blocked by the addition of 200 µL of blocking buffer (2% skimmed 0.1% fat milk in 1X PBS, Tween-20 0.05%, pH 7.4) to all wells of the plate, followed by incubation for 1 hour at 37 °C. The plate was then washed three times in wash buffer before the addition of 100 µL of blocking buffer to all wells except those of column 1. To column 1, 200 µL of immunisation sera was added at a dilution of 1:500 (diluted in blocking buffer). A serial dilutions series on the plate was then initiated by taking 100 µL of this was then added into column 2, mixed by pipetting up and down 5 times, and the serial dilution continued as per for the successive columns up to until column 11. Column 12 saw no addition of sera. The plate was covered as before with Clingfilm and incubated for 2 hours at 37 °C. The plate was then washed three times with wash solution before the addition of 100 µL of Anti-Mouse IgG –Peroxidase antibody diluted to 1:10,000 in blocking buffer was added to all the wells of the plate. The plate was covered as before and incubated for 1 hour at 37 °C before washing three times with wash buffer. This was followed by the addition of 100 µL of substrate to all wells and the plate was then covered with foil for 30 minutes. After the 30 minutes had elapsed, 20 µL of 0.2 M sulphuric acid was added to all wells to stop the reaction and the absorbance was read at 450 nm.

5.2.6 Analysis of anti-NadA3 (24-170) IgG1 and IgG2a antibody titres by ELISA

The wells of a Nunc MaxiSorp flat-bottom plate were coated with 100 µL of NadA3 (24-170) at 2 ug/µL diluted in 1X PBS, pH 7.4 The plate was then covered with Clingfilm and left to incubate at 4°C overnight. The following morning, the plate was washed three times with wash buffer (1 X PBS, Tween-20 0.05%, pH 7.4) and then blocked by the addition of 200 µL of blocking buffer (2% skimmed 0.1% fat milk in 1X PBS, Tween-20 0.05%, pH 7.4) to all wells of the plate, followed by incubation for 1 hour at 37 °C. The plate was then washed three times in wash buffer before the addition of 100 µL of blocking buffer to all wells except those of column 1. To column

1, 200 µL of immunisation sera was added at a dilution of 1:500 (diluted in blocking buffer). A serial dilutions series on the plate was then initiated by taking 100 µL of this was then added into column 2, mixed by pipetting up and down 5 times, and the serial dilution continued as per for the successive columns up to until column 11. Column 12 saw no addition of sera. The plate was covered as before with Clingfilm and incubated for 2 hours at 37 °C. The plate was then washed three times with wash solution before the addition of 100 µL of goat anti-mouse IgG1-HRP or rat anti-mouse IgG2a, HRP antibody (diluted to 1: 20,000 or 1:5000 in blocking buffer, respectively) was added to all the wells of the plate. The plate was covered as before and incubated for 1 hour at 37 °C before washing three times with wash buffer. This was followed by the addition of 100 µL of substrate to all wells and the plate was then covered with foil for 30 minutes. After the 30 minutes had elapsed, 20 µL of 0.2 M sulphuric acid was added to all wells to stop the reaction and the absorbance was read at 450 nm.

5.2.7 Multiplex cytokine analysis of cellular immune response

Supernatants from stimulated splenocytes were measured using the LEGENDplexTM mouse inflammation panel (13-plex) flow cytometry kit (BioLegend) in conjunction with a BD FACSCanto system (BD Biosciences).

5.2.8 Serum bactericidal activity of immunisation sera

The serum bactericidal activity (SBA) of immunisation sera against *N. meningitidis* strains was evaluated using baby rabbit complement at 25% of the total volume of the reaction (12.5 µL of complement in 50 µL of the reaction volume). SBA titres were defined as the serum dilution that resulted in a 50% decrease in colony-forming units (CFUs) per ml after a 60 minute incubation of the *N. meningitidis* bacteria with the reaction mixture compared to the control CFU per mL at time 0.

5.2.9 Biodistribution studies by IVIS

Both adjuvants and protein antigens were fluorescently labelled for *in vivo* imaging. For the AddaVax and liposome adjuvants, both were labelled with 1,1'-Dioctadecyl-3,3,3',3'-Tetramethylindodicarbocyanine (DiD). Before antigen association to adjuvant, both the DDA liposomes and the AddaVax were prepared to a final DiD concentrations of 32 µg/mL (for the liposomes, concentrated DiD was added to the lipid stock prior to production on the NanoAssemblr, while for the AddaVax the DiD was directly added and vortexed). For fluorescent labelling of the protein antigens,

the infrared fluorescent Alexa Fluor 790 label was conjugated using an Alexa Fluor 790 Antibody Labelling Kit as according to the manufacturer's instructions.

All animal studies were ethically reviewed and carried out in accordance with European Directive 2010/63/EEC. All protocols were subjected to ethical review and were carried out in a designated establishment. 3 female BALB/c mice (7-9 weeks old) per group were housed in study groups and allowed free access to food and water. The mice were anesthetized under continuous flow of isoflurane (2% in oxygen). For the AddaVax adjuvanted groups, each immunisation dose consisted of 12.5 µL Addavax and 37.5 µL of 10 mM PBS containing 10 µg of antigen, while the liposome group contained 10 ug of antigen in the liposome formulation at a final concentration of 5 mg/mL. The 50 µL immunisation dose was administered intramuscularly into the thigh.

Mice were scanned for fluorescence over an 11-day period using an IVIS Spectrum (PerkinElmer Inc., Waltham, MA, USA). DiD fluorescence was detected using excitation and emission wavelengths of 605 nm and 680 nm respectively, while for the Alexa Fluor 790 excitation at 745 nm and emission at 820 nm were used. At the end of the study, mice were terminated by cervical dislocation and select organs harvested for fluorescence analysis.

Captured images were analysed using the Living Image 4.1 software (PerkinElmer Inc.). The fluorescence signal data were in all cases corrected by subtracting the signal detected in the control mouse that had not been immunised with a fluorescent marker. Fluorescent signal data from all tissues were obtained considering the lateral view. All captured fluorescence signal obtained was expressed as the radiance, technically defined as fluorescence emission radiance per incident excitation intensity: photons/s/cm_2/sr (steradian).

5.2.10 Statistical analysis

Statistical analysis of data was calculated by one-way analysis of variance (ANOVA). Where significant differences are indicated, differences between means were determined by the Tukey Simultaneous Tests for Differences of Means. All the calculations were made using Minitab 17 statistical software.

5.3 Results and discussion

5.3.1 Immunisation schedule

Five female BALB/c mice (7 – 9 weeks old) were immunised with NadA3-PorA-Ferritin (equivalent to 10 µg of NadA3-PorA per dose) adjuvanted with the DDA-based cationic liposomes. An adjuvant free group of three mice was also included as a control. The immunisation schedule is depicted in Figure 5-1 and consisted of three doses administered intramuscularly.

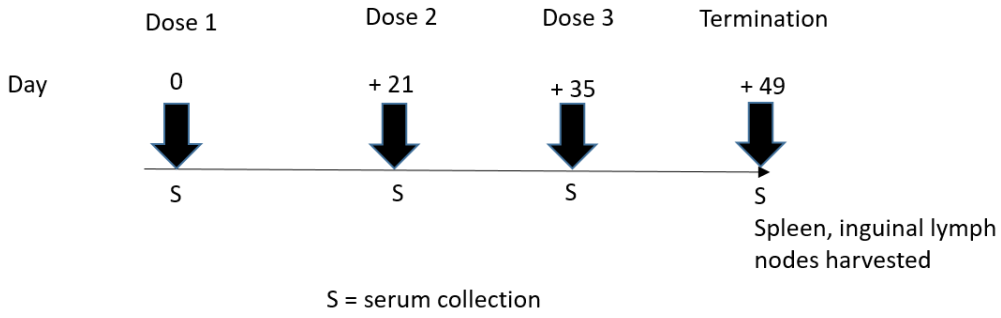

Figure 5-1 A diagram of the *in vivo* study immunisation schedule

5.3.2 Preparation of DDA-liposome formulation for *in vivo* immunisation

On the day of immunisation, DDA liposomes were prepared freshly on the NanoAssemblr from an initial lipid stock of 40 mg/mL and using the process parameters of 12 mL/min TFF, 3:1 FRR as described in chapter 4. In order to absorb NadA3-PorA-Ferritin to the liposome surface, a concentrated solution of the antigen was added to the DDA liposome formulation such that the final protein concentration was 0.44 mg/mL (giving an equivalent of 10 µg of NadA3-PorA antigen per 50 µL liposome dose) and the final lipid concentration was 5 mg/mL. A summary of the NadA3-PorA-Ferritin adsorbed liposomes used in this study is shown in Table 5-1. The increase in liposome size and PDI, and reduction in zeta potential on adsorption are consistent with observations detailed in section 4.3.8.

Table 5-1 Summary of Nada3-PorA-Ferrin adsorbed DDA-liposome formulations used the *in vivo* adjuvant comparison study. Results are represented as mean± SD of the three doses administered

Formulation	Size (nm)	PDI	Zeta potential (mV)
DDA liposomes: Nad3-PorA-Ferritin	112 ± 10	0.24 ± 0.03	16 ± 5

5.3.3 DDA-based liposome formulation induces high total IgG antibody

Sera collected at the various timepoints (detailed in Figure 5-1) was assayed for total anti-NadA3 (24-170) IgG antibodies by ELISA. Figure 5-2 shows the anti-NadA3 (24-170) total IgG endpoint titres for sera collected on the A) day 21 and B) day 35.

A)

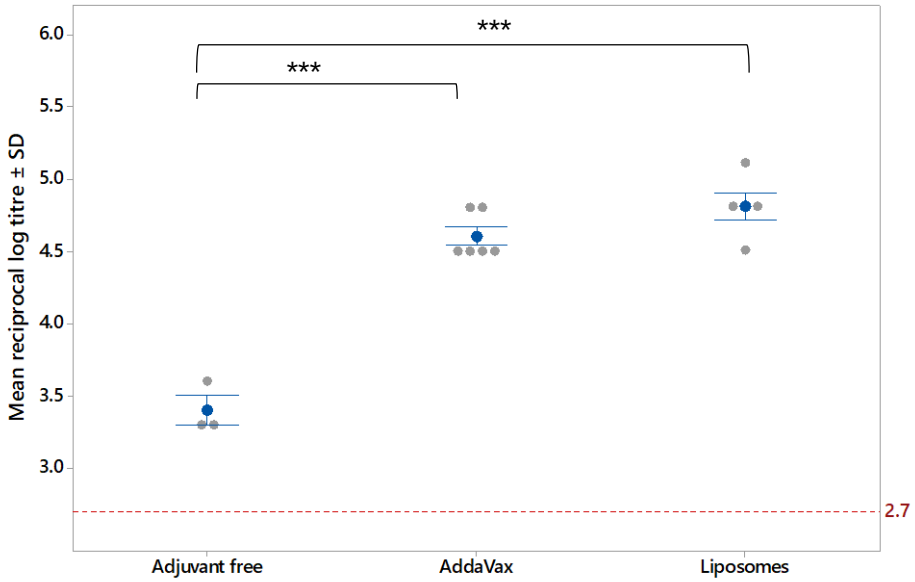

B)

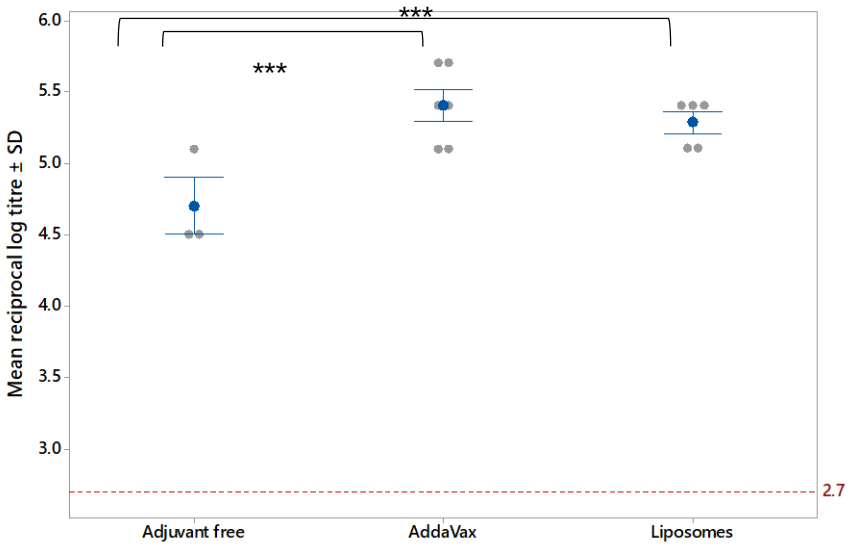

Figure 5-2 Anti-NadA3 (24-170) total IgG titres after immunisation with NadA3-PorA-Ferritin adjuvanted with either AddaVax or cationic DDA-based liposomes. Titres displayed derive from sera collected either A) 21 days after immunisation with the first dose or B) At the 35 day timepoint, 2 weeks after the second dose. The x-axis displays the adjuvant categories; Adjuvant free, AddaVax or liposomes. The dashed red-line at a titre of 2.7 represents the titre obtained at the starting sera dilution. Grey dots ● indicate titres from individual mice while the dark blue dot ● represents the mean reciprocal endpoint log titre ± SD.

At the day 21 timepoint (21 days following the first immunisation with NadA3-PorA-Ferritin), there are significantly higher titres ($p<0.001$) obtained for the adjuvanted groups in comparison to the non-adjuvanted group. Moving to the day 35 timepoint

(14 days following the second immunisation dose), these differences are still significant ($p<0.05$). For both timepoints, the differences between the AddaVax and liposome-adjuvanted titres are not significant.

The statistically significant increase in IgG anit-NadA3 antibody titres seen here when the NadA3-PorA-Ferritin is adjuvanted with either the AddaVax or DDA-liposomes conforms to what is known about the immuno-stimulating role of adjuvants. Highly purified, subunit antigens such as the NadA3-PorA-Ferritin, show reduced immunogenicity due to the absence of exogenous immune-activating components that would otherwise be present in a whole-cell vaccine formulation (Zepp, 2010), and so for this reason adjuvants are included to provide the innate immunopotentiation which leads into an adaptive immune response (Tandrup Schmidt et al., 2016). Kanekiyo et al. showed that when their hemagglutinin-presenting ferritin nanoparticles were administered unadjuvanted, they were able to induce higher titres than a licensed inactivated influenza vaccine. However, these increases in titres only reached statistical significance when the nanoparticle was adjuvanted with Ribi adjuvant (Kanekiyo et al., 2013).

As previously described, the MF59-similar adjuvant AddaVax is able to enhance both cellular and humoral immune responses (Calabro et al., 2013). As demonstrated here, it is able along with the DDA-liposomes to significantly elevate the anti-NadA3 IgG titres over those of the unadjuvanted group. The adjuvant effect of DDA-based liposomes has been purported to be primarily due to enhanced targeting of antigen to the cellular membrane of APCs, which subsequently increases both the uptake and presentation of that antigen by the APCs (Korsholm et al., 2007).

5.3.4 Analysis of IgG1 and IgG2a anti-NadA3 antibody titres elicited by the AddaVax and DDA-based liposomes

The humoral response to immunisation was further investigated by analysing the IgG1 and IgG2a subclass titres. Figure 5-3 (IgG1) and Figure 5-4 (IgG2a) display titres obtained at timepoints day 21 and 35.

A)

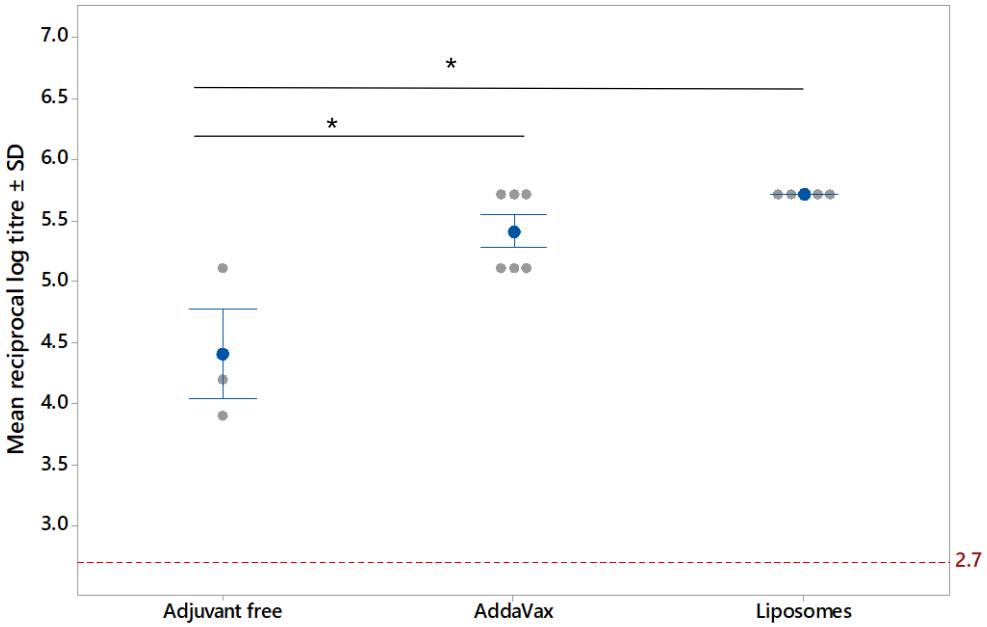

B)

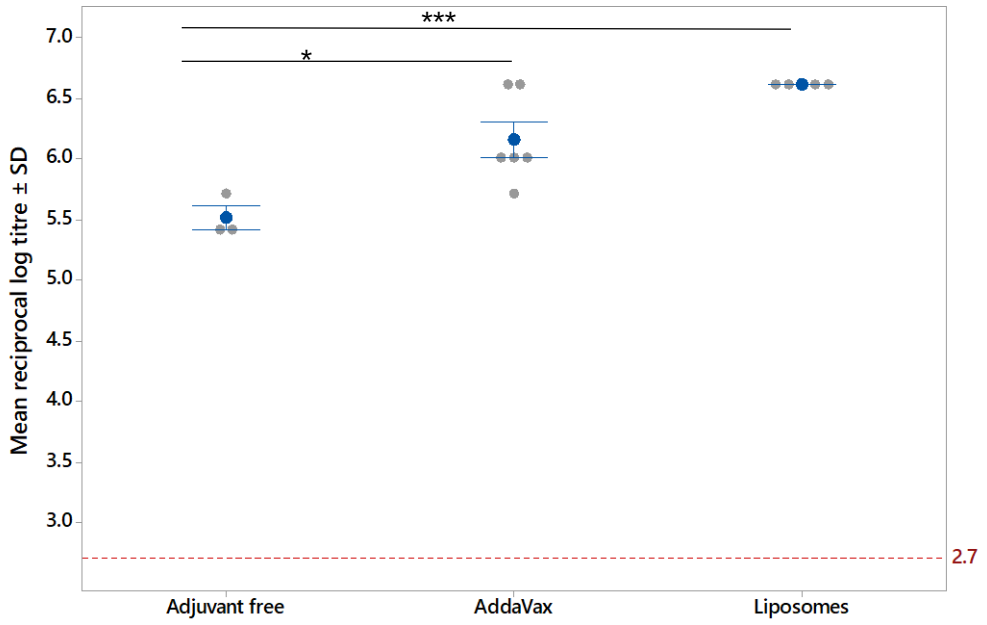

Figure 5-3 Anti-NadA3 (24-170) IgG1 titres after immunisation with NadA3-PorA-Ferritin adjuvanted with either AddaVax or cationic DDA-based liposomes. Titres displayed derive from sera collected either A) 21 days after immunisation with the first dose or B) At the 35 day timepoint, 2 weeks after the second dose. The x-axis displays the adjuvant categories; Adjuvant free, AddaVax or liposome. The dashed red-line at a titre of 2.7 represents the titre obtained at the starting sera dilution. Grey dots ● indicate titres from individual mice while the dark blue dot ● represents the mean reciprocal endpoint log titre ± SD. Significant differences between means were determined by the Tukey Simultaneous Tests for Differences of Means, with significance denoted as ***$p < 0.001$ and p*< 0.05.

A)

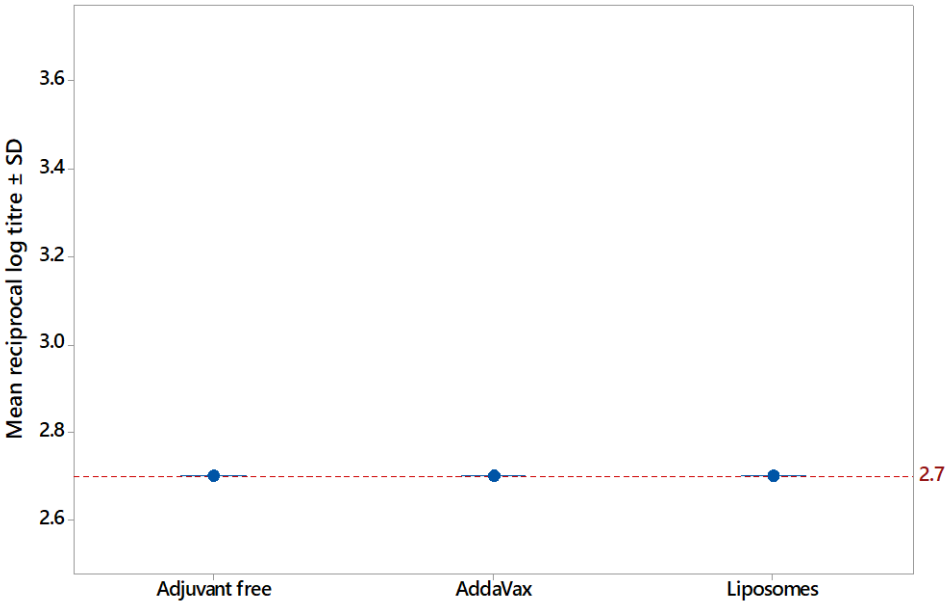

B)

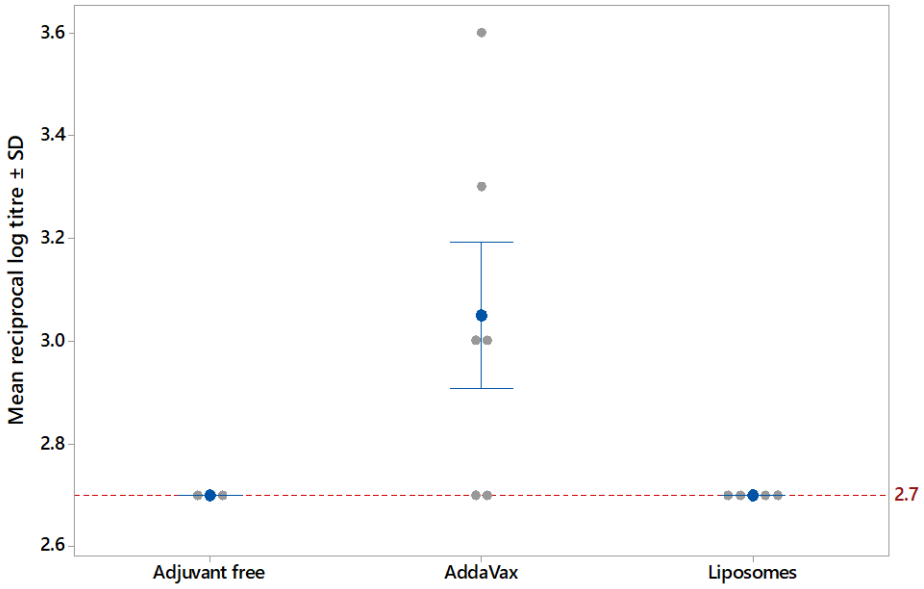

Figure 5-4 Anti-NadA3 (24-170) IgG2a titres after immunisation with NadA3-PorA-Ferritin adjuvanted with either AddaVax or cationic DDA-based liposomes. Titres displayed derive from sera collected either A) 21 days after immunisation with the first dose or B) At the 35 day timepoint, 2 weeks after the second dose. The x-axis displays the adjuvant categories; Adjuvant free, AddaVax or liposome. The dashed red-line at a titre of 2.7 represents the titre obtained at the starting sera dilution. Grey dots ● indicate titres from individual mice while the dark blue dot ● represents the mean reciprocal endpoint log titre ± SD.

Figure 5-3 shows the IgG1 anti-NadA3 (24-170) titres obtained at the day 21 and 35 timepoints. At day 21, the titres obtained for both adjuvanted groups are significantly higher ($p<0.05$) than those obtained for the adjuvant free group. This is also observed at day 35, with both adjuvant groups inducing IgG1 titres significantly greater than the non-adjuvanted group ($p<0.05$ and 0.001 for the AddaVax and liposome-adjuvanted groups, respectively). At the day 35 timepoint, there are also now significantly higher ($p<0.05$) titres obtained for the liposome group over the AddaVax group.

IgG2a anti-NadA3 (24-710) are displayed in Figure 5-4. At the day 21 timepoints, IgG2a titres are at background for all groups. Titres remain low at the day 35 timepoint, with only the higher dose NadA3-PorA-Ferritin group inducing IgG2a titres above background, though not significantly so.

In comparing the IgG1 and IgG2a titres overall, all the antibody responses induced are strongly skewed towards a Th2-type response, with the choice of adjuvant not appearing to alter the Th1-Th2 balance significantly. As described in chapter 3, the NadA3-PorA-Ferritin being a soluble protein would be expected to primarily induce an IgG1 response (Vidarsson et al., 2014).

In terms of what is known about the adjuvants, the MF59-like AddaVax also induces an IgG1 bias (Knudsen et al., 2016). Mice immunised with secreted antigens from *Mycobacterium tuberculosis* adjuvanted with DDA (not in the form of liposomes) gave a response skewed towards IgG2a (Lindblad et al., 1997). Further to this, DDA in form of liposomes formulation was able to shift the predominant IgG1 response induced by the Respiratory Syncytial Virus RSV antigen BBG2Na towards a more balanced IgG1/IgG2a profile (Klinguer-Hamour et al., 2002). In the same study where DDA-based liposomes were demonstrated to promote antigen retention at the injection site through a depot effect, DDA-based liposomes were also shown to be able to significantly raise both IgG1 and IgG2c antibody titres against the soluble antigen Ag85B-ESAT-6 (Henriksen-Lacey et al., 2010a).

However, in accounting for the low Th1 response in this study, it is also important to consider that the liposomes also contain the neutral lipid DSPC and cholesterol. In one study to investigate the role of cholesterol inclusion in the DDA:TDB formulation, it was found that cholesterol inclusion at ~30 mol % resulted in reduction of Th1-based immune responses (in particular with regards to Th1 cytokine profile) (Kaur et al., 2014). While fluidity of the DDA:TDB was enhanced, there was no increased movement to the local lymphatics nor an impact on monocyte recruitment to the injection site, which suggested that the reduction seen in the immune response was

likely due to reduced APC uptake. Hussain et al. demonstrated using a DDA:DSPC:TDB formulation that a reduction in the DDA content and its gradual replacement with DPSC resulted in reduced IgG2b responses, which suggested that higher levels of DDA potentiated a stronger Th1-skewed response (Hussain et al., 2014). To further investigate the role of DSPC, two DDA:DSPC:TDB formulations were prepared in which the DDA content was kept constant for both but only one of the formulations had DSPC added. When the immune responses of these two formulations were compared, IgG1 and IgG2b were not found to be significantly different but spleen proliferation and Th1 cytokines (IFNγ and IL-2) were significantly higher for the formulation without DSPC included, reinforcing the suggestion that DSPC reduces Th1-type responses.

5.3.5 Cellular immune response induced by the adjuvants AddaVax and DDA-based liposomes

The cellular immune response to immunisation with the NadA3-PorA-Ferritin adjuvanted with either the AddaVax or cationic liposomes was measured in a similar manner as described in chapter 3. Splenocytes isolated from the AddaVax and liposome-adjuvanted groups were then stimulated with the homologous subunit antigen NadA3-PorA for 72 hours. After the 72-hour stimulation period, cytokine levels in the culture supernatant were measured using the LEGENDplex mouse inflammation panel flow cytometry kit.

Figure 5-5 through to Figure 5-7 details the cytokine responses as classified by T-cell helper subsets. In this assay, control groups were also included; ‘NadA-PorA control’ are non-immunised spleens stimulated with the Nada3-PorA subunit antigen. The RPMI negative control group consists of immunised splenocytes from each group stimulated with no antigen.

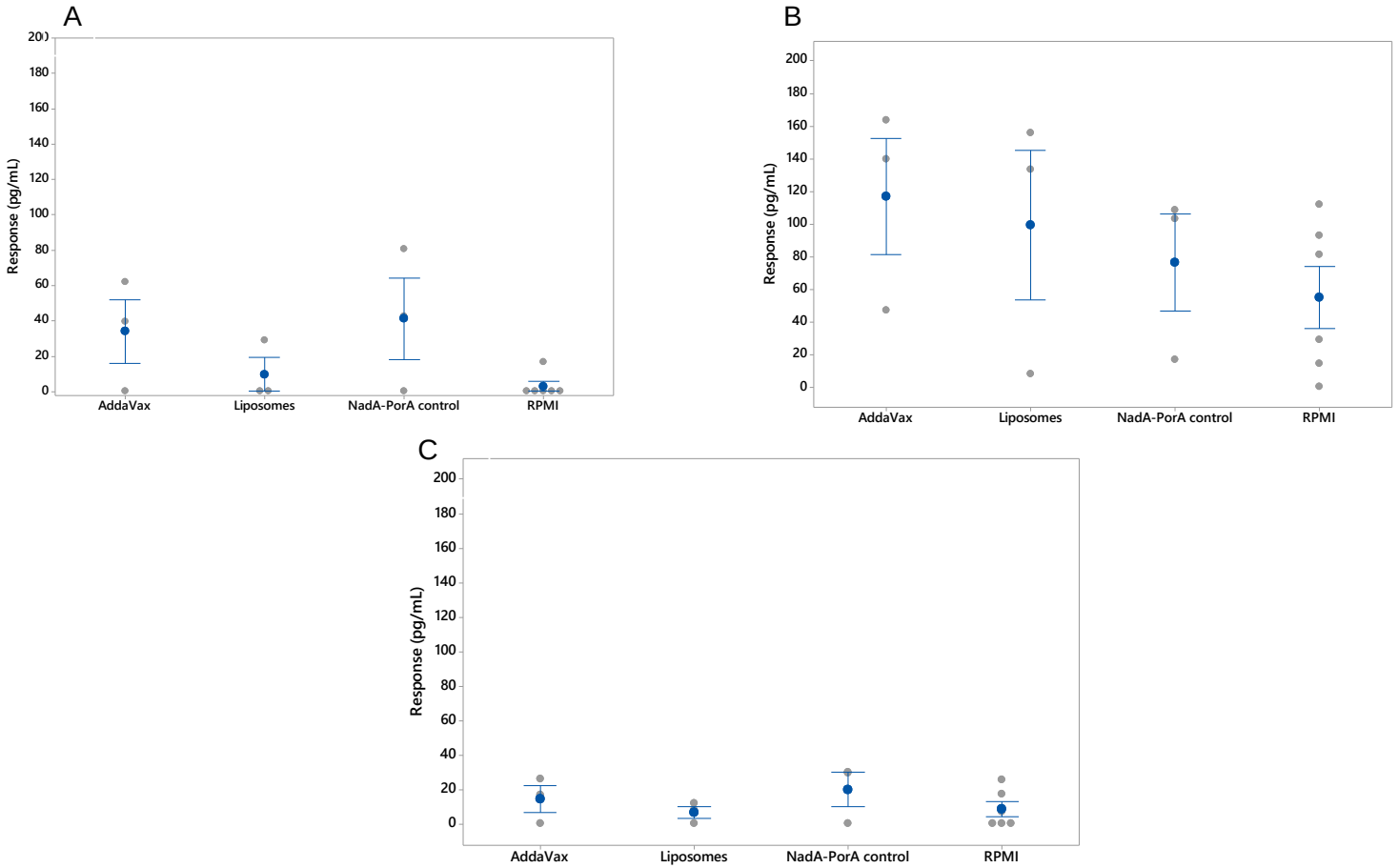

Figure 5-5 Cellular immune responses in terms of Th1 cytokines A) IFNγ B) IL-2. C) TNF-α. After 72 hours of stimulation with NadA3-PorA the supernatants were assayed for the presence of cytokines using the LEGENDplex mouse inflammation kit. Along the x-axis are the adjuvanted groups represented by 'AddaVax' and 'Liposomes'. 'NadA-PorA control' refers to control non-immunised spleens stimulated with NadA3-PorA while 'RPMI' represents immunised splenocytes stimulated with only RPMI. Grey dots ● represent individual mice and the dark blue dot ● represents the group mean, with the interval bar representing the standard error of the mean. Three mice per group were analysed, except for the RPMI group where n=6.

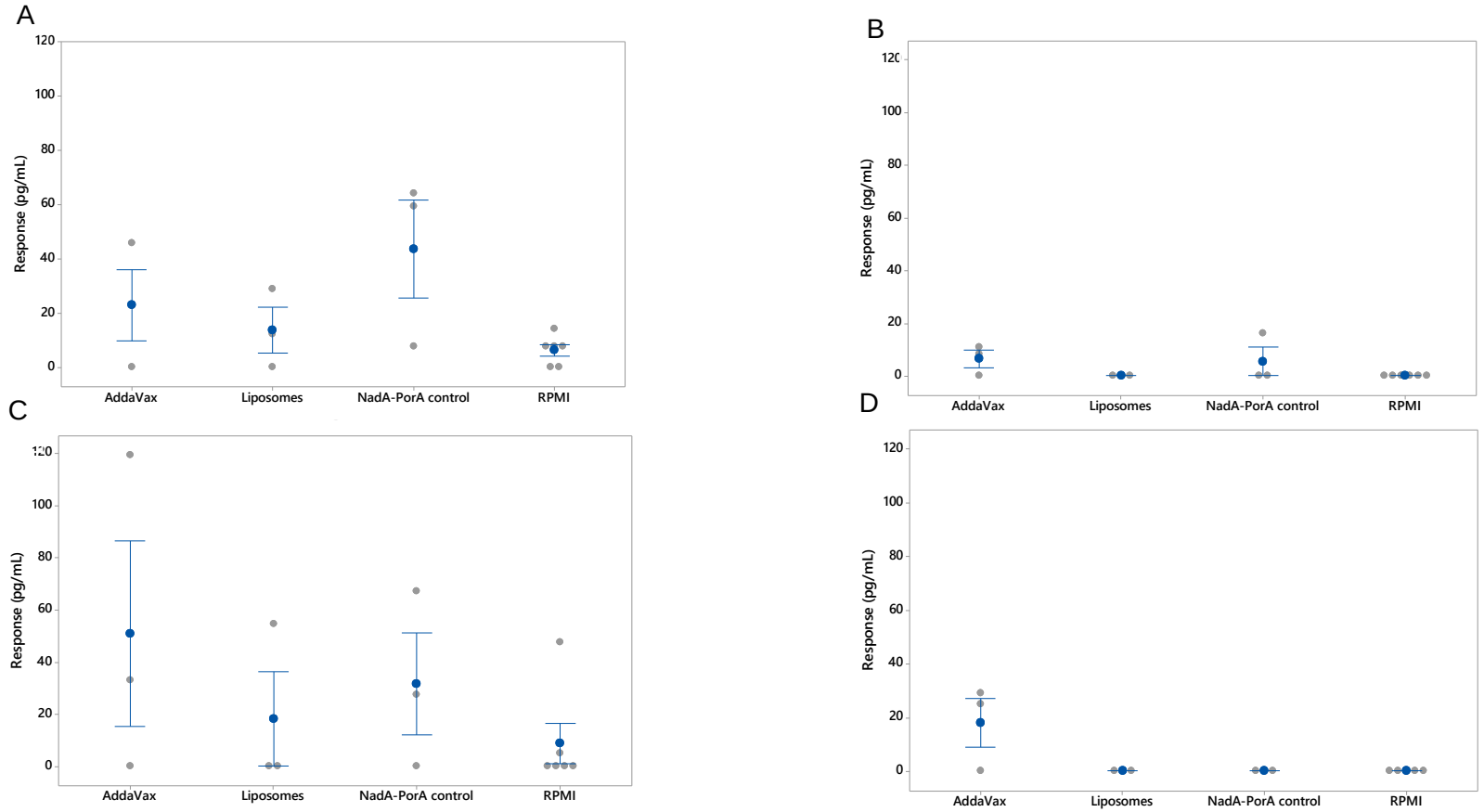

Figure 5-6 Cellular immune responses in terms of Th2 cytokines A) IL-10 B) IL-4 C) IL-5 D) IL-13. After 72 hours of stimulation with NadA3-PorA the supernatants were assayed for the presence of cytokines using the LEGENDplex mouse inflammation kit. Along the x-axis are the adjuvanted groups represented by 'AddaVax' and 'Liposomes'. 'NadA-PorA control' refers to control non-immunised spleens stimulated with NadA3-PorA while 'RPMI' represents immunised splenocytes stimulated with only with RPMI. Grey dots ● represent individual mice and the dark blue dot ● represents the group mean, with the interval bar representing the standard error of the mean. Three mice per group were analysed, except for the RPMI group where n=6.

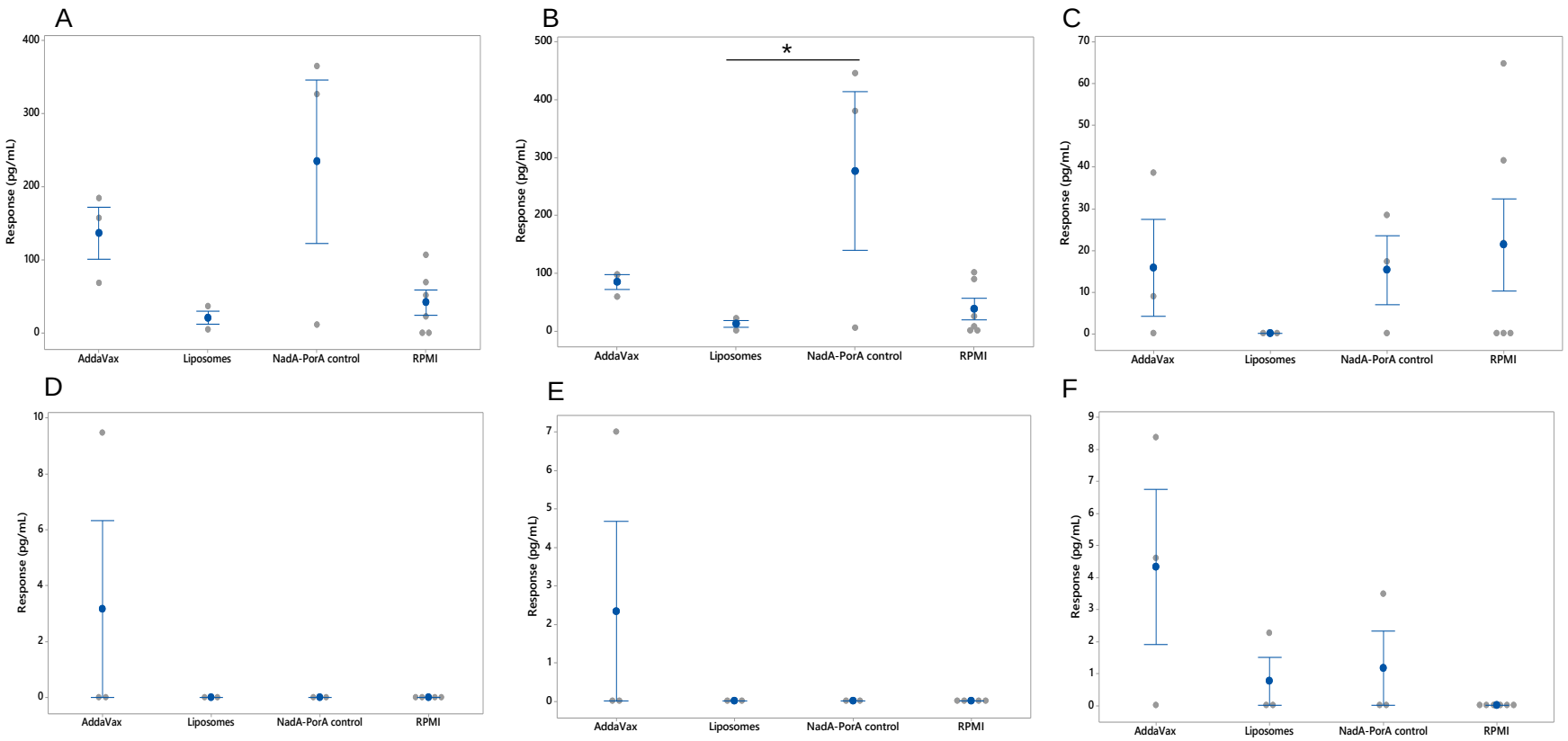

Figure 5-7 Cellular immune responses in terms of Th17, Th22, T_{FH} and Th9 cytokines A) IL-6 B) IL-22 C) IL-17A D) IL-17F E) IL-21 F) IL-9. After 72 hours of stimulation with NadA3-PorA the supernatants were assayed for the presence of cytokines using the LEGENDplex mouse inflammation kit. Along the x-axis are the adjuvanted groups represented by 'AddaVax' and 'Liposomes'. 'NadA-PorA control' refers to control non-immunised spleens stimulated with NadA3-PorA while 'RPMI' represents immunised splenocytes stimulated with only with RPMI. Grey dots ● represent individual mice and the dark blue dot ● represents the group mean, with the interval bar representing the standard error of the mean. Three mice per group were analysed, except for the RPMI group where n=6. Significant differences between means were determined by the Tukey Simultaneous Tests for Differences of Means, with significance denoted as *$p < 0.05$.

Across all the cytokines measured, there are no significant differences found when the AddaVax and liposome-adjuvanted groups are compared. The IgG1, IgG2a titres presented in section 3.3.6 showed no clear differences in the Th1/Th2 balance of the immune responses when NadA3-PorA-Ferritin was adjuvanted with AddaVax or liposomes and this lack of differences is also reflected here in the cytokine responses. The only cytokine that gives a significant difference between the two groups is the Th2 cytokine IL-13 (the responses remain low at less than 25 pg/mL), which may be as a result of the Th-2 skewing AddaVax adjuvant.

Liposomal adjuvants based on DDA have been found to induce stronger Th1 responses, which can be characterised by high levels of IFNγ production (Henriksen-Lacey et al., 2011a). An explanation for the poor IFNγ response observed for NadA3-PorA-Ferritin adjuvanted with the DDA liposome formulation may be due to the lack of an immunostimulator. In a study by Henriksen-Lacey et al, incorporation of the immunostimulator TDB into a DDA formulation was able to induce significantly higher IFNγ responses, while the IgG1 and IgG2c responses remained unchanged (Henriksen-Lacey et al., 2010a).

However, the cholesterol and DSPC components of the DDA liposome formulation may also have an effect on the resulting immune response. Incorporation of cholesterol into DDA-based liposomes was found to result in a decrease in the measured IFNγ response (Kaur et al., 2014). The potential immune effects of DSPC were explored in another study by Henriksen-Lacey et al. who found that substituting the cationic DDA for the neutral DSPC in a DDA:TDB formulation resulted in significantly decreased Th1 (IFNγ) and Th17 (IL-17) responses (Henriksen-Lacey et al., 2010b). This is in addition to the aforementioned study by Hussain et al, showing that addition of DSPC into a DDA:TDB formulation made no significant differences to IL-5 and IL-10 responses (Th2 cytokines) yet significantly reduced the IFNγ and IL-2 cytokine responses (Hussain et al., 2014).

A further point to consider is the cationic lipid content, as the liposomes described here in this study have a molar DDA content of 10%, whereas in the aforementioned papers the content was higher. Though differing in their choice of cationic lipid (another important consideration with regards to the immune response), Ma et al. found that DOTAP:DOPC (a neutral lipid) liposomes with higher cationic charge density enhanced dendritic cell maturation, antigen uptake and increased the production of antigen-specific IgG2a and IFNγ responses (Ma et al., 2011).

5.3.6 Analysis of bactericidal antibody titres by SBA

The total IgG ELISA assays detailed in section 5.3.3 revealed that when NadA3-PorA-Ferritin was administered with either the AddaVax and DDA-liposome adjuvants, high anti-NadA3 (24-170) IgG titres were obtained. To further compare immunisation of NadA3-PorA-Ferritin co-administered with these adjuvants, an SBA assay was performed to analyze bactericidal titre of the humoral response. The tested MenB strains are as described in chapter 3.

Table 5-2 SBA of sera taken from day 35 to assess bactericidal titres elicited by immunisation with the NadA3-PorA-Ferritin. Assay was performed in the presence of baby rabbit complement.

Immunisation sera	MenB strain		
	5/99	M08-0240104	M14933
NadA3-PorA-Ferritin + AddaVax	64	<64	<64
NadA3-PorA-Ferritin + DDA liposomes	<64	<64	<64
Non-immunised BALB/c control sera	<64	<64	<64
Internal control NadA3 clinical lot	>=32768	-	4096

As can be seen from Table 5-2, neither adjuvant groups is able induce bactericidal titres; a titre of 64 or less is classed as being negative for bactericidal activity. The NadA3 clinical lot, acting as a positive control in this assay, is the only group able to elicit bactericidal titres against all MenB strains except from the M08-0240104 strain, which lacks the NadA3.

To see if sera from another timepoint might elicit improved bactericidal titres, sera deriving from day 49, collected 2 weeks following the third dose was used in a repeat SBA assay against the same strains. Only three mice per group were used to supply sera in this assay. Figure 5-8 shows the anit-NadA3 titres antibody (total IgG, IgG1 and IgG2a) for this timepoint.

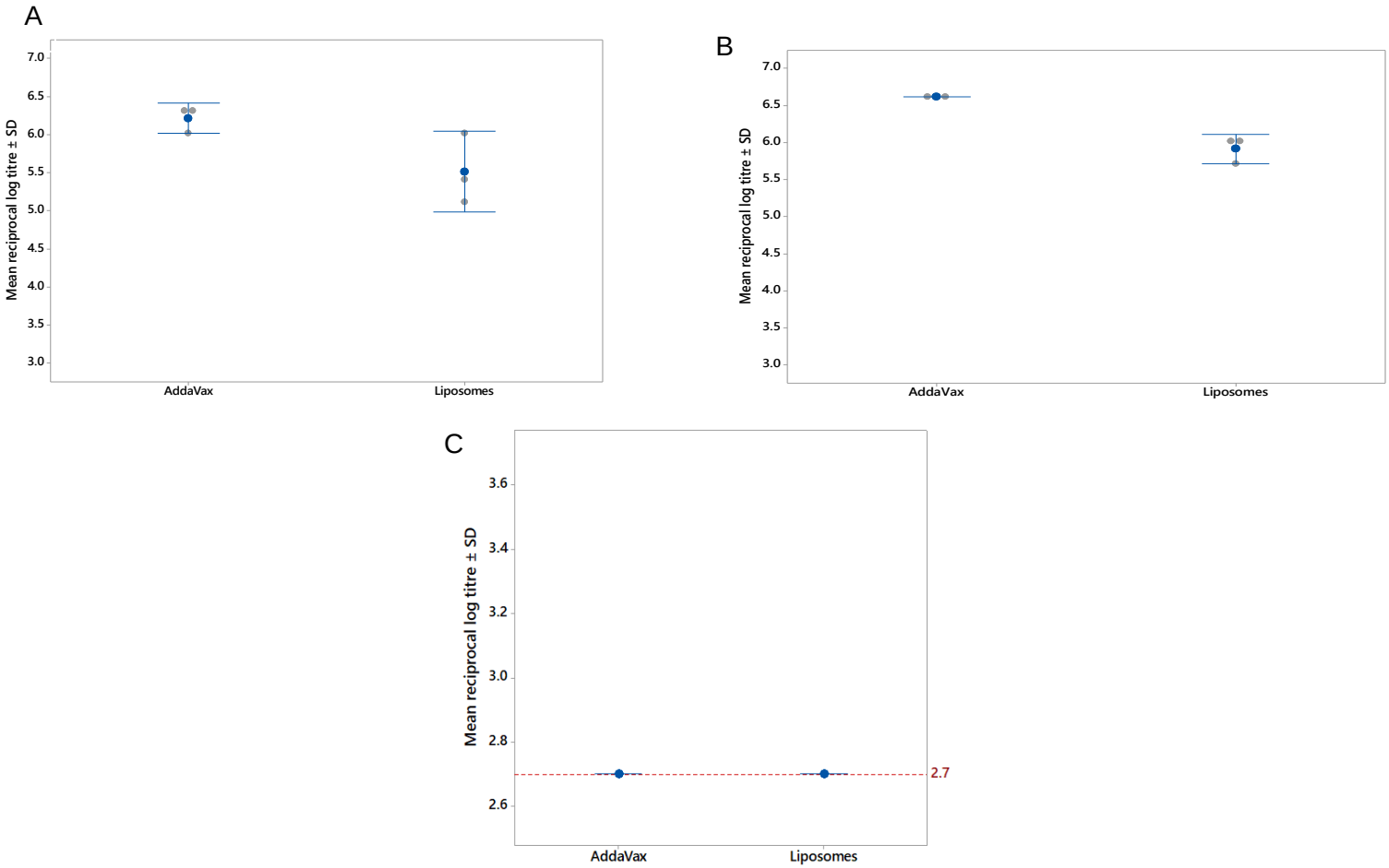

Figure 5-8 Anti-NadA3 (24-170) antibody titres collected at day 49, 2 weeks following the third dose. A) Total IgG B) IgG1 C) IgG2a. Along the x-axis is the immunisation group, in which NadA3-PorA-Ferritin was adjuvanted with either AddaVax or DDA liposomes. For the IgG2a titres, the dashed red-line at a titre of 2.7 represents the titre obtained at the starting sera dilution Each individual mouse is represented by a grey dot ●, the dark blue dot ● represents the mean reciprocal endpoint log titre ± SD.

Figure 5-8 shows the day 49 anti-NadA3 (24-170) antibody titres obtained as measured by total IgG, IgG1 and IgG2a. Total IgG follows a similar trend as for day 35, with no significant differences between both adjuvant groups. For IgG1, the differences between the AddaVax and liposome-adjuvanted groups are no longer significant. IgG2a again fits the same trend, with titres remaining low at background levels. Table 5-3 shows the SBA bactericidal titres obtained using these day 49 sera.

Table 5-3 SBA of sera taken from day 49 to assess bactericidal titres elicited by immunisation with the NadA3-PorA-Ferritin. Assay was performed in the presence of baby rabbit complement.

Immunisation sera	MenB strain		
	5/99	M08-0240104	M14933
NadA3-PorA-Ferritin + AddaVax	64	<16	16
NadA3-PorA-Ferritin + DDA liposomes	<16	<16	32
Non-immunised BALB/c control sera	<16	<16	<16
Internal control NadA3 clinical lot	>4096	<16	4096

As can be seen from Table 5-3, the obtained bactericidal titres are similar to those obtained for day 35, with neither of the adjuvant groups being able to elicit titres that can be classed as bactericidal. Again, the NadA3 clinical lot is the only sera able to result in bactericidal killing of the NadA3-expressing strains 5/99 and M14933. A discussion of the negative results obtained when using these antigens is given in section 3.3.10.

5.3.7 Biodistribution comparison of the NadA3-PorA and the nanoparticle NadA3-PorA-Ferritin

A further method to examine the differences between the two adjuvant systems is through performing a biodistribution study. Cationic liposomes aggregate upon contacting extracellular proteins at the site of injection, leading to the formation of a depot effect that is able to prolong antigen presentation to APCs (Perrie et al., 2013). MF59, on the other hand, generates an immunocompetent environment at the injection site which promotes cell migration and antigen uptake by APCs (Calabro et al., 2011; Dupuis et al., 2001).

Another interesting analysis would be the biodistribution of the subunit NadA3-PorA compared to the nanoparticle NadA3-PorA-Ferritin. Nanoparticle size can dictate tissue distribution and kinetics, cellular distribution within draining lymph nodes, uptake by APCs and intracellular processing pathways, all of which can contribute towards the quality of the resulting immune response (Irvine et al., 2013). For instance, the NadA3-PorA-Ferritin has an overall particle diameter of about 40 nm, which is an optimal size for lymphatic draining (Reddy et al., 2007).

The In Vivo Imaging System (IVIS) can be used to monitor the biodistribution of fluorescently-labelled molecules of interest in real-time in live animals. It represents a non-invasive and relatively simple technique to perform that also allows for a reduction in the number of animals used since multiple timepoints in the same group of animals can be assessed (Arms et al., 2018).

In order to do this, both the adjuvants and protein antigens are labelled using fluorescent dyes via lipophilic interaction or covalent chemical conjugation. Fluorescent dyes that have absorption and emission wavelengths in the near-infrared (NIR) spectrum (650-900 nm) are useful for whole body imaging as NIR light is able to penetrate deep into tissues and there is minimal background tissue interference in this spectral region (Liu et al., 2016; Ntziachristos et al., 2003)

For labelling of the AddaVax and DDA-liposomes, the long-chain dialkylcarbocyanine lipophilic marker 1,1'-Dioctadecyl-3,3,3',3'-Tetramethylindodicarbocyanine (DiD) was used as the fluorescent marker, whereas for the protein antigens the Alexa Fluor 790 label was chemically conjugated to the antigens.

The biodistribution study was intended to explore two different aspects. The first was to study the distribution profiles of the subunit NadA3-PorA to that of the nanoparticle NadA3-PorA-Ferritin. The second aspect was to complement the adjuvant

comparison study by monitoring the distribution profile of the NadA3-PorA-Ferritin when using either the AddaVax or DDA-liposome adjuvants. This was achieved by monitoring over a period of 11 days the fluorescence of Alexa Fluor 790-conjugated protein antigen and DiD-labelled adjuvant following intramuscular injection.

The biodistribution profile of the subunit NadA3-PorA to that of the nanoparticle NadA3-PorA-Ferritin is discussed first. Figure 5-9 shows the biodistribution results for the Alexa Fluor 790-conjugated protein antigens NadA3-PorA and NadA3-PorA-Ferritin.

A)

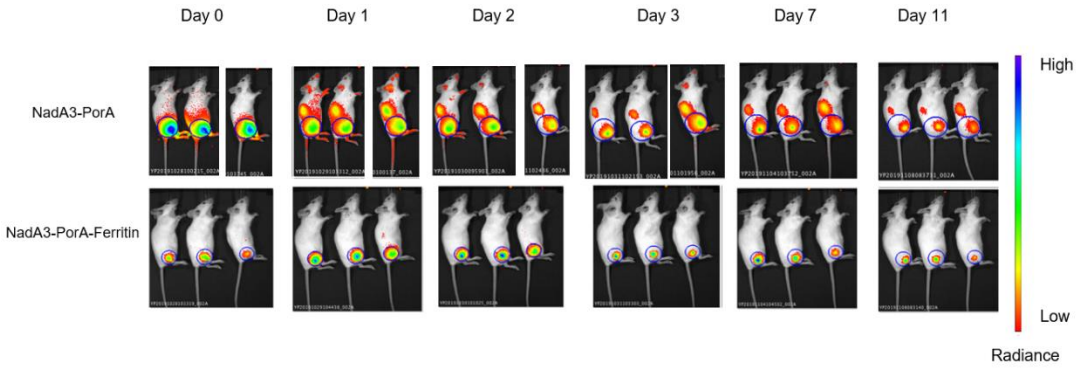

B)

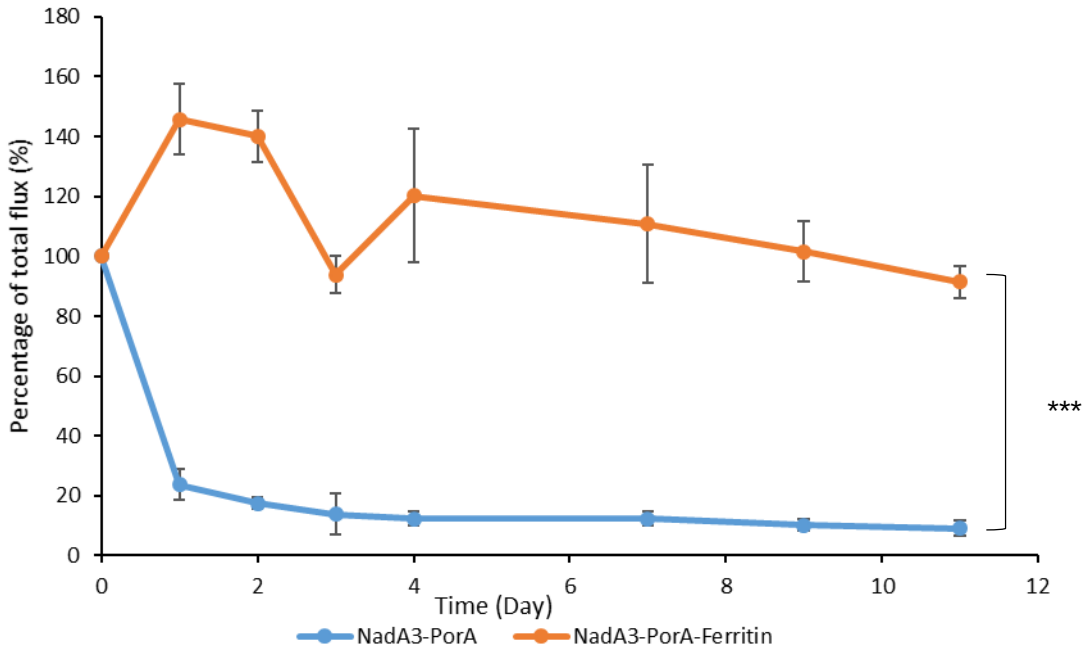

Figure 5-9 IVIS biodistribution results for detection of Alexa Fluor 790 labelled protein antigens adjuvanted with AddaVax A) Real-time biodistribution of Alexa Fluor 790-labelled NadA3-PorA and NadA3-PorA-Ferritin adjuvanted with AddaVax. Mice were imaged every 24 hours using the IVIS. The pseudocolor scale bar for radiance is located on the right. The region of interest selected is shown by the blue circles. B) Analysis of captured IVIS data monitoring percentage of total flux (normalised at day 0) over the course of 11 days. Results are represented as the mean ± SD (n=3), except for day 4 where only 2 mice were imaged for the NadA3-PorA immunisation group (the imaging schedule for the third mouse was staggered by one day, with the IVIS not available on the 4th day). Significant differences between means were determined by the Tukey Simultaneous Tests for Differences of Means, with significance denoted as ***$p < 0.001$.

For both the labelled NadA3-PorA and the NadA3-PorA-Ferritin, a strong signal for the Alexa Fluor 790-label antigens localised at the site of injection is observed immediately after injection at 0 hours. This total fluorescence flux at day 0 was used

to normalise the fluorescence for subsequent days of the study, such that day 0 represents 100% of the total flux. After 24 hours the subunit NadA3-PorA protein signal diminished significantly ($p<0.001$) in the vicinity of the site of injection and there is detectable signal in what could potentially be the kidneys (and this detectable throughout the duration of the study). By day 11, the detected signal at the site of injection has decreased to around 20%. For the nanoparticle NadA3-PorA-Ferritin in contrast, the detectable signal is localised in the vicinity of the site of injection and does not diminish significantly throughout the study. In comparing the groups when the region of interest is centred around the site of injection in the thigh, the Alexa Fluor 790 labelled protein signal throughout the study is significantly higher ($p<0.001$) for the NadA3-PorA-Ferritin immunisation group.

The biodistribution of the DiD-labelled AddaVax present in the administered dose for the both antigens was also analysed, with the results shown in Figure 5-10.

A)

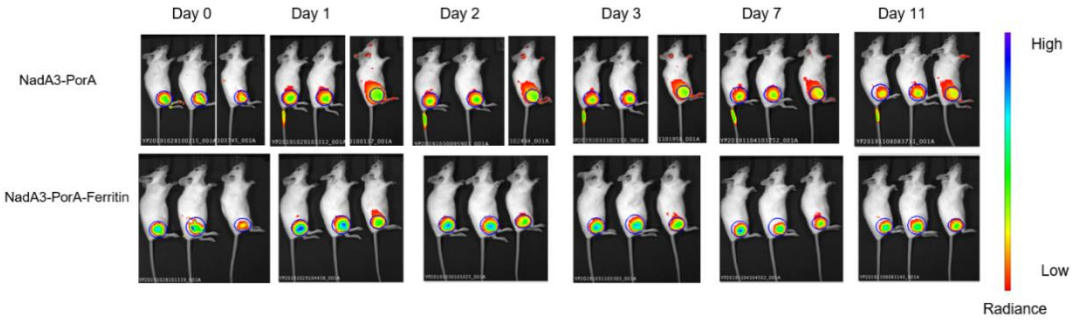

B)

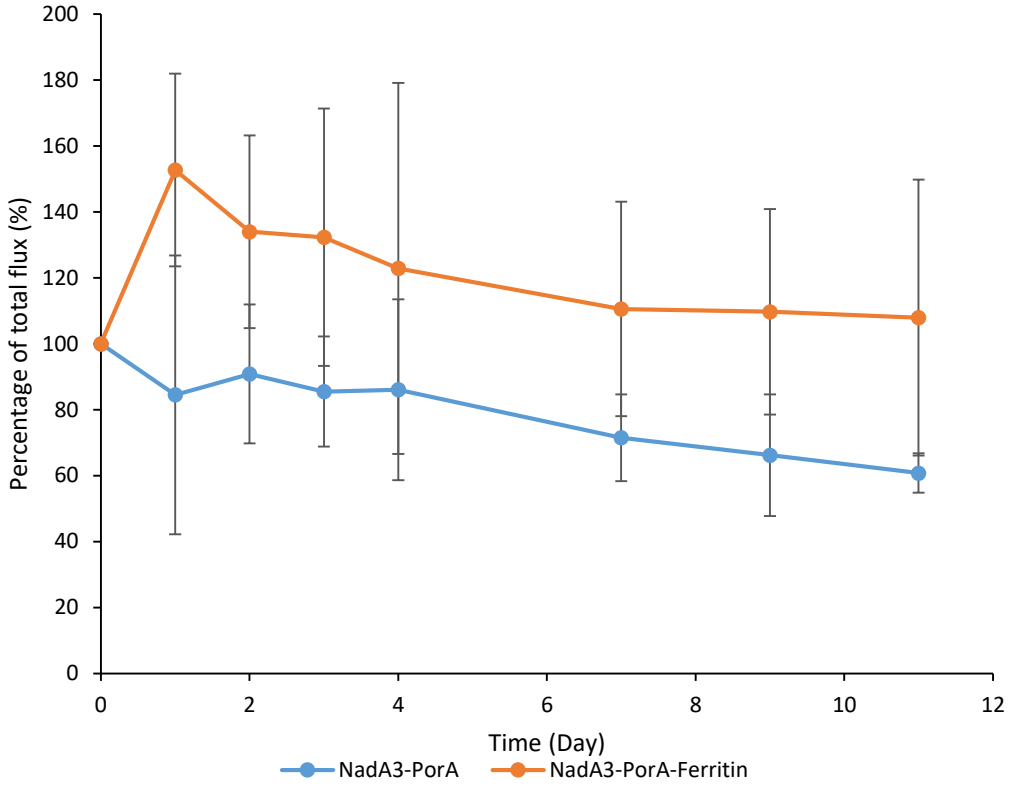

Figure 5-10 IVIS biodistribution results for detection of DiD-labelled AddaVax used as adjuvant for NadA3-PorA and NadA3-PorA-Ferritin A) Real-time biodistribution of DiD-labelled AddaVax. Mice were imaged every 24 hours using the IVIS. The pseudocolor scale bar for radiance is located on the right. The region of interest selected is shown by the blue circles. B) Analysis of captured IVIS data monitoring percentage of total flux (normalised at day 0) over the course of 11 days. Results are represented as the mean ± SD (n=3), except for day 4 where only 2 mice were imaged for the NadA3-PorA immunisation group.

As shown in Figure 5-10A, it can be seen that fluorescence signal from the DiD-labelled AddaVax remains localised at the site of injection in the mouse thigh muscle for both the NadA3-PorA and the NadA3-PorA-Ferritin immunisations. When

comparing the fluorescence (measured as percentage of total flux normalised at day 0) over the course of 11 days (Figure 5-10B), there is a trend of decreasing fluorescence for the DiD-labelled AddaVax used to adjuvant the NadA3-PorA, reducing to around 60% of the initial total flux by day 11. For the NadA3-PorA-Ferritin immunisation, the signal does not diminish over the course of the study; however, when these two groups are compared, the differences in flux are not found to be significant.

In conclusion, based on the signal owing from the Alexa Fluor 790 fluorophore, there is a significant difference in distribution of Alexa Fluor 790-conjugated antigens NadA3-PorA and NadA3-PorA-Ferritiin protein antigens over the 11-day study, with a strong signal remaining at the site of injection in the case of NadA3-PorA-Ferritin immunisation, whereas for the subunit NadA3-PorA administration, the signal rapidly disappears from the site of injection. For the NadA3-PorA group, there is a strong signal in what could potentially be the kidneys, however it is unknown if the fluorescence is due to intact NadA3-PorA or broken down antigen. In a biodistribution study of a radioactively labelled self-assembling protein nanoparticle, radioactivity in the urine confirmed the presence of broken down nanoparticles since intact nanoparticle had a molecular weight exceeding the 50 kDa cut off of the kidney glomerulum (Yang et al., 2013). However, intact NadA3-PorA with a molecular weight of around 42 kDa could in theory pass through this cut off barrier.

Ex vivo imaging of the organs harvested at day 14 was performed and fluorescence from the Alexa Fluor 790 (Figure 5-11Figure 5-11A) and DiD (Figure 5-11B) fluorophores measured. The presence of the Alexa Fluor 790 fluorophore in the kidneys can be observed even at this late timepoint, with particularly strong signals in the kidneys of the NadA3-PorA group but a weaker signal in the NadA3-PorA-Ferritin group. For both fluorophores, signal in the spleen and liver (not shown) was below the background but a strong signal was observed in the inguinal lymph node at the site of injection only for the DiD fluorophore but not the Alexa Fluor 790 fluorophore (though a weak signal is seen for the subunit NadA3-PorA), suggesting perhaps that

antigen was cleared at this late day 14 timepoint from the inguinal lymph node but AddaVax adjuvant remained

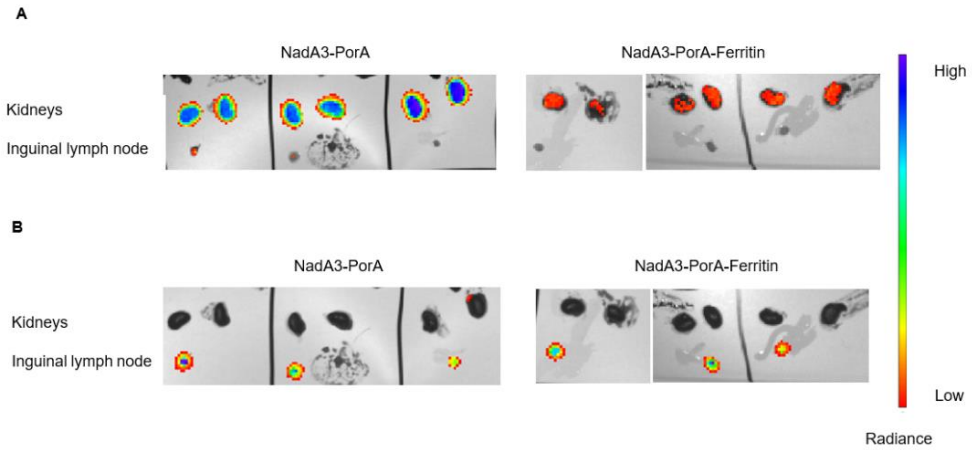

Figure 5-11 *Ex vivo* imaging of kidneys and inguinal lymph nodes from the Alexa Fluor 790-conjugated antigens NadA3-PorA and NadA3-PorA-Ferritin immunisations adjuvanted with DiD-labelled AddaVax **A**) Alexa Fluor 790 fluorescence **B**) DiD fluorescence. Organs were harvested from each of the three mice of both immunisation groups

The diameter of the NadA3-PorA-Ferritin nanoparticle is around 40 nm, while the subunit NadA3-PorA is smaller with a width of around 4 nm and a length of 16 nm. A possible explanation for the more rapid dissemination away from the site of injection seen for the NadA3-PorA could be due to size differences between the antigens. Particulate vaccines in the 20 - 100 nm size range have been shown to traffic preferentially into lymphatic vessels towards the lymph nodes, while in contrast smaller molecules instead disseminate into the systemic circulation and see poorer uptake by the lymphatics (Moyer et al., 2016). This could also be one factor that contributes towards the observation that the nanoparticle NadA3-PorA-Ferritin is able to induce superior humoral responses compared to the subunit NadA3-PorA antigen.

5.3.8 Biodistribution of the NadA3-PorA-Ferritin depending on the choice of adjuvant

The second aspect of the biodistribution study was to assess the impact of choice of adjuvant on the biodistribution of the NadA3-PorA-Ferritin. Figure 5-12 shows the biodistribution results for the Alexa Fluor 790-conjugated NadA3-PorA-Ferritin when administered to three different adjuvant scenarios; AddaVax, DDA liposomes and adjuvant free.

A)

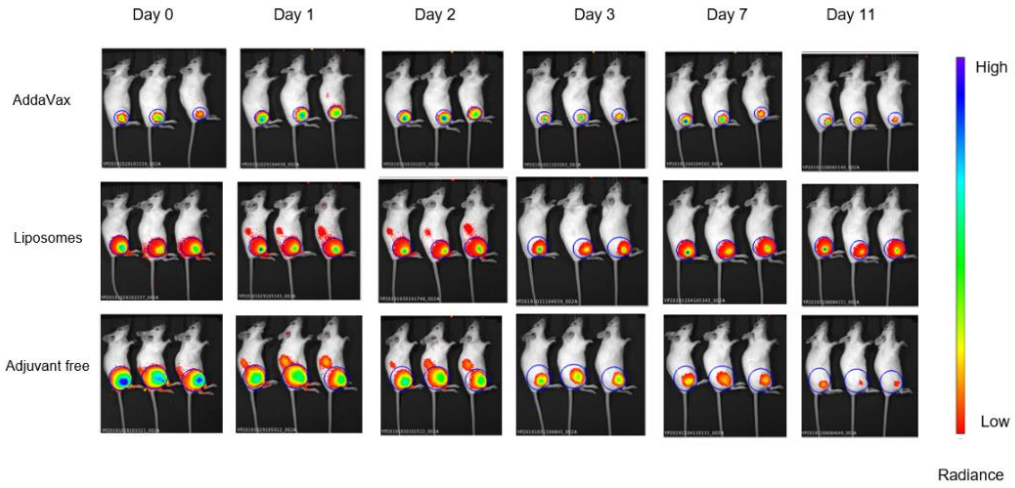

B)

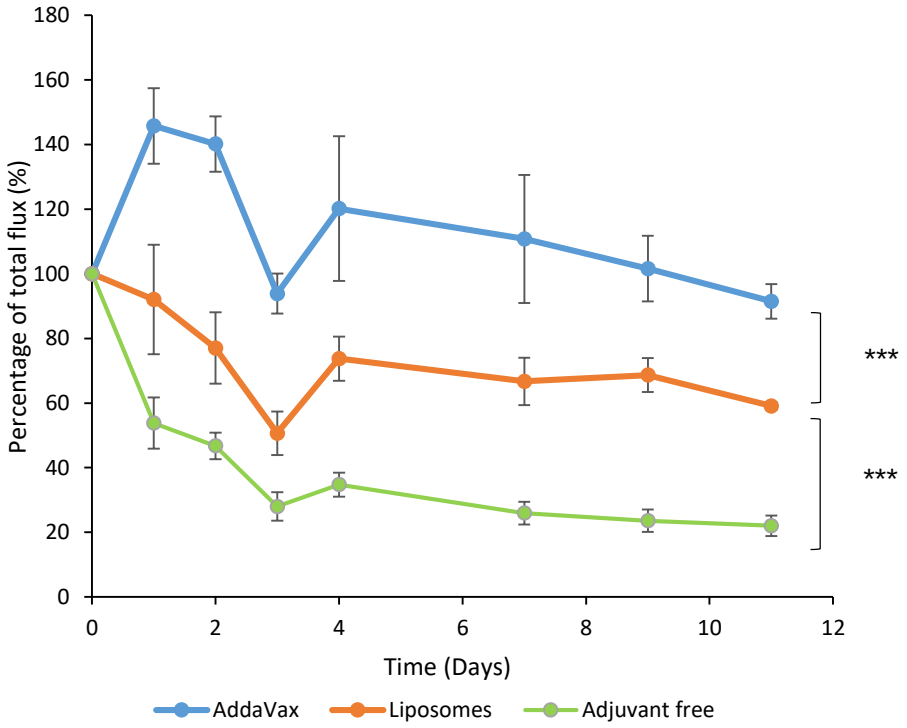

Figure 5-12 IVIS biodistribution results for detection of Alexa Fluor 790-conjugated NadA3-PorA-Ferritin when adjuvanted under three different adjuvant scenarios; AddaVax, DDA liposomes or adjuvant free A) Real-time biodistribution of Alexa Fluor 790-labelled NadA3-PorA-Ferritin. Mice were imaged every 24 hours using the IVIS. The pseudocolor scale bar for radiance is located on the right. The region of interest selected is shown by the blue circles B) Analysis of captured IVIS data monitoring percentage of total flux (normalised at day 0) over the course of 11 days. Results are represented as the mean ± SD (n=3). Significant differences between means were determined by the Tukey Simultaneous Tests for Differences of Means, with significance denoted as ***$p < 0.001$.

As can be seen from Figure 5-12A, a strong signal for the Alexa Fluor 790-label antigens localised at the site of injection is observed immediately after injection on

day 0 for all three adjuvant scenarios. After 24 hours, the fluorescence signal for the liposome and adjuvant free group diminishes, significantly so for the adjuvant free group ($p<0.001$), in the vicinity of the site of injection and there is detectable signal in what could potentially be the kidneys for both of these groups. By day 11, the fluorescence signal for the AddaVax adjuvanted group has remained constant, though for the liposome and adjuvant free groups it has reduced, significantly so in both cases to 60% and 20%, respectively. In comparing the groups when the region of interest is centred around the site of injection, the Alexa Fluor 790 labelled protein signal throughout the study is significantly higher ($p<0.001$) for the AddaVax group when compared to the liposome and adjuvant free groups. The adjuvant free group is significantly lower ($p<0.001$) in comparison to both adjuvanted groups.

The biodistribution of the DiD-labelled AddaVax and liposomes was also analysed, with the results shown in Figure 5-13.

A)

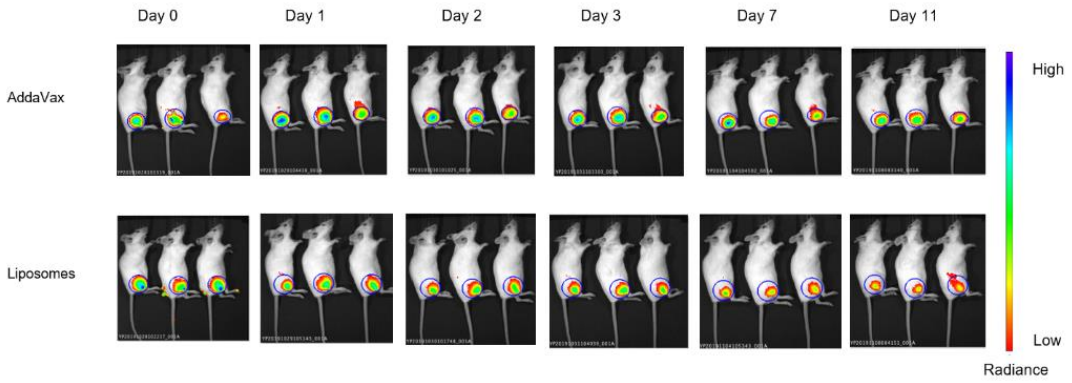

B)

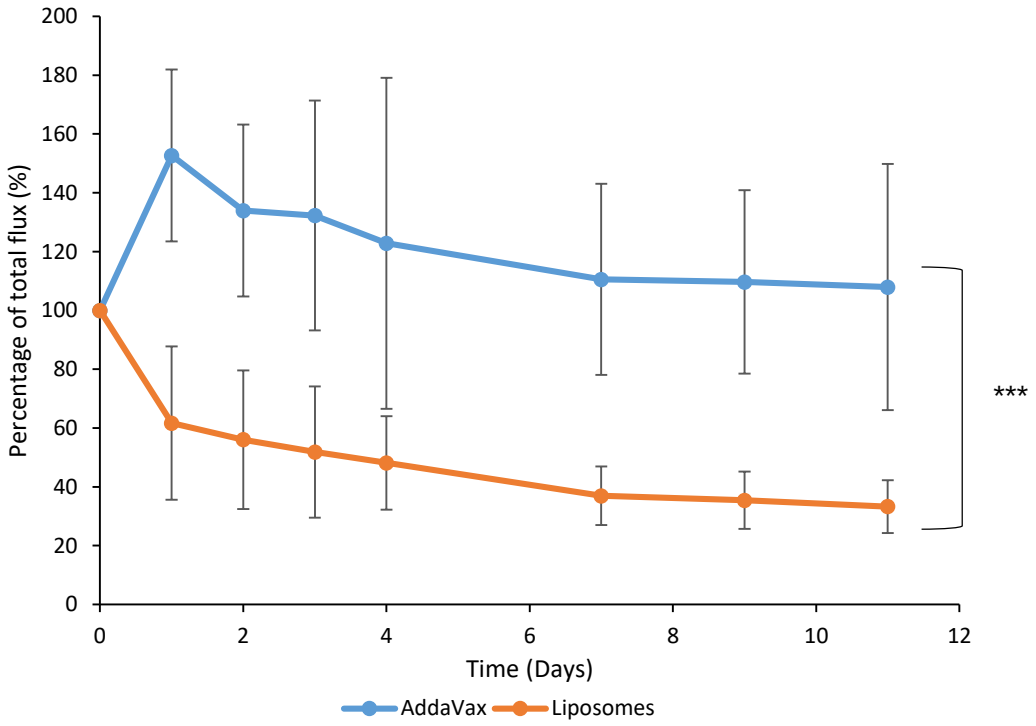

Figure 5-13 IVIS biodistribution results for detection of DiD labelled AddaVax and liposomes when used as adjuvants to deliver NadA3-PorA-Ferriitn. A) Real-time biodistribution of DiD-labelled AddaVax and liposomes. Mice were imaged every 24 hours using the IVIS. The pseudocolor scale bar for radiance is located on the right. The region of interest selected is shown by the blue circles B) Analysis of captured IVIS data monitoring percentage of total flux (normalised at day 0) over the course of 11 days. Results are represented as the mean ± SD (n=3).

As shown in Figure 5-13A, it can be seen that the fluorescence signal from the DiD-labelled AddaVax and liposomes remains localised at the site of injection in the mouse thigh for both groups. When comparing the fluorescence over the course of 11 days (Figure 5-13B), the signal remains constant at the site of injection for the

Addavax adjuvanted group throughout the course of the study. However, the signal in the liposome group deceases to around 60% after 24 hours and then has fallen significantly so ($p<0.001$) to 30 % by the end of the study at day 11. When the adjuvant groups are compared the differences in flux throughout the study remains significant ($p<0.001$).

At day 14, organs were harvested and *ex vivo* imaging of the organs was performed, with the fluorescence from the Alexa Fluor 790 (shown Figure 5-14A) and DiD (in Figure 5-14B) fluorophores measured. The presence of the Alexa Fluor 790 fluorophore in the kidneys can be observed for all adjuvant scenarios, though is strongest in the adjuvant free group. Weak to no signal is seen in the inguinal lymph nodes. For the DiD-labelled adjuvants, strong signals are seen in the inguinal lymph node for both adjuvants.

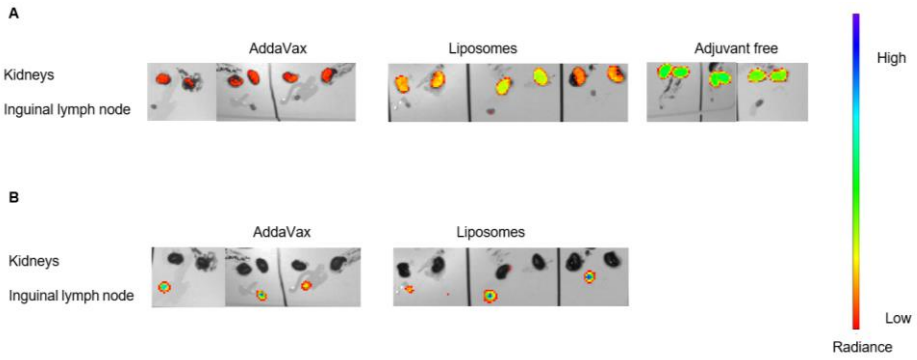

Figure 5-14 *Ex vivo* imaging of kidneys and inguinal lymph nodes from the Alexa Fluor 790-conjugated antigens NadA3-PorA and NadA3-PorA-Ferritin immunisations adjuvanted with DiD-labelled AddaVax, DDA-liposomes or without adjuvant **A**) Alexa Fluor 790 fluorescence **B**) DiD fluorescence. Organs were harvested from each of the three mice of both immunisation groups

When NadA3-PorA-Ferritin is delivered with either adjuvant, it is retained for longer at the site of injection whereas without adjuvant it disseminates more rapidly away from the site of injection. Both DiD and Alexa Fluor signal at the site of injection in the NadA3-PorA-Ferritin adjuvanted with AddaVax group is in agreement with observations made for the MF59 adjuvant (on which AddaVax is based). MF59 has been found to promote the uptake of both antigen and adjuvant in the muscle by several myeloid cells and induces their efficient transport to the draining lymph nodes (Calabro et al., 2011), though the low spatial resolution of the IVIS technique means that any potential fluorescence signal in the draining lymph nodes at the site of

injection cannot be resolved. In addition, Cantisani et al. further showed that MF59 is detectable in the draining lymph nodes at least 7 days after immunisation and is able promote the overall accumulation of unprocessed antigen within lymph nodes, which correlates with its ability to enhance the humoral response (Cantisani et al., 2015).

The immunogenicity of cationic liposomes can in part be explained due to their ability to form a depot at the site of injection, which increases antigen presentation to APCs. Using radioactively labelled antigen and liposomes, Henriksen-Lacey et al. showed that antigen adsorbed to DDA cationic liposomes was released much slower from the site of injection compared to when antigen was injected in the absence of cationic liposome adjuvant (Henriksen-Lacey et al., 2010a), in agreement with the IVIS results obtained here. The retention of antigen was also found to coincide with the retention of the liposomes, with the levels of liposomes not found to have decreased significantly after 4 days and more than 40% of the original dose was still present after 14 days, again not dissimilar to the results obtained here by IVIS.

5.4 Conclusion

This study sought to compare the immune response generated against the NadA3-PorA-Ferritin nanoparticle when adjuvanted with AddaVax compared to a cationic DDA liposome formulation.

Both adjuvants resulted in significantly higher total IgG NadA3 titres over the non-adjuvanted nanoparticle, demonstrating that the liposome formulation produced in-house by microfluidics was able to achieve a comparable immune response to a commercially available adjuvant. For IgG1 titres against the NadA3 component of the nanoparticle, significantly higher titres over the adjuvant-free nanoparticle immunisation were again observed for both adjuvants, however this increase was less pronounced post-second dose. IgG2a titres remained low throughout all groups and so the Th2 bias still remained when the DDA liposomes were used to adjuvant the formulation. No significant differences in the cellular immune response between the two adjuvants was seen, with no indication seen for a Th1 bias observed in past studies that used DDA liposomes. Explanations for the low Th1 cytokine markers like IFNγ include the DDA cationic content of the liposomes (low at 10%) and the lack of an immunopotentiator such as TDB.

Though both adjuvants induce high NadA3 IgG antibody titres, an SBA using sera from both adjuvant immunisation groups was again found to be bactericidal negative

using the same panel of MenB strains as used in chapter 3. To further probe the functional activity of antibodies induced by immunisation with these adjuvants, alternative assays may need to be performed. A biodistribution study revealed that the subunit NadA3-PorA disseminates more rapidly from the site of injection compared to the NadA3-PorA-Ferritin, an observation which might be a factor in the reduced immunogenicity seen for the subunit antigen compared to the nanoparticle administration. Comparing the biodistribution of the NadA3-PorA-Ferritin when adjuvanted with either AddaVax or liposomes showed that the nanoparticle is retained for longer at the site of injection with respect to when the nanoparticle is delivered without adjuvant, in good agreement with past observations of adjuvant mechanisms of action.

6. Chapter 6

Conclusions and future perspectives

6.1 Rational-structure based design of a protein nanoparticle presenting a chimeric MenB antigen

Neisseria meningitidis serogroup B (MenB) infection is a leading cause of meningitis and septicaemia both of which are manifestations of invasive meningococcal disease (IMD). Born out of the reverse vaccinology approach, the Bexsero vaccine represents the first of its kind multicomponent vaccine formulation against MenB and is composed of multiple surface-exposed meningococcal proteins (Serruto et al., 2012). Though these subunit antigen formulations have better safety profiles than live-attenuated or inactivated vaccines, the lack of microbial PAMPs renders them inherently less immunogenic and so immunostimulatory agents (adjuvants) are often needed (Moyle and Toth, 2013).

While research is ongoing to establish new adjuvant formulations, subunit antigen vaccine immunogenicity can also be improved through the use of nanoparticle delivery systems. Moreover, advances have been made in structural and computational techniques which have increased our capacity to determine antigen structures and form the basis of a new era of vaccine development and discovery dubbed ‘structural vaccinology’. The central premise of structural vaccinology is the rational structure-based design of improved vaccine antigens measured in terms of epitope presentation, stability and ease of production.

Here, a rational structure-based design approach was undertaken toward a ferritin-based self-assembling protein nanoparticle system presenting a chimeric MenB protein antigen known as NadA3-PorA. The chimera confers broader strain coverage against MenB. while its presentation in a multi-copy format on the surface of the ferritin was hypothesized to enhance the subsequent immune response compared to if the NadA3-PorA subunit antigen was administered alone.

6.2 Purification and characterisation of NadA3-PorA-Ferritin

In this chapter, the expression, purification and structural characterisation of the rationally-designed Nada3-PorA-Ferritin nanoparticle was described. X-ray crystallography data was first used to design a feasible structure for the nanoparticle, from which a DNA construct encoding the NadA3-PorA-Ferritin nanoparticle could be realised. This DNA construct was then cloned into a suitable *E. coli* expression strain to enable its successful and subsequent purification.

An initial structural analysis of a purified NadA3-PorA-Ferritin sample served as an indication that the nanoparticle could successfully self-assemble, as had been envisioned. However, a high resolution cryo-EM single particle reconstruction was hindered by the flexibility of the NadA3-PorA appendage, which introduced too large an amount of structural heterogeneity in the captured cryo-EM data of the NadA3-PorA-Ferritin sample. Other electron microscopy approaches, such as single particle tomography, to determine the structure of the NadA3-PorA presented on the ferritin surface were also unsuccessful.

Further characterisation of presented epitopes on the NadA3-PorA-Ferritin was performed by a variety of antibody-based techniques. Using a small panel of anit-NadA3 antibodies, immunogold EM indicated that insertion of the PorA VR2 loop may compromise NadA3 epitope presentation in the N-terminal head region. NadA3 stalk epitopes were more difficult to assess by this technique, potentially due to steric hindrance of the antibody. To further explore epitope presentation, SPR was performed with a limited pool of anti-NadA3 antibodies, which again showed that modifications made to accommodate the PorA VR2 loop may have induced structural changes in the NadA3 by compromising epitopes both in the N-terminal head region as well as in the stalk. To expand the pool of potential antibodies available to probe epitope presentation, a competitive SBA using anti-NadA3 sera was instead able to confirm that NadA3 bactericidal epitopes were optimally presented. SPR and immunoblots using an anti-PorA VR2 14 antibody also showed in a similar manner that the PorA VR2 epitope was presented by the nanoparticle.

This work served as a validation of the rational structure-based design process, demonstrated that not only could a novel, self-assembling protein nanoparticle be both expressed and purified, but presents immunogenic epitopes optimally for the potential induction of an immune response. Following on from this *in vitro* characterisation, an

in vivo assessment of the NadA3-PorA-Ferritin as a potential vaccine antigen candidate was then undertaken, described in chapter 3.

6.3 *in vivo* immunisation with the NadA3-PorA-Ferritin nanoparticle

Work carried out in chapter 3 demonstrated that protective epitopes on the NadA3-PorA-Ferritin nanoparticle were optimally presented. The nanoparticle system could then be though to an *in vivo* assessment for its efficacy in conferring broad and potent protection against MenB.

Following stability confirmation of the antigens by SEC-HPLC and SDS-PAGE prior to immunisation, a pilot study was conducted as an initial assessment of the humoral responses to immunisation with the NadA3-PorA-Ferritin nanoparticle which was able to confirm the induction of anti-NadA3 responses.

A larger *in vivo* study was designed to ultimately investigate whether multicopy presentation can enhance the immune response over the administration of subunit antigen alone, as well as examine whether the presented chimeric NadA3-PorA antigen conferred broad protection against MenB. The NadA3-PorA-Ferritin nanoparticle was able to induce significantly higher total IgG and IgG1 anti-NadA3 titres than the subunit antigen. A comparison of the immune responses induced by antigen NadA3-PorA to the wildtype NadA3 revealed significant differences, with the wildtype inducing higher antibody tires. This result suggested that modifications made to accommodate the PorA VR 12 epitope may have removed or even compromised some immunogenic epitopes of the wildtype NadA3. However, presentation of the NadA3-PorA on the surface of the ferritin was able to raise antibody titres to levels of the wildtype NadA3, confirming that a multivalent nanoparticle presentation can be beneficial.

As shown by antibody IgG1/IgG2a ELISAs, nanoparticle immunisation did alter the Th1/Th2 balance. This was in disagreement with cytokine responses of stimulated splenocytes, which showed no significant differences between subunit and nanoparticle immunisations. Germinal centre B cell analysis by FACS revealed nanoparticle immunisation induced a non-significant increase in germinal centre B cells over subunit NadA3-PorA administration.

The design of the NadA3-PorA chimeric antigen may have compromised or even removed T-cell epitopes native to NadA3. To investigate this, predicted T-cell peptide

epitopes from NadA3 were synthesised and used to stimulate splenocytes deriving from immunisations with the nanoparticle NadA3-PorA-Ferritin. The assay was ultimately unsuccessful, as neither the predicted peptide epitopes nor the complete antigens NadA3 and NadA3-PorA were able to induce significantly different cytokine responses.

Serum bactericidal activity, a crucial component of host defense against meningococcal disease, is mediated by antigen-specific IgG antibodies and a functional complement system (Goldschneider et al., 1969). From the ELISAs, it was shown that immunisation with the nanoparticle could induce high anti-nadA3 antibody titres, however SBAs were required to determine the bactericidal activity of these antibodies raised. However, sera from all the immunisation groups was found to be bactericidal negative against a panel of MenB strains, despite all sera having been confirmed for the presence of anti-NadA3 titres by ELISA. This could suggest that bactericidal antibodies are not raised *in vivo*, perhaps due to sub optimal presentation of epitopes that elicit bactericidal antibodies. The only serum sample that yielded positive bactericidal titres was the clinical lot of NadA3, the full length version. In contrast, the truncated NadA3 (24-170), which was the scaffold antigen for insertion of the PorA VR2 epitope, was bactericidal negative. This could also suggest that in this truncated version, bactericidal epitopes are no longer optimally presented. It should also be noted that this is also in contrast with the results of the competitive inhibition SBA, detailed in section 2.3.13, where bactericidal antibodies present in anti-NadA3 (24-170) were seemingly sequestered by NadA3-PorA-Ferritin when added into the sera, resulting in a reduction in the bactericidal titre.

6.4 Formulation of a cationic liposome adjuvant by microfluidics

A comparative study was planned to examine the differences in immunogenicity induced when the NadA3-PorA-Ferritin was adjuvanted with either the AddaVax emulsion or cationic liposomes. This cationic liposome adjuvant would be formulated by microfluidics, which represents a high-throughput technique for the reproducible and controlled production of liposomes (Joshi et al., 2016; Kastner et al., 2015; Perrie et al., 2016).

initially a DOTAP-based formulation underwent composition and microfluidic process parameter optimisation. The molar percentage of the cationic lipid DOTAP was first

selected for on the basis of liposome size, PDI and zeta potential. Following this, the microfluidic process parameters, TFR and FRR were optimised to give a formulation with favourable liposomal attributes. Lipid recovery was quantified throughout to validate the liposome production method. PEGylation of the liposomes resulted in a reduction in the zeta potential which was deemed unfavourable for association of the NadA3-PorA-Ferriin, so was not pursued further.

The DOTAP cationic lipid was then replaced with another cationic lipid, DDA, and the formulation was then optimised for composition and microfluidic process parameters. Antigen adsorption studies were conducted to establish a ratio of NadA3-PorA-Ferritin-to-lipid that gave a stable liposome formulation for immunisation.

6.5 Adjuvant head-to-head study and biodistribution

Chapter 4 had established a cationic liposome formulation for the delivery of the NadA3-PorA-Ferritin nanoparticle. The immune responses of this in-house, microfluidic-produced liposome adjuvant were compared to those seen for when the NadA3-PorA-Ferritin nanoparticle was adjuvanted with AddaVax.

In terms of total IgG and IgG1 NadA3 titres, both adjuvants induced similar responses that were significantly greater than when the nanoparticle was derived without adjuvant. IgG2a titres remained low throughout for both adjuvants, indicating that the use of the DDA liposomes did not shift the bias away from a Th2 and towards a Th1-type response. This observation was replicated in the cytokine responses of stimulated splenocytes, with no significant differences noted between the AddaVax and liposome adjuvanted groups. Liposomal adjuvants based on DDA have been found to induce stronger Th1 responses, which can be characterised by high levels of IFNγ production (Henriksen-Lacey et al., 2011a). The lower IFNγ responses seen in this study could be potentially due to the reduced DDA cationic content of the liposomes used and the lack of an immunopotentiator such as TDB.

A biodistribution study showed that the subunit antigen NadA3-PorA clears from the site of injection more rapidly than the NadA3-PorA-Ferritin, and after a period of 11 days the nanoparticle was retained significantly more at the site of the injection compared to the subunit antigen. When NadA3-PorA-Ferritin was adjuvanted with either AddaVax or DDA-liposomes, it was also retained at the site of injection for significantly longer compared to when it was delivered without adjuvant.

6.6 Concluding remarks and future perspectives

The work within this project exemplifies a structural vaccinology approach towards the design of a chimeric protein antigen-presenting self-assembling nanoparticle system with the goal of conferring a broad and efficacious protection against MenB.

Structural vaccinology represents a viable, rational approach for the identification and design of stable, safe and broadly immunogenic antigen candidates. The success of the reverse vaccinology means that today it is relatively straightforward to identify a pool of antigen candidates from pathogen genomes to act as starting points for the development of a new vaccine. Advances underway in both X-ray crystallography and cryo-EM toward the rapid high-resolution structural determination of both antigens and antigen-antibody complexes will see the number of these structures deposited in the PDB rise with ever increasing speed, facilitating the development of improved vaccine antigen candidates. B-cell sequencing for the faster characterisation and cloning of antibodies will likely play an important role in realising this (Liljeroos et al., 2015). Continued integration with proteomics will also be crucial to enable better prediction of post-translational antigen modifications (as these can alter both the structure and antigenic potential of antigens) (van Els et al., 2014).

Here in this work, a natural self-assembling nanoparticle, ferritin, was used as a scaffold for the multicopy presentation of a chimeric antigen. Presentation of the antigen in this way was found to enhance antibody titres against the NadA3 component of the antigen. However, the SBA to investigate functional, protective antibodies against MenB revealed that sera deriving from NadA3-PorA-Ferritin and NadA3-PorA immunisations were bactericidal negative. Significantly however, the truncated NadA3 (24-170) antigen itself was also bactericidal negative. Taken together, these results emphasise how deliberate structural modifications can have deleterious effects on the ability of an antigen to raise a functional response. Though the effect of these structural changes can sometimes only be discovered following experimental analysis, as demonstrated here, continued efforts made in the future to characterise the epitopes recognised by bactericidal antibodies (through a variety of techniques such as X-ray crystallography, NMR, HDX-MS, mutagenesis and peptide scanning (Abbott et al., 2014)) can only aid the rational design of functional antigens.

Recently in a major advancement of this rational, Marcandalli et al. published work that exemplifies the combined advances made in x-ray crystallography, cryo-EM and computational protein design. In their research, they further computationally

engineered an existing RSV protein antigen to enable it to self-assemble into 20 stable trimeric molecules, essentially creating a self-assembling protein nanoparticle from scratch (Marcandalli et al., 2019). Looking to the future, this opens up the possibility of designing *de novo*, self-assembling protein nanoparticles without being confined to natural components such as ferritin.

7. References

Abbas, A.K., Murphy, K.M., and Sher, A. (1996). Functional diversity of helper T lymphocytes. Nature *383*, 787-793.

Abbott, W.M., Damschroder, M.M., and Lowe, D.C. (2014). Current approaches to fine mapping of antigen-antibody interactions. Immunology *142*, 526-535.

Abraham, S., Juel, H.B., Bang, P., Cheeseman, H.M., Dohn, R.B., Cole, T., Kristiansen, M.P., Korsholm, K.S., Lewis, D., Olsen, A.W.*, et al.* (2019). Safety and immunogenicity of the chlamydia vaccine candidate CTH522 adjuvanted with CAF01 liposomes or aluminium hydroxide: a first-in-human, randomised, double-blind, placebo-controlled, phase 1 trial. The Lancet Infectious Diseases.

Ada, G.L. (1990). The immunological principles of vaccination. Lancet *335*, 523-526.

Allen, T.M., Hansen, C., Martin, F., Redemann, C., and Yau-Young, A. (1991). Liposomes containing synthetic lipid derivatives of poly(ethylene glycol) show prolonged circulation half-lives in vivo. Biochimica et biophysica acta *1066*, 29-36.

Almeida, J.D., Edwards, D.C., Brand, C.M., and Heath, T.D. (1975). Formation of virosomes from influenza subunits and liposomes. Lancet *2*, 899-901.

Amanna, I.J., Carlson, N.E., and Slifka, M.K. (2007). Duration of humoral immunity to common viral and vaccine antigens. N Engl J Med *357*, 1903-1915.

Ansari, S., and Yamaoka, Y. (2018). Current understanding and management of Helicobacter pylori infection: an updated appraisal. F1000Res *7*, F1000 Faculty Rev-1721.

Arigita, C., Kersten, G.F.A., Hazendonk, T., Hennink, W.E., Crommelin, D.J.A., and Jiskoot, W. (2003). Restored functional immunogenicity of purified meningococcal PorA by incorporation into liposomes. Vaccine *21*, 950-960.

Arms, L., Smith, D.W., Flynn, J., Palmer, W., Martin, A., Woldu, A., and Hua, S. (2018). Advantages and Limitations of Current Techniques for Analyzing the Biodistribution of Nanoparticles. Front Pharmacol *9*, 802.

Arosio, P., Ingrassia, R., and Cavadini, P. (2009). Ferritins: a family of molecules for iron storage, antioxidation and more. Biochimica et biophysica acta *1790*, 589-599.

Bachmann, M.F., Rohrer, U.H., Kundig, T.M., Burki, K., Hengartner, H., and Zinkernagel, R.M. (1993). The influence of antigen organization on B cell responsiveness. Science *262*, 1448-1451.

Bachmann, M.F., and Zinkernagel, R.M. (1997). Neutralizing antiviral B cell responses. Annu Rev Immunol *15*, 235-270.

Badiee, A., Heravi Shargh, V., Khamesipour, A., and Jaafari, M.R. (2013). Micro/nanoparticle adjuvants for antileishmanial vaccines: present and future trends. Vaccine *31*, 735-749.

Bai, X.C., Fernandez, I.S., McMullan, G., and Scheres, S.H. (2013). Ribosome structures to near-atomic resolution from thirty thousand cryo-EM particles. Elife *2*, e00461.

Bambini, S., De Chiara, M., Muzzi, A., Mora, M., Lucidarme, J., Brehony, C., Borrow, R., Masignani, V., Comanducci, M., Maiden, M.C.J.*, et al.* (2014). Neisseria adhesin A variation and revised nomenclature scheme. Clinical and vaccine immunology : CVI *21*, 966-971.

Banchereau, J., and Steinman, R.M. (1998). Dendritic cells and the control of immunity. Nature *392*, 245-252.

Barrett, D.J., and Ayoub, E.M. (1986). IgG2 subclass restriction of antibody to pneumococcal polysaccharides. Clinical and experimental immunology *63*, 127-134.

Belnap, D.M. (2015). Electron Microscopy and Image Processing: Essential Tools for Structural Analysis of Macromolecules. Curr Protoc Protein Sci *82*, 17 12 11-61.

Berman, H.M., Westbrook, J., Feng, Z., Gilliland, G., Bhat, T.N., Weissig, H., Shindyalov, I.N., and Bourne, P.E. (2000). The Protein Data Bank. Nucleic acids research *28*, 235-242.
Bindon, C.I., Hale, G., Brüggemann, M., and Waldmann, H. (1988). Human monoclonal IgG isotypes differ in complement activating function at the level of C4 as well as C1q. The Journal of Experimental Medicine *168*, 127-142.
Bondos, S.E., and Bicknell, A. (2003). Detection and prevention of protein aggregation before, during, and after purification. Analytical biochemistry *316*, 223-231.
Bowe, F., Lavelle, E.C., McNeela, E.A., Hale, C., Clare, S., Arico, B., Giuliani, M.M., Rae, A., Huett, A., Rappuoli, R*., et al.* (2004). Mucosal vaccination against serogroup B meningococci: induction of bactericidal antibodies and cellular immunity following intranasal immunization with NadA of Neisseria meningitidis and mutants of Escherichia coli heat-labile enterotoxin. Infect Immun *72*, 4052-4060.
Bozzuto, G., and Molinari, A. (2015). Liposomes as nanomedical devices. International journal of nanomedicine *10*, 975-999.
Bretscher, P.A. (2014). On the mechanism determining the TH1/TH2 phenotype of an immune response, and its pertinence to strategies for the prevention, and treatment, of certain infectious diseases. Scandinavian journal of immunology *79*, 361-376.
Brewer, J.M., Tetley, L., Richmond, J., Liew, F.Y., and Alexander, J. (1998). Lipid vesicle size determines the Th1 or Th2 response to entrapped antigen. J Immunol *161*, 4000-4007.
Brgles, M., Habjanec, L., Halassy, B., and Tomašić, J. (2009). Liposome fusogenicity and entrapment efficiency of antigen determine the Th1/Th2 bias of antigen-specific immune response. Vaccine *27*, 5435-5442.
Bryan, J.T. (2007). Developing an HPV vaccine to prevent cervical cancer and genital warts. Vaccine *25*, 3001-3006.
Bulbake, U., Doppalapudi, S., Kommineni, N., and Khan, W. (2017). Liposomal Formulations in Clinical Use: An Updated Review. Pharmaceutics *9*, 12.
Burgess, P., Hutt, P.B., Farokhzad, O.C., Langer, R., Minick, S., and Zale, S. (2010). On firm ground: IP protection of therapeutic nanoparticles. Nat Biotechnol *28*, 1267-1270.
Calabro, S., Tortoli, M., Baudner, B.C., Pacitto, A., Cortese, M., O'Hagan, D.T., De Gregorio, E., Seubert, A., and Wack, A. (2011). Vaccine adjuvants alum and MF59 induce rapid recruitment of neutrophils and monocytes that participate in antigen transport to draining lymph nodes. Vaccine *29*, 1812-1823.
Calabro, S., Tritto, E., Pezzotti, A., Taccone, M., Muzzi, A., Bertholet, S., De Gregorio, E., O'Hagan, D.T., Baudner, B., and Seubert, A. (2013). The adjuvant effect of MF59 is due to the oil-in-water emulsion formulation, none of the individual components induce a comparable adjuvant effect. Vaccine *31*, 3363-3369.
Campbell, M.G., Cheng, A., Brilot, A.F., Moeller, A., Lyumkis, D., Veesler, D., Pan, J., Harrison, S.C., Potter, C.S., Carragher, B., and Grigorieff, N. (2012). Movies of ice-embedded particles enhance resolution in electron cryo-microscopy. Structure *20*, 1823-1828.
Campbell, R.B., Balasubramanian, S.V., and Straubinger, R.M. (2001). Phospholipid-cationic lipid interactions: influences on membrane and vesicle properties. Biochimica et Biophysica Acta (BBA) - Biomembranes *1512*, 27-39.
Cantisani, R., Pezzicoli, A., Cioncada, R., Malzone, C., De Gregorio, E., D'Oro, U., and Piccioli, D. (2015). Vaccine Adjuvant MF59 Promotes Retention of Unprocessed Antigen in Lymph Node Macrophage Compartments and Follicular Dendritic Cells. The Journal of Immunology *194*, 1717-1725.
Capecchi, B., Adu-Bobie, J., Di Marcello, F., Ciucchi, L., Masignani, V., Taddei, A., Rappuoli, R., Pizza, M., and Arico, B. (2005). Neisseria meningitidis NadA is a new

invasin which promotes bacterial adhesion to and penetration into human epithelial cells. Mol Microbiol *55*, 687-698.
Cariccio, V.L., Domina, M., Benfatto, S., Venza, M., Venza, I., Faleri, A., Bruttini, M., Bartolini, E., Giuliani, M.M., Santini, L.*, et al.* (2016). Phage display revisited: Epitope mapping of a monoclonal antibody directed against Neisseria meningitidis adhesin A using the PROFILER technology. MAbs *8*, 741-750.
Cheng, Y., Grigorieff, N., Penczek, P.A., and Walz, T. (2015). A primer to single-particle cryo-electron microscopy. Cell *161*, 438-449.
Cho, K.J., Shin, H.J., Lee, J.H., Kim, K.J., Park, S.S., Lee, Y., Lee, C., Park, S.S., and Kim, K.H. (2009). The crystal structure of ferritin from Helicobacter pylori reveals unusual conformational changes for iron uptake. J Mol Biol *390*, 83-98.
Christensen, D., Korsholm, K.S., Andersen, P., and Agger, E.M. (2011). Cationic liposomes as vaccine adjuvants. Expert Rev Vaccines *10*, 513-521.
Cohen, J., Nussenzweig, V., Nussenzweig, R., Vekemans, J., and Leach, A. (2010). From the circumsporozoite protein to the RTS, S/AS candidate vaccine. Hum Vaccin *6*, 90-96.
Comanducci, M., Bambini, S., Caugant, D.A., Mora, M., Brunelli, B., Capecchi, B., Ciucchi, L., Rappuoli, R., and Pizza, M. (2004). NadA diversity and carriage in Neisseria meningitidis. Infect Immun *72*, 4217-4223.
Cordeiro, A.S., Crecente-Campo, J., Bouzo, B.L., Gonzalez, S.F., de la Fuente, M., and Alonso, M.J. (2019). Engineering polymeric nanocapsules for an efficient drainage and biodistribution in the lymphatic system. Journal of drug targeting *27*, 646-658.
Correa, S., Choi, K.Y., Dreaden, E.C., Renggli, K., Shi, A., Gu, L., Shopsowitz, K.E., Quadir, M.A., Ben-Akiva, E., and Hammond, P.T. (2016). Highly scalable, closed-loop synthesis of drug-loaded, layer-by-layer nanoparticles. Advanced functional materials *26*, 991-1003.
Crotty, S. (2014). T follicular helper cell differentiation, function, and roles in disease. Immunity *41*, 529-542.
Danaei, M., Dehghankhold, M., Ataei, S., Hasanzadeh Davarani, F., Javanmard, R., Dokhani, A., Khorasani, S., and Mozafari, M.R. (2018). Impact of Particle Size and Polydispersity Index on the Clinical Applications of Lipidic Nanocarrier Systems. Pharmaceutics *10*.
Davidsen, J., Rosenkrands, I., Christensen, D., Vangala, A., Kirby, D., Perrie, Y., Agger, E.M., and Andersen, P. (2005). Characterization of cationic liposomes based on dimethyldioctadecylammonium and synthetic cord factor from M. tuberculosis (trehalose 6,6'-dibehenate)-a novel adjuvant inducing both strong CMI and antibody responses. Biochimica et biophysica acta *1718*, 22-31.
Del Giudice, G., Rappuoli, R., and Didierlaurent, A.M. (2018). Correlates of adjuvanticity: A review on adjuvants in licensed vaccines. Semin Immunol *39*, 14-21.
Derrick, J.P., Urwin, R., Suker, J., Feavers, I.M., and Maiden, M.C. (1999). Structural and evolutionary inference from molecular variation in Neisseria porins. Infect Immun *67*, 2406-2413.
Dimov, N., Kastner, E., Hussain, M., Perrie, Y., and Szita, N. (2017). Formation and purification of tailored liposomes for drug delivery using a module-based micro continuous-flow system. Scientific Reports *7*, 12045.
Ding, P., Zhang, T., Li, Y., Teng, M., Sun, Y., Liu, X., Chai, S., Zhou, E., Jin, Q., and Zhang, G. (2017). Nanoparticle orientationally displayed antigen epitopes improve neutralizing antibody level in a model of porcine circovirus type 2. International journal of nanomedicine *12*, 5239-5254.
Domina, M., Lanza Cariccio, V., Benfatto, S., D'Aliberti, D., Venza, M., Borgogni, E., Castellino, F., Biondo, C., D'Andrea, D., Grassi, L.*, et al.* (2014). Rapid profiling of the antigen regions recognized by serum antibodies using massively parallel sequencing of antigen-specific libraries. PLoS One *9*, e114159.

Donnelly, J., Medini, D., Boccadifuoco, G., Biolchi, A., Ward, J., Frasch, C., Moxon, E.R., Stella, M., Comanducci, M., Bambini, S.*, et al.* (2010). Qualitative and quantitative assessment of meningococcal antigens to evaluate the potential strain coverage of protein-based vaccines. Proc Natl Acad Sci U S A *107*, 19490-19495.
Dormitzer, P.R., Grandi, G., and Rappuoli, R. (2012). Structural vaccinology starts to deliver. Nat Rev Microbiol *10*, 807-813.
Dreborg, S., and Akerblom, E.B. (1990). Immunotherapy with monomethoxypolyethylene glycol modified allergens. Critical reviews in therapeutic drug carrier systems *6*, 315-365.
Drescher, D.G., Ramakrishnan, N.A., and Drescher, M.J. (2009). Surface plasmon resonance (SPR) analysis of binding interactions of proteins in inner-ear sensory epithelia. Methods in molecular biology (Clifton, N.J.) *493*, 323-343.
Drulyte, I., Johnson, R.M., Hesketh, E.L., Hurdiss, D.L., Scarff, C.A., Porav, S.A., Ranson, N.A., Muench, S.P., and Thompson, R.F. (2018). Approaches to altering particle distributions in cryo-electron microscopy sample preparation. Acta crystallographica. Section D, Structural biology *74*, 560-571.
Dubochet, J., Adrian, M., Chang, J.J., Homo, J.C., Lepault, J., McDowall, A.W., and Schultz, P. (1988). Cryo-electron microscopy of vitrified specimens. Q Rev Biophys *21*, 129-228.
Dupuis, M., Denis-Mize, K., LaBarbara, A., Peters, W., Charo, I.F., McDonald, D.M., and Ott, G. (2001). Immunization with the adjuvant MF59 induces macrophage trafficking and apoptosis. Eur J Immunol *31*, 2910-2918.
Egerton, R.F., Li, P., and Malac, M. (2004). Radiation damage in the TEM and SEM. Micron *35*, 399-409.
Elamanchili, P., Lutsiak, C.M., Hamdy, S., Diwan, M., and Samuel, J. (2007). "Pathogen-mimicking" nanoparticles for vaccine delivery to dendritic cells. J Immunother *30*, 378-395.
Esther, M.L., and Pedro, A.R. (2009). Prediction of MHC-Peptide Binding: A Systematic and Comprehensive Overview. Current Pharmaceutical Design *15*, 3209-3220.
Fagnocchi, L., Biolchi, A., Ferlicca, F., Boccadifuoco, G., Brunelli, B., Brier, S., Norais, N., Chiarot, E., Bensi, G., Kroll, J.S.*, et al.* (2013). Transcriptional regulation of the nadA gene in Neisseria meningitidis impacts the prediction of coverage of a multicomponent meningococcal serogroup B vaccine. Infect Immun *81*, 560-569.
Fagnocchi, L., Pigozzi, E., Scarlato, V., and Delany, I. (2012). In the NadR regulon, adhesins and diverse meningococcal functions are regulated in response to signals in human saliva. J Bacteriol *194*, 460-474.
Fan, K., Cao, C., Pan, Y., Lu, D., Yang, D., Feng, J., Song, L., Liang, M., and Yan, X. (2012). Magnetoferritin nanoparticles for targeting and visualizing tumour tissues. Nat Nanotechnol *7*, 459-464.
Feavers, I.M., and Pizza, M. (2009). Meningococcal protein antigens and vaccines. Vaccine *27 Suppl 2*, B42-50.
Fernandez, I.S., Bai, X.C., Hussain, T., Kelley, A.C., Lorsch, J.R., Ramakrishnan, V., and Scheres, S.H.W. (2013). Molecular architecture of a eukaryotic translational initiation complex. Science *342*, 1240585.
Findlow, J., Lowe, A., Deane, S., Balmer, P., van den Dobbelsteen, G., Dawson, M., Andrews, N., and Borrow, R. (2005). Effect of sequence variation in meningococcal PorA outer membrane protein on the effectiveness of a hexavalent PorA outer membrane vesicle vaccine in toddlers and school children. Vaccine *23*, 2623-2627.
Findlow, J., Taylor, S., Aase, A., Horton, R., Heyderman, R., Southern, J., Andrews, N., Barchha, R., Harrison, E., Lowe, A.*, et al.* (2006). Comparison and correlation of neisseria meningitidis serogroup B immunologic assay results and human antibody responses following three doses of the Norwegian meningococcal outer membrane vesicle vaccine MenBvac. Infection and immunity *74*, 4557-4565.

Fleri, W., Paul, S., Dhanda, S.K., Mahajan, S., Xu, X., Peters, B., and Sette, A. (2017). The Immune Epitope Database and Analysis Resource in Epitope Discovery and Synthetic Vaccine Design. Front Immunol *8*, 278.
Foged, C., Arigita, C., Sundblad, A., Jiskoot, W., Storm, G., and Frokjaer, S. (2004). Interaction of dendritic cells with antigen-containing liposomes: effect of bilayer composition. Vaccine *22*, 1903-1913.
Forbes, N., Hussain, M.T., Briuglia, M.L., Edwards, D.P., Horst, J.H.t., Szita, N., and Perrie, Y. (2019). Rapid and scale-independent microfluidic manufacture of liposomes entrapping protein incorporating in-line purification and at-line size monitoring. International Journal of Pharmaceutics *556*, 68-81.
Franzoso, S., Mazzon, C., Sztukowska, M., Cecchini, P., Kasic, T., Capecchi, B., Tavano, R., and Papini, E. (2008). Human monocytes/macrophages are a target of Neisseria meningitidis Adhesin A (NadA). J Leukoc Biol *83*, 1100-1110.
Galaz-Montoya, J.G., and Ludtke, S.J. (2017). The advent of structural biology in situ by single particle cryo-electron tomography. Biophysics Reports *3*, 17-35.
Gall, D. (1966). The adjuvant activity of aliphatic nitrogenous bases. Immunology *11*, 369-386.
Garcon, N., and Van Mechelen, M. (2011). Recent clinical experience with vaccines using MPL- and QS-21-containing adjuvant systems. Expert Rev Vaccines *10*, 471-486.
Geninatti Crich, S., Bussolati, B., Tei, L., Grange, C., Esposito, G., Lanzardo, S., Camussi, G., and Aime, S. (2006). Magnetic resonance visualization of tumor angiogenesis by targeting neural cell adhesion molecules with the highly sensitive gadolinium-loaded apoferritin probe. Cancer Res *66*, 9196-9201.
Germann, T., Bongartz, M., Dlugonska, H., Hess, H., Schmitt, E., Kolbe, L., Kölsch, E., Podlaski, F.J., Gately, M.K., and Rüde, E. (1995). Interleukin-12 profoundly up-regulates the synthesis of antigen-specific complement-fixing IgG2a, IgG2b and IgG3 antibody subclasses in vivo. European Journal of Immunology *25*, 823-829.
Giuliani, M., Bartolini, E., Galli, B., Santini, L., Lo Surdo, P., Buricchi, F., Bruttini, M., Benucci, B., Pacchiani, N., Alleri, L.*, et al.* (2018). Human protective response induced by meningococcus B vaccine is mediated by the synergy of multiple bactericidal epitopes. Sci Rep *8*, 3700.
Gluck, R., Moser, C., and Metcalfe, I.C. (2004). Influenza virosomes as an efficient system for adjuvanted vaccine delivery. Expert Opin Biol Ther *4*, 1139-1145.
Goldschneider, I., Gotschlich, E.C., and Artenstein, M.S. (1969). Human immunity to the meningococcus. I. The role of humoral antibodies. J Exp Med *129*, 1307-1326.
Granier, T., Langlois d'Estaintot, B., Gallois, B., Chevalier, J.M., Precigoux, G., Santambrogio, P., and Arosio, P. (2003). Structural description of the active sites of mouse L-chain ferritin at 1.2 A resolution. J Biol Inorg Chem *8*, 105-111.
Guex, N., and Peitsch, M.C. (1997). SWISS-MODEL and the Swiss-PdbViewer: an environment for comparative protein modeling. Electrophoresis *18*, 2714-2723.
Guimarães Sá Correia, M., Briuglia, M.L., Niosi, F., and Lamprou, D.A. (2017). Microfluidic manufacturing of phospholipid nanoparticles: Stability, encapsulation efficacy, and drug release. International Journal of Pharmaceutics *516*, 91-99.
Guy, B. (2007). The perfect mix: recent progress in adjuvant research. Nat Rev Microbiol *5*, 505-517.
Hamborg, M., Jorgensen, L., Bojsen, A.R., Christensen, D., and Foged, C. (2013). Protein antigen adsorption to the DDA/TDB liposomal adjuvant: effect on protein structure, stability, and liposome physicochemical characteristics. Pharmaceutical research *30*, 140-155.
Han, J.A., Kang, Y.J., Shin, C., Ra, J.S., Shin, H.H., Hong, S.Y., Do, Y., and Kang, S. (2014). Ferritin protein cage nanoparticles as versatile antigen delivery nanoplatforms for dendritic cell (DC)-based vaccine development. Nanomedicine *10*, 561-569.
He, Y., Fang, J., Taatjes, D.J., and Nogales, E. (2013). Structural visualization of key steps in human transcription initiation. Nature *495*, 481-486.

Heesters, B.A., van der Poel, C.E., Das, A., and Carroll, M.C. (2016). Antigen Presentation to B Cells. Trends in Immunology *37*, 844-854.
Henriksen-Lacey, M., Bramwell, V.W., Christensen, D., Agger, E.M., Andersen, P., and Perrie, Y. (2010a). Liposomes based on dimethyldioctadecylammonium promote a depot effect and enhance immunogenicity of soluble antigen. Journal of controlled release : official journal of the Controlled Release Society *142*, 180-186.
Henriksen-Lacey, M., Christensen, D., Bramwell, V.W., Lindenstrom, T., Agger, E.M., Andersen, P., and Perrie, Y. (2010b). Liposomal cationic charge and antigen adsorption are important properties for the efficient deposition of antigen at the injection site and ability of the vaccine to induce a CMI response. Journal of controlled release : official journal of the Controlled Release Society *145*, 102-108.
Henriksen-Lacey, M., Christensen, D., Bramwell, V.W., Lindenstrøm, T., Agger, E.M., Andersen, P., and Perrie, Y. (2011a). Comparison of the Depot Effect and Immunogenicity of Liposomes Based on Dimethyldioctadecylammonium (DDA), 3β-[N-(N′,N′-Dimethylaminoethane)carbomyl] Cholesterol (DC-Chol), and 1,2-Dioleoyl-3-trimethylammonium Propane (DOTAP): Prolonged Liposome Retention Mediates Stronger Th1 Responses. Molecular pharmaceutics *8*, 153-161.
Henriksen-Lacey, M., Devitt, A., and Perrie, Y. (2011b). The vesicle size of DDA:TDB liposomal adjuvants plays a role in the cell-mediated immune response but has no significant effect on antibody production. Journal of controlled release : official journal of the Controlled Release Society *154*, 131-137.
Hewitt, E.W. (2003). The MHC class I antigen presentation pathway: strategies for viral immune evasion. Immunology *110*, 163-169.
Hobb, R.I., Tzeng, Y.L., Choudhury, B.P., Carlson, R.W., and Stephens, D.S. (2010). Requirement of NMB0065 for connecting assembly and export of sialic acid capsular polysaccharides in Neisseria meningitidis. Microbes Infect *12*, 476-487.
Hollingshead, S., Jongerius, I., Exley, R.M., Johnson, S., Lea, S.M., and Tang, C.M. (2018). Structure-based design of chimeric antigens for multivalent protein vaccines. Nature Communications *9*, 1051.
Holst, J., Feiring, B., Naess, L.M., Norheim, G., Kristiansen, P., Hoiby, E.A., Bryn, K., Oster, P., Costantino, P., Taha, M.K.*, et al.* (2005). The concept of "tailor-made", protein-based, outer membrane vesicle vaccines against meningococcal disease. Vaccine *23*, 2202-2205.
Holst, J., Martin, D., Arnold, R., Huergo, C.C., Oster, P., O'Hallahan, J., and Rosenqvist, E. (2009). Properties and clinical performance of vaccines containing outer membrane vesicles from Neisseria meningitidis. Vaccine *27 Suppl 2*, B3-12.
Hong, P., Koza, S., and Bouvier, E.S.P. (2012). Size-Exclusion Chromatography for the Analysis of Protein Biotherapeutics and their Aggregates. J Liq Chromatogr Relat Technol *35*, 2923-2950.
Hussain, M.J., Wilkinson, A., Bramwell, V.W., Christensen, D., and Perrie, Y. (2014). Th1 immune responses can be modulated by varying dimethyldioctadecylammonium and distearoyl-sn-glycero-3-phosphocholine content in liposomal adjuvants. Journal of Pharmacy and Pharmacology *66*, 358-366.
Immordino, M.L., Dosio, F., and Cattel, L. (2006). Stealth liposomes: review of the basic science, rationale, and clinical applications, existing and potential. International journal of nanomedicine *1*, 297-315.
Irvine, D.J., Swartz, M.A., and Szeto, G.L. (2013). Engineering synthetic vaccines using cues from natural immunity. Nat Mater *12*, 978-990.
Iwasaki, K., Mitsuoka, K., Fujiyoshi, Y., Fujisawa, Y., Kikuchi, M., Sekiguchi, K., and Yamada, T. (2005). Electron tomography reveals diverse conformations of integrin αIIbβ3 in the active state. Journal of Structural Biology *150*, 259-267.
Jahn, A., Vreeland, W.N., DeVoe, D.L., Locascio, L.E., and Gaitan, M. (2007). Microfluidic Directed Formation of Liposomes of Controlled Size. Langmuir *23*, 6289-6293.

Jandl, C., Loetsch, C., and King, C. (2017). Cytokine Expression by T Follicular Helper Cells. In Germinal Centers: Methods and Protocols, D.P. Calado, ed. (New York, NY: Springer New York), pp. 95-103.
Jardine, J., Julien, J.P., Menis, S., Ota, T., Kalyuzhniy, O., McGuire, A., Sok, D., Huang, P.S., MacPherson, S., Jones, M.*, et al.* (2013). Rational HIV immunogen design to target specific germline B cell receptors. Science *340*, 711-716.
Jarva, H., Ram, S., Vogel, U., Blom, A.M., and Meri, S. (2005). Binding of the complement inhibitor C4bp to serogroup B Neisseria meningitidis. J Immunol *174*, 6299-6307.
Jeong, H.-S., Park, H.-N., Kim, J.-G., and Hyun, J.-K. (2013). Critical importance of the correction of contrast transfer function fortransmission electron microscopy-mediated structural biology. Journal of Analytical Science and Technology *4*, 14.
Jin, J., Tarrant, R.D., Bolam, E.J., Angell-Manning, P., Soegaard, M., Pattinson, D.J., Dulal, P., Silk, S.E., Marshall, J.M., Dabbs, R.A.*, et al.* (2018). Production, quality control, stability, and potency of cGMP-produced Plasmodium falciparum RH5.1 protein vaccine expressed in Drosophila S2 cells. npj Vaccines *3*, 32.
Joshi, S., Hussain, M.T., Roces, C.B., Anderluzzi, G., Kastner, E., Salmaso, S., Kirby, D.J., and Perrie, Y. (2016). Microfluidics based manufacture of liposomes simultaneously entrapping hydrophilic and lipophilic drugs. Int J Pharm *514*, 160-168.
Kamath, A.T., Mastelic, B., Christensen, D., Rochat, A.-F., Agger, E.M., Pinschewer, D.D., Andersen, P., Lambert, P.-H., and Siegrist, C.-A. (2012). Synchronization of Dendritic Cell Activation and Antigen Exposure Is Required for the Induction of Th1/Th17 Responses. The Journal of Immunology *188*, 4828.
Kanekiyo, M., Bu, W., Joyce, M.G., Meng, G., Whittle, J.R., Baxa, U., Yamamoto, T., Narpala, S., Todd, J.P., Rao, S.S.*, et al.* (2015). Rational Design of an Epstein-Barr Virus Vaccine Targeting the Receptor-Binding Site. Cell *162*, 1090-1100.
Kanekiyo, M., Wei, C.J., Yassine, H.M., McTamney, P.M., Boyington, J.C., Whittle, J.R., Rao, S.S., Kong, W.P., Wang, L., and Nabel, G.J. (2013). Self-assembling influenza nanoparticle vaccines elicit broadly neutralizing H1N1 antibodies. Nature *499*, 102-106.
Kastner, E., Kaur, R., Lowry, D., Moghaddam, B., Wilkinson, A., and Perrie, Y. (2014). High-throughput manufacturing of size-tuned liposomes by a new microfluidics method using enhanced statistical tools for characterization. International Journal of Pharmaceutics *477*, 361-368.
Kastner, E., Verma, V., Lowry, D., and Perrie, Y. (2015). Microfluidic-controlled manufacture of liposomes for the solubilisation of a poorly water soluble drug. Int J Pharm *485*, 122-130.
Kaur, R., Bramwell, V.W., Kirby, D.J., and Perrie, Y. (2012a). Manipulation of the surface pegylation in combination with reduced vesicle size of cationic liposomal adjuvants modifies their clearance kinetics from the injection site, and the rate and type of T cell response. Journal of controlled release : official journal of the Controlled Release Society *164*, 331-337.
Kaur, R., Bramwell, V.W., Kirby, D.J., and Perrie, Y. (2012b). Pegylation of DDA:TDB liposomal adjuvants reduces the vaccine depot effect and alters the Th1/Th2 immune responses. Journal of controlled release : official journal of the Controlled Release Society *158*, 72-77.
Kaur, R., Henriksen-Lacey, M., Wilkhu, J., Devitt, A., Christensen, D., and Perrie, Y. (2014). Effect of incorporating cholesterol into DDA:TDB liposomal adjuvants on bilayer properties, biodistribution, and immune responses. Molecular pharmaceutics *11*, 197-207.
Kelly, D.F., and Rappuoli, R. (2005). Reverse vaccinology and vaccines for serogroup B Neisseria meningitidis. Adv Exp Med Biol *568*, 217-223.
Khatami, A., and Pollard, A.J. (2010). The epidemiology of meningococcal disease and the impact of vaccines. Expert Rev Vaccines *9*, 285-298.

Kim, Y.-S., Son, A., Kim, J., Kwon, S.B., Kim, M.H., Kim, P., Kim, J., Byun, Y.H., Sung, J., Lee, J.*, et al.* (2018). Chaperna-Mediated Assembly of Ferritin-Based Middle East Respiratory Syndrome-Coronavirus Nanoparticles. Frontiers in Immunology *9*.
Kirby, C., Clarke, J., and Gregoriadis, G. (1980). Effect of the cholesterol content of small unilamellar liposomes on their stability in vivo and in vitro. Biochemical Journal *186*, 591-598.
Klinguer-Hamour, C., Libon, C., Plotnicky-Gilquin, H., Bussat, M.C., Revy, L., Nguyen, T., Bonnefoy, J.Y., Corvaia, N., and Beck, A. (2002). DDA adjuvant induces a mixed Th1/Th2 immune response when associated with BBG2Na, a respiratory syncytial virus potential vaccine. Vaccine *20*, 2743-2751.
Klock, H.E., and Lesley, S.A. (2009). The Polymerase Incomplete Primer Extension (PIPE) method applied to high-throughput cloning and site-directed mutagenesis. Methods Mol Biol *498*, 91-103.
Knudsen, N.P.H., Olsen, A., Buonsanti, C., Follmann, F., Zhang, Y., Coler, R.N., Fox, C.B., Meinke, A., D'Oro, U., Casini, D.*, et al.* (2016). Different human vaccine adjuvants promote distinct antigen-independent immunological signatures tailored to different pathogens. Scientific reports *6*, 19570-19570.
Kool, M., Fierens, K., and Lambrecht, B.N. (2012). Alum adjuvant: some of the tricks of the oldest adjuvant. J Med Microbiol *61*, 927-934.
Korsholm, K.S., Agger, E.M., Foged, C., Christensen, D., Dietrich, J., Andersen, C.S., Geisler, C., and Andersen, P. (2007). The adjuvant mechanism of cationic dimethyldioctadecylammonium liposomes. Immunology *121*, 216-226.
Lawson, D.M., Artymiuk, P.J., Yewdall, S.J., Smith, J.M., Livingstone, J.C., Treffry, A., Luzzago, A., Levi, S., Arosio, P., Cesareni, G., and et al. (1991). Solving the structure of human H ferritin by genetically engineering intermolecular crystal contacts. Nature *349*, 541-544.
Leenaars, M., and Hendriksen, C.F.M. (2005). Critical Steps in the Production of Polyclonal and Monoclonal Antibodies: Evaluation and Recommendations. ILAR Journal *46*, 269-279.
Lefeber, D.J., Benaissa-Trouw, B., Vliegenthart, J.F.G., Kamerling, J.P., Jansen, W.T.M., Kraaijeveld, K., and Snippe, H. (2003). Th1-Directing Adjuvants Increase the Immunogenicity of Oligosaccharide-Protein Conjugate Vaccines Related to Streptococcus pneumoniae Type 3. Infection and Immunity *71*, 6915-6920.
Lehmann, A.K., Halstensen, A., Aaberge, I.S., Holst, J., Michaelsen, T.E., Sornes, S., Wetzler, L.M., and Guttormsen, H. (1999). Human opsonins induced during meningococcal disease recognize outer membrane proteins PorA and PorB. Infection and immunity *67*, 2552-2560.
Li Pira, G., Ivaldi, F., Moretti, P., and Manca, F. (2010). High throughput T epitope mapping and vaccine development. J Biomed Biotechnol *2010*, 325720.
Liguori, A., Dello Iacono, L., Maruggi, G., Benucci, B., Merola, M., Lo Surdo, P., López-Sagaseta, J., Pizza, M., Malito, E., and Bottomley, M.J. (2018). NadA3 Structures Reveal Undecad Coiled Coils and LOX1 Binding Regions Competed by Meningococcus B Vaccine-Elicited Human Antibodies. mBio *9*.
Liljeroos, L., Malito, E., Ferlenghi, I., and Bottomley, M.J. (2015). Structural and Computational Biology in the Design of Immunogenic Vaccine Antigens. J Immunol Res *2015*, 156241.
Lin, H.H., Zhang, G.L., Tongchusak, S., Reinherz, E.L., and Brusic, V. (2008). Evaluation of MHC-II peptide binding prediction servers: applications for vaccine research. BMC bioinformatics *9 Suppl 12*, S22-S22.
Lindblad, E.B., Elhay, M.J., Silva, R., Appelberg, R., and Andersen, P. (1997). Adjuvant modulation of immune responses to tuberculosis subunit vaccines. Infection and immunity *65*, 623-629.
Litt, D.J., Savino, S., Beddek, A., Comanducci, M., Sandiford, C., Stevens, J., Levin, M., Ison, C., Pizza, M., Rappuoli, R., and Kroll, J.S. (2004). Putative vaccine antigens

from Neisseria meningitidis recognized by serum antibodies of young children convalescing after meningococcal disease. J Infect Dis *190*, 1488-1497.
Liu, T.-M., Conde, J., Lipiński, T., Bednarkiewicz, A., and Huang, C.-C. (2016). Revisiting the classification of NIR-absorbing/emitting nanomaterials for in vivo bioapplications. NPG Asia Materials *8*, e295-e295.
Lofano, G., Mancini, F., Salvatore, G., Cantisani, R., Monaci, E., Carrisi, C., Tavarini, S., Sammicheli, C., Rossi Paccani, S., Soldaini, E.*, et al.* (2015). Oil-in-Water Emulsion MF59 Increases Germinal Center B Cell Differentiation and Persistence in Response to Vaccination. The Journal of Immunology *195*, 1617-1627.
López-Sagaseta, J., Malito, E., Rappuoli, R., and Bottomley, M.J. (2016). Self-assembling protein nanoparticles in the design of vaccines. Computational and Structural Biotechnology Journal *14*, 58-68.
Lou, G., Anderluzzi, G., Woods, S., Roberts, C.W., and Perrie, Y. (2019). A novel microfluidic-based approach to formulate size-tuneable large unilamellar cationic liposomes: formulation, cellular uptake and biodistribution investigations. Eur J Pharm Biopharm.
Lyskowski, A., Leo, J.C., and Goldman, A. (2011). Structure and biology of trimeric autotransporter adhesins. Adv Exp Med Biol *715*, 143-158.
Ma, Y., Zhuang, Y., Xie, X., Wang, C., Wang, F., Zhou, D., Zeng, J., and Cai, L. (2011). The role of surface charge density in cationic liposome-promoted dendritic cell maturation and vaccine-induced immune responses. Nanoscale *3*, 2307-2314.
MacDonald, N.E., Halperin, S.A., Law, B.J., Forrest, B., Danzig, L.E., and Granoff, D.M. (1998). Induction of immunologic memory by conjugated vs plain meningococcal C polysaccharide vaccine in toddlers: a randomized controlled trial. Jama *280*, 1685-1689.
Madico, G., Gursky, O., Fairman, J., and Massari, P. (2017). Structural and Immunological Characterization of Novel Recombinant MOMP-Based Chlamydial Antigens. Vaccines (Basel) *6*.
Maisonneuve, C., Bertholet, S., Philpott, D.J., and De Gregorio, E. (2014). Unleashing the potential of NOD- and Toll-like agonists as vaccine adjuvants. Proc Natl Acad Sci U S A *111*, 12294-12299.
Malito, E., Biancucci, M., Faleri, A., Ferlenghi, I., Scarselli, M., Maruggi, G., Lo Surdo, P., Veggi, D., Liguori, A., Santini, L.*, et al.* (2014). Structure of the meningococcal vaccine antigen NadA and epitope mapping of a bactericidal antibody. Proc Natl Acad Sci U S A *111*, 17128-17133.
Malmqvist, M. (1993). Surface plasmon resonance for detection and measurement of antibody-antigen affinity and kinetics. Curr Opin Immunol *5*, 282-286.
Mamo, T., and Poland, G.A. (2012). Nanovaccinology: the next generation of vaccines meets 21st century materials science and engineering. Vaccine *30*, 6609-6611.
Manolova, V., Flace, A., Bauer, M., Schwarz, K., Saudan, P., and Bachmann, M.F. (2008). Nanoparticles target distinct dendritic cell populations according to their size. Eur J Immunol *38*, 1404-1413.
Marasini, N., Ghaffar, K.A., Skwarczynski, M., and Toth, I. (2017). Liposomes as a Vaccine Delivery System. 221-239.
Marcandalli, J., Fiala, B., Ols, S., Perotti, M., de van der Schueren, W., Snijder, J., Hodge, E., Benhaim, M., Ravichandran, R., Carter, L.*, et al.* (2019). Induction of Potent Neutralizing Antibody Responses by a Designed Protein Nanoparticle Vaccine for Respiratory Syncytial Virus. Cell *176*, 1420-1431.e1417.
Martin, D.R., Ruijne, N., McCallum, L., O'Hallahan, J., and Oster, P. (2006). The VR2 epitope on the PorA P1.7-2,4 protein is the major target for the immune response elicited by the strain-specific group B meningococcal vaccine MeNZB. Clinical and vaccine immunology : CVI *13*, 486-491.
Masignani, V., Comanducci, M., Giuliani, M.M., Bambini, S., Adu-Bobie, J., Arico, B., Brunelli, B., Pieri, A., Santini, L., Savino, S.*, et al.* (2003). Vaccination against

Neisseria meningitidis using three variants of the lipoprotein GNA1870. J Exp Med *197*, 789-799.
Mastelic Gavillet, B., Eberhardt, C.S., Auderset, F., Castellino, F., Seubert, A., Tregoning, J.S., Lambert, P.-H., de Gregorio, E., Del Giudice, G., and Siegrist, C.-A. (2015). MF59 Mediates Its B Cell Adjuvanticity by Promoting T Follicular Helper Cells and Thus Germinal Center Responses in Adult and Early Life. The Journal of Immunology *194*, 4836-4845.
Mazzon, C., Baldani-Guerra, B., Cecchini, P., Kasic, T., Viola, A., de Bernard, M., Arico, B., Gerosa, F., and Papini, E. (2007). IFN-gamma and R-848 dependent activation of human monocyte-derived dendritic cells by Neisseria meningitidis adhesin A. J Immunol *179*, 3904-3916.
Mbow, M.L., De Gregorio, E., Valiante, N.M., and Rappuoli, R. (2010). New adjuvants for human vaccines. Curr Opin Immunol *22*, 411-416.
McAleer, W.J., Buynak, E.B., Maigetter, R.Z., Wampler, D.E., Miller, W.J., and Hilleman, M.R. (1984). Human hepatitis B vaccine from recombinant yeast. Nature *307*, 178-180.
McIntosh, E.D., Broker, M., Wassil, J., Welsch, J.A., and Borrow, R. (2015). Serum bactericidal antibody assays - The role of complement in infection and immunity. Vaccine *33*, 4414-4421.
McNeil, S.E., Rosenkrands, I., Agger, E.M., Andersen, P., and Perrie, Y. (2011). Subunit vaccines: distearoylphosphatidylcholine-based liposomes entrapping antigen offer a neutral alternative to dimethyldioctadecylammonium-based cationic liposomes as an adjuvant delivery system. Journal of pharmaceutical sciences *100*, 1856-1865.
Meiring, H.D., Kuipers, B., van Gaans-van den Brink, J.A., Poelen, M.C., Timmermans, H., Baart, G., Brugghe, H., van Schie, J., Boog, C.J., de Jong, A.P., and van Els, C.A. (2005). Mass tag-assisted identification of naturally processed HLA class II-presented meningococcal peptides recognized by CD4+ T lymphocytes. J Immunol *174*, 5636-5643.
Metruccio, M.M., Pigozzi, E., Roncarati, D., Berlanda Scorza, F., Norais, N., Hill, S.A., Scarlato, V., and Delany, I. (2009). A novel phase variation mechanism in the meningococcus driven by a ligand-responsive repressor and differential spacing of distal promoter elements. PLoS Pathog *5*, e1000710.
Michaelsen, T.E., Garred, P., and Aase, A. (1991). Human IgG subclass pattern of inducing complement-mediated cytolysis depends on antigen concentration and to a lesser extent on epitope patchiness, antibody affinity and complement concentration. Eur J Immunol *21*, 11-16.
Michaelsen, T.E., Kolberg, J., Aase, A., Herstad, T.K., and Hoiby, E.A. (2004). The four mouse IgG isotypes differ extensively in bactericidal and opsonophagocytic activity when reacting with the P1.16 epitope on the outer membrane PorA protein of Neisseria meningitidis. Scandinavian journal of immunology *59*, 34-39.
Mogensen, T.H. (2009). Pathogen recognition and inflammatory signaling in innate immune defenses. Clin Microbiol Rev *22*, 240-273, Table of Contents.
Montanari, P., Bozza, G., Capecchi, B., Caproni, E., Barrile, R., Norais, N., Capitani, M., Sallese, M., Cecchini, P., Ciucchi, L.*, et al.* (2012). Human heat shock protein (Hsp) 90 interferes with Neisseria meningitidis adhesin A (NadA)-mediated adhesion and invasion. Cell Microbiol *14*, 368-385.
Moon, J.J., Suh, H., Polhemus, M.E., Ockenhouse, C.F., Yadava, A., and Irvine, D.J. (2012). Antigen-displaying lipid-enveloped PLGA nanoparticles as delivery agents for a Plasmodium vivax malaria vaccine. PLoS One *7*, e31472.
Mosmann, T.R., and Coffman, R.L. (1989). TH1 and TH2 cells: different patterns of lymphokine secretion lead to different functional properties. Annu Rev Immunol *7*, 145-173.
Moyer, T.J., Zmolek, A.C., and Irvine, D.J. (2016). Beyond antigens and adjuvants: formulating future vaccines. The Journal of clinical investigation *126*, 799-808.

Moyle, P.M., and Toth, I. (2013). Modern Subunit Vaccines: Development, Components, and Research Opportunities. ChemMedChem *8*, 360-376.
Naess, L.M., Aarvak, T., Aase, A., Oftung, F., Hoiby, E.A., Sandin, R., and Michaelsen, T.E. (1999). Human IgG subclass responses in relation to serum bactericidal and opsonic activities after immunization with three doses of the Norwegian serogroup B meningococcal outer membrane vesicle vaccine. Vaccine *17*, 754-764.
Naess, L.M., Oftung, F., Aase, A., Michaelsen, T.E., and Pollard, A.J. (2001). T-cell responses against meningococcal antigens. Methods in molecular medicine *66*, 339-348.
Nagele, V., Heesemann, J., Schielke, S., Jimenez-Soto, L.F., Kurzai, O., and Ackermann, N. (2011). Neisseria meningitidis adhesin NadA targets beta1 integrins: functional similarity to Yersinia invasin. J Biol Chem *286*, 20536-20546.
Naito, Y., Takematsu, H., Koyama, S., Miyake, S., Yamamoto, H., Fujinawa, R., Sugai, M., Okuno, Y., Tsujimoto, G., Yamaji, T.*, et al.* (2007). Germinal center marker GL7 probes activation-dependent repression of N-glycolylneuraminic acid, a sialic acid species involved in the negative modulation of B-cell activation. Mol Cell Biol *27*, 3008-3022.
Nakanishi, T., Kunisawa, J., Hayashi, A., Tsutsumi, Y., Kubo, K., Nakagawa, S., Fujiwara, H., Hamaoka, T., and Mayumi, T. (1997). Positively charged liposome functions as an efficient immunoadjuvant in inducing immune responses to soluble proteins. Biochemical and biophysical research communications *240*, 793-797.
Needham, D., McIntosh, T.J., and Lasic, D.D. (1992). Repulsive interactions and mechanical stability of polymer-grafted lipid membranes. Biochimica et biophysica acta *1108*, 40-48.
Nguyen, H.H., Park, J., Kang, S., and Kim, M. (2015). Surface plasmon resonance: a versatile technique for biosensor applications. Sensors (Basel, Switzerland) *15*, 10481-10510.
Noad, R., and Roy, P. (2003). Virus-like particles as immunogens. Trends Microbiol *11*, 438-444.
Nogales, E. (2016). The development of cryo-EM into a mainstream structural biology technique. Nat Methods *13*, 24-27.
Nowakowski, A.B., Wobig, W.J., and Petering, D.H. (2014). Native SDS-PAGE: high resolution electrophoretic separation of proteins with retention of native properties including bound metal ions. Metallomics *6*, 1068-1078.
Ntziachristos, V., Bremer, C., and Weissleder, R. (2003). Fluorescence imaging with near-infrared light: new technological advances that enable in vivo molecular imaging. European Radiology *13*, 195-208.
Nutt, S.L., and Tarlinton, D.M. (2011). Germinal center B and follicular helper T cells: siblings, cousins or just good friends? Nature immunology *12*, 472-477.
O'Hagan, D.T., and De Gregorio, E. (2009). The path to a successful vaccine adjuvant--'the long and winding road'. Drug Discov Today *14*, 541-551.
O'Hagan, D.T., Ott, G.S., Nest, G.V., Rappuoli, R., and Giudice, G.D. (2013). The history of MF59® adjuvant: a phoenix that arose from the ashes. Expert Review of Vaccines *12*, 13-30.
Oftung, F., Korsvold, G.E., Aase, A., and Naess, L.M. (2016). Cellular Immune Responses in Humans Induced by Two Serogroup B Meningococcal Outer Membrane Vesicle Vaccines Given Separately and in Combination. Clin Vaccine Immunol *23*, 353-362.
Ohi, M., Li, Y., Cheng, Y., and Walz, T. (2004). Negative Staining and Image Classification - Powerful Tools in Modern Electron Microscopy. Biol Proced Online *6*, 23-34.
Ohtake, S., Schebor, C., Palecek, S.P., and de Pablo, J.J. (2005). Phase behavior of freeze-dried phospholipid–cholesterol mixtures stabilized with trehalose. Biochimica et Biophysica Acta (BBA) - Biomembranes *1713*, 57-64.

Oliver, A.M., Martin, F., and Kearney, J.F. (1997). Mouse CD38 is down-regulated on germinal center B cells and mature plasma cells. The Journal of Immunology *158*, 1108-1115.
Oomen, C.J., Hoogerhout, P., Kuipers, B., Vidarsson, G., van Alphen, L., and Gros, P. (2005). Crystal Structure of an Anti-meningococcal Subtype P1.4 PorA Antibody Provides Basis for Peptide–Vaccine Design. Journal of Molecular Biology *351*, 1070-1080.
Oyewumi, M.O., Kumar, A., and Cui, Z. (2010). Nano-microparticles as immune adjuvants: correlating particle sizes and the resultant immune responses. Expert Rev Vaccines *9*, 1095-1107.
Parry, D., and Squire, J. (2017). Fibrous Proteins: Structures and Mechanisms, Vol 82.
Patronov, A., and Doytchinova, I. T-cell epitope vaccine design by immunoinformatics. Open biology *3*, 120139-120139.
Perrie, Y., Crofts, F., Devitt, A., Griffiths, H.R., Kastner, E., and Nadella, V. (2016). Designing liposomal adjuvants for the next generation of vaccines. Adv Drug Deliv Rev *99*, 85-96.
Perrie, Y., Kastner, E., Kaur, R., Wilkinson, A., and Ingham, A.J. (2013). A case-study investigating the physicochemical characteristics that dictate the function of a liposomal adjuvant. Hum Vaccin Immunother *9*, 1374-1381.
Pettersen, E.F., Goddard, T.D., Huang, C.C., Couch, G.S., Greenblatt, D.M., Meng, E.C., and Ferrin, T.E. (2004). UCSF Chimera--a visualization system for exploratory research and analysis. Journal of computational chemistry *25*, 1605-1612.
Rappuoli, R. (2000). Reverse vaccinology. Current Opinion in Microbiology *3*, 445-450.
Rappuoli, R., Mandl, C.W., Black, S., and De Gregorio, E. (2011). Vaccines for the twenty-first century society. Nat Rev Immunol *11*, 865-872.
Rappuoli, R., and Serruto, D. (2019). Self-Assembling Nanoparticles Usher in a New Era of Vaccine Design. Cell *176*, 1245-1247.
Raynal, B., Lenormand, P., Baron, B., Hoos, S., and England, P. (2014). Quality assessment and optimization of purified protein samples: why and how? Microbial cell factories *13*, 180.
Reddy, S.T., van der Vlies, A.J., Simeoni, E., Angeli, V., Randolph, G.J., O'Neil, C.P., Lee, L.K., Swartz, M.A., and Hubbell, J.A. (2007). Exploiting lymphatic transport and complement activation in nanoparticle vaccines. Nat Biotechnol *25*, 1159-1164.
Rodig, S.J., Shahsafaei, A., Li, B., and Dorfman, D.M. (2005). The CD45 isoform B220 identifies select subsets of human B cells and B-cell lymphoproliferative disorders. Human Pathology *36*, 51-57.
Rosano, G.L., and Ceccarelli, E.A. (2014). Recombinant protein expression in Escherichia coli: advances and challenges. Frontiers in Microbiology *5*.
Rosenstein, N.E., Perkins, B.A., Stephens, D.S., Popovic, T., and Hughes, J.M. (2001). Meningococcal disease. N Engl J Med *344*, 1378-1388.
Rosenthal, J.A., Chen, L., Baker, J.L., Putnam, D., and DeLisa, M.P. (2014). Pathogen-like particles: biomimetic vaccine carriers engineered at the nanoscale. Curr Opin Biotechnol *28*, 51-58.
Rouphael, N.G., and Stephens, D.S. (2012). Neisseria meningitidis: biology, microbiology, and epidemiology. Methods Mol Biol *799*, 1-20.
Rouppe van der Voort, E.M., Kuipers, B., Brugghe, H.F., van Unen, L.M., Timmermans, H.A., Hoogerhout, P., and Poolman, J.T. (1997). Epitope specificity of murine and human bactericidal antibodies against PorA P1.7,16 induced with experimental meningococcal group B vaccines. FEMS immunology and medical microbiology *17*, 139-148.
Roy, S., and Awasthi, A. (2019). ATP Triggers Human Th9 Cell Differentiation via Nitric Oxide-Mediated mTOR-HIF1α Pathway. Frontiers in Immunology *10*.

Russell, J.E., Jolley, K.A., Feavers, I.M., Maiden, M.C., and Suker, J. (2004). PorA variable regions of Neisseria meningitidis. Emerg Infect Dis *10*, 674-678.
Sanchez-Trincado, J.L., Gomez-Perosanz, M., and Reche, P.A. (2017). Fundamentals and Methods for T- and B-Cell Epitope Prediction. J Immunol Res *2017*, 2680160.
Scarselli, M., Arico, B., Brunelli, B., Savino, S., Di Marcello, F., Palumbo, E., Veggi, D., Ciucchi, L., Cartocci, E., Bottomley, M.J.*, et al.* (2011). Rational design of a meningococcal antigen inducing broad protective immunity. Sci Transl Med *3*, 91ra62.
Scheiblhofer, S., Laimer, J., Machado, Y., Weiss, R., and Thalhamer, J. (2017). Influence of protein fold stability on immunogenicity and its implications for vaccine design. Expert Rev Vaccines *16*, 479-489.
Scheres, S.H. (2012). RELION: implementation of a Bayesian approach to cryo-EM structure determination. J Struct Biol *180*, 519-530.
Schiller, J.T., and Lowy, D.R. (2012). Understanding and learning from the success of prophylactic human papillomavirus vaccines. Nat Rev Microbiol *10*, 681-692.
Schonbrunn, A. (2014). Editorial: Antibody Can Get It Right: Confronting Problems of Antibody Specificity and Irreproducibility. Molecular Endocrinology *28*, 1403-1407.
Schur, P.H. (1988). IgG subclasses. A historical perspective. Monographs in allergy *23*, 1-11.
Sellers, R.S., Clifford, C.B., Treuting, P.M., and Brayton, C. (2011). Immunological Variation Between Inbred Laboratory Mouse Strains. Veterinary Pathology *49*, 32-43.
Serruto, D., Bottomley, M.J., Ram, S., Giuliani, M.M., and Rappuoli, R. (2012). The new multicomponent vaccine against meningococcal serogroup B, 4CMenB: immunological, functional and structural characterization of the antigens. Vaccine *30 Suppl 2*, B87-97.
Sharma, G., and Holt, R.A. (2014). T-cell epitope discovery technologies. Hum Immunol *75*, 514-519.
Shinall, S.M., Gonzalez-Fernandez, M., Noelle, R.J., and Waldschmidt, T.J. (2000). Identification of murine germinal center B cell subsets defined by the expression of surface isotypes and differentiation antigens. J Immunol *164*, 5729-5738.
Sliepen, K., Ozorowski, G., Burger, J.A., van Montfort, T., Stunnenberg, M., LaBranche, C., Montefiori, D.C., Moore, J.P., Ward, A.B., and Sanders, R.W. (2015). Presenting native-like HIV-1 envelope trimers on ferritin nanoparticles improves their immunogenicity. Retrovirology *12*, 82.
Snape, M.D., and Pollard, A.J. (2005). Meningococcal polysaccharide-protein conjugate vaccines. Lancet Infect Dis *5*, 21-30.
Soema, P.C., Willems, G.J., Jiskoot, W., Amorij, J.P., and Kersten, G.F. (2015). Predicting the influence of liposomal lipid composition on liposome size, zeta potential and liposome-induced dendritic cell maturation using a design of experiments approach. Eur J Pharm Biopharm *94*, 427-435.
Steers, N.J., Peachman, K.K., McClain, S., Alving, C.R., and Rao, M. (2009). Liposome-encapsulated HIV-1 Gag p24 containing lipid A induces effector CD4+ T-cells, memory CD8+ T-cells, and pro-inflammatory cytokines. Vaccine *27*, 6939-6949.
Stephens, D.S. (1999). Uncloaking the meningococcus: dynamics of carriage and disease. Lancet *353*, 941-942.
Stephens, D.S. (2009). Biology and pathogenesis of the evolutionarily successful, obligate human bacterium Neisseria meningitidis. Vaccine *27*, B71-B77.
Stephens, D.S., Greenwood, B., and Brandtzaeg, P. (2007). Epidemic meningitis, meningococcaemia, and Neisseria meningitidis. Lancet *369*, 2196-2210.
Sun, B., and Zhang, Y. (2014). Overview of Orchestration of CD4+ T Cell Subsets in Immune Responses. In T Helper Cell Differentiation and Their Function, B. Sun, ed. (Dordrecht: Springer Netherlands), pp. 1-13.

Sutter, M., Boehringer, D., Gutmann, S., Gunther, S., Prangishvili, D., Loessner, M.J., Stetter, K.O., Weber-Ban, E., and Ban, N. (2008). Structural basis of enzyme encapsulation into a bacterial nanocompartment. Nat Struct Mol Biol *15*, 939-947.
Tandrup Schmidt, S., Foged, C., Korsholm, K.S., Rades, T., and Christensen, D. (2016). Liposome-Based Adjuvants for Subunit Vaccines: Formulation Strategies for Subunit Antigens and Immunostimulators. Pharmaceutics *8*.
Tauseef, I., Ali, Y.M., and Bayliss, C.D. (2013). Phase variation of PorA, a major outer membrane protein, mediates escape of bactericidal antibodies by Neisseria meningitidis. Infect Immun *81*, 1374-1380.
Tavano, R., Capecchi, B., Montanari, P., Franzoso, S., Marin, O., Sztukowska, M., Cecchini, P., Segat, D., Scarselli, M., Arico, B., and Papini, E. (2011). Mapping of the Neisseria meningitidis NadA cell-binding site: relevance of predicted {alpha}-helices in the NH2-terminal and dimeric coiled-coil regions. J Bacteriol *193*, 107-115.
Tavano, R., Franzoso, S., Cecchini, P., Cartocci, E., Oriente, F., Arico, B., and Papini, E. (2009). The membrane expression of Neisseria meningitidis adhesin A (NadA) increases the proimmune effects of MenB OMVs on human macrophages, compared with NadA- OMVs, without further stimulating their proinflammatory activity on circulating monocytes. J Leukoc Biol *86*, 143-153.
Thompson, R.F., Walker, M., Siebert, C.A., Muench, S.P., and Ranson, N.A. (2016). An introduction to sample preparation and imaging by cryo-electron microscopy for structural biology. Methods *100*, 3-15.
Tokatlian, T., Read, B.J., Jones, C.A., Kulp, D.W., Menis, S., Chang, J.Y.H., Steichen, J.M., Kumari, S., Allen, J.D., Dane, E.L.*, et al.* (2019). Innate immune recognition of glycans targets HIV nanoparticle immunogens to germinal centers. Science *363*, 649-654.
Tommassen, J., Vermeij, P., Struyve, M., Benz, R., and Poolman, J.T. (1990). Isolation of Neisseria meningitidis mutants deficient in class 1 (porA) and class 3 (porB) outer membrane proteins. Infect Immun *58*, 1355-1359.
Tondella, M.L., Popovic, T., Rosenstein, N.E., Lake, D.B., Carlone, G.M., Mayer, L.W., and Perkins, B.A. (2000). Distribution of Neisseria meningitidis serogroup B serosubtypes and serotypes circulating in the United States. The Active Bacterial Core Surveillance Team. J Clin Microbiol *38*, 3323-3328.
Torchilin, V.P. (2005). Recent advances with liposomes as pharmaceutical carriers. Nat Rev Drug Discov *4*, 145-160.
Truffi, M., Fiandra, L., Sorrentino, L., Monieri, M., Corsi, F., and Mazzucchelli, S. (2016). Ferritin nanocages: A biological platform for drug delivery, imaging and theranostics in cancer. Pharmacol Res *107*, 57-65.
Ulmer, J.B., Valley, U., and Rappuoli, R. (2006). Vaccine manufacturing: challenges and solutions. Nature Biotechnology *24*, 1377-1383.
Uria, M.J., Zhang, Q., Li, Y., Chan, A., Exley, R.M., Gollan, B., Chan, H., Feavers, I., Yarwood, A., Abad, R.*, et al.* (2008). A generic mechanism in Neisseria meningitidis for enhanced resistance against bactericidal antibodies. J Exp Med *205*, 1423-1434.
Vagenende, V., Yap, M.G.S., and Trout, B.L. (2009). Mechanisms of Protein Stabilization and Prevention of Protein Aggregation by Glycerol. Biochemistry *48*, 11084-11096.
Valenzuela, P., Medina, A., Rutter, W.J., Ammerer, G., and Hall, B.D. (1982). Synthesis and assembly of hepatitis B virus surface antigen particles in yeast. Nature *298*, 347-350.
van der Ende, A., Hopman, C.T., Keijzers, W.C., Spanjaard, L., Lodder, E.B., van Keulen, P.H., and Dankert, J. (2003). Outbreak of meningococcal disease caused by PorA-deficient meningococci. J Infect Dis *187*, 869-871.
van der Ende, A., Hopman, C.T., Zaat, S., Essink, B.B., Berkhout, B., and Dankert, J. (1995). Variable expression of class 1 outer membrane protein in Neisseria meningitidis is caused by variation in the spacing between the -10 and -35 regions of the promoter. J Bacteriol *177*, 2475-2480.

van Els, C.A.C.M., Corbière, V., Smits, K., van Gaans-van den Brink, J.A.M., Poelen, M.C.M., Mascart, F., Meiring, H.D., and Locht, C. (2014). Toward Understanding the Essence of Post-Translational Modifications for the Mycobacterium tuberculosis Immunoproteome. Frontiers in Immunology *5*.
van Heel, M., and Keegstra, W. (1981). IMAGIC: A fast, flexible and friendly image analysis software system. Ultramicroscopy *7*, 113-129.
Vedadi, M., Niesen, F.H., Allali-Hassani, A., Fedorov, O.Y., Finerty, P.J., Wasney, G.A., Yeung, R., Arrowsmith, C., Ball, L.J., Berglund, H.*, et al.* (2006). Chemical screening methods to identify ligands that promote protein stability, protein crystallization, and structure determination. Proceedings of the National Academy of Sciences *103*, 15835-15840.
Vermont, C., and van den Dobbelsteen, G. (2002). Neisseria meningitidis serogroup B: laboratory correlates of protection. Pathogens and Disease *34*, 89-96.
Vidarsson, G., Dekkers, G., and Rispens, T. (2014). IgG subclasses and allotypes: from structure to effector functions. Front Immunol *5*, 520.
Vidarsson, G., and van de Winkel, J.G. (1998). Fc receptor and complement receptor-mediated phagocytosis in host defence. Current opinion in infectious diseases *11*, 271-278.
Vidarsson, G., van Der Pol, W.L., van Den Elsen, J.M., Vile, H., Jansen, M., Duijs, J., Morton, H.C., Boel, E., Daha, M.R., Corthesy, B., and van De Winkel, J.G. (2001). Activity of human IgG and IgA subclasses in immune defense against Neisseria meningitidis serogroup B. J Immunol *166*, 6250-6256.
Vipond, C., Suker, J., Jones, C., Tang, C., Feavers, I.M., and Wheeler, J.X. (2006). Proteomic analysis of a meningococcal outer membrane vesicle vaccine prepared from the group B strain NZ98/254. Proteomics *6*, 3400-3413.
Vita, R., Mahajan, S., Overton, J.A., Dhanda, S.K., Martini, S., Cantrell, J.R., Wheeler, D.K., Sette, A., and Peters, B. (2019). The Immune Epitope Database (IEDB): 2018 update. Nucleic acids research *47*, D339-d343.
Wang, C., Liu, P., Zhuang, Y., Li, P., Jiang, B., Pan, H., Liu, L., Cai, L., and Ma, Y. (2014). Lymphatic-targeted cationic liposomes: a robust vaccine adjuvant for promoting long-term immunological memory. Vaccine *32*, 5475-5483.
Whitesides, G.M. (2006). The origins and the future of microfluidics. Nature *442*, 368-373.
Wiertz, E.J., van Gaans-van den Brink, J.A., Schreuder, G.M., Termijtelen, A.A., Hoogerhout, P., and Poolman, J.T. (1991). T cell recognition of Neisseria meningitidis class 1 outer membrane proteins. Identification of T cell epitopes with selected synthetic peptides and determination of HLA restriction elements. J Immunol *147*, 2012-2018.
Wilson, N.R., Pandey, P.A., Beanland, R., Young, R.J., Kinloch, I.A., Gong, L., Liu, Z., Suenaga, K., Rourke, J.P., York, S.J., and Sloan, J. (2009). Graphene Oxide: Structural Analysis and Application as a Highly Transparent Support for Electron Microscopy. ACS Nano *3*, 2547-2556.
Winey, M., Meehl, J.B., O'Toole, E.T., and Giddings, T.H., Jr. (2014). Conventional transmission electron microscopy. Mol Biol Cell *25*, 319-323.
Wu, X., Tian, J., and Wang, S. (2018). Insight Into Non-Pathogenic Th17 Cells in Autoimmune Diseases. Frontiers in Immunology *9*.
Yang, Y., Neef, T., Mittelholzer, C., Garcia Garayoa, E., Blauenstein, P., Schibli, R., Aebi, U., and Burkhard, P. (2013). The biodistribution of self-assembling protein nanoparticles shows they are promising vaccine platforms. J Nanobiotechnology *11*, 36.
Yassine, H.M., Boyington, J.C., McTamney, P.M., Wei, C.J., Kanekiyo, M., Kong, W.P., Gallagher, J.R., Wang, L., Zhang, Y., Joyce, M.G.*, et al.* (2015). Hemagglutinin-stem nanoparticles generate heterosubtypic influenza protection. Nature medicine *21*, 1065-1070.

Yogev, R., and Tan, T. (2011). Meningococcal disease: the advances and challenges of meningococcal disease prevention. Hum Vaccin *7*, 828-837.
Zepp, F. (2010). Principles of vaccine design-Lessons from nature. Vaccine *28 Suppl 3*, C14-24.
Zhang, L.F., Zhou, J., Chen, S., Cai, L.L., Bao, Q.Y., Zheng, F.Y., Lu, J.Q., Padmanabha, J., Hengst, K., Malcolm, K., and Frazer, I.H. (2000). HPV6b virus like particles are potent immunogens without adjuvant in man. Vaccine *18*, 1051-1058.
Zhang, X., Goel, V., Attarwala, H., Sweetser, M.T., Clausen, V.A., and Robbie, G.J. (2019). Patisiran Pharmacokinetics, Pharmacodynamics, and Exposure-Response Analyses in the Phase 3 APOLLO Trial in Patients With Hereditary Transthyretin-Mediated (hATTR) Amyloidosis. The Journal of Clinical Pharmacology *0*.
Zhigaltsev, I.V., Belliveau, N., Hafez, I., Leung, A.K.K., Huft, J., Hansen, C., and Cullis, P.R. (2012). Bottom-Up Design and Synthesis of Limit Size Lipid Nanoparticle Systems with Aqueous and Triglyceride Cores Using Millisecond Microfluidic Mixing. Langmuir *28*, 3633-3640.
Zhu, J., Yamane, H., and Paul, W.E. (2010). Differentiation of effector CD4 T cell populations (*). Annual review of immunology *28*, 445-489.
Zimmer, S.M., and Stephens, D.S. (2006). Serogroup B meningococcal vaccines. Curr Opin Investig Drugs *7*, 733-739.
Zizzari, A., Bianco, M., Carbone, L., Perrone, E., Amato, F., Maruccio, G., Rendina, F., and Arima, V. (2017). Continuous-Flow Production of Injectable Liposomes via a Microfluidic Approach. Materials (Basel, Switzerland) *10*.